PERFORMANCE CHARACTERISATION OF COMPRESSION IGNITION ENGINE USING TRUNCATED CONE PISTON CROWNS

BY

TOWOJU, OLUMIDE ADEWOLE

B. Tech. Hons (Ogbomoso), M.Sc. (Ibadan), Mechanical Engineering

(Matric No. 136044)

A Thesis in the Department of Mechanical Engineering

Submitted to the Faculty of Technology in partial fulfilment of

the requirement for the Degree of

DOCTOR OF PHILOSOPHY

of the

UNIVERSITY OF IBADAN

Department of Mechanical Engineering
University of Ibadan
Ibadan.

October 2018

ABSTRACT

Compression Ignition (CI) engines are widely used in transportation and power generation industries in Nigeria. However, their low thermal efficiency and high emissions have necessitated continuous efforts at redesigning the Combustion Chamber (CC). There is still sparse literature on effect of using non-cylindrical piston crown in addressing these limitations. This study was therefore designed to investigate the performance characteristics of a CI engine equipped with Truncated Cone Piston Crown (TCPC) and Inverted Truncated Cone Piston Crown (ITCPC) using selected fuels.

A model based on mass balance, momentum, energy, and k-ε turbulent equations was developed and solved using finite-element technique to obtain Temperature, Pressure and Emission History (TPEH) inside the CC of a CI engine. The model was applied to two standard CI engines utilising Automotive Gas Oil (AGO) with equivalence-ratio, initial pressure and temperature of 0.5, 100 kPa, and 313 K respectively. The standard CI engines are Kirloskar-TV1 (KTV) with 87.5 mm cylinder-bore, Compression Ratio (CR) of 17.5 and Yoshita-165F (Y165) with 70 mm cylinder-bore, CR of 20.5. The TPEH was used to estimate Engine Thermal Efficiency (ETE), Specific Fuel Consumption (SFC), and Carbon Monoxide Emissions (CME). The model was further applied to KTV with TCPC (KTV-TCPC), KTV with ITCPC (KTV-ITCPC), Y165 with TCPC (Y165-TCPC), and Y165 with ITCPC (Y165-ITCPC) at Truncated Cone Base Angles (TCBA) of 25, 30, 35, 40 and 45°. Biodiesel was prepared from Shea-butter and its physicochemical properties determined using standard techniques. The ETE, SFC and CME were determined experimentally for Y165 and Y165-TCPC with the selected TCBA using AGO and 100% biodiesel. Data were analysed using ANOVA at $\alpha_{0.05}$.

The ETE, SFC, and CME for KTV were 30.90%, 0.194 kg/kWh, and 1558.70 ppm, respectively, while for Y165 were 32.20%, 0.347 kg/kWh, and 1545.24 ppm. The best TCBA for KTV-TCPC, KTV-ITCPC, Y165-TCPC, and Y165-ITCPC was 40°. At TCBA of 40°, ETE, SFC, and CME were 30.91%, 0.192 kg/kWh, and 1557.99 ppm, respectively for KTV-TCPC, 30.93%, 0.193 kg/kWh, and 1558.00 ppm, respectively for KTV-ITCPC, 32.26%, 0.346 kg/kWh, and 1542.94 ppm, respectively for Y165-TCPC, and 32.26%, 0.346 kg/kWh, and 1542.92 ppm, respectively for Y165-ITCPC. The determined specific gravity, calorific value, kinematic viscosity, and cetane number for biodiesel were 0.923, 40.10 MJ/kg, 5.40 mm/s^2, and 44.80, respectively. The ETE, SFC, and CME obtained experimentally for Y165 operated

on AGO were 13.74%, 0.728 kg/kWh, and 1598.00 ppm respectively, while that of biodiesel were 16.05%, 0.599 kg/kWh, and 1859.00 ppm respectively. The ETE, SFC, and CME for Y165-TCPC operated on AGO were 12.60%, 0.794 kg/kWh, and 1463.00 ppm respectively, while for biodiesel were 25.08%, 0.329 kg/kWh, and 780.00 ppm respectively. The CI engine with TCPC and ITCPC showed better performance than KTV and Y165. There was no significant difference between the numerical and experimental results.

The use of conical piston crown improved the performance of compression ignition engines. The forty degree base angle truncated conical piston crown gave the best engine performance.

Keywords: Compression-ignition engine, Finite element method, Piston crown, Biodiesel
Word count: 481

CERTIFICATION

I certify that this work was carried out by O. A. Towoju in the Department of Mechanical Engineering, University of Ibadan

…….

Supervisor
Dr A. A. Dare
B.Sc., M.Sc., Ph.D. (Ibadan), MNSE, MNIMechE, COREN Regd.
Associate Professor, Department of Mechanical Engineering
University of Ibadan, Nigeria

DEDICATION

This work is dedicated to the Almighty God, the Alpha and Omega, the author and the finisher of our faith.

AKNOWLEDGEMENTS

My sincere appreciation to the Almighty God, the eternal Rock of Ages, the creator of the universe, who out of His infinite love, grace, mercy, and favour had made this work a success. To Him alone be all the glory and adoration for graciously bestowing on me wisdom, knowledge and understanding during the course of this work, and for the gift of life.

I sincerely appreciate my supervisor, Dr A. A. Dare for his support, tutelage, understanding, and guidance right from the inception of my programme. I am immensely grateful to him for devoting sufficient time to ensure speedy completion of the research work. I have gained immensely from his wealth of experience and vast knowledge. I pray he will enjoy a long life in good health and prosperity. I do pray that he will always have cause to praise the name of the Lord together with his entire household.

My appreciation goes to all the lecturers in the Department of Mechanical Engineering, University of Ibadan for advice, support, and encouragement towards the completion of the programme. I sincerely thank Prof O. M. Oyewola, Prof O. O. Oluwole, Dr T. A. O. Salau, Dr K. M. Odunfa, Dr A. Falana, Dr C. J. Diji, Dr O. S. Ismail, Dr D. A. Fadare, Dr I. F. Odesola, Dr O. E. Simolowo, Dr O. O. Ajide, Dr R. Abu, Dr A. S. Adebayo, Dr S. K. Fasogbon, Dr N. Idusuyi, and Engr. Temilola T. Olugasa. Dr M. O. Petinrin, you were not just a member of the department staff, a colleague and friend, but also a brother who assisted in the time of need.

I am very grateful to a former lecturer turned father of the Department of Mechanical Engineering, University of Ibadan, Prof. R. O. Fagbenle, for his constant words of advice and encouragement.

I appreciate all staff in the Laboratory for their unwavering supports and assistance rendered while conducting the laboratory experiments. I really appreciate Mr J. S. Bolade.

To the administrative staff of the Department, thank-you very much for your support, God bless you all.

I acknowledge my colleagues at the doctoral research degree level, Dr A. A. Adegbola, Dr R. A. Kazeem, Mr Olorunfemi for their words of encouragement and helpful insights provided to my research work.

My gratitude also goes to the entire members of staff of the Department of Mechanical Engineering, and staff of the Faculty of Engineering, Adeleke University, Ede for their love and support. Prof J.O. Ojediran (former Dean, Faculty of Engineering, Adeleke University, now Vice-Chancellor Bells University of Technology, Ota), Prof S. Jekayinfa and a host of others are highly appreciated for their advice and moral support.

My sincere appreciation also goes to Engr. John. Ipadeola; chief technologist, LAUTECH, Mr. Jimoh, and Mr. David Ogunsola of LAUTECH, Ogbomoso for their numerous support.

I appreciate the support, show of concern and prayer of my Pastor, Pastor (Dr) O. Ojo, I pray the Lord will continue to increase you on all sides.

My profound gratitude also goes to my loving parents, Mr M.A. Towoju (JP) and Mrs F.F. Towoju, my siblings and their spouses: Mrs O.O. Towoju, Dr and Dr (Mrs) Olugbenga A. Towoju, Mr and Mrs Olubukola A. Towoju, and Dr Opeyemi A. Towoju, not forgetting my Aunty and her spouse, Mr and Mrs Ogunniyi and my uncle Pastor Kunle Towoju for their prayers, advice, encouragement and moral support towards the successful completion of my programme.

I will be an ingrate if I fail to specially acknowledge and appreciate my loving and understanding wife, Titilayo Omorinola Towoju (aca). I thank you for your care, belief in me, moral and emotional support, and continued endurance. I am grateful to my God given kids, Oluwadarasimi and Oluwadunmininu. I pray that God will keep them and prosper their ways in all their endeavours.

TABLE OF CONTENTS

LIST OF TABLES

LIST OF PLATES

LIST OF FIGURES

NOMENCLATURE

c_p	Specific Heat Capacity at Constant Pressure (J/kgK)
d	Piston Diameter (m)
f	Body Forces (N)
h	Heat Transfer Coefficient (W/m^2K)
k	Thermal Conductivity (W/mK)
k	Turbulence Kinetic Energy (m^2/s^2)
l	Connecting Rod Length (m)
$\dot{m}$	Mass Flow Rate (kg/s)
n_c	Number of Cycles
Pm	Mean Effective Pressure (N/m^2)
q	Volumetric Flow Rate (m^3/s)
Q	Heat Energy per unit Volume (J/m^3)
$\mathcal{Q}$	Heat due to Chemical Reaction (J/s)
rc	Crank Radius (m)
R	Gas Constant (J/kg.K)
S	Stroke Length
T	Temperature (K)
Upp	Instantaneous Velocity (m/s)
V_c	Clearance Volume (m^3)
V_d	Displacement Volume (m^3)
V_o	Initial Engine Volume (m^3)
V_s	Swept Volume (m^3)
W	Work-done (J)
x_p	Piston Displacement (m)
σ	Stress Tensor
ε	Dissipation Rate (m^2/s^3)
ρ	Density (kg/m^3)
Π	Efficiency (%)
ψ	Equivalence Ratio
θ	Angle of Taper (°)
μ	Dynamic Viscosity (Pas)

μ_T	Turbulent Eddy Viscosity (Pas)
φ	Heat Flux (J/m^2)
Υ	Shear Stress (N/m^2)

ABBREVIATIONS

A/F	Air-Fuel Ratio
AGO	Automotive Gas Oil
aTDC	After Top Dead Centre
bTDC	Before Top Dead Centre
CC	Combustion Chamber
CI	Compression Ignition
CO	Carbon Monoxide
CO_2	Carbon Dioxide
CR	Compression Ratio
D	Cylinder Bore Diameter (m)
DI	Direct Injection
EGR	Exhaust Gas Recirculation
EGT	Exhaust Gas Temperature (K)
HC	Hydrocarbon
ITCPC	Inverted Truncated Cone Piston Crown
PM	Particulate Matters
SFC	Specific Fuel Consumption
TCPC	Truncated Cone Piston Crown
TCBA	Truncated Cone Base Angle

Subscripts

atm	Atmospheric
av	Average
init	Initial
stoc	Stoichiometric
Th	Thermal

CHAPTER ONE
INTRODUCTION

1.1 General Background

An internal combustion engine is one in which fuel burns in an oxidizer (air) within a confined space known as a combustion chamber. This is different from external combustion engines in which a separate working fluid is made to do work while being energized by the heat of an external combustion process (Internal combustion engine, 2018).

The combustion of a fuel with an oxidizer such as oxygen creates gases of high temperature and pressure. The expansion of the energized gases inside the combustion chamber is used to generate useful work by using it to cause a movement.

The engines are a class of heat engines and are presently its most common form, and are widely employed in the transportation and power generation sectors (Hanania, et al., 2018).

It has witnessed a development over time from the first engines which do not rely on compression, but rather depend on the amount of air and fuel mixture admitted during the first part of the intake/induction stroke, to the modern day internal combustion engines which are compression dependent as it relies on the in-cylinder compression.

The internal combustion engine powered automobiles will still be available for a long time to come despite the different nation's government legislation to outlaw it due to emission problems and the thought of the future of automobiles as electric. Despite the clamour for the electric powered vehicles, it is yet to muster the capacity to overthrow it because the mass production of such vehicles is yet to commence coupled with the issue of very high cost of production.

The electricity has to be generated from other sources such as fossil fuels, hydraulic, nuclear or solar sources, as things stand, about sixty-six percent of the world's electricity generation is from fossil fuels, a pointer to the fact that the electric vehicle cannot be said to have zero emission (its major argument point), because the production of its batteries involves the use of heavy machinery that is powered by electricity coupled with the subsequent requirement of electricity for the charging and recharging of its batteries. (Fischer and Keating, 2017; Wade, 2016; Franco, 2017)

The global market shares of its competitor, the electric powered vehicles currently stand at a very low value of a little above one percent (Electric car use by country, 2018).

Engineers around the world are now more than before concerned with the design of better engines that squeeze more power out of less fuel and their research is tailored towards making the engines cleaner with the major focus on computer control of fuel and air handling and materials selection. To achieve this, the in-cylinder flow is refined, combustion process and fuel mixture formation are carried out with the utilization of an optimal combustion chamber geometry design which leads to higher efficiency and lower emission parameters.

1.2 Types of Internal Combustion Engine

While the reciprocating and Wankel rotary engines are the most popular types of internal combustion engines, worthy of note is to state that internal combustion engines also refers to jet engines and many turbine engines where the combustion process is continuous.

According to the method of fuel ignition, internal combustion engines can be categorized into the following two types;

1) Spark-ignition engines (SI Engine) and
2) Compression-ignition engines (CI Engine)

A spark-ignition engine is a type of an internal combustion engine generally referred to as a petrol engine. The combustion process of the air-fuel (air – petrol) mixture is ignited by a spark generated from a spark plug, while a compression ignition engine also generally referred to as diesel engines are internal combustion engines where the heat produced from the compression of air together with the injection of fuel is enough to initiate and sustain the combustion process (Khemani, 2008a; Sankararaj, 2013).

The major difference between spark ignition and compression ignition engines is a function of the type of fuel used in each case. Spark-ignition engines use petrol or gasoline as fuel, while compression ignition engines use diesel as fuel. The spark-ignition engines operate on the Otto cycle; in this cycle, the process of the addition of heat or fuel combustion occurs at a constant volume. The basis of the working of compression ignition engines, on the other hand, is the diesel cycle; the process of the addition of heat or fuel combustion occurs at a constant pressure.

Spark-ignition and compression ignition internal combustion engines can also be classified or grouped into either a two-stroke or a four-stroke depending on the number of strokes which is required to complete a full cycle.

A two-stroke engine is one which completes its full cycle with two strokes of the piston in a revolution of the crankshaft. The end of combustion and the beginning of compression happen simultaneously while the intake and exhaust functions occur at the same time. These

engines have a high power to weight ratio, but with greater exhaust emissions in comparison to four-stroke engines.

Four-stroke engines, on the other hand, complete a power cycle with four separate strokes of the piston which involves two complete revolutions of the crankshaft. The strokes are clearly differentiated into the processes of induction, compression, power and the exhaust.

The limited (scarce) nature of petroleum resources from which automotive gas oil (diesel) and premium motor spirit (petrol), are derived led to the first major impetus for a search to alternative fuels from renewable energy sources. Also, the environmental impact of the emission products of combustion of these fuels necessitated this further, hence the continued search for lower emission alternative fuels and the development of better efficient (increased performance and reduced emission) engines to meet the demands of time.

1.3 Impact of the Internal Combustion Engine on Transportation and Power Sector

The internal combustion engine brought about a change, in fact, a revolution in man's mode of movement and existence; the movement of humans and goods from one designation to another place in comfort became possible turning the world into a global village as it allows for their unhindered movement thereby enhancing trades between parties and also provided a means to access remote locations like space which brought about many discoveries and inventions (Bell, 2014; Ma, 2014).

The transport sector owes its transformation and modernization to the development of the internal combustion engine. It serves as the major tool for ground transport (Serrano, 2017) and enjoys wide applications in the other modes of transportation; air and maritime (Arcoumanis, 2011).

The aircraft existence and development is indebted to the internal combustion engine. The development of the internal combustion engine was what brought about the establishment of the aviation industry as a powered flight was impossible before then. The internal combustion engine thus plays an integral part in globalization as it allows for international and intercontinental movement of people and goods.

The maritime industry is the cheapest means of transportation of people and goods. Many countries trade with another using this medium and it forms the basis for the freight of heavy cargoes. The maritime industry relies mainly on the internal combustion engine, and the compression ignition type has continued to live up to the expectation.

As it stands today, internal combustion engines account for about ninety-nine percent of vehicles used in land transportation, and the remaining percentage is accounted for by

electric powered vehicles (Electric car use by country, 2018). With this statistical figure, the importance of the internal combustion engine to the movement of people and goods on land cannot be overemphasised as it is the engine utilized in automobiles and locomotives.

Agriculture was boosted by the mechanization of tools and implements, thanks to the revolutionary internal combustion engines used in powering the farm equipment and implements. This has led to increased food production to meet the demands of man and the attendant increased efficiency ensuring reduced prices.

The use of compression (diesel) ignition internal combustion engines in providing food security cannot be overemphasised, as this is the reason why some nations continue to be more productive than others. The construction industry is also in no small way being impacted by the internal combustion engine. Earth movement equipment are powered by them, and this equipment without mincing words have changed the construction industry for good.

Internal combustion engines also find wide applications in power generation industries especially for backup power applications, nuclear energy generation plants start-ups, as a prime mover for combined-heat and power plants, and for base-load power generation. With the need of the internal combustion engines even for start-ups of nuclear plants, its relevance in the functioning of a sector that caters for about eleven percent of the total worlds energy output cannot be downplayed (Nuclear power in the world today, 2018). “Wartsila Sulzer RTA-96C” with a peak capacity of 80MW is the world’s biggest diesel engine (Hanlon, 2004; Puiu, 2017; Wartsila-Sulzer RTA96-C, 2018), and the largest internal combustion engine based power generating plant has a combined capacity for generation of 573 MW of energy (Larson, 2015).

1.4 Impact of Internal Combustion Engines on the Environment

Over the years the negative impact of the internal combustion engine has continually reduced, however, the concept of global warming resulting mainly from the greenhouse effect caused by the emission of the products of fossil fuels combustion, which is the energy source of the engine has continued to rear its ugly head. Another harmful impact attributed to the combustion of fossil fuels is the concept of acid rain which is believed to be due to the emission of the oxides of nitrogen and sulphur.

The lion share of the application of the internal combustion engine lies in its use in the transport sector and standby power generation; statistics show that eighty-five percent of the consumption of petroleum products in the transport sector in the United States of America is due to on-road vehicles operated on the internal combustion engines, while about thirty-three

percent of her greenhouse gas emissions comes from this sector (U.S. Department of Energy, 2015).

The primary source of energy for the internal combustion engine is petroleum, but of recent with extensive research on alternative fuels, bio-fuels are coming into play. The process of its extraction has an impact on the environment not just at the drilling site, but also in form of spillage at times during the course of transportation which endangers marine life.

However, recent studies on internal combustion engines continue to focus on better fuel efficiency with reduced emission and alternative energy sources. Noise pollution is another area where the environment is impacted upon by the internal combustion engines, but with the advancement in the design of its exhaust systems, internal combustion engines have become quieter.

1.5 Thermal Efficiencies of Internal Combustion Engines

The thermal efficiency is the measurement of the performance of devices that utilizes thermal energy. It is the amount of useful work that is obtainable from an amount of heat input.

The thermal efficiency of internal combustion engines is believed to be incredibly small as it hovers between twenty and forty percent. Compression ignition engines have higher thermal efficiencies in comparison to spark-ignition engines. Traditional spark-ignition engines have typical thermal efficiency values that hover between twenty and twenty-five percent, while that of compression ignition engine hovers between thirty and forty percent (Ingram, 2014).

The difference in thermal efficiencies between the standard spark-ignition and compression ignition engines is attributable to the differences in compression ratio and throttling process that exist between them. The compression ignition engine has a relatively high compression ratio, favours lean combustion, and undergoes an un-throttled operation which makes it have higher thermal efficiency values over the spark-ignition engine variant (Khemani, 2008b).

Recent advances in the design and manufacture of internal combustion engines have led to its increased thermal efficiencies. Thermal efficiency of new spark-ignition engines can reach a value of about thirty-eight percent (Ingram, 2014), and based on the concept of Homogenous Charge Compression Ignition Engines (HCCI), although yet to be a practical engine, the spark-ignition engine is expected to approach an efficiency of around fifty-six percent as this will allow for higher compression ratio of about 15:1 as against traditional values of 9:1.

However, as encouraging and promising this new concept is, the complexity it will add to the design of the engine is enormous, coupled with the fact that the governing process of the engine ignition is yet to be well understood asides the fact that the current understanding of material science, chemistry and turbulence is not sufficient to master the development of the engine because of the prevalence of the difficulty in controlling the auto-ignition of the mixture, operating range and the attendant high emission of carbon-monoxide and un-burn hydrocarbon (Gowthaman and Sathiyagnanam, 2015; Najafabadi and Aziz, 2013; Pokharkar et al., 2016).

Engine combustion chamber geometry is a major determinant of its thermal efficiency. The combustion process that takes place in an engine cylinder is to a great extent governed by the geometry of its combustion chamber. Thermal efficiency is a function of the brake power which in turn is dependent on the combustion process.

The optimisation of the combustion chamber geometry to favour an improved thermal efficiency cannot thus be overemphasised.

1.6 Problem Statement

With the considerable efforts already expended on engine development coupled with the development of hybrid fuel (bio-diesel), optimal power generation and emission reduction still pose a great challenge. Although there has been a growing interest in NOx emission reduction by catalyst, the major drawback has continued to be cost and complexity of the exhaust after-treatment systems.

Also, the use of different piston crown configurations in obtaining modified combustion chamber geometries have in no small way led to the improvement in brake power and emission reduction, however, the low thermal ratings and emission levels of such engines still leaves a great gap waiting to be filled. There is, therefore, the need to consider some new designs that can assist in improved power generation and reduced emission

1.7 Aim and Objectives

The aim of this work is to explore a new compression ignition engine design, equipped with truncated cone piston crown that will lead to an improvement in its performance characteristics.

The aim is to be achieved by the following objectives

1) Performance characterization of compression ignition engine operating with truncated cone piston crown using Automotive Gas Oil (AGO) as fuel

2) Performance characterization of compression ignition engine operating with inverted truncated cone piston crown using Automotive Gas Oil (AGO) as fuel
3) Performance characterization of compression ignition engine operating with truncated cone piston crown using Bio-diesel as fuel

1.8 Significance of Study

Optimizing power generation and emission reduction of compression ignition engines is still a great challenge. The dreaded global warming caused by climate change is largely in part attributable to the emission of combustion products of petroleum, of which the compression ignition engines are a major contributor. Improvements on the derivable power from a given quantity of fuel; that is making the fuel more efficient is of utmost priority to engine manufacturers, as this will in no small way lead to a reduction in running cost of the engines, but will also help in the reduction of emission.

1.9 Scope

This work has only considered a thermodynamic analysis of a compression ignition engine operating with some modified piston crowns. Impact of the modified piston crowns on the structural integrity of the compression ignition engine has not been considered

1.10 Expected Outcome

It is expected that the research work will lead to a better understanding of the performance of a compression ignition engine with a modified design of piston crown.

CHAPTER TWO
LITERATURE REVIEW

2.1 Early Development of the Internal Combustion Engine

Several scientists contributed in one way or the other to the evolvement of present day internal combustion engines as its history lacks a single flashpoint. The first commercially successful internal combustion engine was patented by J. J. Étienne Lenoir in 1860 by a Belgian Engineer (Laukkonei, 2013) (Internal combustion engine, 2014). However, before his invention, based on modern ideas, the credit of the first internal combustion engine invention goes to Robert Street who got patent for his engine in 1794 (History of internal combustion engine, 2018; Havens, 2015) and was the first invented internal combustion engine to utilize liquid fuel.

The modern day compression ignition engine has its root on the Diesel engine shown in Figure 2.1 named after its inventor; Rudolf Diesel. The engine was built in 1892, and was the first internal combustion engine developed based on the principles of compressed charge, compression ignition engine. It utilizes the very high temperature of compressed air to ignite the injected fuel at nearly constant pressure (History of internal combustion engine, 2018; Havens, 2015). The engine has similarities to the Brayton engine but with high thermal efficiency incomparable to the other invented internal combustion engines.

Although there have been a number of incremental improvements over the years, modern gasoline and diesel engines operation still relies on the same basic principles as those of the early pioneers in the field.

The modern gasoline operates on the Otto cycle while the diesel engines operate on the diesel cycle. The processes of the two cycles for a four stroke engine is shown in Figure 2.2.

The result of some innovations like fuel injection and computer controls on today's internal combustion engines are largely noticed in better fuel efficiency and creation of less pollution due to emission control systems. But be as it may, numerous studies are still being undertaken by scholars to improve its performance in terms of power output, efficiency, and emission reduction.

Compression ignition engines are the most fuel efficient engines ever developed for transportation purposes, due largely to their high compression ratio and lack of throttling losses.

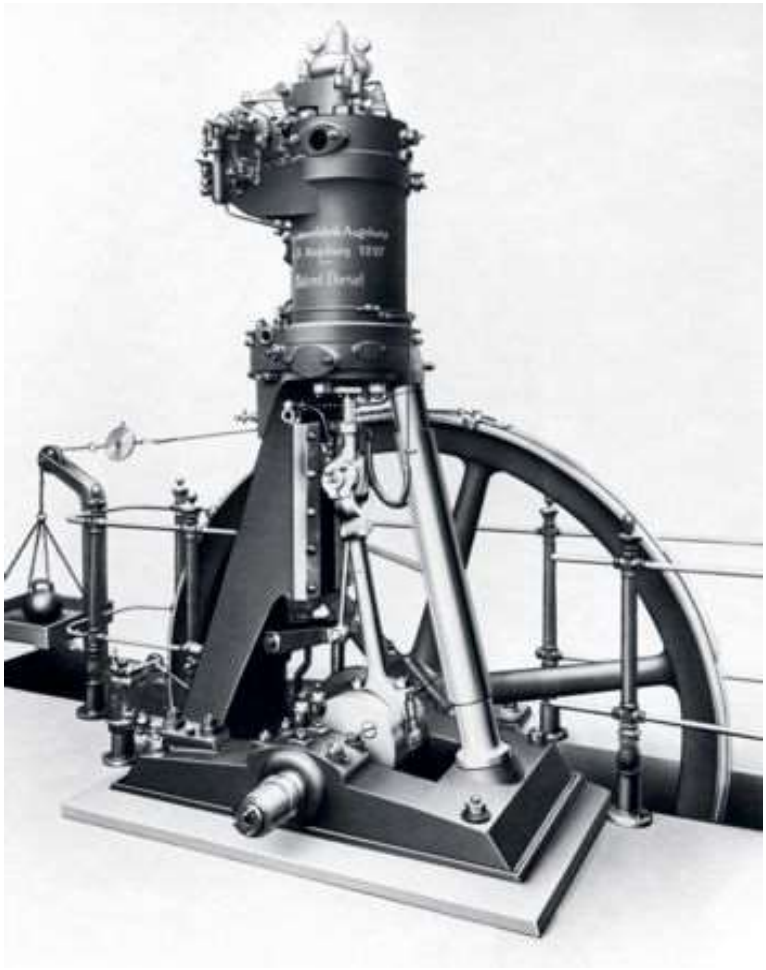

Figure 2.1. Diesel engine

(Jääskeläinen, 2013)

Sourced from https://www.dieselnet.com/tech/diesel_history.php

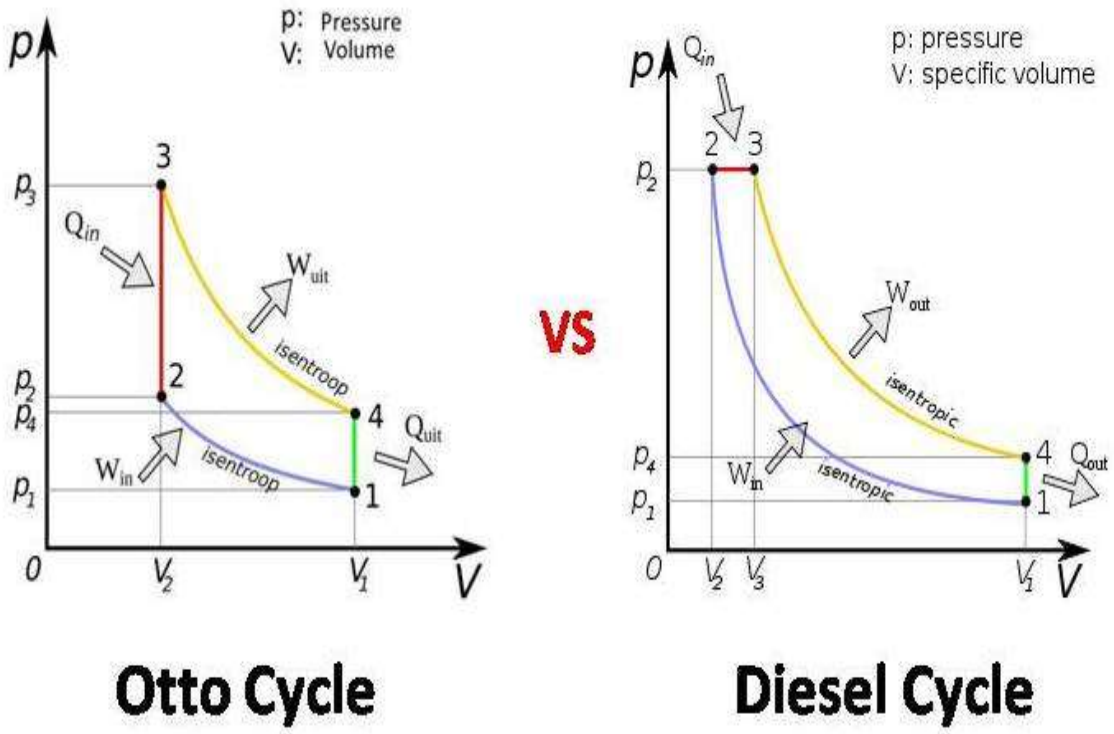

Figure 2.2. Otto cycle and Diesel cycle

(Diesel cycle vs Otto cycle, 2016)

Sourced from http://mech4study.com/2016/08/diesel-cycle-vs-otto-cycle.html

However, conventional compression ignition engines have high emission rates of Nitric oxides (NOx) and particulate matters (PM) than spark ignition engines. The high emission of the toxic substances coupled with the stringent legislation imposed by many nations' government gingered the interest for research on compression ignition engines, which has significantly led to the design of better fuel efficient engines.

The interventions are being carried out majorly in the areas of fuels, injection modes, types of process, and combustion chamber type.

2.2 Fuel

Working on MAN bus diesel; a four-stroke, six-cylinders in-line water-cooled engine, the density, viscosity, sound velocity, bulk modulus and oxygen content of fuels were found to have significant effects not only on the start of injection but also on the start of combustion and diffusion burn peak and influenced its emission and other performances (Zelimir *et al*., 2009).

The lubricating nature of fuel is governed by its kinematic viscosity and has a significant impact on its delivery and power output; a higher value of kinematic viscosity affects its delivery and power output negatively. The brake specific fuel consumption was also observed to be dependent on the fuel's cetane number and its heat content; lower values of cetane number and heat content results in increased brake specific fuel consumption (Li *et al*., 2005; Parvaneh *et al*., 2017).

The brake thermal energy was found to be a function of the oxygen content and boiling points; higher oxygen content and lower boiling points improve the brake thermal efficiency of engines operated on such fuels (Li *et al*., 2005). The fuel oxygen content of fuel also has a relationship with the emission characteristics of diesel engines; increased oxygen values reduces the emission of particulate matters (PM) and carbon II oxide (CO) due to better oxidation in the combustion chamber, however, the formation of NOx increases. This disadvantage can be addressed by increasing the engine speed, as this leads to a shorter time for NOx formation inside the combustion chamber (Parvaneh *et al*., 2017).

The performance and emission characteristics of a four-stroke single cylinder of 5.2 kW rated power at 1500 rev/min HCCI engine operated on Uppage oil methyl ester and compressed natural gas shows that the NOx emission of the engine in the HCCI mode reduced by 98%, the smoke by 94 %, and the brake thermal efficiency by between 12-14% when compared to the conventional compression ignition engine of the same specifications operated on diesel. Operating the compression ignition engine on the dual fuel operation mode showed inferior performance in terms of indicated power with respect to the HCCI and diesel operated mode,

however, lower NOx and smoke were obtained when compared to the diesel operation mode (Banapurmath *et al*., 2014).

Using a four-stroke single cylinder constant speed direct injection compression engine with rated power of 3.78 kW at 1500 rev/min, Bhabani *et al*., (2013) studies established that the engine brake thermal efficiency when fuelled in a dual mode using biogas and Karanja oil biodiesel on one hand, and biogas and diesel on another was lower in comparison to that of single fuelled mode at all engine loads. The NOx, HC and CO emissions were lower for the dual fuelled modes compared to the single fuel mode.

Ravi *et al*., (2015) treated biogas with lime to reduce its Carbon IV Oxide (CO_2) level and determined the impact of CO_2 on engine performance and emission characteristics of a dual fuelled 4-stroke single cylinder compression ignition engine with a power rating of 3.7 kW. They observed that treatment of biogas with lime resulted in reduced CO, NOx, HC and particulate matters in comparison to untreated biogas. Higher brake thermal efficiency and lower specific fuel consumption were also noticed.

The performance and emission characteristics of four-stroke single cylinder 5.9 kW rated power compression ignition engine operated on liquefied petroleum gas and Pongamia biodiesel have been studied; brake thermal efficiency increased from medium to high load operations for the dual fuel with lower brake specific fuel consumption. HC emission was higher for the dual fuel when compared to diesel; however, it showed a reduced NOx emission (Periyasamy and Vadivel, 2015).

The brake thermal efficiency of the pure Canola biodiesel utilized in a four-stroke direct injection variable compression ratio engine was found to be 98.2% the value of that obtained with the utilization of pure diesel. Brake specific fuel consumption decreased with increasing loads and was higher for the biodiesel (113%) when compared to pure diesel. When blended with diesel as B20, B40, and B60 (20%, 40% and 60% by volume), the brake thermal efficiency of the test engine increased with increasing load up to 75% load after which it remained almost constant. Increasing the blend of the biodiesel with diesel gives a reduction in HC and NOx emissions (Anbarasu and Karthikeyan, 2014).

Basavarajappa *et al*. (2014) carried-out performance, combustion and emission characteristics studies using a four-stroke single cylinder direct injection engine with rated power of 5.2 kW operated on dual fuels of compressed natural gas and Honge, Jatropha biodiesels, and extended the studies to include the effects of injection timing, compression ratio, compressed natural gas flow rate, and exhaust gas recirculation (EGR). It was concluded that dual fuel engine operated with optimized parameters of injection timing of 27^0 bTDC

(before Top Dead Centre), a compression ratio of 17.5:1, 6 mm diameter venturi hole carburettor and 10% EGR resulted in overall improved performance. Dual fuel operation using compressed natural gas and diesel showed the best performance in terms of brake thermal efficiency followed by compressed natural gas/Honge combination. This trend was also observed for smoke opacity, CO, and HC emissions while compressed natural gas/Jatropha combination fared better than the others for NOx emission, diesel combination coming last.

Instead of using compressed natural gas, a blend of diesel and jatropha was utilized in dual fuel mode in a single cylinder air cooled direct injection compression ignition engine of rated power 4.4 kW and speed 1500 rev/min by Anandan *et al*. (2014a) and they discovered that a 30% blend of jatropha biodiesel with diesel dual fuel gives improved brake thermal efficiency values than pure diesel at compression ratio of 17.5:1 and above. Conducting further studies by incorporating exhaust gas recirculation (EGR) to the combustion, it was concluded that a blend of 20% Jatropha biodiesel with diesel at a compression ratio of 20:1 and 20% EGR resulted in improved combustion, decreased NOx, better brake thermal efficiency, and exhaust gas temperature. A slight increase in smoke, HC and CO emissions were however, also observed (Anandan *et al*., 2014b).

Since the start of ignition in the cylinders and the duration of the combustion have a direct impact on the engine performance and its emission characteristics, Valipour (2014) studied the effect of injection pressure on combustion and ignition delay period of Jatropha biodiesel blended with diesel while varying ambient pressure between 5 and 25 bar. Using a constant volume combustion chamber of 54.2 mm length, 95 mm diameter and 7.5 mm thickness, the study revealed that ignition delay period reduced with the increase in injection pressure for all test fuel (20%, 40% blend of biodiesel and diesel, and pure diesel) and the combustion duration though least for pure diesel, also showed a marked reduction with increases in injection pressure.

The results were corroborated by Agarwal *et al*. (2015) who extended the studies to include different compression ratio "16.5:1, 17.5:1 and 18.5:1" and injection pressures of 200, 225 and 250 bar respectively. With the use of Methanol, Ethanol, and Pangomia, as biodiesel sources other than Jatropha, NOx increased while HC and CO emissions decreased with increasing values of compression ratio and injection pressure for all the test fuels.

Al-Dawody and Bhatti (2014) reported that the cylinder pressure and heat release rate increases with the increase in compression ratio of their engine operated on diesel/soybean biodiesel dual fuel. The brake thermal efficiency, HC, CO and smoke opacity decreased with the increase in compression ratio of the engine, each found to be greatest while using pure

diesel and decreases as the percentage of the soybean biodiesel increases in the blend. The case of NOx emission was however different; it was observed that it increased with increase in compression ratio and percentage of soybean biodiesel in the dual fuel blend.

With a blend of diesel and Ziziphus Jujuba biodiesel as the dual fuel, Naveen *et al*. (2014) carried out an experimental investigation of varying compression ratio on the performance of a single cylinder compression ignition engine having a power rating of 3.5 kW and speed 1500 rev/min. Using compression ratio range of 15:1 to 18:1 and a blended volume of 20%, 40%, and 60% biodiesel, it was reported that the specific fuel consumption decreased with increasing load for the entire test compression ratio, and increased with increasing percentage blend of biodiesel. The brake thermal efficiency increased with increasing load for all compression ratios and with decreasing percentage of the biodiesel blend.

At full open throttle, Balki *et al*. (2014) gave a slightly different report in terms of emission while utilizing alcohols (methanol and ethanol used separately) in spark ignition engines HC, CO, and NOx decreased while CO_2 increased. However, an increase was reported for brake specific fuel consumption, torque, thermal efficiency and combustion efficiency in agreement with the findings of Argakiotis *et al*. (2014) where ethanol-blended fuel was utilized.

Utilization of natural gas in dual fuel mode with diesel in a common rail 4-stroke four-cylinder compression ignition engine with a compression ratio of 19:1 was studied by Abagnale *et al*. (2014) together with the evaluation of computational fluid dynamics (CFD) potential to predict the main features of the engine. It was observed that the numerical results from the CFD cases were in agreement with the experimental results and hence making a good case for the use of CFD analyses as a tool for searching for optimal solutions to dual fuel operations. Results showed that for 50% natural gas rates, engine behaviour is similar to that of full diesel operation both in terms of lean combustion development and as it relates to NOx formation, while on increasing the rates to 70 – 90% levels an engine condition comparable to a spark ignition engine knocking is induced. CO emissions of the dual fuel mode at all range of operation were greater than that of full diesel, but the reverse was the case for CO_2 emissions at all operation range.

Joshi *et al.* (2012) carried out the mathematical modelling of an engine cycle used for the prediction of the peak value of the cylinder gas pressure, indicated mean effective pressure, brake power, brake thermal efficiency and ignition delay period to an accuracy of between 0.2 - 2.5 % in relation to experimental values and thus developed a model which was used for the optimization of a number of design parameters of a dual fuelled engine.

Yuhua *et al*. (2013) conducted extensive numerical simulations to evaluate parameters that influence diesel micro pilot in their studies on combustion characteristics of a diesel micro-pilot ignited gasoline engine employing direct injection of gasoline and diesel, as well as turbo-charging and cooled EGR. Diesel micro-pilot approach to spark ignition combustion was compared, and likewise, the impact of diesel micro-pilot injection timing, mass fraction, injection strategies, EGR and in-homogeneity tolerance of diesel micro-pilot combustion.

Diesel micro pilot injection timing plays an important role in combustion performance and the mass fraction of the total fuel also affects the combustion performance. The diesel micro pilot combustion not only delivered a potential for improved lean burn performance but also extended actual lean burn limit, while also showing a better tolerance to EGR than spark ignition combustion. Using three diesel micro-pilot injection strategies; single, double, and triple, the double case fared better in respect of NOx emission but at a minor price in thermal efficiency when compared to that of the single.

Vancoillie and Verhelst (2010) did preliminary studies on modelling of the combustion of light alcohols in spark ignition engines where they discussed on the requirements for the construction of a two-zone thermodynamic model that can be used to predict the power cycle, knock onset and pollutant emissions in alcohol engines. It was reported that similar models used for gasoline engines can be adapted for alcohols engines in the prediction of emissions, the only particularity been for aldehydes formation, and for which a suitable model was identified. The auto-ignition behaviour of alcohols revealed that the fuels exhibit a single stage auto-ignition in contrast to the two-stage behaviour of gasoline.

The complexity in the composition of typical commercial diesel fuel makes its modelling very tedious if not impossible to be as exact as it should be, hence of major concern is the creation of surrogate fuels which are simpler mixtures that capture the vital performance characteristics of diesel fuel to an adequate precision level, however, it contains approximately only ten or fewer pure “palette” compounds for the sake of computational tractability (Mueller et al., 2012).

Diesel surrogates can have lower-compositional accuracy or higher-compositional accuracy; one which is often with lower purities and contains a smaller number of compounds which are readily available, making them a good choice because they are relatively inexpensive, easy to procure, blend, and computationally model. The other are usually of higher purity and contain a larger number of palette compounds, and have weights and molecular structures which are more of a true representation of those found in commercial diesel fuels. (Mueller et al., 2016).

The lower-compositional accuracy diesel surrogates suffers from insufficient property matching, unknown or large effects of the impurities and it is not unusual that some of their primary constituents are not representative of compounds which exists in commercial diesel fuels while the major drawbacks for the higher-compositional accuracy diesel surrogates are associated higher costs, ultralow-sulphur, the increased intricacies of treating and blending processes, and greater difficulties in kinetic modelling (Pitz and Mueller, 2011).

Chemical kinetic models for n-alkanes up to sixteen (16) carbon atoms have been developed. Experimental and modelling work on lower molecular weight surrogate components such as n-decane and n-dodecane which are most relevant to jet fuel surrogates, but are also relevant to diesel surrogates where simulation of the full boiling point range is desired have been undertaken (Pitz and Mueller, 2011).

Due to the very large size of detailed chemical kinetic models for surrogate fuels tremendous energy has been invested in making these hitherto large models practicable in simulations of even multi-dimensional reacting flow of diesel combustion by improving the reduction mechanism tools, however, several research gaps still exist as bulk of the studies have focussed on diesel: iso-cetane whereas in modelling and experimental investigations of the treatment of real diesel the inclusion of these higher molecular weight components is required (Pitz and Mueller, 2011).

Alessio *et al.* (2015), knowing fully that a realistic simulation of diesel engines combustion process can only be achieved with its detailed chemistry which is a fundamental pre-requisite, were able to validate a reduced mechanism of n-dodecane which accurately described its high and low-temperature reactivity for a wide range of operations.

Pei *et al*. (2015) conducted an investigation on a mixture of n-dodecane and m-xylene as a diesel fuel surrogate for compression ignition (CI) engine applications. The binary mixture, when compared to neat n-dodecane, was more of a representative of diesel fuel; it contains an alkyl-benzene which represents an important chemical class present in diesel fuels. They were able to develop a skeletal mechanism of a multi-component mixture of *n*-dodecane and *m*-xylene, with 163 species and 887 reactions from a detailed mechanism consisting of 2885 species and 11,754 reactions for multidimensional diesel engine simulations which were validated against available experimental data, and were found to be in good agreement.

A large number of hydrocarbons, organic matter, aromatics and other compounds form the practical fuels such as diesel and gasoline. It is not practical to include all the components of the practical fuels in the modelling of the combustion process because the composition of the automotive fuels varies depending on the fuel's source and production history. The

combustion characteristics of automotive fuels are therefore often represented using blends of hydrocarbons known as primary reference fuels (PRF). Basic hydrocarbon fuels such as methane, ethane, propane, n-heptane, iso-octane, etc are known as primary reference fuel (Periyasamy *et al*., 2012).

n-Heptane have properties that are rather close to typical diesel fuels asides being its simplest representative and well-validated mechanisms; its cetane number (CN~56) is rather close to that of typical diesel fuels (CN~50) which is an indication of similar ignition characteristics (ignition delay) thus eliminating the complexity of modelling several hundreds of components (Tao *et al*., 2007; Curran *et al*., 1998).

2.3 Injection and Ignition Mode

The use of biodiesel as an alternative fuel in compression ignition engines has in most cases resulted in a loss of performance as a penalty for improved emission characteristics mainly due to some properties of the biodiesels.

Kerdsuwan *et al*. (2008) studied the effect of advanced injection timing on the performance of a dual-fuel compression ignition engine run with producer gas. Advancing the injection timing of the engine "a four-stroke four-cylinder direct injection engine" by 5^0 from 12^0 bTDC to 17^0 bTDC, experimentation results gave the indication of the brake thermal efficiency and specific fuel consumption having a marked improvement and even better off than using pure diesel in the normal standard engine. CO and CO_2 emission were lower by advancing the injection but more than the levels obtained from the use of diesel in the standard engine, while higher levels of NOx emission were obtained for the advanced injection than with the use of diesel, but was least for the dual fuel in the normal injection timing state.

Nwafor (2000) also experimented on the effects of advancing injection timing by 3.5^0 from 30^0 bTDC to 33.5^0 bTDC on a four-stroke single cylinder indirect injection compression ignition engine using natural gas as primary fuel in dual fuel mode. A reduction in the brake thermal efficiency and increase in brake specific fuel consumption of the advanced injection was noticed when compared to the normal dual mode and pure diesel fuelled engines.

Goldwine (2008) carried out studies on the effect of fuel injection profile on compression ignition engine performance through the utilization of different multiple injection strategies. He studied the effect of double injection and the timing of the injections using a single cylinder compression ignition engine with four-strokes. His experiment showed that exhaust NOx, soot, and HC were correlated with the location of the second injection while for CO it correlated with the first injection. It was also observed that when the time between the

injections was smaller than 1.4 ms, the injections combusted together but when longer, the injections were ignited and combusted independently. At this point, NOx and soot emissions showed a reduction in values, but CO and HC emissions increased under light load. CO and HC emissions showed no change under medium load with timing between injections longer than 1.4 ms but increased when longer than 2 ms.

The complex in-cylinder process determines premixed flame propagation and onset of auto-ignition in the end gas. The applicability of the CFD for providing insight into this process have been validated by Tatschl *et al*. (2005) in their studies on flame propagation and knock onset analysis for full load spark ignition engine using AVL FIRE software. Comprehensive data on the cause and effect mechanisms of engine design and operating parameters, knock onset characteristics and flame propagation can thus be provided by the tool at the early concept phase.

1-D AVL boost code applied to spark ignition engine for the purpose of determining the knock resistance of the small turbocharged engine revealed that working on the valve timing makes it possible to significantly improve an engine knock resistance and hence its thermal efficiency. At a state of high knock risk, proper retarding of the inlet valve closure, reducing the effective pressure ratio can lead to more favourable engine optimization decreasing the specific fuel consumption (Gustavo and Enzo, 2006).

Outputs from a quasi-dimensional model for compression, combustion and expansion processes in a 4-stroke single cylinder spark ignition engine have shown great accuracy to that obtained experimentally from a Ricardo E6 single cylinder test engine in regards to spark timing, speed, compression and equivalence ratios in their cylinder pressure versus crank angle diagrams. Hence the model can be used as a predictive tool for accurate simulation of spark ignition engine combustion over a wide range of operating conditions (Seyedmohsen *et al*., 2008).

With the notion of dual fuel engines generally having lower thermal efficiency, higher carbon monoxide and HC emissions at part load conditions, Pirouzpanah and Khoshbakhti (2006) worked on the combustion characteristics of a dual fuel (diesel-gas) engine at part loads using a quasi-dimensional multi-zone combustion model for the combustion of the diesel fuel and a single zone model with detailed chemical kinetics for the combustion of the natural gas fuel in order to investigate the combustion phenomena at part loads. Using methods such as advancement of injection timing, pilot fuel quantity increment and intake air throttling they observed the engine's performance and emission characteristics at part loads. There was a little improvement in combustion parameters with an advance in the diesel injection timing,

increasing the pilot fuel quantity provided better combustion and reduction of NOx emission, and air throttling promoted better combustion meaning better dual fuel engine performance but with NOx emission increase. The observations were in good agreement with experimental values.

2.4 Process Types

Advanced compression ignition engines have evolved along two fronts; the homogenous charged compression ignition (HCCI) and the low-temperature combustion (LTC).

Studies conducted on the in-cylinder processes in compression ignition engines, along the two emerging fronts of HCCI and LTC led to substantial progress towards overcoming the main challenges, which includes: improving low-load combustion efficiency, increasing the high-load limit, understanding fuel effects and maintaining low NOx and particulate matters emissions over the operating range (Dec, 2009).

Dual engines operated as HCCI at low load and speed, and as a compression ignition engine at high load and speed using iso-octane as fuel in the determination of temperature-crank angle performance relationship, indicated power-equivalence ratio relationship, and CO emission-equivalence ratio relationship showed higher indicated power and CO emission in comparison with pure HCCI engine (Mozaffari, 2010).

HCCI engine is a hybrid between spark-ignition and compression-ignition engines. The oxidation of the fuel-driven solely by chemical reactions governed by chain breaking mechanisms characterises its combustion. Two different temperature regimes can be said to exist for these reactions – one below 850 K and the other around 1050 K. The combustion can possibly be controlled through temperature stratification; at high load, a local high-temperature in-homogeneity will be the driver of the uniformly slow propagating HCCI combustion and at low load, multiple temperature in-homogeneities can be introduced in the combustion cylinder to simultaneously ignite the charge at multiple locations (Charalambides, 2013).

HCCI engines allow the use of fuels other than diesel and petrol, just as other fuels with properties similar to that of diesel are being utilized in compression ignition engines. The huge sources of renewable energy fuels are thus a big relief to the dwindling fossil fuels, encouraging studies on their utilization in internal combustion engines.

Himmatsinh *et al*. (2015) summarized the effect of alternative fuels on an HCCI engine combustion process. The indicated mean effective pressure (IMEP) increased with increasing premixed ratio of fuel at low and medium loads with a significant reduction in NOx and smoke

in comparison to a conventional diesel engine. However, despite the huge prospects of better fuel economy and emission reductions, the HCCI engines is still taken aback by the effect of rapid pressure rise which is akin to experiencing "knock" as like a spark ignition engine and the problem of combustion timing, which has to be addressed to make the technology a viable one (Prasad *et al*., 2012).

The NOx and soot emissions relationship with the compression ratio of an engine was studied by (Laguitton *et al*., 2006) in the quest of ensuring NOx emission level of an engine meet the 'EURO 6' emission target. The effect of reducing the compression ratio of a single cylinder compression ignition engine from 18.4:1 to 16:1 was investigated, and the studies showed that reducing the compression ratio of a premixed charged in a direct ignition compression ignition engine led to reductions in NOx and soot emission, the same results were gotten for the case of retardation of the ignition timing. However, both methods paid a small penalty with increased CO and HC emissions.

Artificial Neural Networks (ANN) has been employed to study the performance and emission characteristics of HCCI engines. Venkatesan *et al*. (2015) employed the use of a developed radial basis function network (RBFN) which was validated with experimental studies to determine the performance and emission characteristics of HCCI engine operated on hydrous methanol (85% methanol and 15% water) as the primary fuel and diethyl ether as the ignition improver while varying the excess air ratio from 5.6 to 9.5. At an excess air ratio of 9.5, increased brake power, brake thermal efficiency, HC and CO emissions, and reduced NOx emission was deduced in comparison to a normal compression ignition engine of the same capacity. The developed radial basis function network (RBFN) showed closed agreement with experimental outputs, and it was concluded that artificial neural networks (ANN) could be utilized in lieu of experiment to study the performance and emission characteristics of HCCI engines.

Numerical studies of the effect of intermediates and initial conditions of pressure and temperature, exhaust gas recirculation (EGR) and equivalence ratio on the flame propagation in a real HCCI engine showed thus; the flame speed increased unvaryingly with the crank angle increase in a three-region model, equivalence ratio and exhaust gas recirculation ratio distinctly decrease the flame speed and also advance the crank angle of the flame speed, initial pressure and temperature led to an advance of the crank angle of flame speed but with little influence on its value. The flame speed was characterised mainly by the temperature rise due to compression and combustion heat release with the increase of crank angle (Zhang *et al*., 2014).

The impact of engine speed and equivalence ratio on HCCI combustion at three (3) pressure boost cases (0 bar, 1 bar, and 2 bar) using chemistry-based CFD code (KIVA 3-V) was studied by Ghafouri *et al.* (2014). The results obtained from the CFD code tallied with that of experimental investigations; at high engine speeds keeping equivalence ratio constant, combustion tends to misfire as a result of shorter combustion period, whereas at low-speed combustion advances as ignition delay is shortened. Equivalence ratio increment leads to a retardation of the combustion due to compressive heating at 0 bar boost case but had a negligible impact at 1 and 2 bar cases.

An effort to reduce the emission from compression ignition engines operated on diesel have encouraged the study of the process of the use of exhaust gas recirculation (EGR) by researchers.

The two most problematic emission of a conventional compression ignition are NOx and soot, HC and CO emissions are quite low and can be removed by oxidation catalyst from the exhaust. NOx formation can be reduced by the use of EGR; however, the amount of EGR that can be used is limited by different factors which involve the delivery of enough fresh air for the combustion process. A decrease in engine efficiency is however experienced at high EGR rates and also difficulties in establishing the required pressure difference to drive EGR flow in good turbocharged engines. In the case of the latter, an EGR pump is utilized. The route taken by EGR back to the intake charge of the engine is also of importance on the performance of an engine; long-route EGR path leads to lower fuel consumption, faster response to load changes but a slower response to changes in EGR demand than the short-route (Reifarth, 2010).

Kumar *et al*. (2013) carried out studies to determine the effect of cooled EGR on the performance, combustion and emissions of a direct injection single cylinder variable compression ratio engine with a rated power of 4 kW at a speed of 1500 rev/min. Increasing the compression ratio increased the brake thermal efficiency and reduced the specific fuel consumption. For the test volume of 0, 5 and 10% EGR, brake thermal efficiency was observed to be greatest for 10% and least for 0% EGR, while the NOx level was least for 10% and greatest for 0% EGR. Combustion duration and smoke opacity decreased with increased compression ratio.

At a compression ratio of 15:1 and diesel injection pressure of 150 bars, hot EGR has a negligible effect on the delay period of liquefied petroleum gas-diesel dual fuel combustion in a 4-stroke single cylinder direct injection compression ignition engine. However, it was affected by cold EGR by an increase. Both cold and hot EGR leads to an increase in the rate of pressure rise and therefore is not recommended as a means for reduction of combustion knock

at higher loads. EGR increases the duration of combustion and relative cycle efficiency is maximum at optimum hot EGR (Poonia and Mathur, 2012).

Sorathia *et al*. (2012) investigated the effect of EGR in the reduction of NOx emission from the tailpipe of HCCI engines operated on jatropha and liquefied petroleum gas for constant speed and heavy duty direct injection compression ignition engines. 15% EGR value in HCCI engine operated on Jatropha resulted in the reduction of NOx emission at all loads without adverse effect in performance compared with using diesel with no EGR. Further increase of EGR values showed remarkable reductions in NOx emission but with an attendant increase in HC, CO, and smoke emissions. A reduction in NOx emission was observed for the other fuel with the use of EGR and there exist a critical value at which increment of EGR fraction in the charge results into the increased release of other emission products which makes it unsafe.

Studies conducted on a 4-stroke four-cylinder spark ignition engine with a compression ratio of 9:1, bore diameter of 80mm and stroke of 90mm by Shehata and Razek (2008) on emission reduction methods for spark ignition engines using catalyst, EGR rates of 5, 7, 8 and 10% and air injection rates of 3, 4, 5 and 6% in the tests revealed that catalyst and air injection reduced the emission of HC and CO, while EGR increases the emission of HC and CO but reduces NOx. They found out that brake power increased with engine speed up to 3000 rev/min after which it began to decrease due to increased engine friction, while brake specific fuel consumption was a minimum at a speed of 2400 rev/min. Brake specific fuel consumption increased with increases in EGR values while brake thermal efficiency decreased with increasing EGR values for different engine speeds.

Working with EGR rates of 0%, 9%, 12%, 15%, 18% and 21% on a two-cylinder direct injection air cooled compression ignition engine, exhaust gas temperature and NOx emission were found to decrease with increasing rate of EGR. Also, EGR rates of up to 21% had a negligible effect on thermal efficiency for low and medium loads, but with high loads, a slight reduction in thermal efficiency was observed for EGR rates above 15%. The smoke opacity at low loads was also found to be proportional to the increase in EGR, but at higher loads and EGR, it showed a rapid increase (Agrawal *et al*., 2004).

Fumigating EGR with ethanol was found to have a positive influence on the performance and emission characteristics of a compression ignition engine. Hebbar and Bhat (2012) while working on a four-stroke single cylinder engine rated 3.7 kW at 1500 rev/min observed a reduction in exhaust gas temperature with ethanol fumigation of hot EGR. With ethanol added to EGR at 5, 10, 15 and 20% rate by volume, there was no appreciable change

in level of CO_2 emission for fumigated hot EGR, there was, however, a marked reduction in the level of HC emission by fumigating hot EGR with up to 10% ethanol after which it began to show an increase. The same trend was observed for the brake thermal efficiency. NOx emissions were reduced with ethanol fumigation of hot EGR.

Krishnan *et al*. (2006) devised a simple means for the evaluation of the effect of EGR on NOx emission reduction based on the flame temperature correlation. A procedure for calculating the reduction in NOx levels due to EGR, given only engine base-data was developed. Their approach utilized the flame temperature correlation technique to obtain NOx predictions with sufficient accuracy of approximately 6.5% at low loads. The correlation coefficient was found to be high for medium to low loads conditions however significant errors were observed at 100% load condition and high EGR rates at all speeds. They suggested getting a more accurate prediction by accurate calculation of flame temperature by the inclusion of CO_2 dissociation and other effects.

Yang *et al*. (2008) developed a transport equation residual model with incorporated Damkohler number criterion. It was implemented in the ERC KIVA-3V code to predict flame propagation in a direct injection gasoline turbocharged engine. The developed transport equation residual model was employed to differentiate CO_2 and Water from the previous engine cycle or EGR from the combustion products of the current engine cycle. This led to the accurate tracing of the local and instantaneous residual values in the flame front cells that have a great effect on the laminar flame speed. The Damkohler criterion was used as a determinant for the use of either the chemical kinetics or G-equation model in the assessment of the combustion processes in the flame containing cells based on the comparison between the chemical kinetics timescale and laminar flame propagation timescale. There was a good agreement between the model and experimental results for in-cylinder pressure, heat release rates and mass fraction burned.

Etheridge *et al*. (2008) developed a PDF-based stochastic reactor model for the simulation in spark ignition engines. The cycle to cycle variation in a spark ignition engine was simulated using the model and it was found to be in good agreement with data obtained from experimentations. Average NOx emissions and the variation of peak pressures and crank angles showed a great level of matching.

2.5 Combustion Chamber Geometry

Research and development in the area of internal combustion engines emphasised thoroughly on better efficiency and reduced emission parameter; this requires refinement of

the fuel mixture formation, in-cylinder flow, and combustion process. The combustion chamber geometry affects the combustion process in internal combustion engines and ultimately has a decisive effect on its performance and emission characteristics because the compression ignition engine is greatly influenced by air turbulence which is created by it.

Researchers believe that by optimizing the combustion chamber of these engines, a lot of advantages in terms of performance can be made. The pistons of internal combustion engines have been modified in many ways by researchers and its impact on performance and emission characteristics studied.

The combustion chamber geometry and engine speed affect the velocity flow fields and high-temperature domains which are pivotal in the formation and progression of NOx and soot, and the combustion process in an internal combustion engine.

Mamilla *et al*. (2013) conducted studies on the effect of combustion chamber design on the performance and emission characteristics of a single cylinder constant speed air-cooled four-stroke direct injection compression ignition engine having a power rating of 4.4 kW using Jatropha oil – diesel blend as fuel. 20% Jatropha oil – diesel blend provided the best alternative to diesel fuel, and this was used as a test fuel for spherical, toroidal and re-entrant combustion chamber geometry experiments. The brake thermal efficiency of the test fuel has lower values than that of pure diesel using the standard compression ignition engine, but with the toroidal combustion chamber, it was higher. CO, HC, and smoke emissions were reported to be lower for the blended fuel using the three test combustion chamber geometry in comparison to the standard engine operated on diesel. NOx emission was lower in standard engine operated on diesel than that of the test geometries using diesel-jatropha blend. The toroidal geometry has the least NOx emission of the three.

Simulation studies on different combustion chamber geometry of a single cylinder compression ignition engine with a power rating of 3.73 kW at 1500 rev/min using toroidal and re-entrant geometries showed higher charge velocity, higher volumetric efficiency, lesser NOx emission and an improvement on overall efficiency by a value range of 3-5% was also observed (Indrodia *et al*., 2014).

The combustion chamber geometry and engine speed impact on velocity flow fields and high-temperature domains which are significant factors in the formation and evolution of NOx and soot emissions was undertaken by De Risi and Manieri (1999) employing KIVA-3V as a simulator, while also conducting experiments at engine speeds of between 1500 rev/min and 4000 rev/min using different modified bowl geometries and re-entrants. The influence of the bowl geometries on emissions was observed to be more pertinent at lower engine regimes,

while highly re-entrant bowl showed less sensitivity to engine speed but affects engine emission characteristics. NOx reduced with increase in engine speed

The complexity of the in-cylinder combustion process in internal combustion engines poses a great difficulty in understanding it. Lehtiniemi *et al*. (2014) developed transient flame-let models "transient interactive flame-let mode (TIF), and transient flame-let progress variable model (TFPV)" for use with STAR-CD to model advanced combustion in a compression ignition engine. Consistent handling of turbulence interactions, efficient treatment of chemistry and complex soot, and emission was allowed for with the TIF model. The TFPV model on its part allowed for consideration of effects of local in-homogeneities and local variations of scalar dissipation rate on the chemistry, coupling to models, and use of arbitrary large chemistry in the tabulation without influencing the CFD simulation computer processing time. They went further to provide sample 3D CFD simulations using the two models.

Jafarmadar and Khanbabazadeh (2008) carried out computational studies on the effects of combustion chamber geometries on combustion process and emission in a direct injection compression ignition engine and validated the studies with experiments. The shape of the combustion chamber was found to have significant effects on combustion and emission behaviour. Their results also proved that lesser soot and NOx emissions are released by re-entrant combustion chambers; the depth of the chamber is an effective parameter on the formation of soot and NOx.

With a four-stroke single cylinder engine with rated power of 5.2 kW and speed 1500 rev/min. Cylindrical, trapezoidal, shallow depth and toroidal shaped combustion chambers and three, four and five holes' injector of diameter 3 mm were used to conduct experiments on the impact of injection timing, combustion chamber shape and nozzle geometry on the performance of the engine. It was observed that brake thermal efficiency had a peak value at 23^0 bTDC. Smoke, CO and HC emissions were also at least values at this injection timing. NOx emission levels increased with increased retardation but became more rapid after injection timing of 23^0 bTDC.

Using an injection timing of 23^0 bTDC and compression ratio of 17.5:1, the different combustion chamber shapes were put to test, and they found out that the toroidal shape gave better brake thermal efficiency in comparison to the others, the standard engine shape inclusive. The same results were gotten in terms of CO, HC and smoke emissions as the toroidal shaped combustion chamber gave least values. NOx emission was highest for the toroidal combustion chamber and least for the trapezoidal combustion chamber which fared least on all other indications. The engine performance and emission characteristics were also reported to be of

optimum values with the increase of injector holes, except for the case of NOx emission where the reverse was the case (Ranganatha *et al*., 2014).

Nataraj *et al*. (2015) got similar results to Ranganatha *et al*., 2014 while working with similar conditions with a four-stroke direct injection single cylinder compression ignition engine with rated speed of 1500 rev/min with compression ratio of 17.5:1 and injection timing of 23^0 bTDC. The engine was operated on Mahua and Neem biodiesel in single fuel mode for the determination of the effect of combustion chamber geometry on performance and emission characteristics. The performance and emission characteristics (HC, smoke, and CO) were best for toroidal shaped combustion chamber operated on the biodiesel fuels and least for trapezoidal shaped chambers, however in comparison, conventional compression ignition engine operated on diesel fared better.

Air swirl is a major determinant of in-cylinder fluid motion in internal combustion engines and is one of the most important factors that control the combustion process. Fuel-air mixing and burning rates in compression ignition engines is governed by air swirl. Bharathi and Prasanthi (2013) studied the influence of air swirl on the combustion and emissions properties of compression ignition engines. Using a number of grooves (six, nine and twelve) on the piston of a four-stroke single cylinder direct injection compression ignition engine rated 3.68 kW and 1500 rev/min operated on diesel fuel, it was observed that the smoke density, NOx, HC and CO emissions showed improvements over the standard engine.

Grooved pistons operated on blended fuel of 80% cotton biodiesel and 20% diesel utilized in a test engine of a four-stroke single cylinder direct injection compression ignition engine with rated power of 3.72 kW and speed of 1500 rev/min showed better performance in terms of brake thermal efficiency and specific fuel consumption and reduced CO, HC and smoke emissions in comparison with diesel operated engine without tangential groves (Reddy, *et al*., 2012).

Using Pongamia biodiesel blended with diesel in the ratio 20:80, and combustion chamber shapes of toroidal, hemispherical and shallow in a 4-stroke single cylinder direct injection compression ignition engine with rated power of 5.2 kW and speed 1500 rev/min, Jaichander and Annamalai (2012a) reported that the toroidal shaped combustion chamber performed better of the three in terms of brake thermal efficiency, CO, HC, and PM emission levels but least in emission of NOx.

The motion of the gas inside the engine cylinder plays a pivotal role in the determination of an engine thermal efficiency, and a better understanding of in-cylinder gas motion is germane to the optimization of engine design parameters. Basha *et al*. (2009) conducted studies on the

combustion processes in a compression ignition engine. Simulating using a computational fluid dynamic code "FLUENT", a detailed CFD model was developed for predicting the fluid flow and combustion for a flat piston 4-stroke compression ignition engine. Injection of fuel at 18° before TDC was observed to be the most effective, resulting into reasonable growth in the pressure, temperature, and turbulence kinetic energy were also observed.

Nureddin and Nuri (2008) modelled an axi-symmetric homogenous charged spark ignition engine while considering the turbulent flow conditions in order to investigate the fluid motion and combustion process taking place in the engine. They studied the effects of valve angle on the fluid flow, combustion at constant air/fuel, compression ratios, and observed that fuel consumption dependency was weakly related to the valve angle while the combustion velocity showed a marked relationship with valve angle, decreasing with increase in valve angle. The combustion velocity and tumble strength increase in-cylinder flow and flame propagation, and thus the valve angles have effects on flame propagation and by extension on the performance and emission characteristics of the engine.

Rajashekhar *et al*. (2012) carried out studies on the effects of injection pressure and combustion chamber geometry on biodiesel (20% jatropha with 80% diesel) combustion. They modified the piston of a four-stroke single cylinder compression ignition engine with a rated power of 5.2 kW at a speed of 1500 rev/min to a multi-chambered one by cutting three small cavities 120^0 apart on the piston land. With injection pressures of 175, 200 and 225 bar, they noticed that the performance and emission characteristics of the test engine were optimum at an injection pressure of 200 bar. Using this optimum value of injection pressure, the specific fuel consumption, brake thermal efficiency, HC and CO emissions were all reported to be of better values with the multi-chambered piston in comparison with the standard one.

Mikalsen and Roskilly (2009) while using OpenFOAM CFD toolkit worked on a coupled dynamic-multidimensional simulation model for the simulation of free-piston engines. The influence of the operational variables of the engine on the piston motion was modelled by incorporated solution dependent mesh motion, and demonstrated the use of the coupled solver with the simulation of a spark ignited free piston engine. The coupled dynamic multidimensional solver can be used to make detailed investigations into the effects changes in TDC position and clearance distance on the combustion process and engine performance as it provides a powerful tool for the investigation of the operating characteristics and performance of free-piston engines.

The studies on combustion chamber geometry modification using different piston crown shapes is an ongoing one, however, findings from literature have shown that the different

piston crown geometry being investigated have remained cylindrical. Literature on the use of non-cylindrical piston crown is sparse. This study is therefore focussed on the performance characterisation of non-cylindrical piston crown equipped compression ignition engine.

CHAPTER THREE
MATERIALS AND METHODS

Numerical and experimental investigations were carried out in the course of this research work.

3.1 Numerical Approach

The combustion and fluid motion inside an engine cylinder is governed by the heat energy and Navier – Stokes equation;

The Navier – Stokes equation which solves the pressure and velocity of fluid flow was derived from the continuity equation and the conservation of momentum (Cauchy momentum equation)

3.1.1 Continuity Equation

The continuity equation which is a statement of conservation of mass states that the rate at which mass enters a system equals to the rate at which it leaves the system plus the accumulation of mass within the system.

$$\frac{\partial}{\partial x}(\rho U) + \frac{\partial}{\partial y}(\rho V) + \frac{\partial}{\partial z}(\rho W) + \frac{\partial \rho}{\partial t} = 0 \quad \ldots (3.1)$$

Equation (3.1) is the general equation of continuity in three dimensions and is applicable to all types of fluid flow whether compressible or incompressible.

Noting that

$$\nabla . u = \frac{\partial}{\partial x} U + \frac{\partial}{\partial y} V + \frac{\partial}{\partial z} W$$

Equation (3.1) can thus be expressed as

$$\frac{\partial \rho}{\partial t} + \nabla . (\rho u) = 0 \quad \ldots (3.2)$$

3.1.2 Momentum Equation

The momentum equation is based on the conservation of momentum, and states that the rate of momentum accumulation is equal to the difference in the rate of momentum inflow and the momentum outflow plus the sum of the forces acting on the system.

Applying the conservation relation as obtained in Equation (3.2) to momentum while denoting momentum as ρu, we have;

$$\frac{\partial (\rho u)}{\partial t} + \nabla . (\rho u u) = 0 \quad \ldots (3.3)$$

uu is a dyad, a special case of tensor product, which results in a second rank tensor.

The Cauchy momentum equation is expressed as

$$\rho \frac{Du}{Dt} = \nabla . \sigma + F \quad \ldots (3.4)$$

where σ is stress and,

F are external forces due to gravity.

Expressing the momentum equation in the form of Navier-Stokes equation, we have

$$\rho \frac{Du}{Dt} = -\nabla p + \nabla . T + F \quad \ldots (3.5)$$

where T is the stress tensor.

To apply the Navier – Stokes equation to our fluid of interest, we adopt the following three assumptions;

i) The stress tensor is a direct function of strain rates

ii) The fluid is isotropic

iii) When a fluid is at rest, $\nabla . T$ must be equal to zero

The equation in compact form is thus expressed as;

$$\rho \frac{\partial u}{\partial t} + \rho\, u . \nabla\, u = -\nabla . \rho + \nabla . \left[\mu\, (\nabla u + (\nabla u)^T) - \frac{2}{3}\, \mu \nabla (\nabla .\, u)\right] + F \quad \ldots (3.6)$$

3.1.3 Energy Equation

The energy equation has its roots in the first law of thermodynamics also referred to as the law of conservation of energy. It states that the total energy of an isolated system remains constant, and can be said to be conserved over time. In other words, energy can neither be created nor destroyed but can be transformed from one form to another.

The first law is expressed mathematically as;

$$d(E + Ek) = \delta Q + \delta W \quad \ldots (3.7)$$

E and Ek are the potential and kinetic energy variations respectively, δQ and δW are the path dependent heat and work contributions to the energy variations.

From the conservation of energy,

$$\frac{\partial E_{in}}{\partial t} + \frac{\partial E_g}{\partial t} - \frac{\partial E_{out}}{\partial t} = \frac{\partial E_{st}}{\partial t} \quad \ldots (3.8)$$

Energy in the form of heat can be transferred basically through three means: conduction, convection and radiation. For this research, energy transfers in the form of radiation are neglected.

The energy balance equation can thus be expressed as;

$$\rho \frac{Dh}{Dt} = \frac{Dp}{Dt} - \nabla . \varphi + Q \quad \ldots (3.9)$$

where h is the specific enthalpy

p is the fluid pressure

φ is the heat flux and,

Q is the heat energy generated per unit volume

Using the Fourier's law for the heat flux

$$\varphi = -k\nabla T \quad \ldots (3.10)$$

where k is the thermal conductivity, and taking the fluid to be an ideal one, the equation of state can be expressed as;

$$p = \rho RT \quad \ldots (3.11)$$

from which it can be deduced that

$$h = c_p T \quad \ldots (3.12)$$

Where c_p is the specific heat at constant pressure,

T is the absolute temperature and,

R is the gas constant.

Equation (3.9) can be expressed in an explicit form as

$$\rho c_p \frac{\partial T}{\partial t} + \rho c_p \, u.\nabla T = \nabla.(k\nabla T) + Q \quad \ldots (3.13)$$

This is the energy balance equation for the fluid flow.

3.1.4 Engine Simulation

COMSOL Multi-physics software version 4.3 and 5.0 were utilized for the thermodynamic and fluid dynamic solution in the characterization of a truncated cone piston crown compression ignition engine.

COMSOL Multi-physics employs the finite element method for solving physics-based problems.

Partial Differential Equations (PDEs) are expressions of space and time dependent physics based equations, and for a vast number of problems, the analytical method cannot be used to solve the PDEs. An approximation of the equations is usually constructed, typically based upon discretization. The discretization methods are solved using numerical methods which in turn are approximations of the real solutions to the PDEs.

One of the several numerical methods of solution is the Finite Element Method (FEM). Finite element methods are numerical methods for approximating the solutions of mathematical problems that are usually formulated so as to precisely state an idea of some aspect of physical

reality, and it offers great freedom in the selection of discretization, both in the elements that may be used to discretize space and the basic functions.

The reaction engineering module solves the problem in zero dimensions (0 – D) and provides a solution to the combustion chemistry; while the thermo-fluid module solves the problem in two - dimensional axisymmetric (2 – D axisymmetric) providing solutions to the thermodynamic and fluid mechanics models.

n-Heptane was used as petroleum diesel fuel representative. A reduced version containing twenty-nine (29) species and fifty-two (52) chemical reactions in CHEMKIN format was used in the chemical kinetic model.

The modelled engine parameters were those of the Kirloskar TV1 engine with piston length of 106 mm, cylinder bore of 87.5 mm and a compression ratio of 17.5 regarded as category I and as well as the Yoshita 165F engine with piston length of 75 mm, cylinder bore of 70 mm and a compression ratio of 20.5 regarded as category II. The parameters and initial conditions are spelt out in the Table 3.1.

The results of the simulation were validated. Kirloskar TV1 engine simulation results were validated with experimental results from literature, while the results for Yoshita 165F engine simulations were validated using results obtained from conducted experiments.

The Kirloskar TV1 engine was selected as a standard engine because of its popular commercial use, making it an engine to reckon with. However, the difficulty of getting a test dynamometer that can meet the engine's specification around necessitated the use of a second engine "Yoshita 165F" to validate the numerical results using experiments.

Simulations were carried out for the two standard engines namely Kirloskar TV1 and Yoshita 165F with engine details contained in Tables 3.1 and 3.2. Further simulations were carried out using engine details of Kirloskar TV1 and Yoshita 165F but with the flat piston crowns replaced with truncated and inverted truncated cone crowns. Five truncated cone inclination angles (25, 30, 35 40, 45) and five inverted truncated cone inclination angles (25, 30, 35, 40, 45) were used.

Figure 3.1 shows a drawing of an engine cylinder and parameters which are required for the determination of some other parameters.

The engine cylinder volume changes as a function of time and is described by the slider-crank equation;

$$\frac{V}{V_c} = 1 + \frac{(CR-1)}{2}[R + 1 - Cos\alpha - \sqrt{(R^2 - (Sin\alpha)^2)}] \quad \ldots (3.14)$$

(COMSOL, 2012; Scott, 2018)

Table 3.1: Test engines specifications and parameters

Variable Name	**Symbol**	**Kirsloskar TV1**	**Yoshita 165F**
Cylinder bore (m)	D	0.0875	0.0700
Stroke (m)	S	0.11	0.07
Connecting rod length (m)	Lc	0.238	0.130
Crank arm length (m)	La	0.055	0.035
Engine speed (RPM)	N	1500	2600
Compression ratio	CR	17.5:1	20.5:1
Initial temperature (K)	T_init	313	313
Initial Pressure (N/m^2)	P_init	1e5	1e5
Equivalence ratio	ER	0.5	0.5
Length ratio	R	4.3273	3.7143
Initial O_2 mole fraction	X_O_2	0.20801	0.20801
Initial N_2 mole fraction	X_N_2	0.78253	0.78253
Initial C_7H_{16} mole fraction	$X\_C_7H_{16}$	0.00946	0.00946

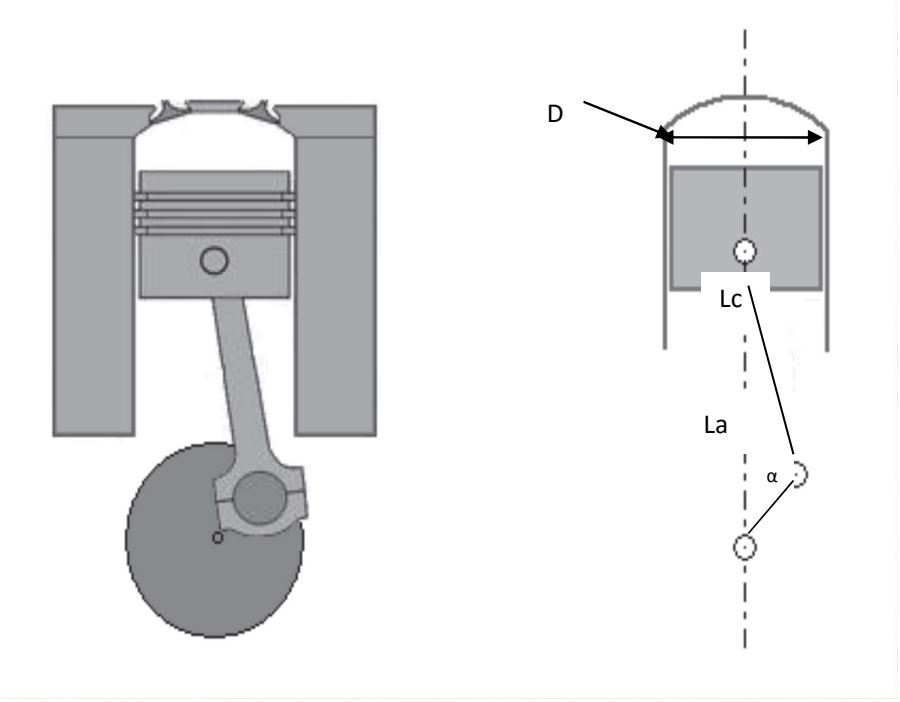

Figure 3.1. Engine cylinder

where;

V is the volume of the cylinder (m^3)

V_c gives the clearance volume (m^3)

CR equals the compression ratio and

R denotes the ratio of the connecting rod to the crank arm

α is the crank angle (rad)

The volume swept by the piston (Vs) for one stroke which is the movement from the bottom dead centre (BDC) to the top dead centre is given by the relation

$$V_s = \frac{\pi D^2 S}{4} \quad \ldots (3.15)$$

D is the bore diameter of the cylinder and

S is the piston stroke.

The engine clearance volume which is the volume between the cylinder head and the top of the piston is given by the relation

$$V_c = \frac{V_s}{(CR-1)} \quad \ldots (3.16)$$

The engine cylinder can be categorized as a perfectly mixed variable volume reactor described by the mass balance relation;

$$VR_i = \frac{d(Vc_i)}{dt} \quad \ldots (3.17)$$

where c_i represents the species concentration (mol/m^3) and R_i denotes the species rate expression ($mol/m^3.s$)

The energy balance taking the mixture in the cylinder as an ideal gas mixture is given as;

$$V_r \sum c_i c_{p,i} \frac{dT}{dt} = \mathcal{Q} + \mathcal{Q}_{external} + V_r \frac{dp}{dt} \quad \ldots (3.18)$$

where;

Cp,i is the species molar heat capacity (J/ mol.K),

T is the temperature (K),

p gives the pressure (Pa),

$\mathcal{Q}$ is the heat due to chemical reaction (J/s) and,

$\mathcal{Q}_{external}$ is the heat from external sources (J/s).

It is assumed that the model is adiabatic and hence, $\mathcal{Q}_{external} = 0$.

The stoichiometric requirement for the combustion of the fuel (n-heptane) is obtained from the overall reaction (assuming air to be composed of 21% Oxygen and 79% Nitrogen)

$$C_7H_{16} + 11(O_2 + 3.76N_2) \rightarrow 7CO_2 + 8H_2O + 41.36N_2 \quad \ldots (3.19)$$

Stoichiometric air-fuel ratio '$(A/F)_{stoc}$' which is the correct amount of air required for the complete combustion of fuel. It is derivable from the relation;

$$(A/F)_{stoc} = \frac{m_{air}}{m_{fuel_{stoc}}} = \frac{4.76*11* m_{air}}{1* m_{fuel}} \quad \ldots (3.20)$$

m_{air} is the mass of air,

m_{fuel} is the mass of fuel and,

$m_{fuel_{stoc}}$ is the stoichiometric mass of fuel.

The equivalence ratio 'ψ' is given by the relation

$$\psi = \frac{(A/F)_{stoc}}{(A/F)} \quad \ldots (3.21)$$

The molar fraction of the reacting mixture is given by

$$x_{fuel} = \frac{1}{(4.76*11)(\psi+1)} \quad \ldots (3.22)$$

while the relation for the initial concentration is

$$C_{fuel} = \frac{x_{fuel*}P_{init}}{RgT_{init}} \quad \ldots (3.23)$$

C_{fuel} is the fuel concentration,

x_{fuel} is the fuel molar fraction,

R is the gas constant,

P_{init} is the initial pressure,

T_{init} is the initial temperature and

g is the force due to gravity.

The simulation was carried out for unmodified flat faced piston, truncated cone and inverted truncated cone pistons at different base-angles of inclination to the vertical; $25°$, $30°$, $35°$, $40°$ and $45°$.

Figure 3.2 and Figure 3.3 shows the modified truncated cone piston crown and the inverted truncated cone piston crown geometries respectively.

The volume of the removed material which was added back to the piston to ensure constant compression ratio for some of the simulated cases was calculated using the relation;

$$V_{rem} = \frac{\pi d^2 Ho}{4} - (\frac{\pi d^2 H}{12} - \frac{\pi}{12}(d - do)^2(H - Ho)) \quad \ldots (3.24)$$

where;

V_{rem} is the volume of material removed during the modification

d is the diameter of the piston

do is the diameter of the tapered section

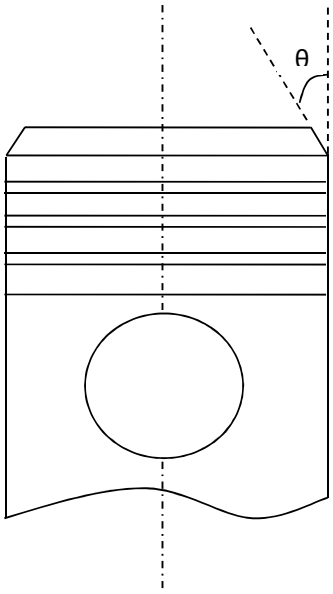

Figure 3.2. Modified truncated cone piston crown geometry

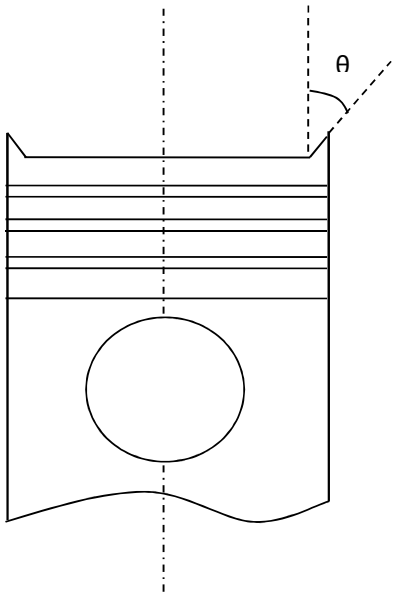

Figure 3.3. Modified inverted truncated cone piston crown geometry

Ho is the height of the tapered section and

H is the height of the cone formed by tapering the piston by an angle.

$$H = \frac{d}{2tan} \quad \ldots (3.25)$$

where θ is the angle of taper

The volume of the material that was removed by the modification (V_{rem}) was first added to the original piston volume, and this was achieved as earlier stated by increasing the piston height. The height increase was calculated using the formula for calculating the volume of a cylinder: $V_{cylinder} = \frac{\pi D^2 H}{4}$.

Hence,

$$Height\ increase = \frac{4V_{rem}}{\pi d^2} \quad \ldots (3.26)$$

The initial pressure was set to 1 bar, an initial temperature of 313 K and an equivalence ratio of 0.5.

The injection starts at 174° before top dead centre (bTDC) and ends at 192° after top dead centre (aTDC)

For the thermodynamic analyses of the mixture of fuel and air inside the engine combustion chamber, the following assumptions were made:

i. The heat energy generated by combustion was added uniformly over the domain, and the combustion assumed to be stoichiometric
ii. All the equations were solved in the original domain, and the effect of change in the cylinder volume was accounted for manually in the equations
iii. Perfect gas laws were used, and the fuel-air mixture was assumed to be an ideal gas
iv. Swirl effects were neglected

The energy balance equation (Equation 3.13) was used to model the temperature distribution of the fuel-air mixture in the cylinder, and the pressure distribution was modelled with the ideal gas equation.

The piston moves continuously inside the engine cylinder, and its displacement as a function of the crankshaft rotation was computed from the relation

$$x_p = \sqrt{l^2 - (r_c Sin\theta)^2} - r_c cos\theta - (l - r_c) \quad \ldots (3.27)$$

(COMSOL, 2014; Scott, 2018)

where;

x_p is the piston displacement,

θ is the crank angle,

l is the connecting rod length and

r_c is the crank radius

Using 'V$_o$' to denote the initial engine cylinder volume, the current engine cylinder volume 'V' = $V_o - \pi {r_p}^2 x_p$ … (3.28)

r_p is the engine cylinder radius

The flow of the fuel-air mixture inside the engine cylinder is governed by the Navier – Stokes equation as stated earlier. The flow is turbulent in nature, and the modelling of turbulence involves the construction and use of a model to predict its effect. A common approach is to average the governing equations of the flow, and for the course of this work, the Reynolds Averaged Navier Stokes (RANS) equations were used, as they are time-averaged equations of motion for the fluid flow.

From Equation (3.26);

$$\rho \frac{\partial u}{\partial t} + \rho\, u.\nabla\, u = -\nabla.\rho + \nabla.\left[\mu\,(\nabla u + (\nabla u)^T) - \frac{2}{3}\,\mu\nabla(\nabla\,.u)\right] + F$$

The Reynolds Averaged Navier Stokes (RANS) equation is expressed as

$$\rho \frac{\partial u}{\partial t} + \rho\, u.\nabla\, u = \nabla.\left[-\rho 2I + (\mu + \mu_T)\,(\nabla u + (\nabla u)^T) - \frac{2}{3}\,(\mu + \mu_T)\nabla(\nabla\,.u)I - \frac{2}{3}\rho k I\right] + F \quad \text{… (3.29)}$$

However, the nonlinearity of the Navier – Stokes equations means that the velocity fluctuations still appears in the Reynolds Averaged Navier Stokes (RANS) equations, and to obtain equations containing only mean values of velocity and pressure, Reynolds Averaged Navier Stokes (RANS) equations were closed using the k-epsilon (k-ε) turbulent model which is based on the Boussinesq hypothesis.

The Boussinesq hypothesis states that the Reynolds stress tensor Υ_{ij} is proportional to the trace-less mean strain rate tensor S_{ij}.

The k-epsilon (k-ε) turbulent model was used because of its relative simplicity of implementation, stable calculations that easily converge and the reasonable predictions for fluid flow problems. It is a two-equation model and allows for history effects like convection and diffusion. One being turbulent kinetic energy 'k' which determines the energy in the turbulence and the other is the turbulent dissipation 'ε' which determines the scale of the turbulence.

The 'k' equation is stated as follows;

$$\rho \frac{\partial k}{\partial t} + \rho(u.\nabla)k = \nabla.\left[(\mu + \frac{\mu_T}{\sigma_k})\nabla k\right] + p_k - p_\varepsilon \quad \text{… (3.30)}$$

and the 'ε' equation is stated as

$$\rho\frac{\partial\varepsilon}{\partial t}+\ \rho(u.\nabla)\varepsilon=\ \nabla.\left[(\mu+\ \frac{\mu_T}{\sigma_\varepsilon})\nabla\varepsilon\right]+\ C_{\varepsilon1}\frac{\varepsilon}{k}P_k-\ C_{\varepsilon2}\rho\frac{\varepsilon^2}{k} \quad \ldots (3.31)$$

where $\mu_T=\ \rho C_\mu\frac{k^2}{\varepsilon}$ and

$$P_k=\ \mu_T\left[\nabla u:\ (\nabla u+(\nabla u)^T)-\frac{2}{3}(\nabla.u)^2\right]-\frac{2}{3}\rho k\nabla.u$$

The turbulent model parameters are spelled out as depicted in Table 3.2.

where;

C_μ is an empirical constant specified in the turbulence model which leads to more mixing and greater change in pressure.

$C_{\varepsilon1}$ and $C_{\varepsilon2}$ are constant coefficients in the k-ε model which also have effects on the mixing, shear generation and pressure change.

σ_k and σ_ε are the turbulent Schmidt numbers.

The boundary conditions used for the simulation are based on the geometry, which comprises of the cylinder head, cylinder wall, and the piston head. The engine cylinder head is stationary, the cylinder side wall is also stationary and the piston slides through it, and the piston head which moves back and forth in the cylinder.

The adopted boundary conditions for the cylinder wall and piston head was the moving wall function making use of its velocity in the radial (r) and axial (z) components, while for the wall function was adopted for the cylinder head being that it was stationary.

The set boundary conditions for the cylinder wall was r = 0 and z = 0, and for the piston head, r = 0 and z = U_{pp}.

U_{pp} is the instantaneous velocity derived from the piston displacement and is written as

$$U_{pp}=\frac{dx_p}{dt} \quad \ldots (3.32)$$

The different classes of the wall boundary showing the cylinder head, to which the wall function was applied, the cylinder wall, and the piston head is shown in Figure 3.4.

The initial velocity 'u' of the air inside the engine cylinder was taken to be zero in all directions, that is $u_r = 0$, $u_z = 0$ and $u_{phi} = 0$.

The values of the net work done by the engine and heat energy derived from the combustion of the fuel-air mixture were determined from the simulation.

The thermal efficiency (η_{Th}) of the engine was computed from the relation

$$\eta_{Th}=\ \frac{W_{net}}{Q_{in}}=\frac{P}{FC*CV} \quad \ldots (3.33)$$

W_{net} is the net work output from the engine

Q_{in} is the heat energy generated by the combustion of the fuel-air mixture

Table 3.2: Turbulent model parameters

Parameters	**Value**
$C_{\varepsilon 1}$	1.44
$C_{\varepsilon 2}$	1.92
C_{μ}	0.09
σ_k	1
σ_{ε}	1.3
k_v	0.41
B	5.2

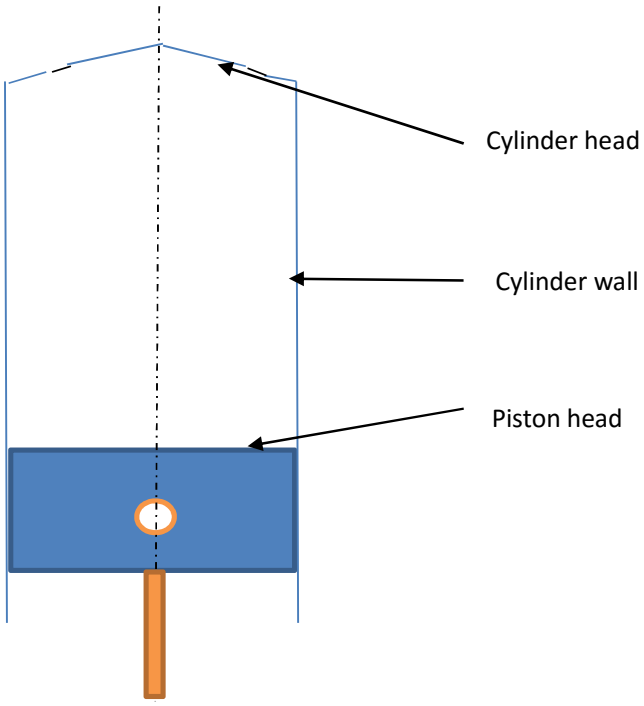

Figure 3.4. Engine cylinder showing the appropriate boundaries

P is the net power of the engine

FC is the fuel consumption rate (kg/s)

CV is the calorific value of a kilogram of fuel

The mean pressure;

$$P_m = \frac{W_{net}}{V_d} \quad \ldots (3.34)$$

where V_d is the displacement volume and is equivalent to the swept volume V_s

The power generated by the engine;

$$P = \frac{P_m LAN}{n_c} \quad \ldots (3.35)$$

A is the area of the cylinder

N is the number of revolutions per minute

n_c is the number of cycles required to make a complete revolution. (For a four-stroke engine, $n_c = 2$)

The engine torque; $T_q = \frac{60}{2\pi N}$ … (3.36)

The specific fuel consumption;

$$SFC = \frac{\rho_{atm}}{(A/F)P_m} = \frac{\dot{m}_f}{P} = \frac{\rho_f q}{P} \quad \ldots (3.37)$$

$\dot{m}_f$ is the mass rate of fuel consumption,

q is the volumetric rate of fuel consumption and,

ρ_f is the fuel density.

3.1.5 Sequence of Analysis using the Numerical Model

The numerical models were used for the performance characterization of a compression ignition engine of piston length of 106 mm, cylinder bore of 87.5 mm. It was fitted with a standard piston, truncated cone piston crown (TCPC), and inverted truncated cone piston crowns (I TCPC) of base-angles of 25°, 30°, 35°, 40° and 45° with compression ratios of 17.5:1 and range of 10.645 to 16.877 respectively. These were classified as category I, and are presented first.

This is followed by category II which is the results of the investigation of performance parameters obtained using the numerical model for a compression ignition engine with piston length of 75 mm, cylinder bore of 70 mm and compression ratio of 20.5:1 and truncated cone and inverted truncated cone piston crown of base-angles of 25°, 30°, 35°, 40° and 45° and constant compression ratio.

The model uses an initial temperature of 313 K, initial pressure of 10^5 N/m^2 and equivalence ratio of 0.5. It also takes the initial mole fractions of oxygen as 0.20801, that of nitrogen as 0.78253 and that of n-heptane as 0.0094589.

The initial concentrations of 7.9931 mol/m^3 of oxygen, 30.0690 mol/m^3 of nitrogen and 0.36347 mol/m^3 of n-heptane were also specified. For each case investigated, the pressure and velocity history inside the combustion chamber were obtained. In addition, the performance parameters namely, indicated mean effective pressure, thermal efficiency and emission history were obtained. The performance parameters were used to determine the most suitable base angle out of all that were investigated.

The flow chart for the numerical approach of solution is shown in Figure 3.5.

3.2 Experimental Approach

To determine the practicality of the results gotten from the numerical approach, experiments were conducted on a horizontal single cylinder four-stroke air-cooled compression ignition engine.

Control experiments was carried out on the test engine using Automotive Gas Oil (AGO) and Shea-butter biodiesel prepared using standard technique from Shea-butter sourced from Ogbomoso town, Nigeria.

Experiments was also conducted on the modified truncated cone piston crown test engine using the most suitable base angle and also using AGO and Shea-butter biodiesel as test fuels. The performance parameters were also evaluated for each of the test case investigated.

3.2.1 Fuel Properties

Physicochemical tests were first conducted on the test fuels namely petroleum diesel and Shea-butter biodiesel to determine their physical and chemical properties. The properties tested for were density, specific gravity, kinematic viscosity, cloud point, pour point, flash point, fire point, carbon content, PH value, calorific value, ash content, cetane number, and sulphur content.

3.2.1.1 Determination of the Fuel Samples Densities

Density is the ratio of mass of a substance to its volume. This property was determined for the test fuels as follows;

Apparatus: density bottle and mass gauge

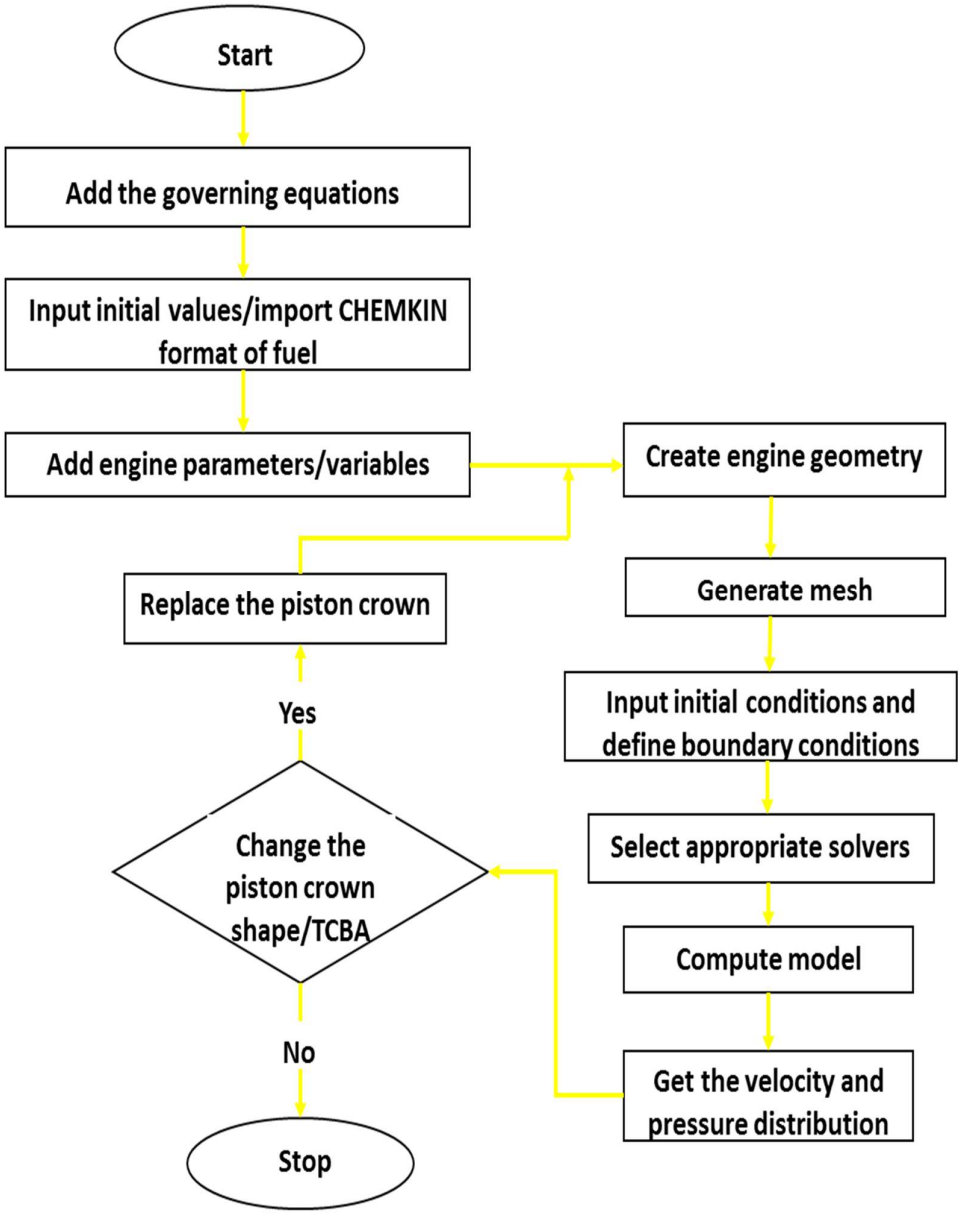

Figure 3.5. Flow chart of the sequence of events for the numerical analysis

Method: The mass of the respective fuel samples was obtained by filling the density bottle with the fuel samples in turn and subtracting the mass of the density bottle from their respective masses. The mass of the fuel samples was denoted as W in each case.

The densities were then computed using the relation

$$\rho = \frac{W_i}{V} \text{ (g/ml)} \quad \ldots (3.38)$$

Where V was the volume of the fuel sample in "ml" used in filling of the density bottle

3.2.1.2 Determination of Specific Gravity of Fuel Samples

Specific gravity is the ratio of the density of the fluid in question to the density of water at 4℃. This property was determined for the test fuels as follows;

Apparatus: density bottle, thermometer and mass gauge

Method: An empty density bottle was weighed and its mass recorded as W_1. The bottle was filled with distilled water maintained at a temperature of 4℃, weighed and its mass recorded as W_2. The bottle was then emptied and filled with the test fuel samples, the mass readings taken accordingly and recorded as W_{31} and W_{32} respectively.

The specific gravity of the fuel samples was then calculated using the relation;

$$\text{S.G} = \frac{W_{3i} - W_1}{W_2 - W_1}. \quad \ldots (3.39)$$

This follows from the formula

$$\text{S.G} = \frac{\rho_{fluid}}{\rho_{water\,@\,4℃}} = \left(\frac{m_{fluid}}{V_{fluid}}\right)\left(\frac{V_{water}}{m_{water}}\right)$$

And since the volume was the same,

$$\text{S.G} = \frac{m_{fluid}}{m_{water}}$$

3.2.1.3 Determination of the Kinematic Viscosity

Kinematic viscosity is the ratio of the fluid dynamic viscosity to its density. It has significant effects on fuel delivery and power output. This property was determined for the test fuels as follows;

Apparatus: Capillary viscometer, Digital stopwatch

Method: it was done in accordance with ASTM D445-17a procedure.

The time taken for the respective fuel samples to flow under gravity through a calibrated glass capillary viscometer from the upper to the lower mark was taken and recorded. This was repeated until when the difference between two consecutive readings was lesser than one

percent. The average time for the three last readings was then found and used in the computations.

The kinematic viscosity of the respective fuel samples was then calculated using the relation

Kinematic viscosity = kt (mm^2/s) … (3.40)

where $k = \frac{\pi r^4}{8VL}$, "r, L and V" are the radius of the capillary section of viscometer, the length between marked sections and volume of sample respectively.

3.2.1.4 Determination of the Fuel Samples Cloud and Pour Points

Pour point is the temperature at which a liquid just ceases to flow.

Cloud point is the temperature at which a liquid becomes hazy when it is cooled at a specified rate. These properties were determined for the test fuels as follows;

Apparatus: Test jar, high pour thermometer, heater and water bath

Method: A test jar was filled to the level mark with the respective fuel samples at a time. The jar was then closed with a cork carrying a high-pour thermometer. The position of the cork and thermometer were adjusted to ensure a tight fitting, and such that the capillary tube is 3mm below the surface of the fuel sample.

The fuel sample was heated up to a state of free flow and then transferred to a water bath. Its flow characteristics were observed at 3℃ intervals. The temperature at which wax begins to appear in the fuel sample was noted and recorded as its cloud point.

The sample was cooled further, and the lowest temperature at which the movement of the sample was observed was recorded as its pour point.

3.2.1.5 Determination of the Fuel Samples Flash and Fire Points

Flash point is the lowest temperature at which the fuel vapour can be ignited by an externally supplied ignition.

Fire point is the lowest temperature at which the substance gets ignited and burns under specified conditions. These properties were determined for the test fuels as follows;

Apparatus: Cleveland cup, flame exposure device, thermometer, burner

Method: The procedure adopted followed the method of the Federation of Oils, Seeds and Fats Association (FOSFA).

A Cleveland cup was filled with the respective fuel samples in turn. The bulb of a thermometer was immersed in the sample and the sample gently heated. At every 1℃ rise of

temperature, a small flame was passed over the sample until when a flash occurred. The temperature reading at which a flash occurred was then taken as the samples flash point.
The sample was heated further until the volatiles ignites and burns continuously for five (5) seconds. The temperature readings at this stage were recorded and taken as the fuel samples fire point.

3.2.1.6 Determination of Fuel Samples Percentage Carbon Content

Apparatus: weight scale, furnace, crucible

Method: One gram of the sample was poured into a crucible and its weight is taken and recorded. The crucible with its contents was then heated in a furnace until it turned to black char. This was then reweighed and recorded. The respective percentage carbon content of the fuel sample was then calculated using the relation;

$$\% \text{ Carbon content} = \left(\frac{Initial\ weight - Final\ weigh}{Initial\ weigh} * 100\right) \quad \ldots (3.41)$$

3.2.1.7 Determination of Heating Values of the Fuel Samples

Heating value determines the brake power and is the amount of heat released during the combustion of a specified amount of fuel. This property was determined for the test fuels as detailed below.

Apparatus: Bomb calorimeter, 6 volts' battery

Method: The mass of the crucible was measured and recorded. The fuel sample was poured into the crucible, weighed and recorded. The mass of the fuel sample; the difference between the mass of the crucible with fuel sample and the empty crucible was denoted with "m". The crucible with its content was then placed in the calorimeter. The calorimeter was filled with water with mass "W" and its initial temperature taken and recorded as t1. The calorimeter electrodes were then connected to a 6 volts' battery and temperature readings taken at intervals of thirty (30) seconds. The final temperature of the water was taken after two minutes and recorded as t2, and the water equivalent of the calorimeter bomb, stirrer, and thermometer e.t.c. was taken as "w". The higher heating values of the respective fuel samples were determined using the relation;

$$\text{HHV} = \frac{(W+w)(t2-t1)}{m} * 4.184 \text{ (MJ/kg)} \quad \ldots (3.42)$$

And the lower heating value was computed from the relation

$$\text{LHV} = HHV - 2465M_w \text{ (MJ/kg)} \quad \ldots (3.43)$$

M_w is the mass of water vapour liberated from the combustion of 1 kg of fuel.

3.2.1.8 Determination of Fuel Samples Ash Content

Apparatus: Crucible, muffle furnace, scientific balance, fume cupboard

Method: The mass of the dry empty crucible was taken and recorded as W, about 2g of the fuel sample was poured into the crucible, and its mass retaken and recorded as W_1. The crucible was then placed on a burner in a fume cupboard to exclude the organic matters, before transferring it to a furnace maintained at 750℃ for about four hours. The crucible and the residue were then cooled in a desiccator before reweighing and the mass recorded as W_2.

The fuel sample ash content was then calculated using the relation;

$$\text{Ash mass } \% = \frac{W_2 - W}{W_1 - W} * 100 \quad \ldots (3.44)$$

3.2.2 Control Experiment

The design parameters of the experimental test engine are as stated in Table 3.2, and the schematics of the experiment follows in Figure 3.6.

The schematic representation of the experimental set-up which comprises the test engine, exhaust gas analyser, vibrometer, water supply tank, the dynamometer with its instrumentation panel for the display of the engine speed, the torque, and the exhaust gas temperature is shown in Figure 3.6.

The assembled experimental rig which comprised of the test engine, dynamometer, vibrometer, exhaust gas analyser and water receiving tank is shown in Plate 3.1.

Other apparatus/kits used in the conduction of the experiment includes a graduated burette, and a stopwatch

The used dynamometer type was a hydraulic absorption type which uses an enclosed impeller coupled to the output shaft of the test engine. Its power (load) is controlled by the regulation of sluice gates which obstructs the flow of water over the impeller.

The specification of the dynamometer is stated in Table 3.3.

The dynamometer has a power range of 2.5 kW ~ 7.5 kW, with a designed maximum torque value of 15 Nm and speed of 6000 RPM.

The test engine was fastened to the test rig bench with bolts and nuts, and its output shaft coupled to the dynamometer with rubber couplings. Appropriate bushings were used to ensure the alignment of the engine and the dynamometer shaft.

An extension pipe was connected to the exhaust pipe to direct the emission gases outside the workshop.

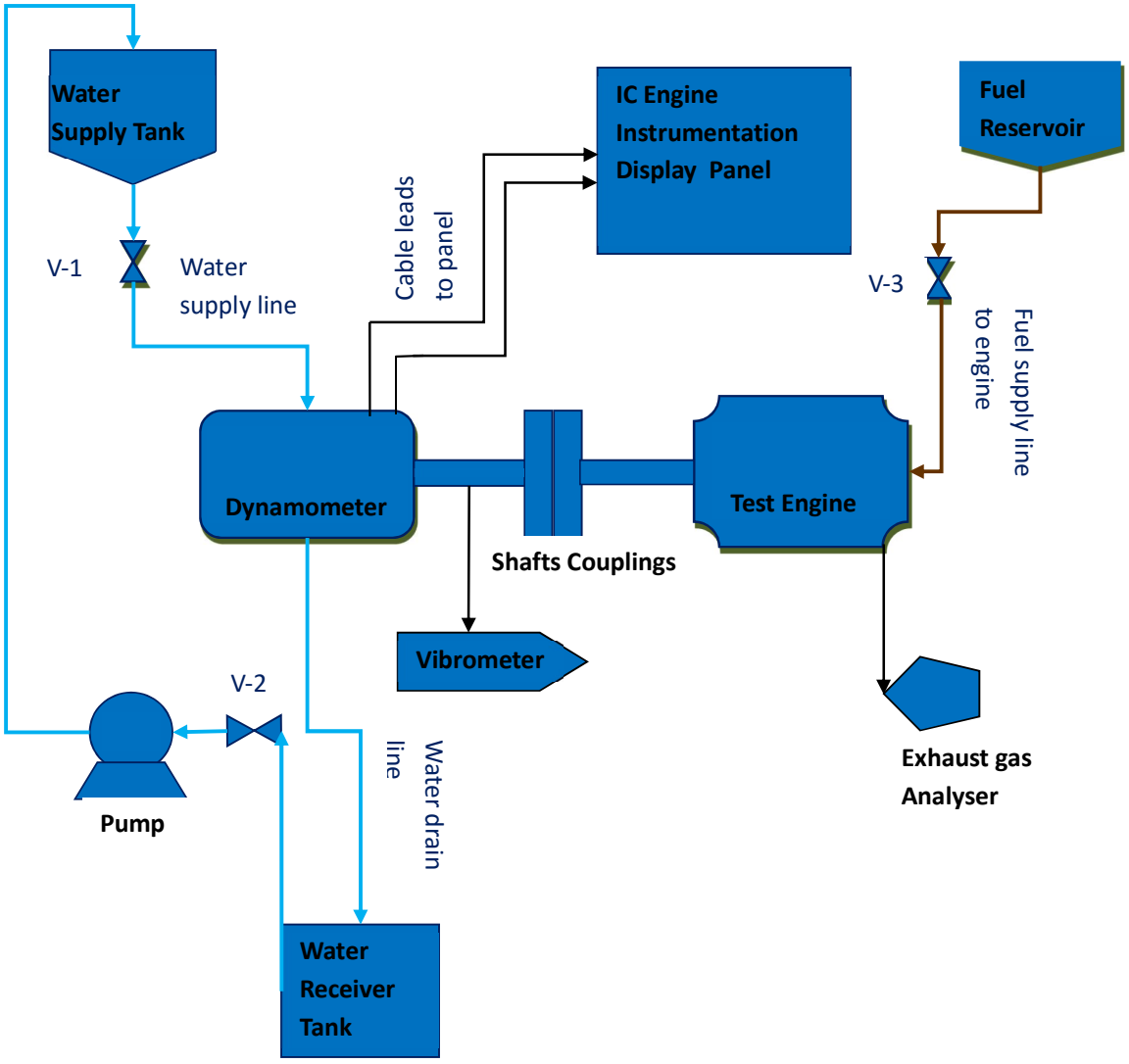

Figure 3.6. Schematic diagram of the experimental set-up

Plate 3.1. Experimental test rig

Table 3.3: Dynamometer specification

Parameters	**Value**
Dynamometer Type	TQ TD115 MKH Absorption Dynamometer
Power Range (kW)	2.5 – 7.5
Torque (Nm)	15 (maximum)
Speed (RPM)	6000 (maximum)

The engine fuel tank was by-passed and the fuel inlet hose connected to a graduated burette to allow for accurate measurement of the fuel flow rate.

The volumetric flow rate 'q' (m^3/s) was computed by taking the time required for the consumption of 2 ml volume of fuel as read from the burette using a stopwatch.

$$q = \frac{V_{fuel}}{t} \quad \ldots (3.45)$$

V_{fuel} is 2 ml

't' is the time taken by the engine to consume 2 ml volume of fuel

The fuel consumption time was taken for at least two instances and the average value was taken and recorded for the engine at no-load and at full-load conditions.

A load was placed on the engine by turning the sluice gates to allow the flow of water through the dynamometer.

The engine speed in rpm at no-load and full load conditions were taken and recorded from the instrumentation panel of the test rig whose probe was attached to the shaft end of the dynamometer.

The temperature probe attached to the test engine's silencer gave the exhaust gas temperature readings in $°C$ on the instrumentation panel; this was taken and recorded for the no-load and full-load conditions.

The engine torque in Nm was also read on the instrumentation panel and recorded. A view of the instrumentation is as depicted in Plate 3.2.

The engine mechanical efficiency is calculated from the relation;

$$\text{Mechanical efficiency in \% } (\eta_M) = \frac{Brake\ power}{Engine\ indicated\ power} \quad \ldots (3.46)$$

Vibration readings in m/s^2 were taken using a vibrometer whose probe was attached to the output shaft of the test engine for the no-load and full-load conditions. The vibrometer is shown in Plate 3.3.

The emitted gas values in ppm were measured using a gas analyzer. The analyzer test probe was placed inside the exhaust pipe and the readings were taken from its digital display interface and recorded accordingly. Plate 3.4 depicts the gas analyser used for taking of the readings.

3.2.3 Modified Piston Engine Test

The piston crown of the test engine was modified to truncated cone geometry after the completion of the control experiment.

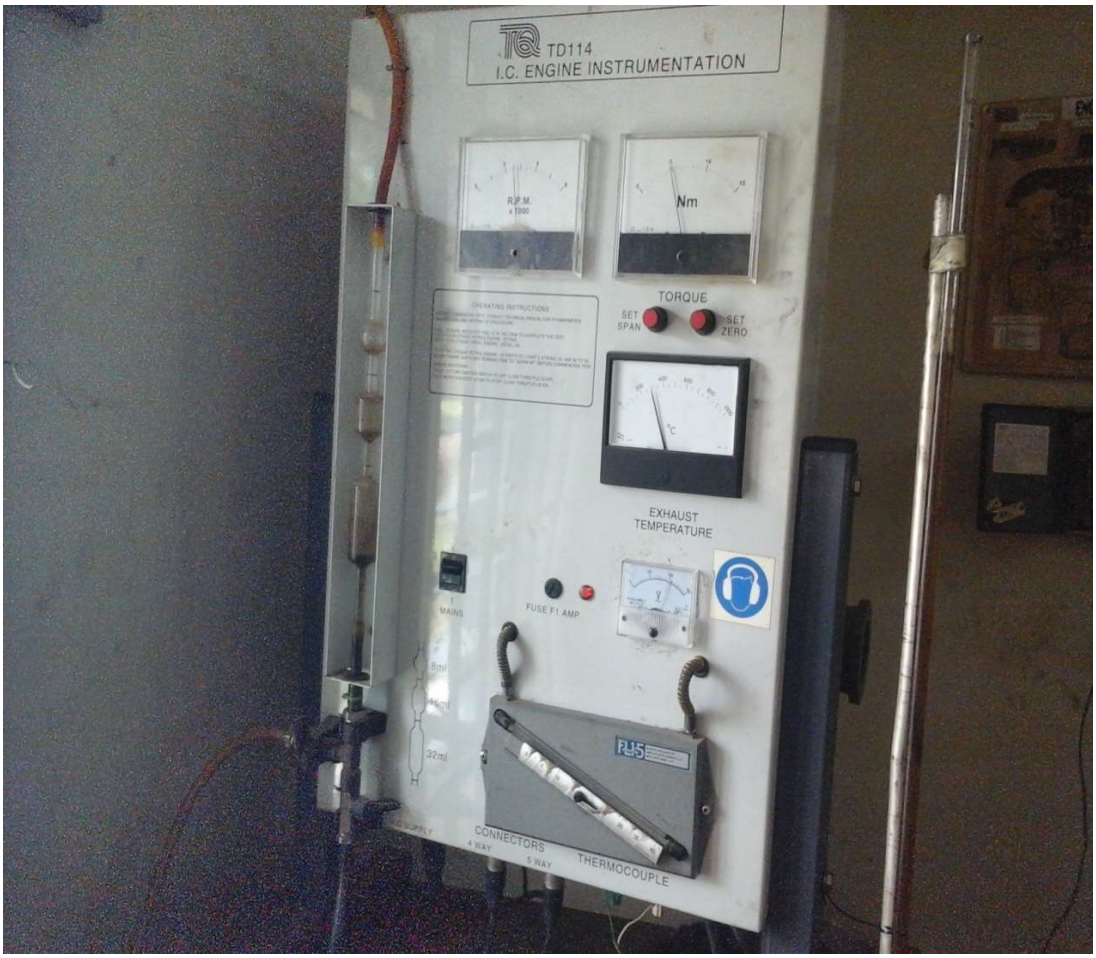

Plate 3.2. Test Rig instrumentation panel

Plate 3.3. Vibrometer

Plate 3.4. Taking measurements with the gas analyzer

The test engine was disassembled to have access to the cylinder block and piston. Plate 3.5 and 3.6 shows the disassembled engine and the unmodified piston respectively.

The test engine unmodified piston as shown in Plate 3.6 was worked upon to produce the truncated cone piston. To maintain the same compression ratio as that of the unmodified piston, the volume of the piston material removed during the reshaping was calculated and added to it thereby increasing the piston height.

Using the results gotten from the simulation studies, the test engine piston was modified towards getting optimal improvement in engine performance characteristics.

The angle of tapering chosen was 40° and a tapered height of 0.005m for the truncated cone piston crown geometry.

The volume of the removed material was calculated using Equation (3.24)

$$V_{rem} = \frac{\pi d^2 H_o}{4} - \left(\frac{\pi d^2 H}{12} - \frac{\pi}{12}(d - d_o)^2(H - H_o)\right)$$

H_o = 0.005 m, d = 0.07 m θ = 40°

H was gotten from Equation (3.47)

$$H = \frac{d}{2tan\theta} = \frac{0.07}{2*tan40^\circ} = 0.0417 \text{ m}$$

$d_o = 2r_o = 2H_o tan\theta$ = 2 x 0.005 x tan40° = 0.0084m

$$V_{rem} = \frac{\pi*0.07^2*0.005}{4} - \left(\frac{\pi*0.07^2*0.0417}{12} - \frac{\pi}{12}(0.07 - 0.0084)^2(0.0417 - 0.005)\right)$$

= $2.2073*10^{-6}$ m^3

The height of the piston was increased in order to compensate for the removed material as a result of the piston crown's taper.

The height increase of the piston is obtained using from Equation (3.26) as

$$Height\ increase = \frac{4* 0.0000022073}{\pi* 0.07^2} = 0.0006 \text{ m}$$

The sketch in Figure 3.7 illustrates the modified geometry.

The piston which was cast from aluminium was filled with the same material to increase the height of the piston crown. This was then turned on a lathe machine to get the required dimensions and geometry. Plate 3.7 shows the filled un-machined piston, and Plate 3.8 shows the modified piston.

The modified piston was fitted back into the test engine and experimental test conducted during the control test was carried out on the engine following the same procedure.

(a)

(b)

Plate 3.5. Test engine showing (a) Cylinder block, (b) Cylinder head with valves

Plate 3.6. Unmodified Piston

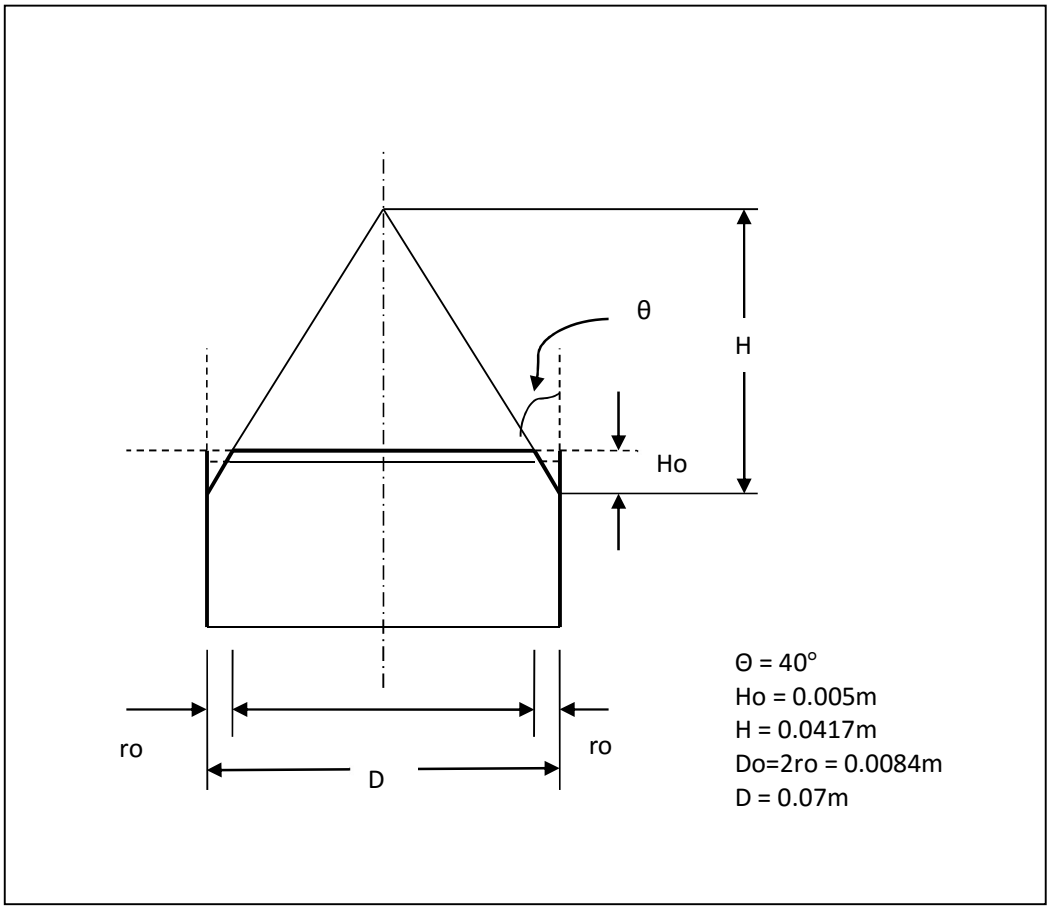

Figure 3.7. Sketch of the modified truncated cone piston crown

Performance parameters were obtained experimentally on the compression ignition engine with piston length of 75 mm, cylinder bore of 70 mm and compression ratio of 20.5:1, and that with truncated cone piston crown of inclination angles of 40°.

Comparative analysis of the numerical and experimental investigations of the compression ignition engine with modified piston crown were also conducted.

Plate 3.7. Aluminium filled piston

Plate 3.8. Modified Aluminium piston for test engine

CHAPTER FOUR
RESULTS AND DISCUSSIONS

4.1 General Remark on the Results

In this chapter the numerical results are presented and analysed. Thereafter, experimental results are presented and then a comparative study of both numerical and experimental studies is presented. All results are fully discussed.

4.2 Numerical Simulation

Detailed pressure and temperature history for each category are presented. For emphasis, in category I, the compression ratios are varied, while the compression ratio in category II is constant.

4.3 Pressure Distribution inside the Engine Cylinder

The details of the pressure distributions inside the engine cylinder when cut-plane sections of the numerical model in the vertical directions are made are presented in the following sections;

4.3.1 The Pressure Distributions in the Engine Cylinder for Category I

The cut-plane sections of the numerical models in the vertical direction indicating the pressure distributions through the engine cylinder for category I at selected time periods are as depicted in Figure 4.1 to 4.4. Figure 4.1 depicts the distribution for the truncated cone piston crown (TCPC) with a compression ratio of 17.5:1 for the indicated inclination angles, Figure 4.2 depicts the pressure distribution for the inverted truncated cone piston crown (ITCPC) also with compression ratio of 17.5:1 and the indicated inclination angles, while Figures 4.3 and 4.4 depicts the pressure distribution for the truncated cone piston crown with compression ratio increasing from 16.243 to 16.877, and inverted truncated cone piston crown with compression ratio increasing from 10.645 to 10.895 for the indicated angles respectively.

The occurrence of active zones (portions with higher pressure) is more conspicuous at an inclination angle of 40° for the truncated cone piston crown and 40° and 45° for the inverted truncated cone piston crown as observed in Figures 4.1 and 4.2 respectively.

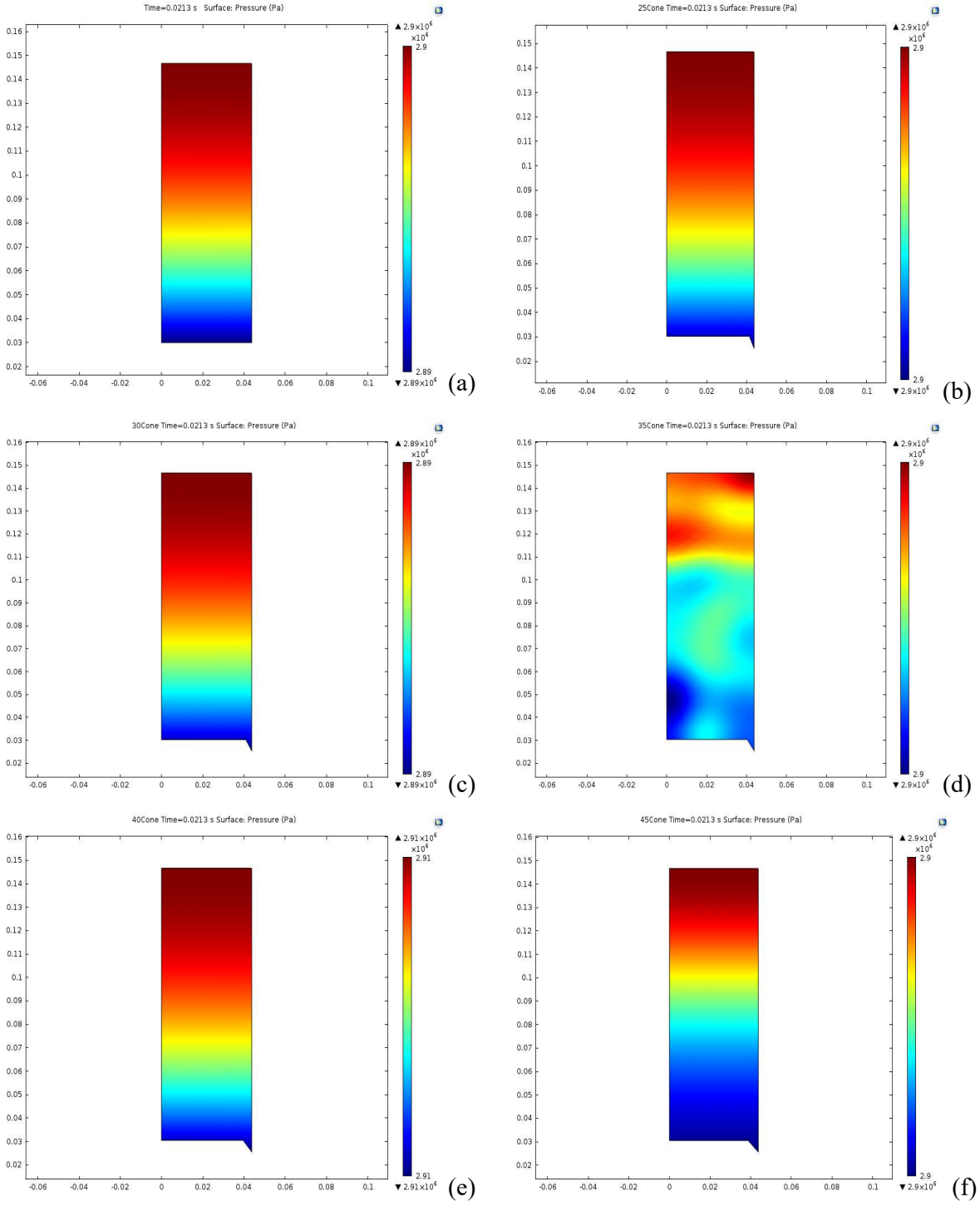

Figure 4.1. Pressure distribution during power stroke in a CI Engine fitted with truncated cone piston crown having a compression ratio of 17.5:1
(a) Unmodified piston crown, (b) 25° TCPC, (c) 30° TCPC, (d) 35° TCPC, (e) 40° TCPC and (f) 45° TCPC

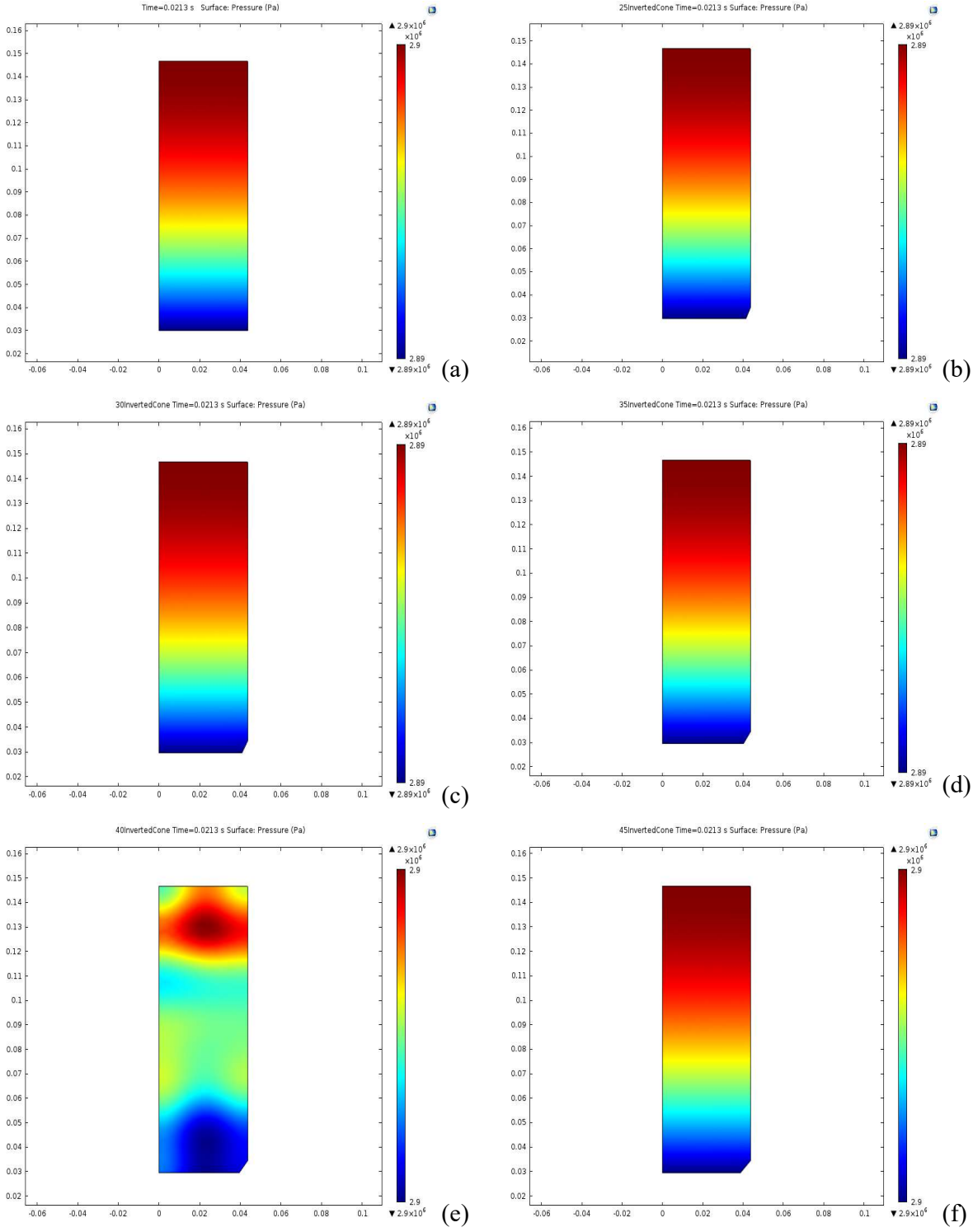

Figure 4.2. Pressure distribution during power stroke in a CI Engine fitted with truncated cone piston crown having a compression ratio of 17.5:1 (a) Unmodified piston crown, (b) 25° ITCPC, (c) 30° ITCPC, (d) 35° ITCPC, (e) 40° ITCPC and (f) 45° ITCPC

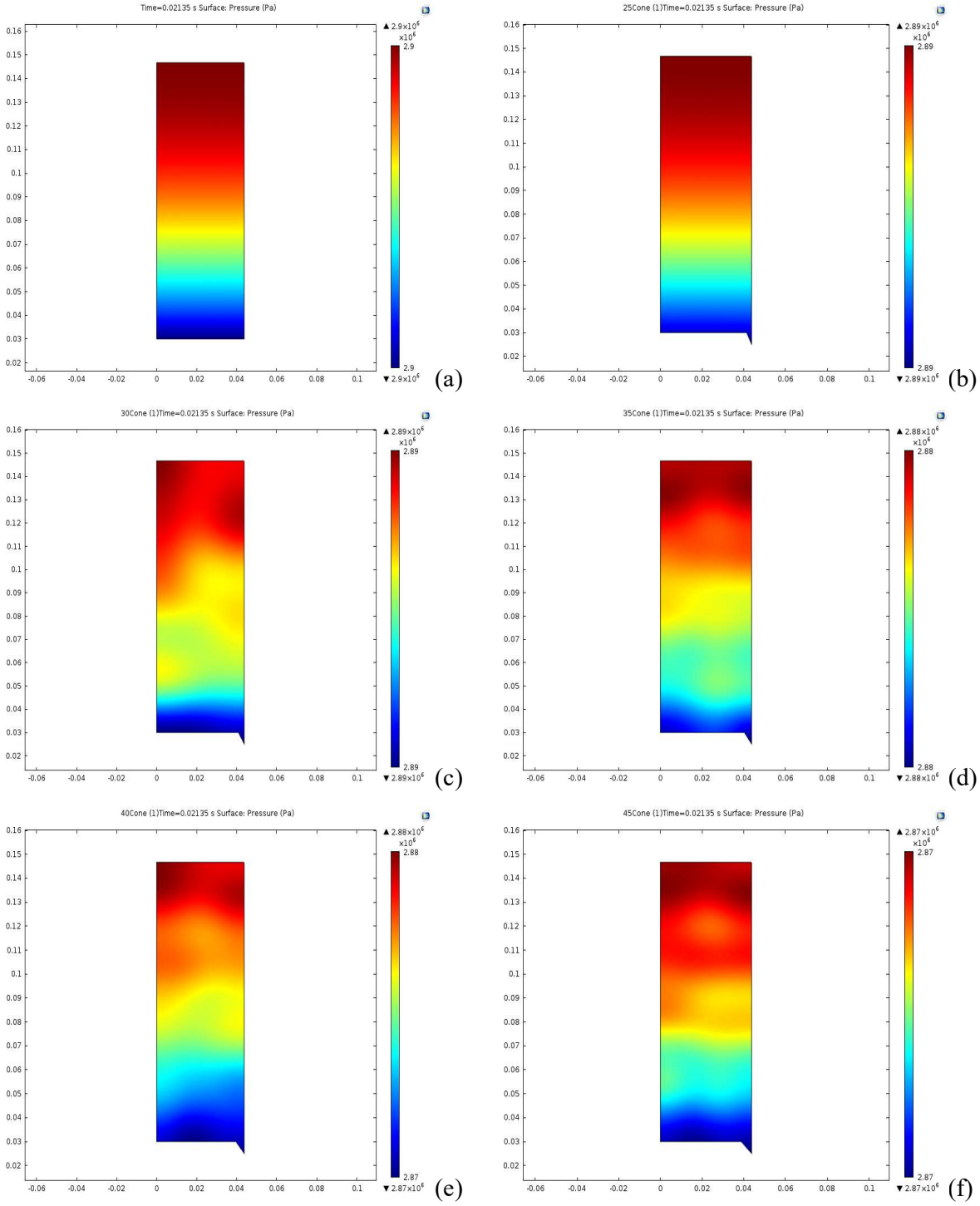

Figure 4.3. Pressure distribution during power stroke in a CI Engine fitted with truncated cone piston crown having different compression ratios (a) Unmodified piston crown, (b) 25° TCPC, CR 16.877:1 (c) 30° TCPC, CR 16.738:1 (d) 35° TCPC, CR 16.589:1 (e) 40° TCPC, 16.426:1 and (f) 45° TCPC, 16.243.

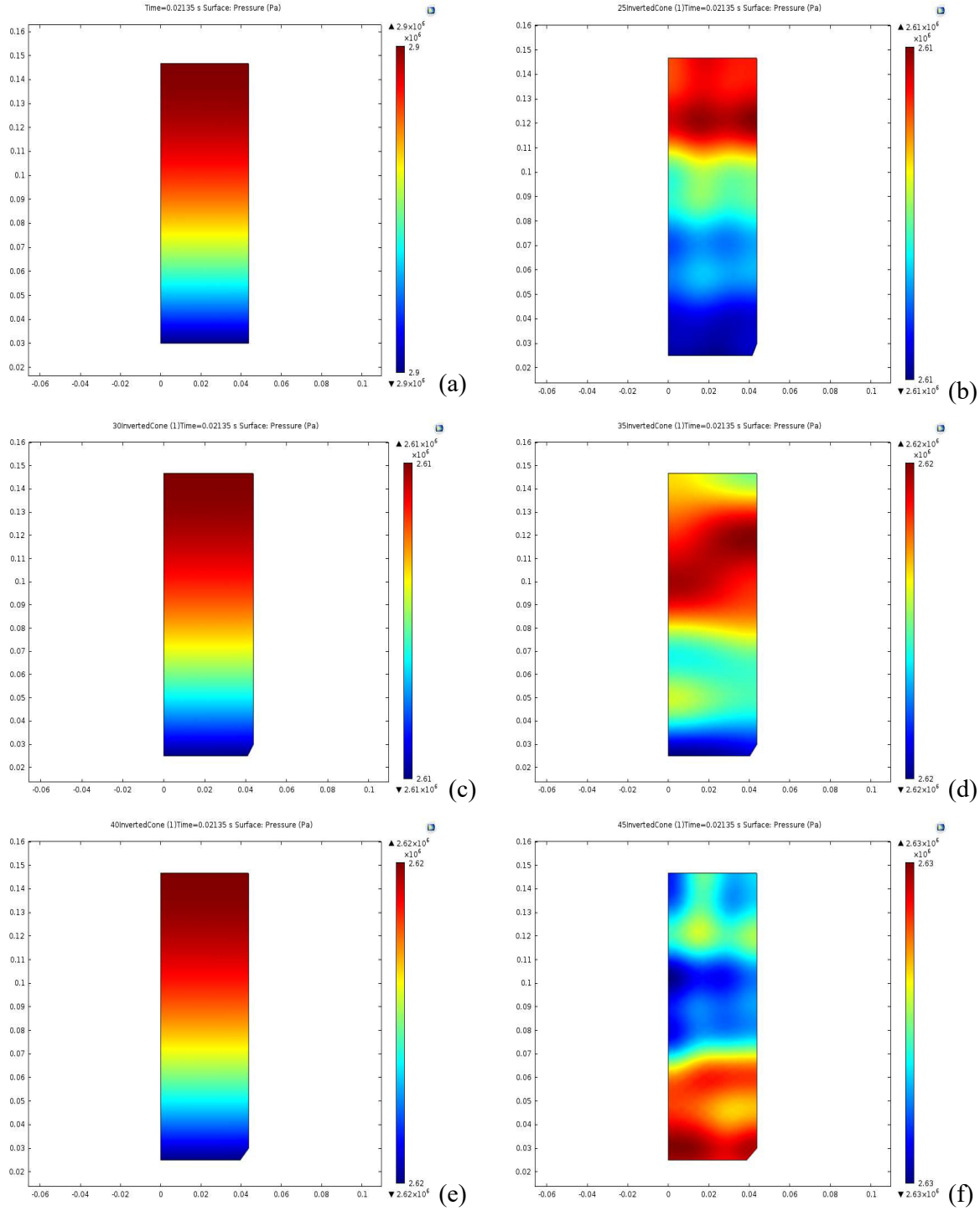

Figure 4.4. Pressure distribution during power stroke in a CI Engine fitted with truncated cone piston crown having different compression ratios (a) Unmodified piston crown, (b) 25° ITCPC, CR 10.6451, (c) 30° ITCPC, CR 10.697:1 (d) 35° ITCPC, CR 10.754:1 (e) 40° ITCPC, 10.819:1 and (f) 45° ITCPC, CR of 10.895:1

As observed from Figure 4.3 the active zone becomes less pronounced as the angle of inclination increases from 25° to 45°, asides from the changes which could have been attributed to the inclination angle of the truncated cone piston crown drawing from the obvious fact that the combustion chamber shape dictates the in-cylinder fluid motion which is a major determinant of a compression ignition engine's performance, another contributing factor is the compression ratio which decreased with the increase of inclination angle. The reverse trend was witnessed for the inverted truncated cone piston crown as observed from Figure 4.4; the active zone becomes more pronounced with the increase in inclination angle, and the compression ratio increased with the increase of inclination angle.

The engine mean pressure has a significant impact on the power output, hence, the area of active pressure zone connotes improved power output.

4.3.2 The Pressure Distributions in the Engine Cylinder for Category II

The cut-plane sections of the numerical models in the vertical direction indicating the pressure distributions through the engine cylinder at selected time periods are as depicted in Figures 4.5 and 4.6. The active zone is more pronounced in the truncated cone piston crown having an inclination angle of 40°, and even as there was a gradual increase in the activeness from an inclination angle of 25° to 40°, a decrease was however observed at 45°. An improved in-cylinder motion facilitated by optimized combustion chamber geometry at a cone base angle of 40^{o} was responsible for the active pressure zone.

4.4 Velocity Distribution inside the Engine Cylinder

The following sections give the details of the velocity distributions inside the engine cylinder when cut-plane sections of the numerical model in the vertical directions are made.

4.4.1 The Velocity Distributions in the Engine Cylinder for Category I

The cut-plane sections of the numerical models in the vertical direction indicating the velocity distributions through the engine cylinder for category I are shown in Figure 4.7, Figure 4.8, Figure 4.9, and Figure 4.10 respectively. As it can be observed from Figures 4.7 to 4.10, the occurrence of active zones (portions with higher velocities) in the engine cylinder is affected by the piston crown geometry. The active velocity zones connote reduced performance, an indication that the kinetic energy was not converted into pressure which is required for doing useful work by the piston.

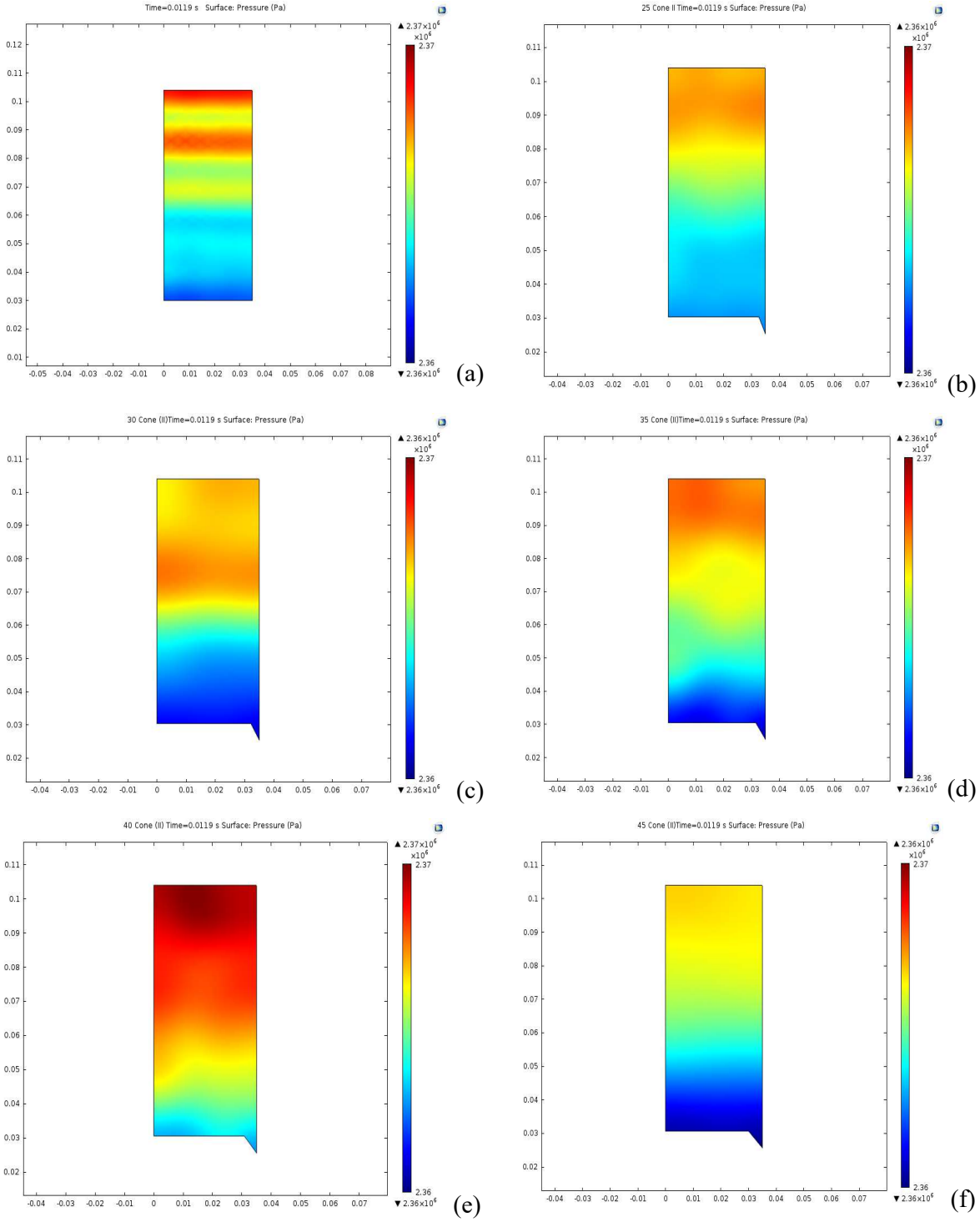

Figure 4.5. Pressure distribution during power stroke in a CI Engine fitted with truncated cone piston crown having a compression ratio of 20.5:1 (a) Unmodified piston crown, (b) 25° TCPC, (c) 30° TCPC, (d) 35° TCPC, (e) 40° TCPC and (f) 45° TCPC

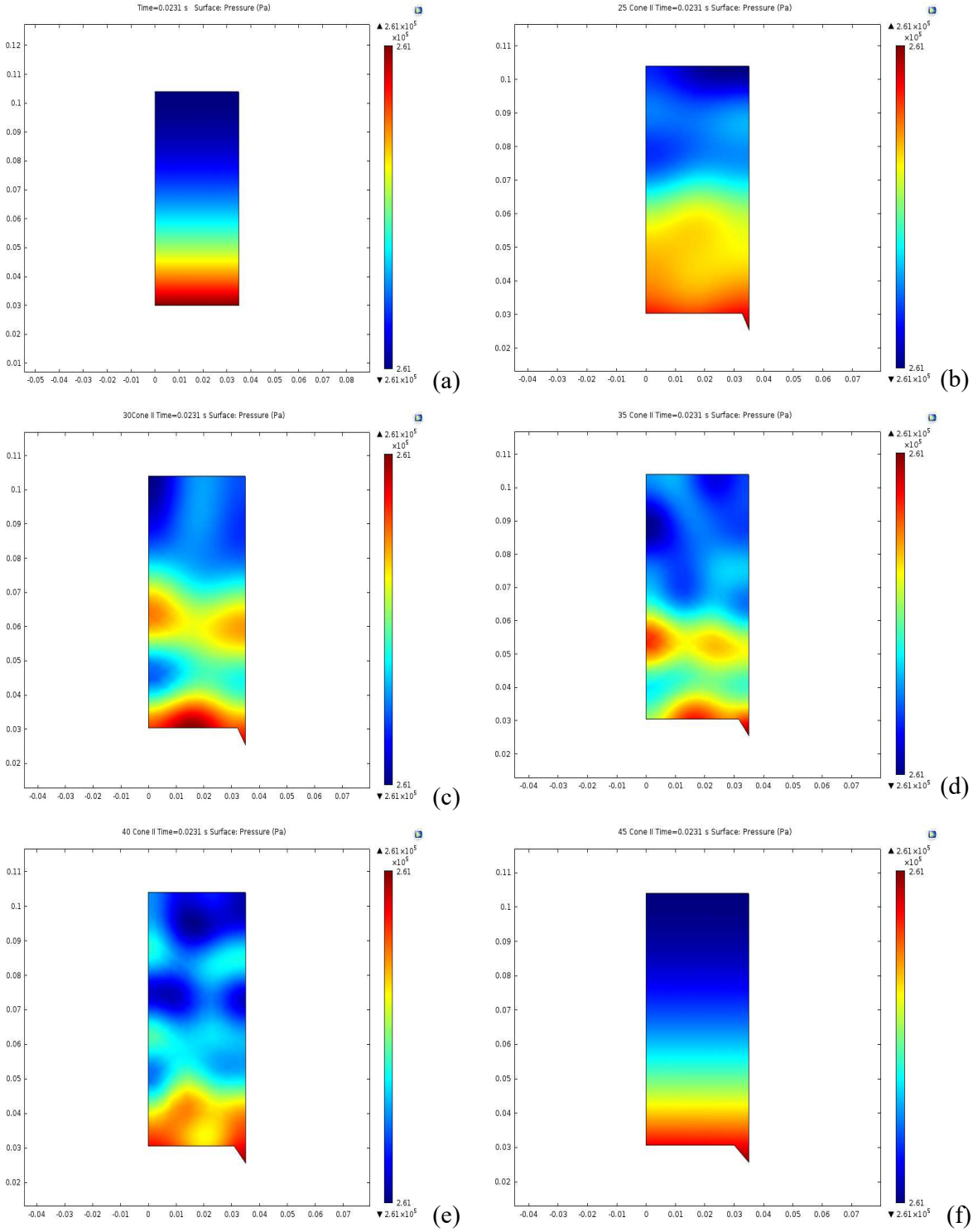

Figure 4.6. Pressure distribution during power stroke in a CI Engine fitted with truncated cone piston crown having a compression ratio of 20.5:1 (a) Unmodified piston crown, (b) 25° TCPC, (c) 30° TCPC, (d) 35° TCPC, (e) 40° TCPC and (f) 45° TCPC

The velocity of the charge inside the engine cylinder was also observed to be a function of the engine's compression ratio as this can be seen by comparing the plots in Figure 4.7 and Figure 4.9, and also Figure 4.8 and Figure 4.10, as the two different categories have the same piston crown configurations but different compression ratios. The lower compression ratio cases have the higher values of charge velocities as the piston moves towards the top dead centre. This is because for high compression ratio, the clearance volume is reduced resulting into reduced space for the combustion charges. The particles of the combustion charge thus collide with each other more often leading to the dissipation of their kinetic energy to a greater extent in comparison to the lower compression ratio cases.

4.4.2 The Velocity Distributions in the Engine Cylinder for Category II

The cut-plane sections of the numerical models in the vertical direction indicating the velocity distributions through the engine cylinder for category II is shown in Figure 4.11. As it can be observed from Figure 4.11, the occurrence of active zones (portions with higher velocities) in the engine cylinder was affected by the piston crown geometry as was in the case of category I.

The velocity of the charge inside the engine cylinder was observed to be least for the truncated cone piston crown with an inclination angle of 40° (Figure 4.11(e)) giving an indication that bulk of its kinetic energy have been converted into pressure energy required for doing useful work than for the other piston crown truncated cone base angles.

4.5 Detailed Graphical Representations of the Numerical Predictions

Here, the discussions of results will be made sequentially according to the selected piston crown shapes and inclination angles investigated to ensure clarity in understanding of presentations. Thus, the presentations are in the following order: for truncated cone piston crown with uniform compression ratio, truncated cone piston crown with different compression ratio, inverted truncated cone piston crown with uniform compression ratio and inverted truncated cone piston crown with different compression ratio under Category I of study, and the unmodified piston crown used as the standard.

The discussions of results for Category II of the studies would follow in the next section for the truncated and inverted truncated cone piston crowns with uniform compression ratio and the unmodified piston crown used as the standard.

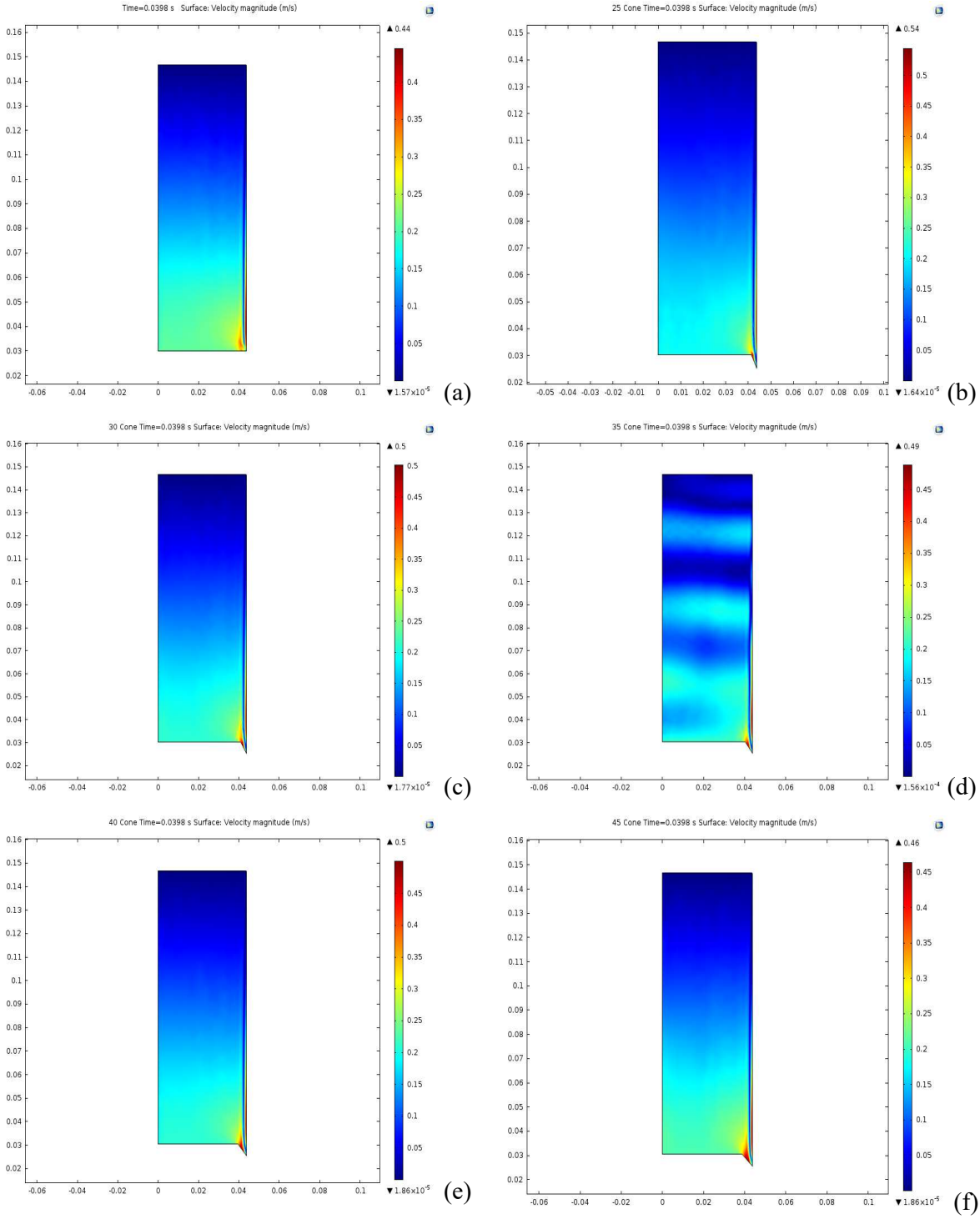

Figure 4.7. Velocity distribution during power stroke in a CI Engine fitted with truncated cone piston crown having a compression ratio of 17.5:1
(a) Unmodified piston crown, (b) 25° TCPC, (c) 30° TCPC, (d) 35° TCPC, (e) 40° TCPC and (f) 45° TCPC

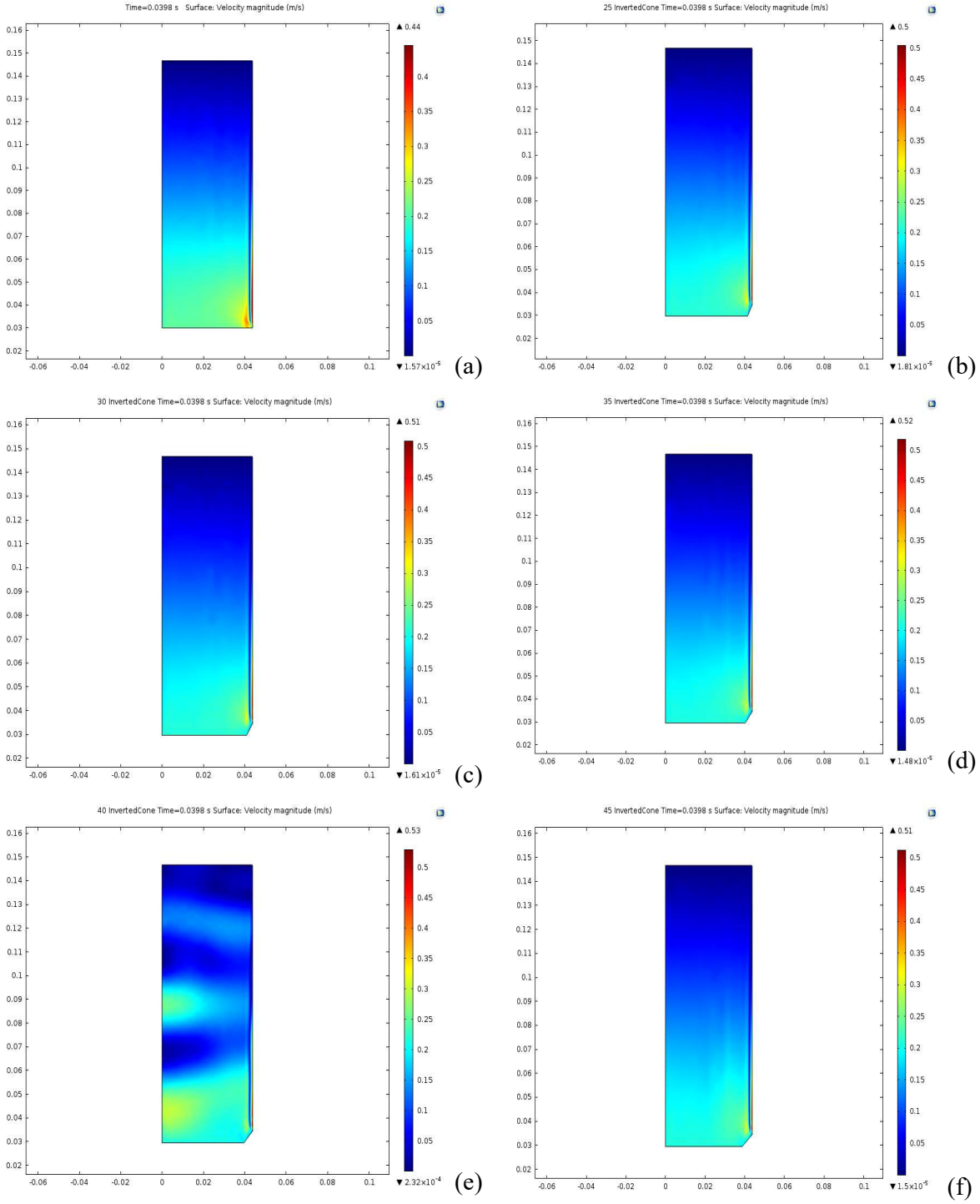

Figure 4.8. Velocity distribution during power stroke in a CI Engine fitted with inverted truncated cone piston crown having a compression ratio of 17.5:1
(a) Unmodified piston crown, (b) 25° ITCPC, (c) 30° ITCPC, (d) 35° ITCPC, (e) 40° ITCPC and (f) 45° ITCPC

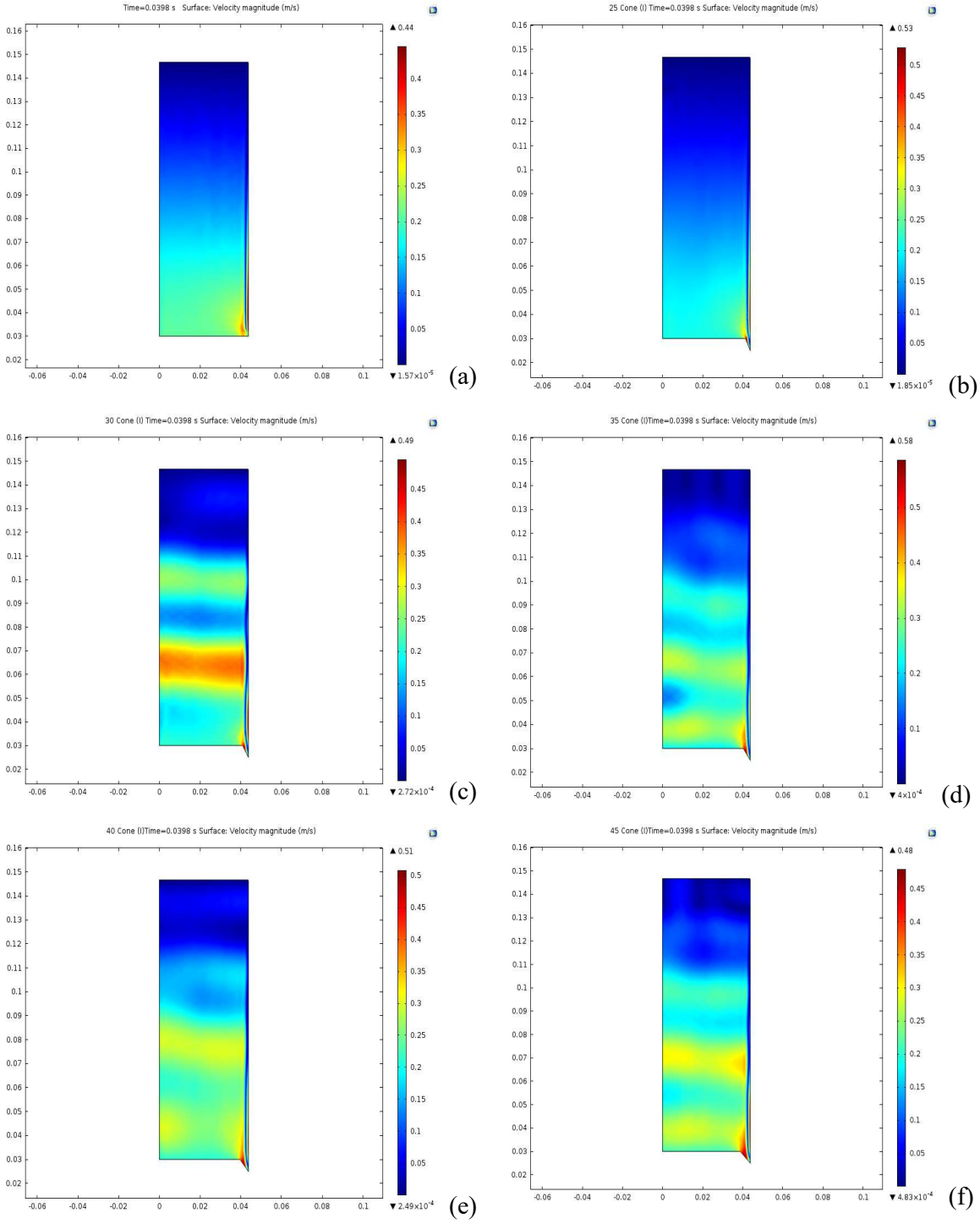

Figure 4.9. Velocity distribution during power stroke in a CI Engine fitted with truncated cone piston crown having different compression ratios (a) Unmodified piston crown, (b) 25° TCPC, CR 16.877:1 (c) 30° TCPC, CR 16.738:1 (d) 35° TCPC, CR 16.589:1 (e) 40° TCPC, 16.426:1 and (f) 45° TCPC, 16.243.

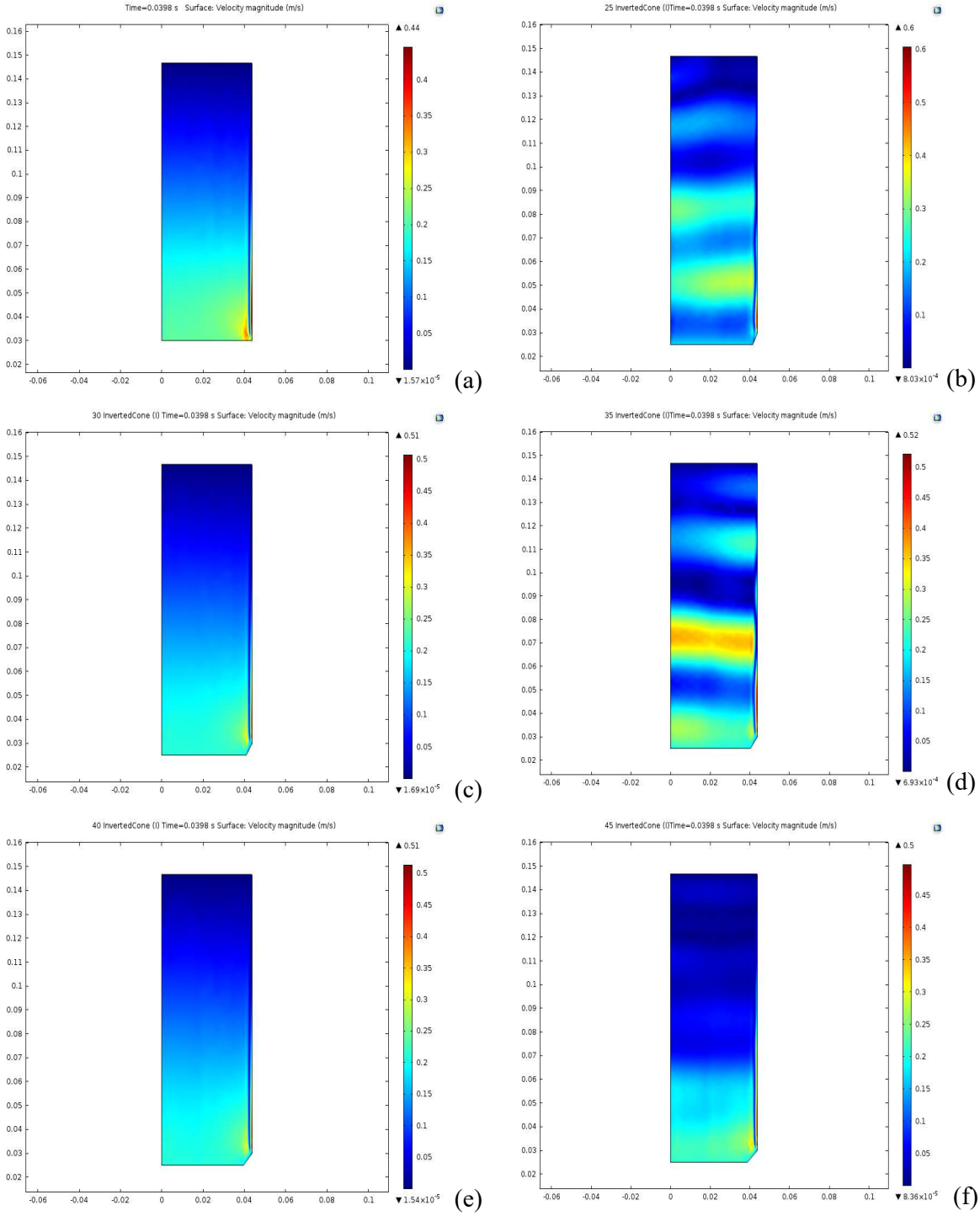

Figure 4.10. Velocity distribution during power stroke in a CI Engine fitted with inverted truncated cone piston crown having different compression ratios (a) Unmodified piston crown, (b) 25° ITCPC, CR 10.6451, (c) 30° ITCPC, CR 10.697:1 (d) 35° ITCPC, CR 10.754:1 (e) 40° ITCPC, 10.819:1 and (f) 45° ITCPC, CR of 10.895:1

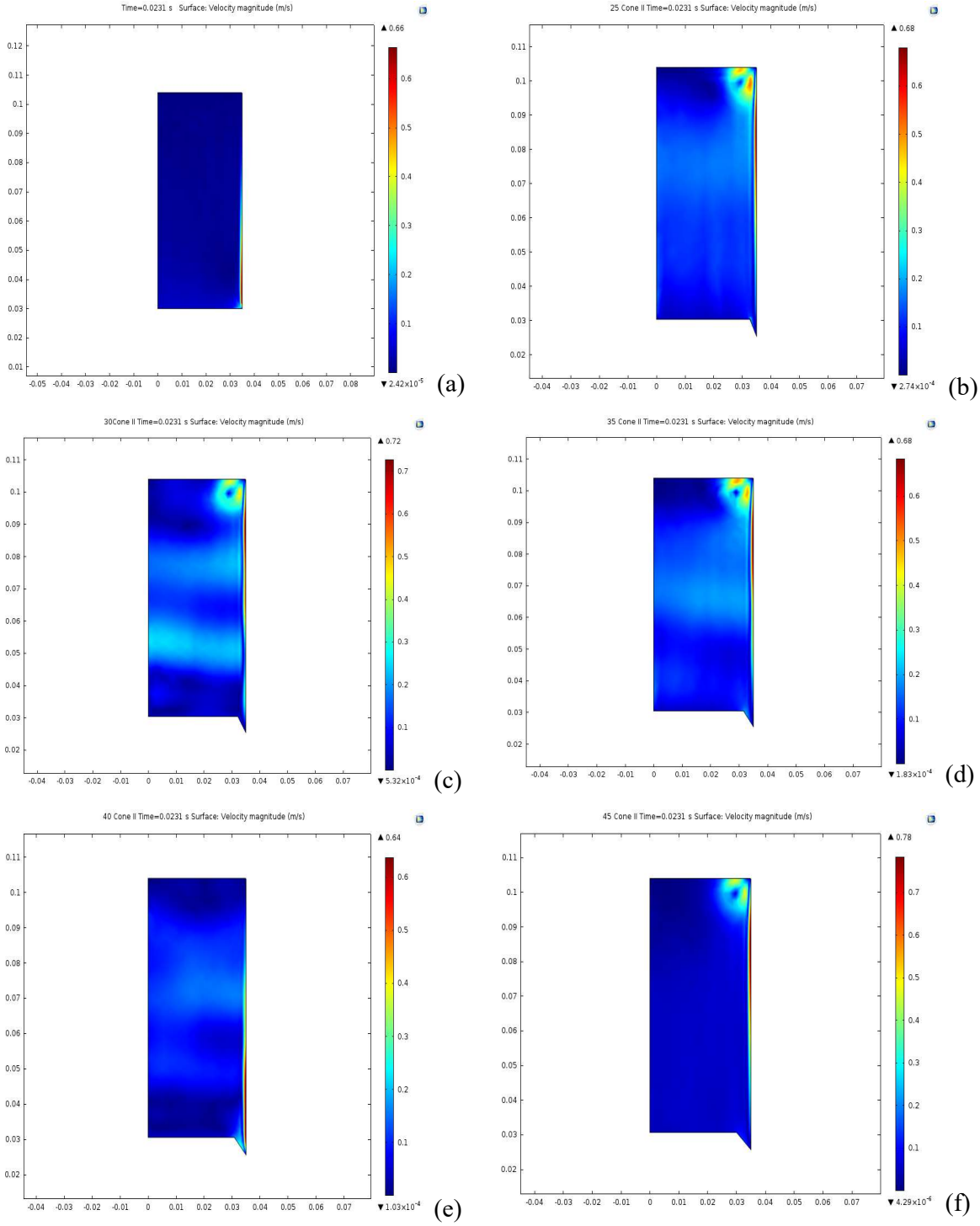

Figure 4.11. Velocity distribution during exhaust stroke fitted with truncated cone piston crown with a compression ratio of 20.5:1
(a) Unmodified piston crown, (b) 25° TCPC, (c) 30° TCPC, (d) 35° TCPC, (e) 40° TCPC and (f) 45° TCPC

4.5.1 Engine Cylinder Pressure Simulations of Truncated Cone Piston Crown with Constant Compression Ratio for Category I

The engine pressures (bar) versus cylinder volume (cc) plots and the corresponding pressure (bar) versus crank angle degrees for the simulation of the unmodified piston and that of the truncated cone piston crown of the different angles of inclination while maintaining a constant compression ratio is depicted in Figure 4.12.

The pressure value of the simulated engine when fitted with the unmodified and the truncated cone piston crown of varying angles of inclination look very close. This is the reason why the last plot (inclination angle of 45° seems to be the most conspicuous, although traces of others too appears in the background giving an indication that there still exists some little differences between the plots which definitely have an effect on the engine performance.

The individual plots are shown in Figure 4.13 to 4.18, and an explanation of the differences observed are stated.

The peak pressure value for the unmodified piston depicted in Figure 4.13 is 92.72 bar and the net work done per cycle by the engine from the heat energy derived from the fuel combustion as calculated from the area enclosed by the pressure – volume curve is -481.64 J.
The heat energy derived by the engine as obtained from the simulation is 1558.62 J.
The engine attains the peak pressure value at 7° after the top dead centre (aTDC)

Peak pressure value for the 25° truncated cone piston crown equipped engine as depicted in Figure 4.14 is 92.83 bar and the net work produced per cycle by the engine as calculated from the area enclosed by the pressure – volume curve is -483.25 J.
The heat energy derived from the combustion of the fuel by the engine is 1564.90 J
The peak pressure value was attained 8° after top dead centre (aTDC)

A peak pressure value of 92.63 bar at 8.5° after top dead centre (aTDC) was gotten for the simulation of the engine when fitted with a modified truncated cone piston crown at an inclination angle of 30° as depicted in Figure 4.15.The net work done as calculated from the area enclosed by the pressure – volume curve is -480.93 J, and the heat energy derived from the fuel combustion is 1560.00 J
The net work obtained from the simulated engine fitted with a modified piston crown of truncated cone geometry at an angle of inclination of 35° to the vertical -483.97 J. The derived heat energy from the fuel combustion in the engine is 1564.74 J. A peak pressure value of 92.95 bar was recorded for the simulated engine and this occurs at 8.6° after the top dead centre (aTDC).

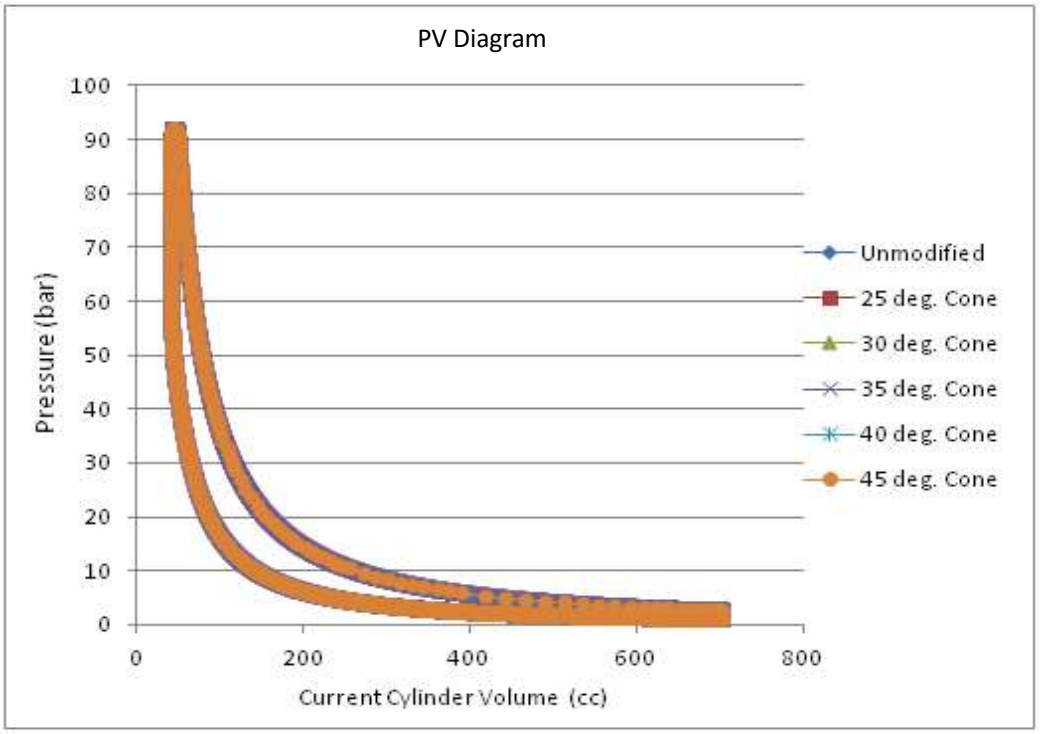

(a)

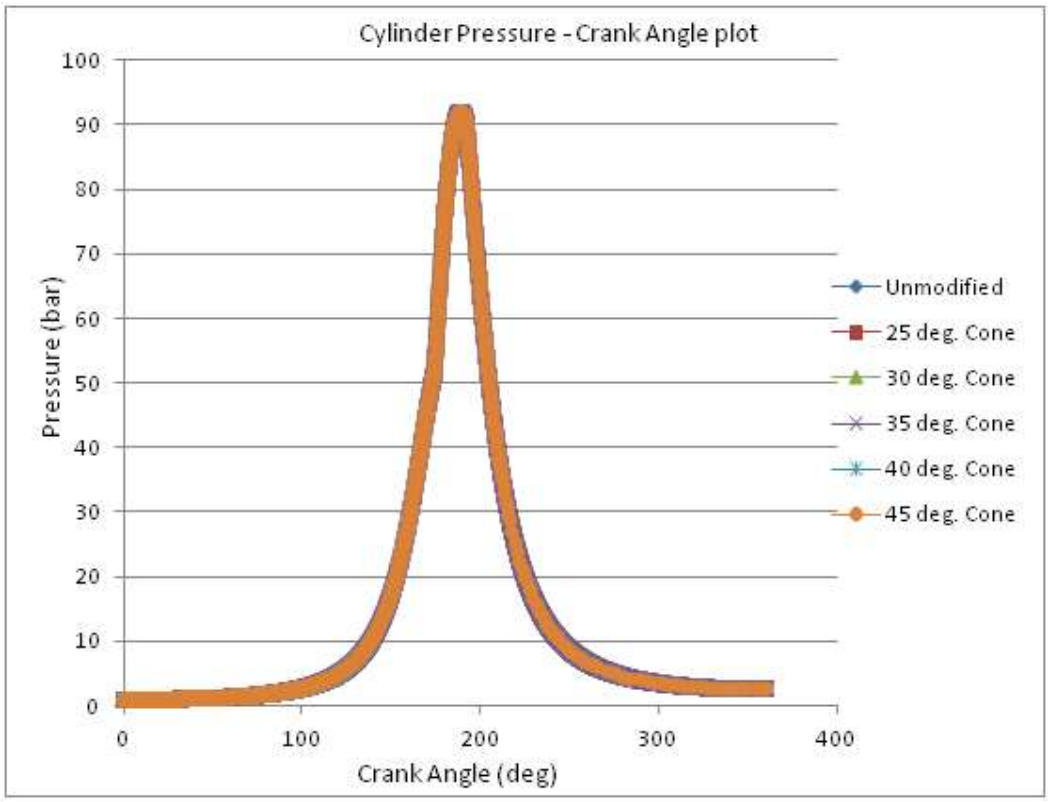

(b)

Figure 4.12. Pressure curve of the simulated CI Engine fitted with truncated cone piston crown with compression ratio of 17.5:1 (a) Pressure-Volume and (b) Pressure-Crank angle

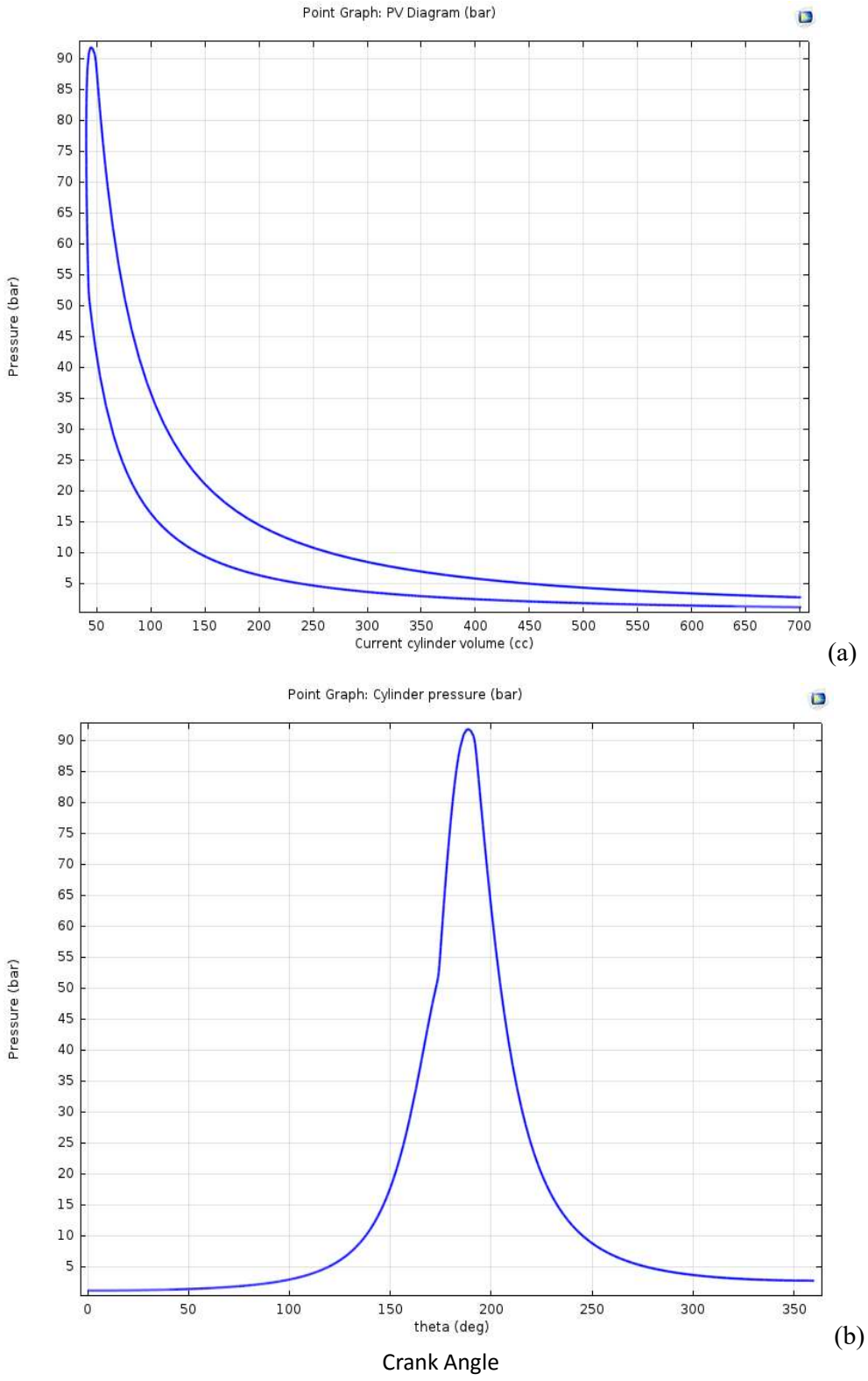

Figure 4.13. Pressure curve of the simulated CI Engine fitted with unmodified piston with compression ratio of 17.5:1 (a) Pressure-Volume and (b) Pressure-Crank angle

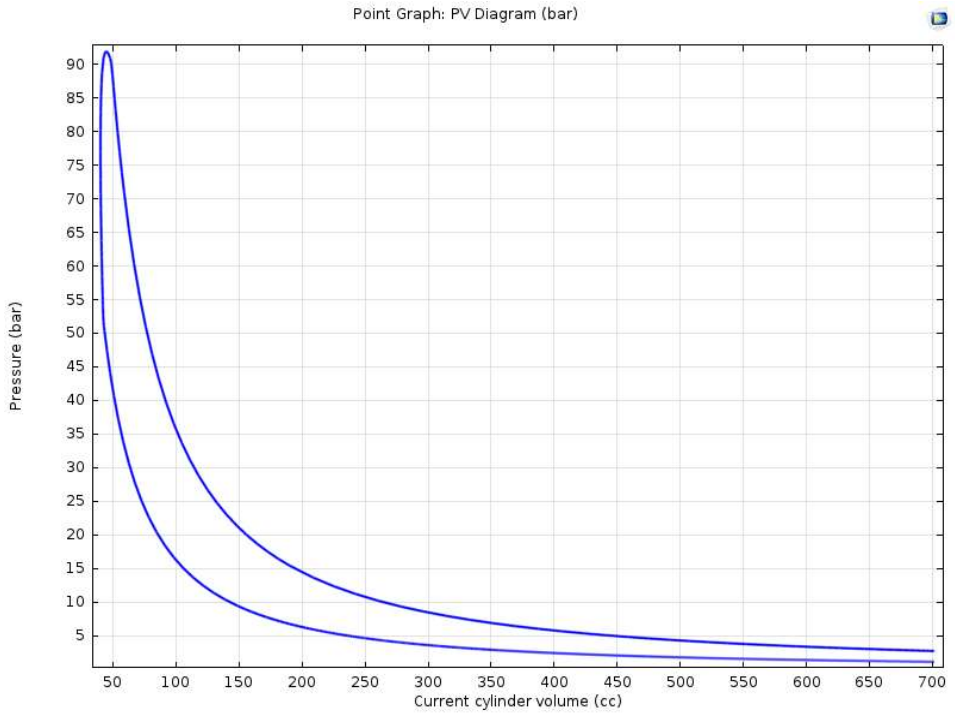

(a)

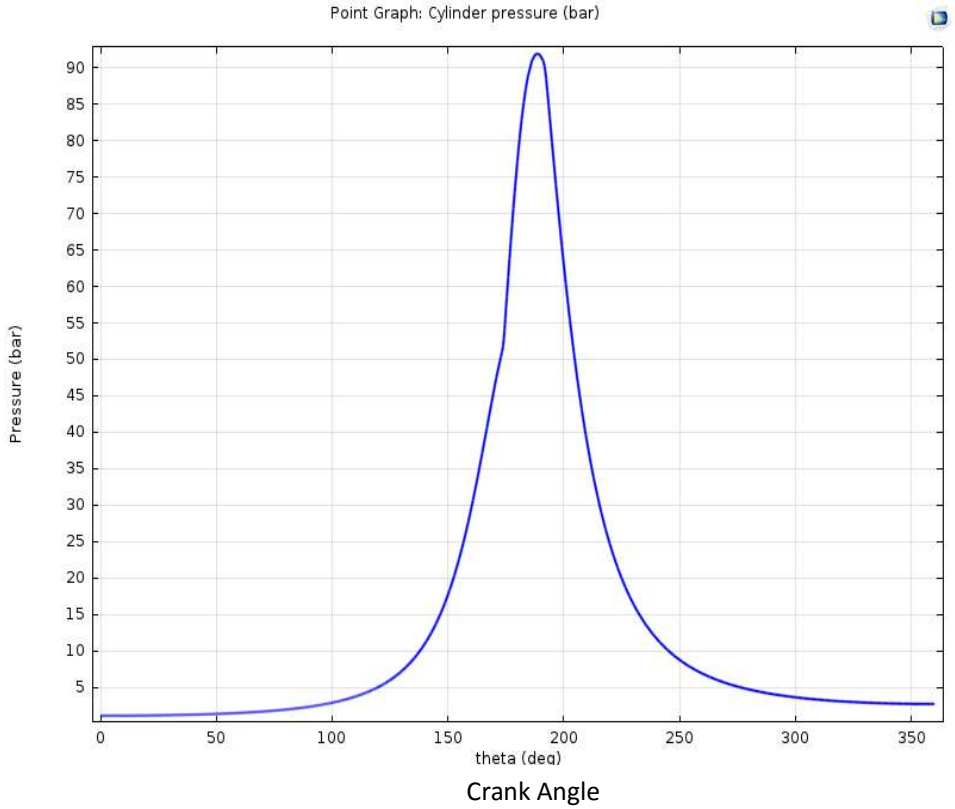

(b)

Crank Angle

Figure 4.14. Pressure curve of the simulated CI Engine fitted with 25^0 truncated cone piston crown with compression ratio of 17.5:1 (a) Pressure-Volume and (b) Pressure-Crank angle

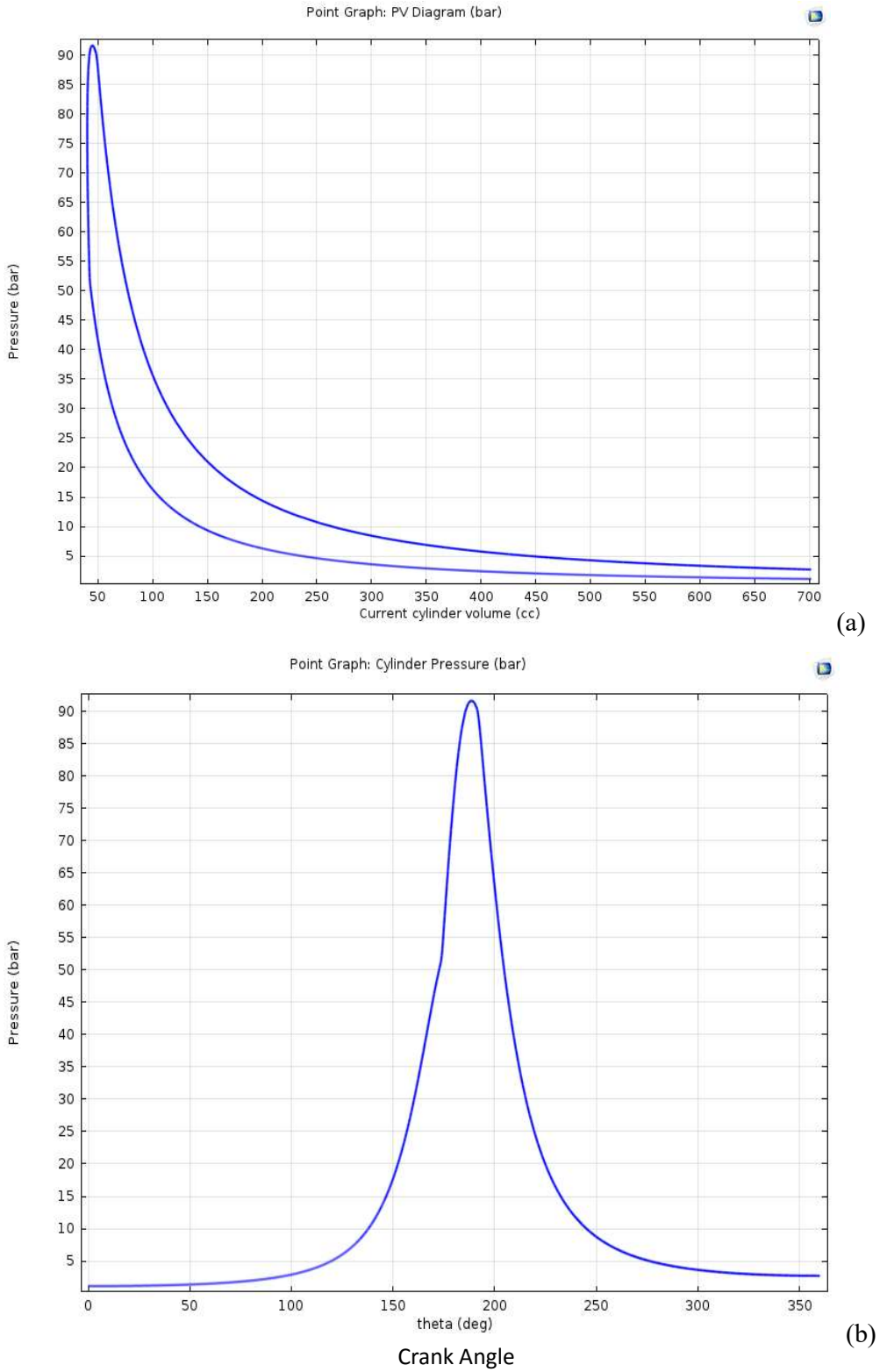

Figure 4.15. Pressure curve of the simulated CI Engine fitted with 30^0 truncated cone piston crown with compression ratio of 17.5:1 (a) Pressure-Volume and (b) Pressure-Crank angle

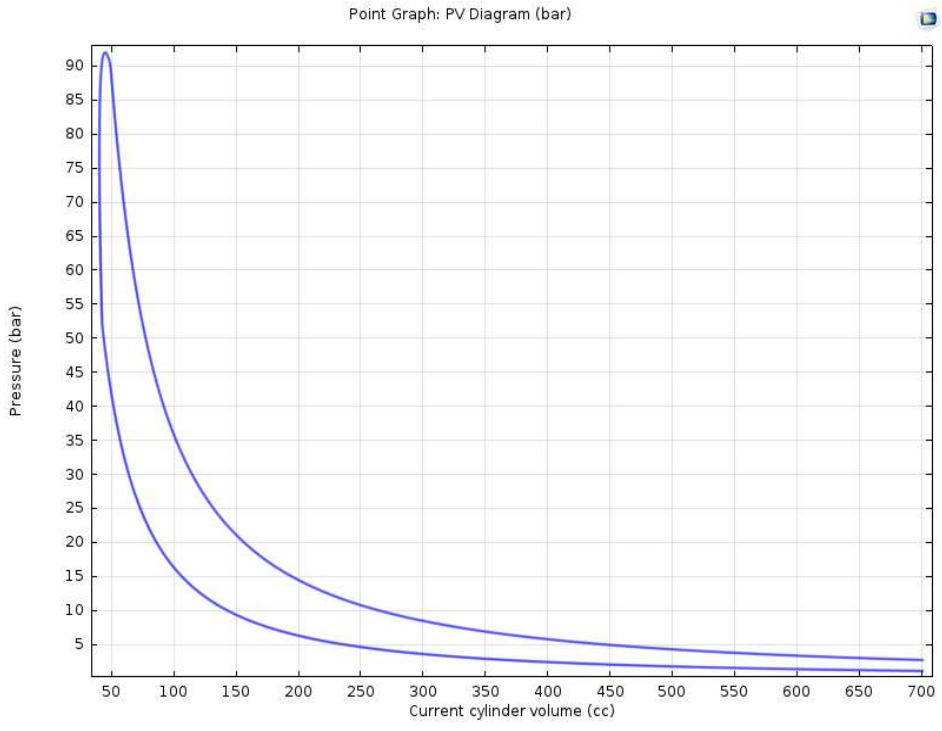

(a)

(b)

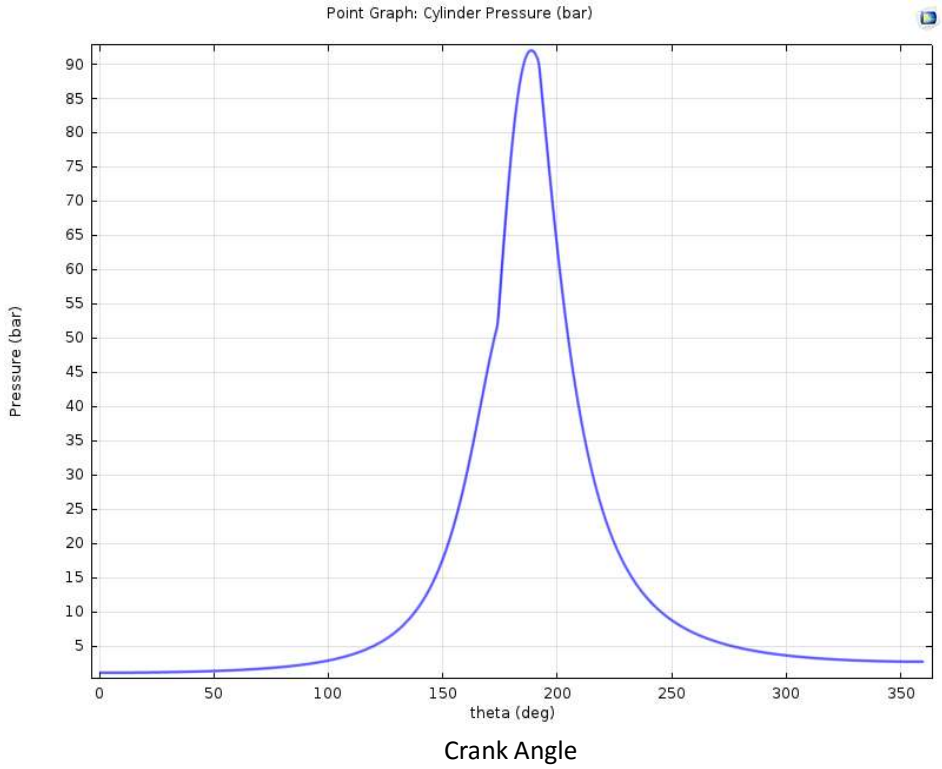

Crank Angle

Figure 4.16. Pressure curve of the simulated CI Engine fitted with 35^0 truncated cone piston crown with compression ratio of 17.5:1 (a) Pressure-Volume and (b) Pressure-Crank angle

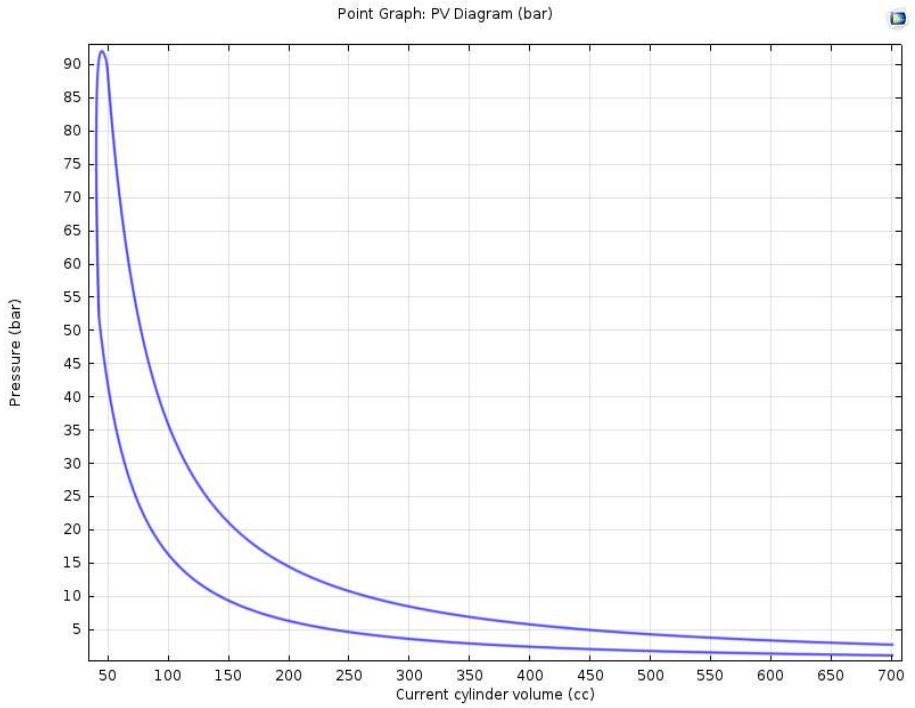

(a)

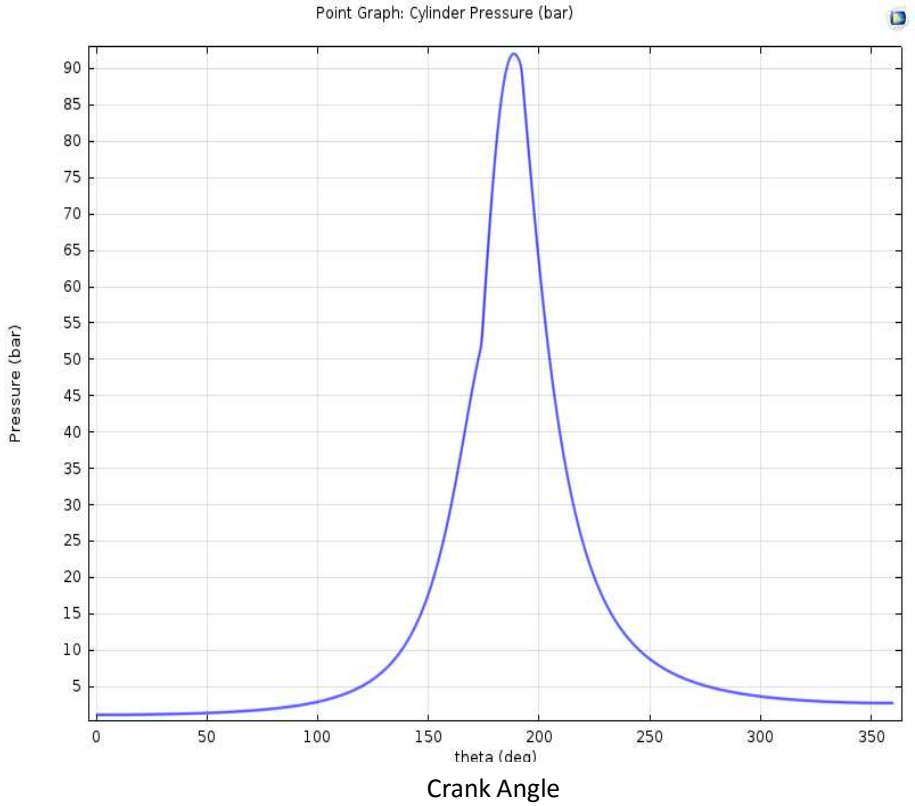

(b)

Crank Angle

Figure 4.17. Pressure curve of the simulated CI Engine fitted with 40^0 truncated cone piston crown with compression ratio of 17.5:1 (a) Pressure-Volume and (b) Pressure-Crank angle

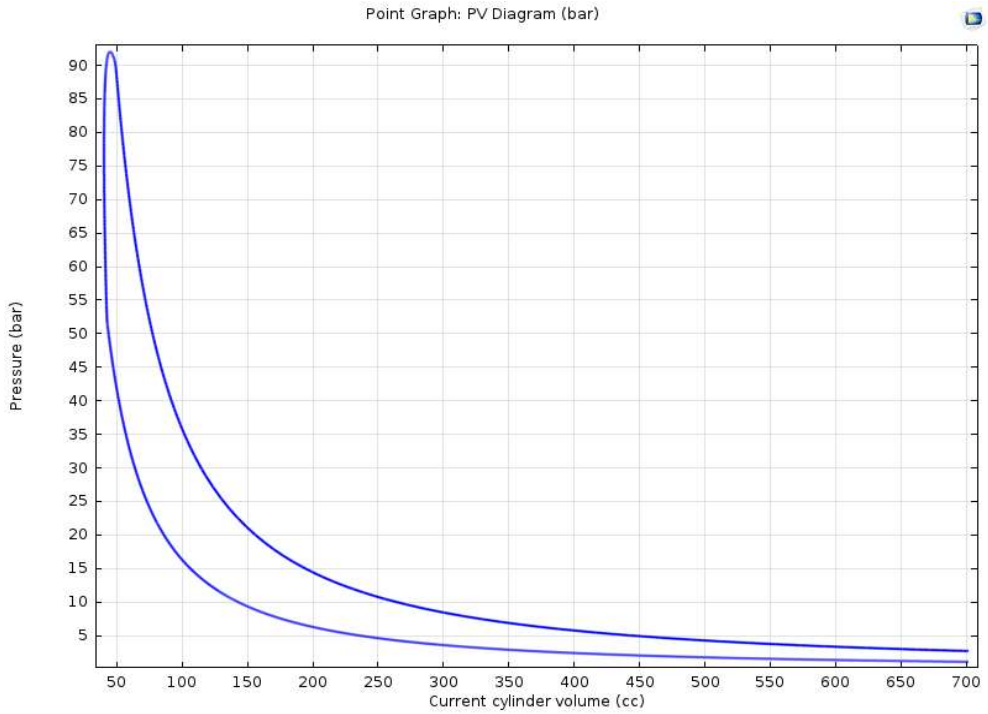

(a)

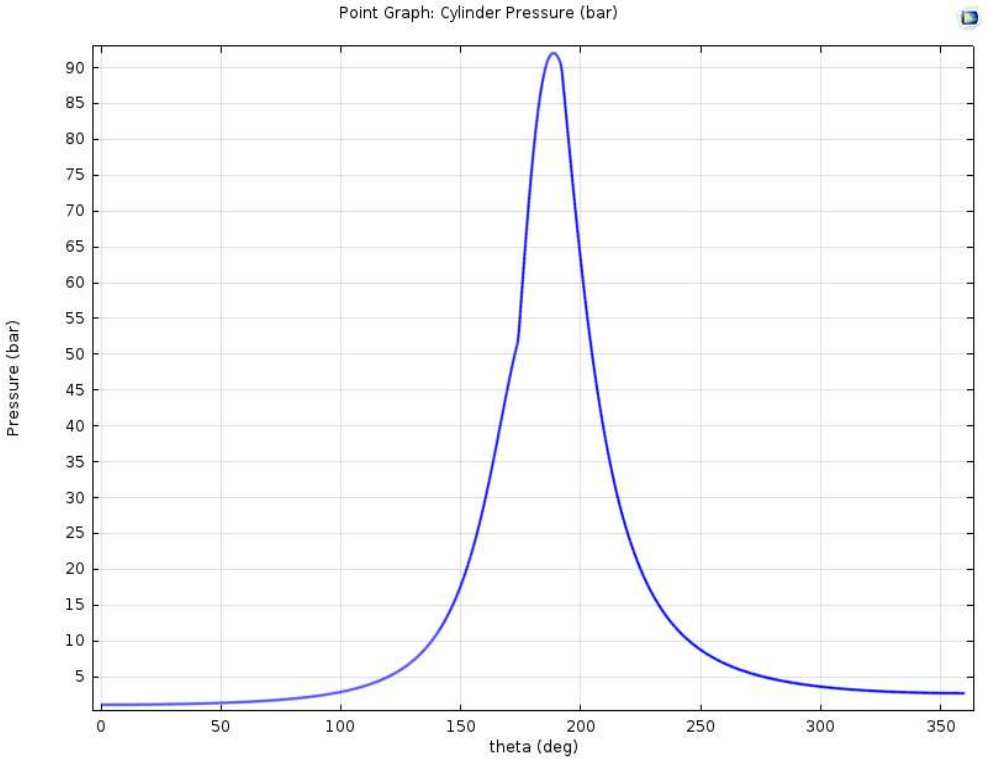

(b)

Crank Angle

Figure 4.18. Pressure curve of the simulated CI Engine fitted with 45^0 truncated cone piston crown with compression ratio of 17.5:1 (a) Pressure-Volume and (b) Pressure-Crank angle

A peak pressure value of 93.04 bar at 8.5° after top dead centre (aTDC) was gotten for the simulation of the engine when fitted with a modified truncated cone piston crown at an inclination angle of 40° as depicted in Figure 4.17. The net work done as calculated from the area enclosed by the pressure – volume curve is -486.41 J, and the heat energy derived from the fuel combustion is 1573.88 J

The net work done as calculated from the area enclosed by the pressure – volume curve is -483.05 J, and the heat energy derived from the fuel combustion is 1564.94 J. A peak pressure value of 92.96 bar at 8.5° after top dead centre (aTDC) was obtained for the simulation of the engine when fitted with a modified truncated cone piston crown at a truncated cone base angle of 45°.

A summary of the findings from the simulation of the engine when fitted with truncated cone piston crown is shown in Table 4.1. The determined pressure values and heat values are important parameters used in the determination of the performance characteristics of the engine.

The derived peak pressure values were in agreement with the peak pressure value of 93 bar reported by Ghafouri *et al.* (2014) while working with a compression ignition engine with bore 120.65 mm, stroke of 140 mm and speed of 1000 rpm. It is not markedly different when compared with the result of Basha *et al,* (2009) who reported peak pressure value of 78 bar while working with a CI engine of 78 mm bore, stroke length of 151 mm, speed of 2400 rpm and with an injection start period of 25^0 bTDC.

The peak pressure values as observed from the plots for the angles of inclination 25°, 35°, 40° and 45° were higher than for the unmodified piston. This leads to greater values of net work done in comparison to the unmodified piston.

The net work produced by the simulated engine fitted with a truncated cone piston at an inclination angle of 40° was the highest in value, and at the same time had the highest value of heat energy derived from the combustion of the fuel.

This is an indication of better performance in terms of power generation in comparison to the engine working on the unmodified piston.

4.5.2 Engine Cylinder Pressure Simulations of Truncated Cone Piston Crown with Different Compression Ratio for Category I

The engine pressure - cylinder volume plots and the corresponding pressure - crank angle plots for the unmodified piston, and for the truncated cone piston crown equipped engine

Table 4.1: Performance parameter estimates for the TCPC with constant CR for category I

Piston Crown Type (TCPC)	**Net Work (J)**	**Heat Energy (J)**	**Peak Pressure (bar)**	**Peak Pressure Position (°aTDC)**
Unmodified	481.64	1558.62	92.72	7
25°	483.25	1564.90	92.83	8
30°	480.93	1560.00	92.63	8.5
35°	483.97	1564.74	92.95	8.6
40°	486.41	1573.89	93.04	8.5
45°	483.05	1564.94	92.96	8.5

using the different cone-base angles is as shown below in Figure 4.19. The compression ratio of the truncated cone equipped compression ignition engine at this instance varies with the cone-base angle.

The pressure versus the volume and pressure versus crank angle of the simulated engine when fitted with the unmodified and the truncated cone piston crown of varying cone base angles having different compression ratios is shown in Figure 4.19.

The peak pressure value attained from the engine simulation was highest for the unmodified piston which has the highest compression ratio value of 17.5:1. The same trend was followed for the modified pistons with the peak pressure value decreasing as the compression ratio reduces.

The plots of the individual modified pistons of the different cone base angles follows in Figure 4.20 to 4.24.

A peak pressure value of 89.45 bar at 8.4° after top dead centre (aTDC) was obtained for the simulation of the engine when fitted with a modified truncated cone piston crown at an inclination angle of 25° and having a compression ratio of 16.877:1.The net work produced is -480.45 J, and the heat energy derived from the fuel combustion is 1567.34 J as shown in Figure 4.20.

A peak pressure value of 88.75 bar at 9° after top dead centre (aTDC) was recorded for the engine when fitted with a modified truncated cone piston crown at an inclination angle of 30° having a compression ratio of 16.738:1 as depicted in Figure 4.21. The net work done is -479.83 J, and the heat energy derived from the fuel combustion is 1567.74 J

The peak pressure was 87.94 bar at 9° after top dead centre (aTDC) for the simulation of the engine when fitted with a modified truncated cone piston crown at an inclination angle of 35° and having a compression ratio of 16.589:1 as depicted in Figure 4.22. The net work done as calculated from the area enclosed by the pressure – volume curve is -478.99 J, and the heat energy derived from the fuel combustion is 1567.74 J

The plots of pressure versus volume and crank angle is as shown in Figure 4.23, the net work done is -478.05 J, and the heat energy derived from the fuel combustion is 1564.74 J. A peak pressure value of 87.04 bar at 9. 2° after top dead centre (aTDC) was derived from the simulation of the engine when fitted with a modified truncated cone piston crown at an inclination angle of 40° and having a compression ratio of 16.426:1.

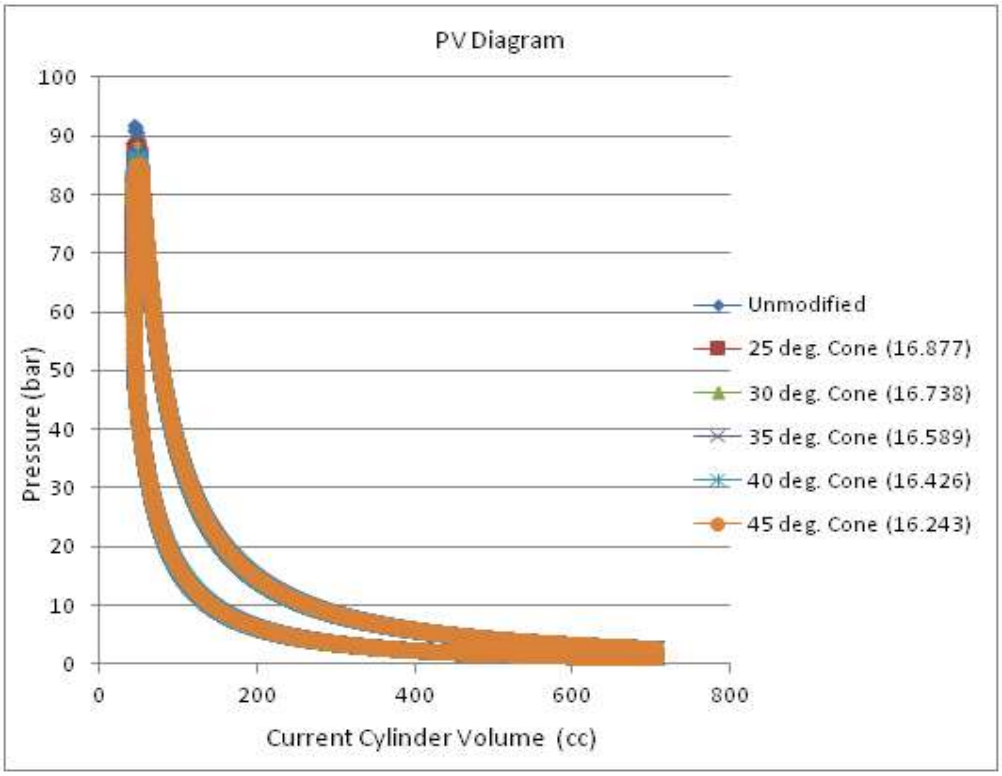

(a)

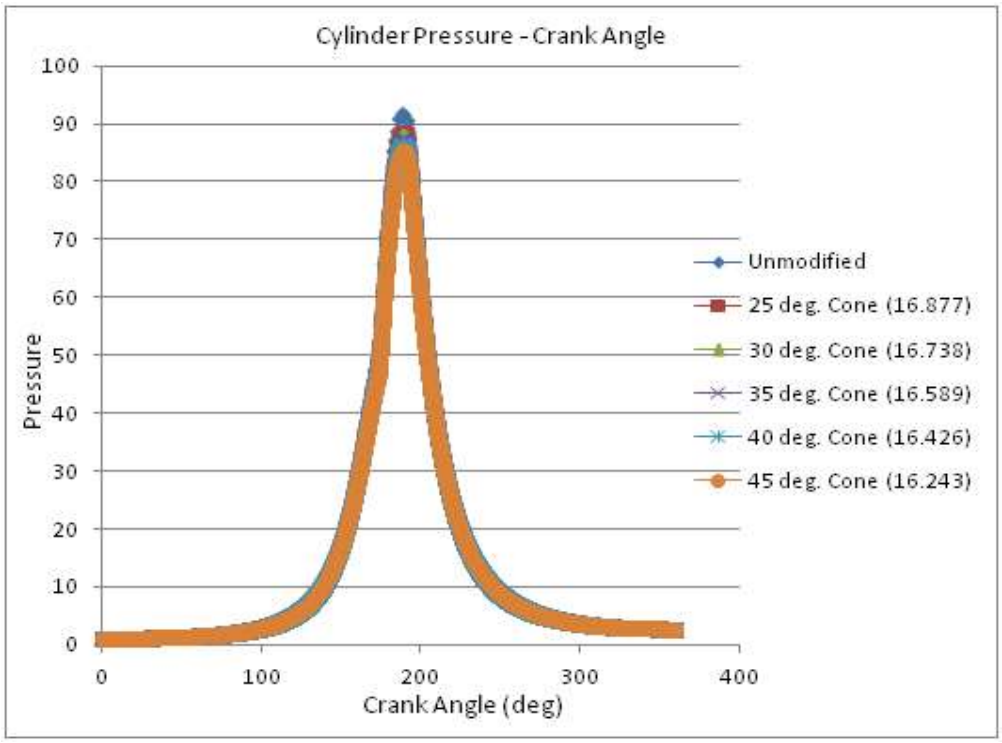

(b)

Figure 4.19. Pressure curve of the simulated CI Engine fitted with truncated cone piston crown at different compression ratios (a) Pressure-Volume, (b) Pressure-Crank angle

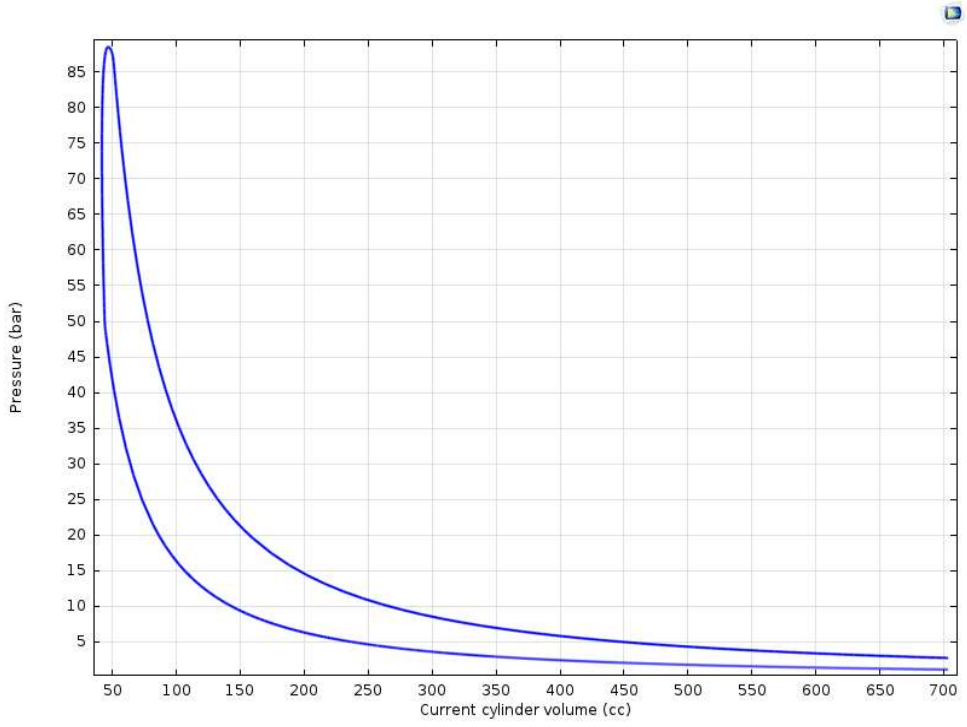

(a)

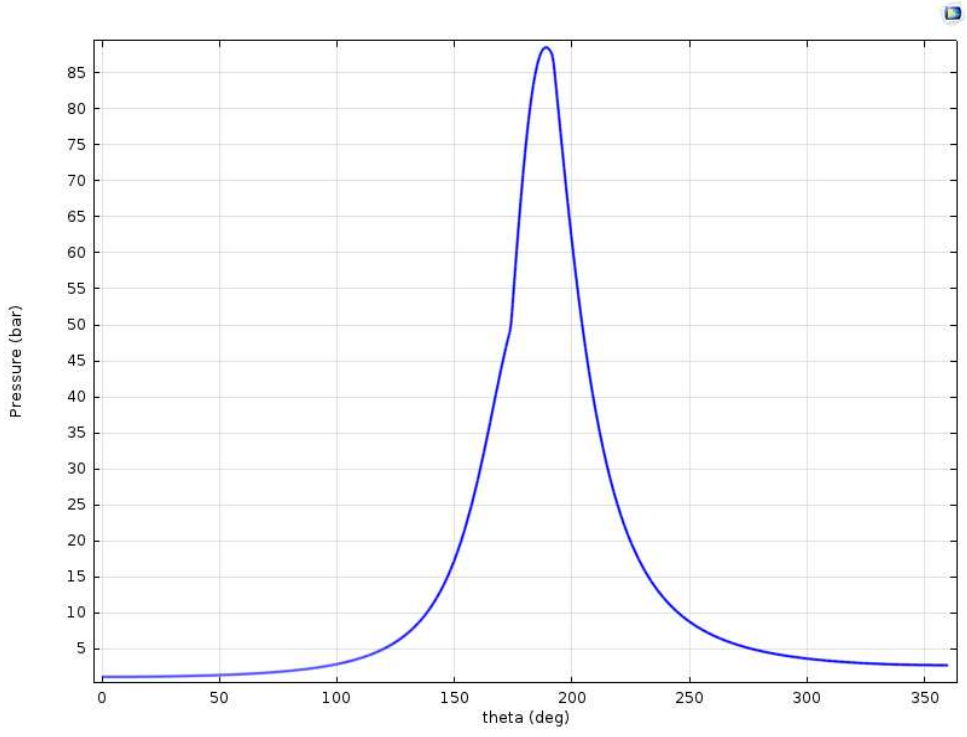

(b)

Crank Angle

Figure 4.20. Pressure curve of the simulated CI Engine fitted with 25^0 truncated cone piston crown with compression ratio of 16.877:1 (a) Pressure-Volume, (b) Pressure-Crank angle

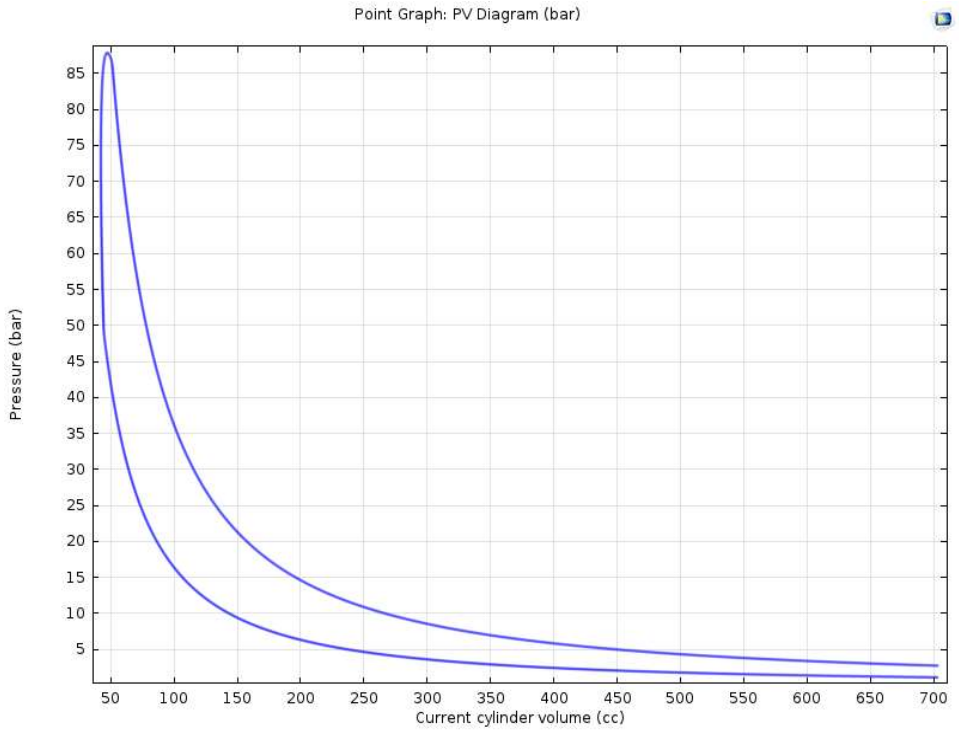

(a)

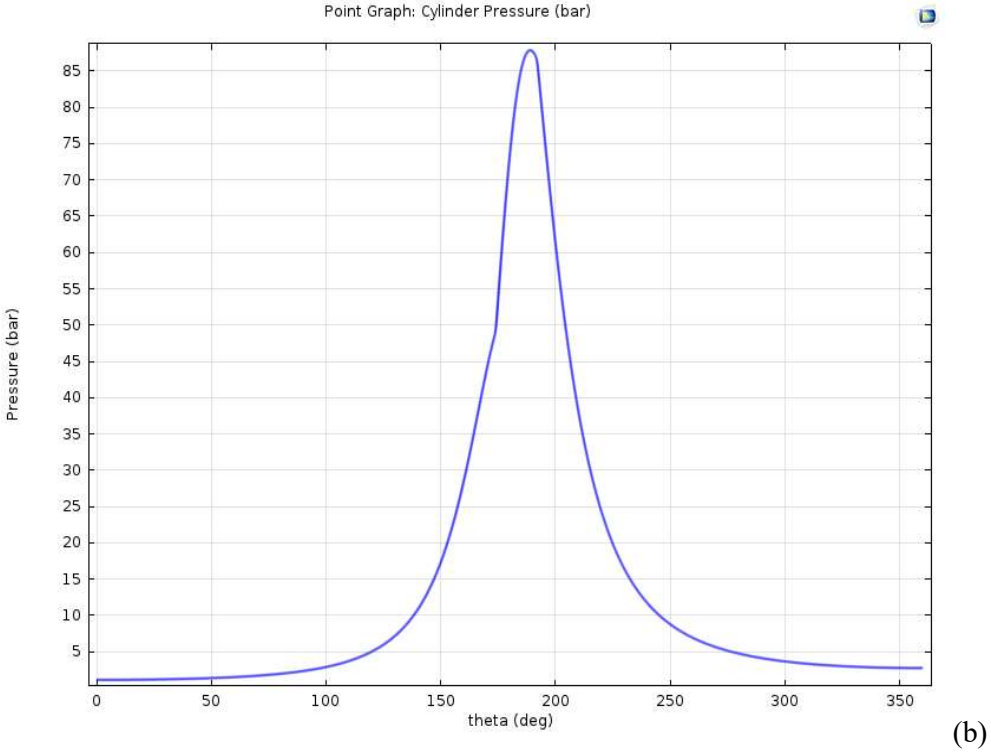

(b)

Crank Angle

Figure 4.21. Pressure curve of the simulated CI Engine fitted with 30^0 truncated cone piston crown with compression ratio of 16.738:1 (a) Pressure-Volume, (b) Pressure-Crank angle

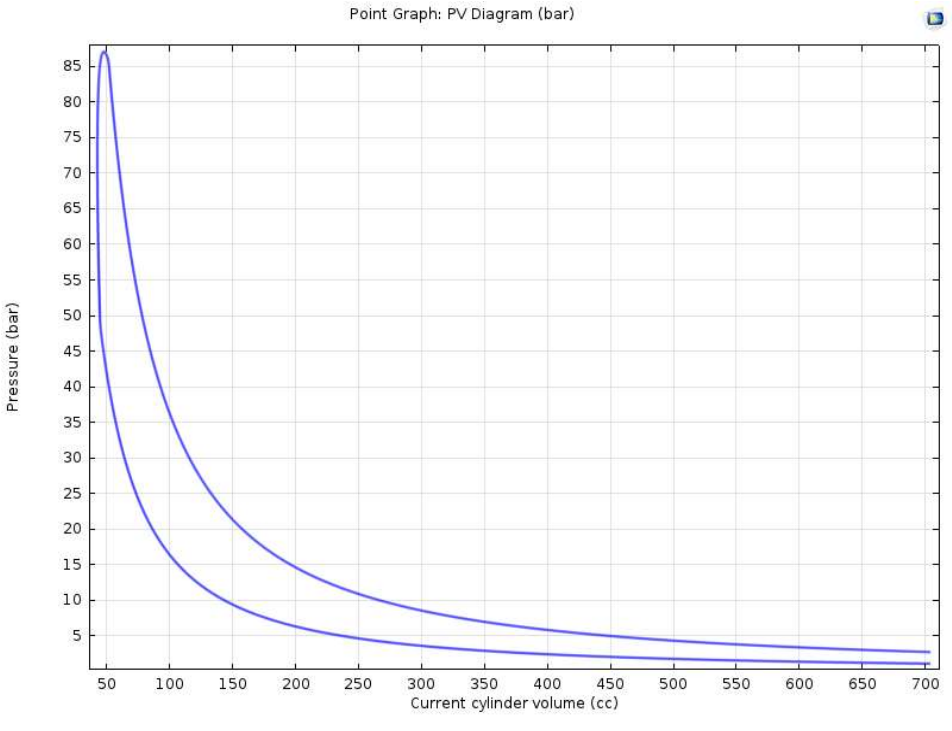

(a)

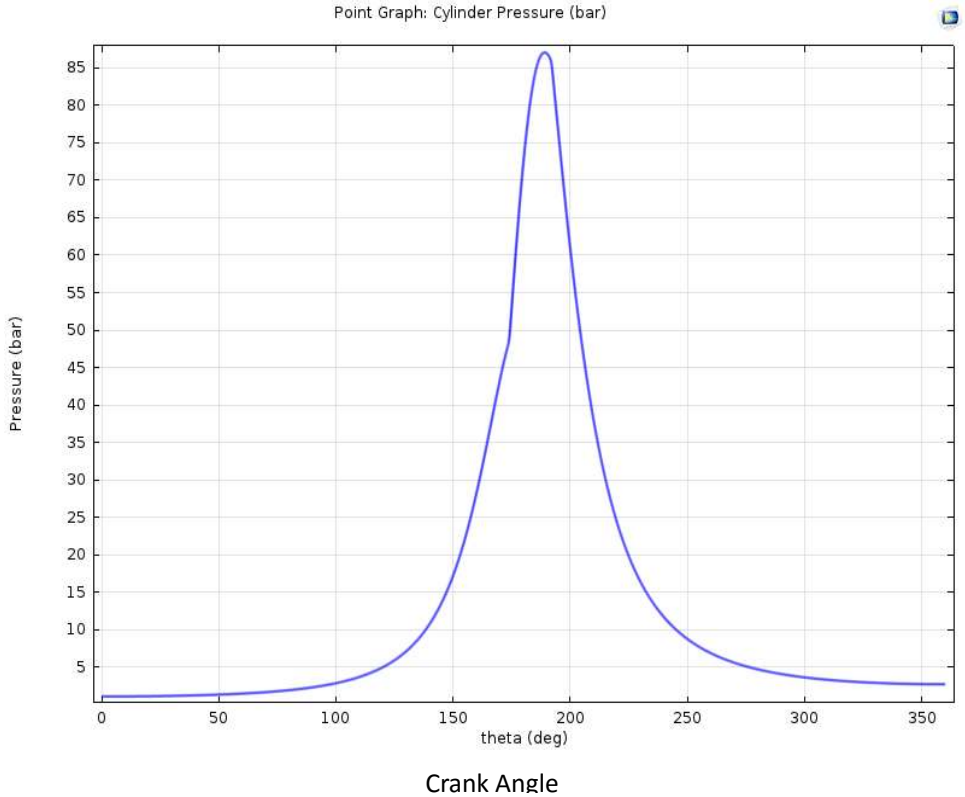

(b)

Crank Angle

Figure 4.22. Pressure curve of the simulated CI Engine fitted with 35^0 truncated cone piston crown with compression ratio of 16.589:1 (a) Pressure-Volume, (b) Pressure-Crank angle

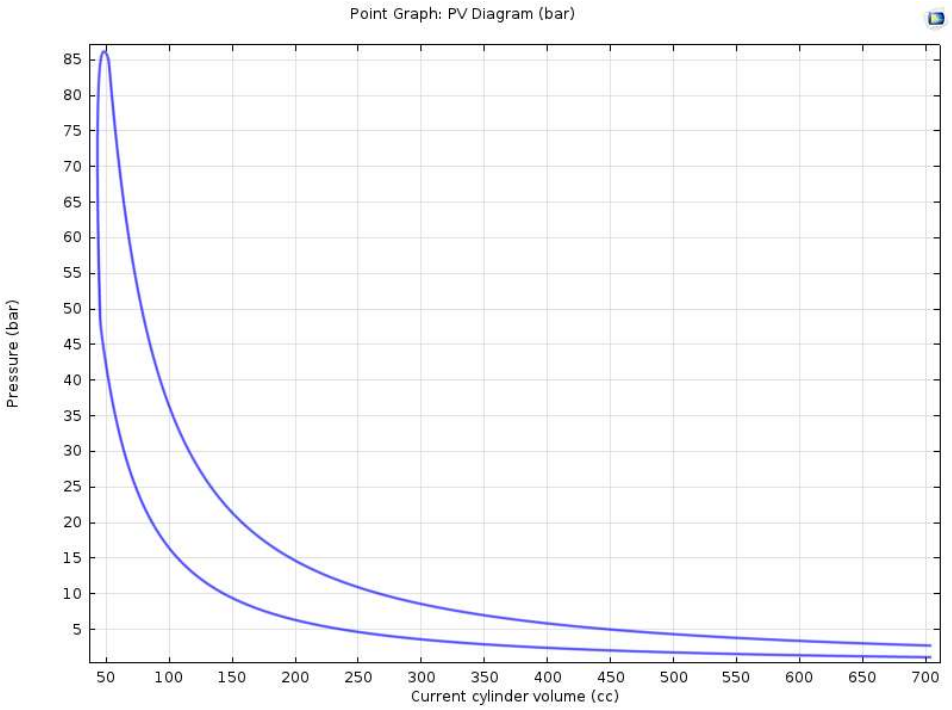

(a)

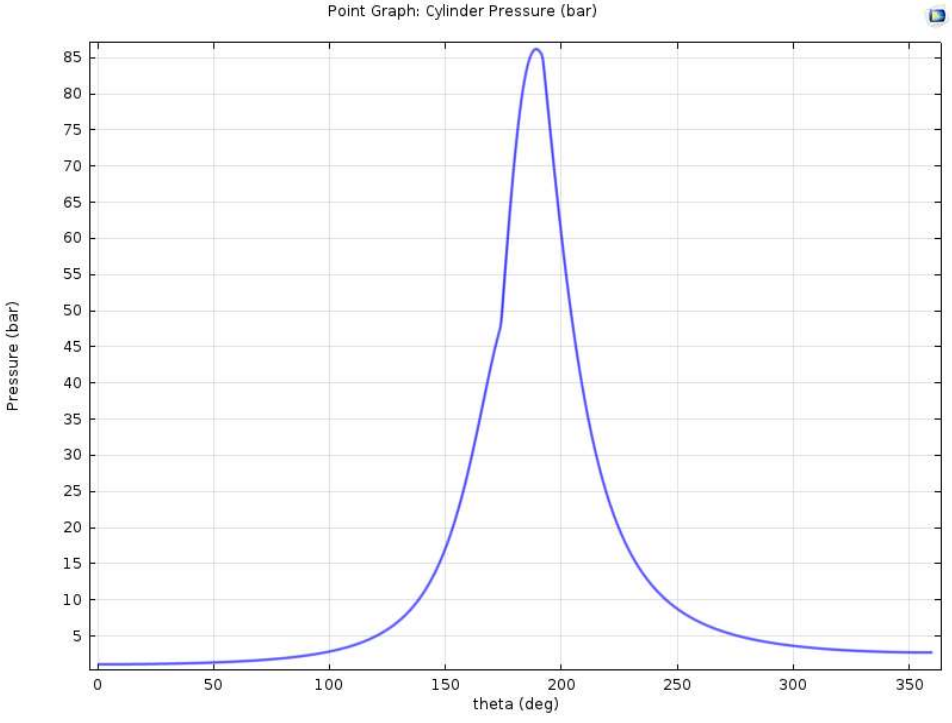

(b)

Crank Angle

Figure 4.23. Pressure curve of the simulated CI Engine fitted with 40^0 truncated cone piston crown with compression ratio of 16.426:1 (a) Pressure-Volume, (b) Pressure-Crank angle

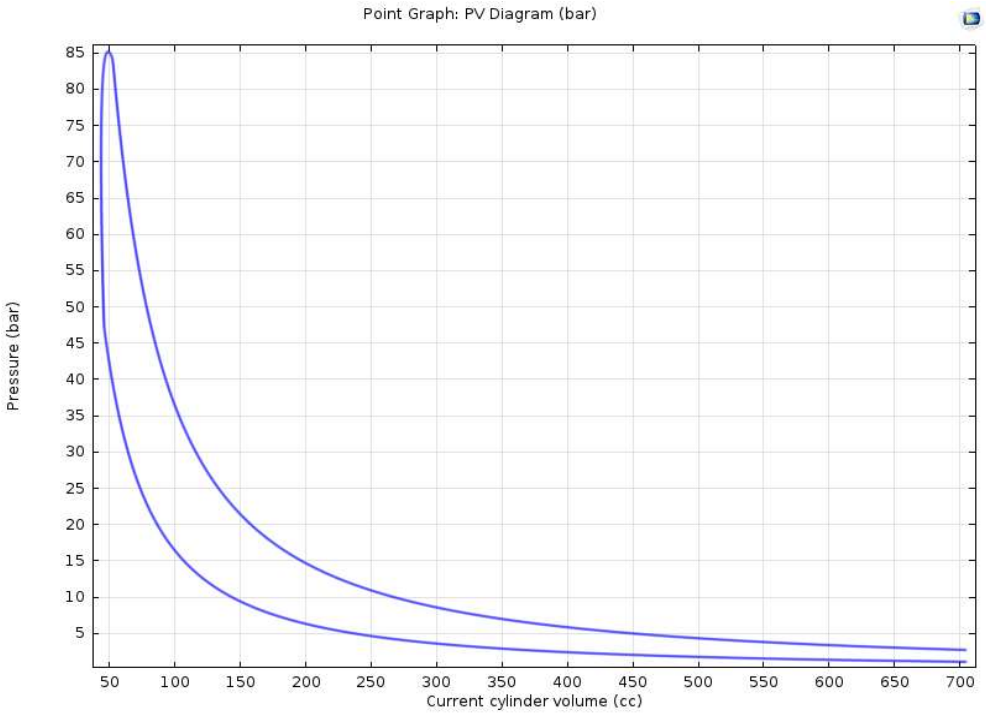

(a)

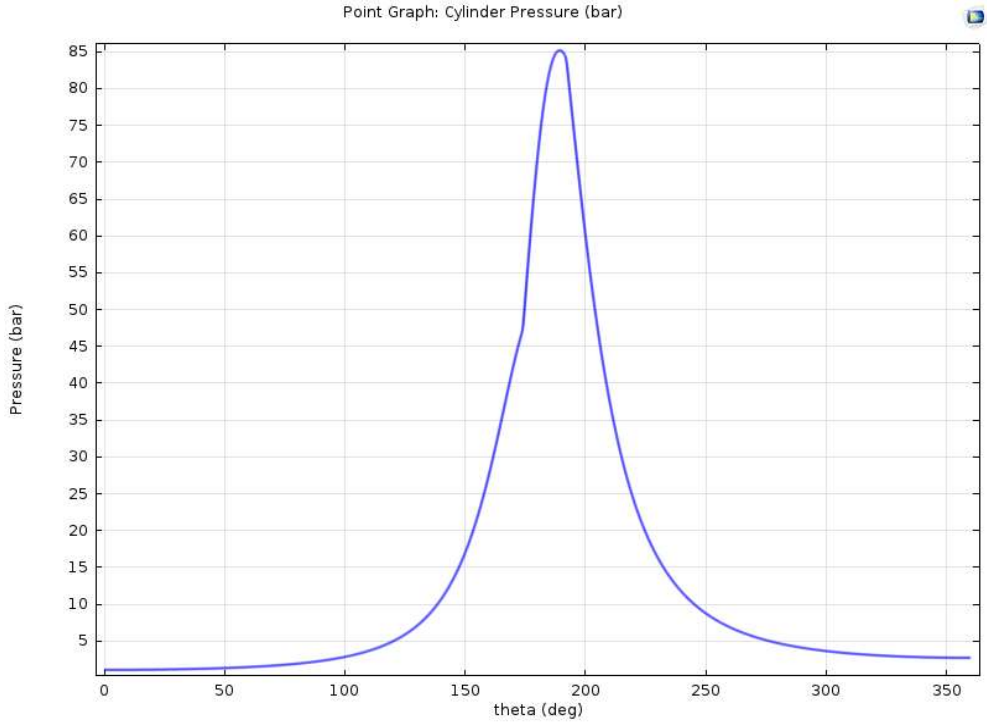

(b)

Crank Angle

Figure 4.24. Pressure curve of the simulated CI Engine fitted with 45^0 truncated cone piston crown with compression ratio of 16.243:1 (a) Pressure-Volume, (b) Pressure-Crank angle

A peak pressure value of 86.04 bar was attained for the 45° truncated cone modified piston crown at 9.2° after the top dead centre (aTDC) position of the piston as depicted in Figure 4.24. The compression ratio for this modified piston was 16.243:1. The net work done by the engine simulation is -476.99 J, while the heat energy derived from the fuel combustion is 1564.74 J.

The summary of the deductions made from the simulation of the engine when fitted with truncated cone piston crowns and of different compression ratios are depicted in Table 4.2. And as stated earlier, the determined pressure values and heat values are important parameters used in the determination of the performance characteristics of the engine.

The derived peak pressure values are to a small extent different from the results reported by Mamilla *et al,* (2013) whose value was in the range of 68 – 70 bars for three different combustion chamber geometry while working with a Kirloskar engine. However, this difference could be attributed in part to the difference in power rating of their own engine (4.4 KW) as against the 5.2 KW engine used in this studies, and at the same time one cannot rule out the impact of differences in the start of injection.

The net work done obtained from the engine simulations using the truncated cone modified pistons as evaluated from the PV diagrams in Figures 4.9 to 4.13 is lower than that evaluated for the unmodified piston. This can be attributed to the reduced values of the compression ratio in each case, as compression ratio is one of the major parameters that determine the performance characteristics of compression ignition engines.

4.5.3 Engine Cylinder Pressure Simulations of Inverted Truncated Cone Piston Crown with Constant Compression Ratio for Category I

The pressure plots result of the simulation carried out using inverted truncated cone piston crown geometries while maintaining a constant compression ratio as that of the unmodified piston are depicted in Figure 4.25.

The pressure versus volume, and crank angle plots for the simulated engine when fitted with the unmodified and the inverted truncated cone piston crown of varying angles of inclination (25°, 30°, 35°, 40° and 45° respectively) just as was for the case of truncated cone piston crown with uniform compression ratios, the pressure plots looks close, however the piston crown of inclination angles of 40° appears domineering, as it is well visible despite the curve of the inclination angle of 45° plotted over it.

Table 4.2: Performance parameter estimates for the TCPC with different CR for category I

Piston Crown Type (TCPC)	**CR**	**Net Work (J)**	**Heat Energy (J)**	**Peak Pressure (bar)**	**Peak Pressure position (°aTDC)**
Unmodified	17.500	481.64	1558.62	92.72	7.0
25°	16.877	480.45	1567.34	89.45	8.4
30°	16.738	479.83	1564.74	88.75	9.0
35°	16.589	478.99	1564.74	87.94	9.0
40°	16.426	478.05	1564.74	87.04	9.2
45°	16.243	476.99	1564.74	86.04	9.2

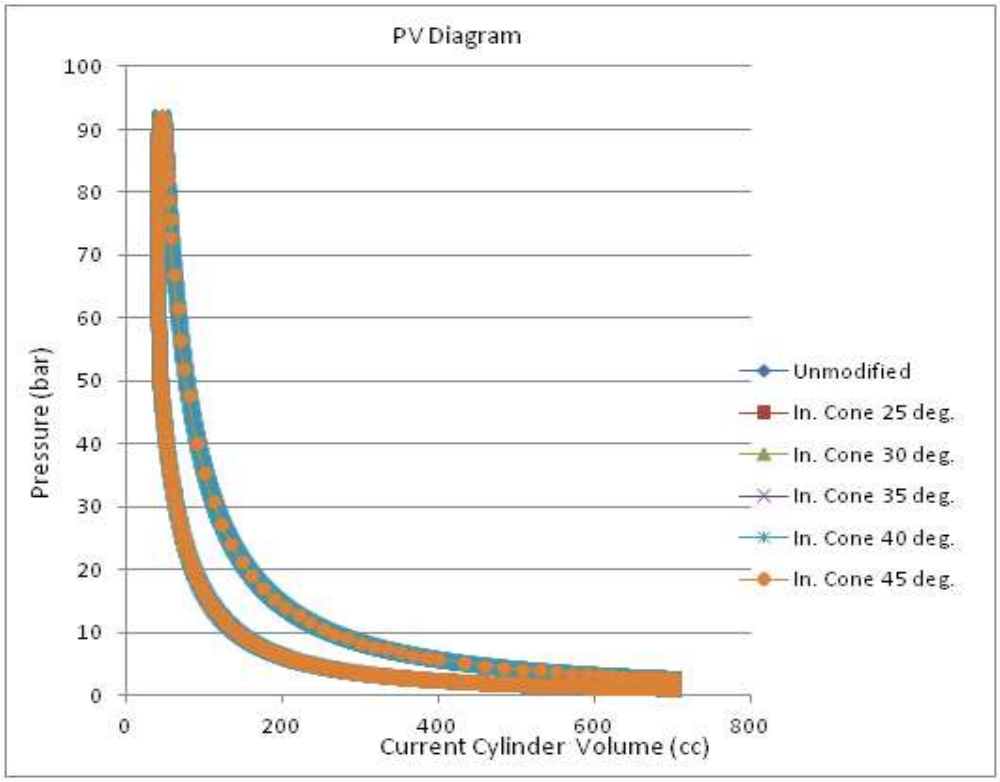

(a)

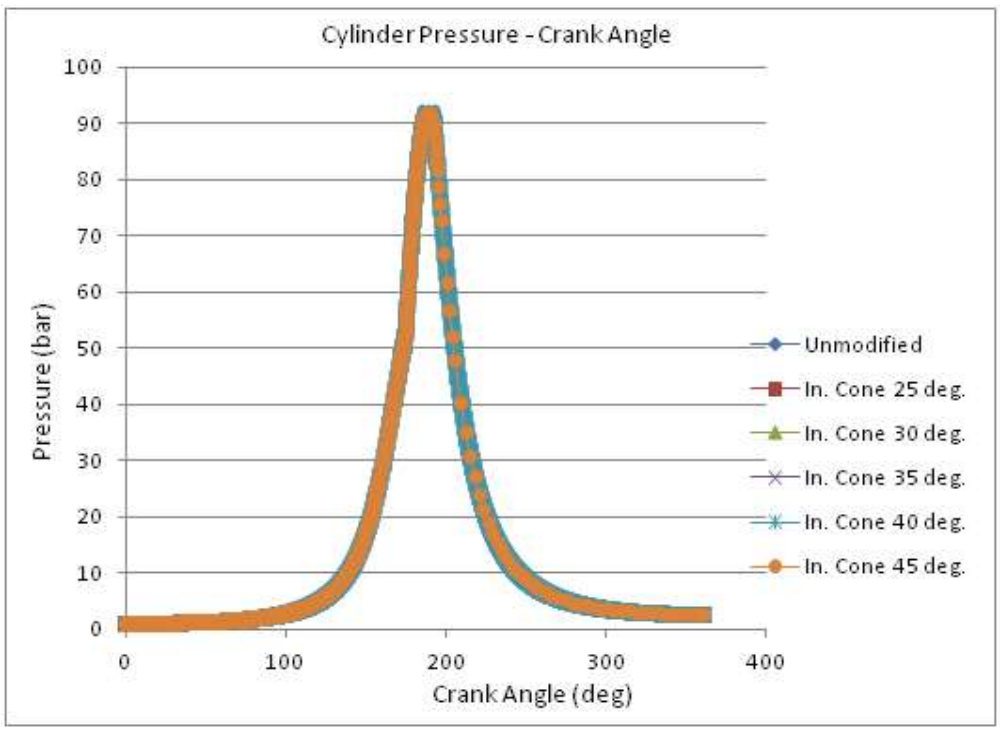

(b)

Figure 4.25. Pressure curve of the simulated CI Engine fitted with inverted truncated cone piston crown with compression ratio of 17.5:1
(a) Pressure-Volume and (b) Pressure-Crank

The domineering appearance of the curve generated from the engine simulation of the 45° cone base angle inverted truncated cone piston crown over the others asides that of the 40° gives an indication of its greater curve area an implication of greater value of net work done.

The individual plots for the pressure versus volume, and pressure versus crank angle are depicted in Figures 4.26 to 4.30.

A peak pressure value of 92.61 bar at 8.3° after top dead centre (aTDC) was derived from the simulation of the engine when fitted with a modified inverted truncated cone piston crown at an inclination angle of 25° as shown in Figure 4.26.The net work done is -480.64 J, and the heat energy derived from the fuel combustion is 1557.74 J

The net work done as derived from the simulation of the engine fitted with a modified piston crown of inverted truncated cone geometry with a cone base angle of 30° as calculated from the plot in Figure 4.27 is -480.86 J, while the heat energy generated from the combustion of fuel is 1558.52 J. A peak pressure value of 92.70 bar at 8.3° after top dead centre (aTDC) was recorded.

At 9.4° after top dead centre (aTDC), a peak pressure of 92.43 bar was derived from the simulation of the engine when fitted with a modified inverted truncated cone piston crown at an inclination angle of 35° as shown in Figure 4.28.The net work done as calculated from the area enclosed by the pressure – volume curve is -480.06 J, and the heat energy derived from the fuel combustion is 1556.82 J.

At 8.7° after the top dead centre (aTDC), a peak pressure of 92.93 bar was recorded in the simulated engine fitted with inverted truncated cone piston crown with inclination angle 40°. The net work done from the plot in Figure 4.29 is -483.95 J, and the heat energy generated from the fuel combustion is 1564.74 J

The peak pressure value recorded for the engine simulation fitted with an inverted truncated cone piston of inclination angle of 45° to the vertical was 92.91 bar attained at 8.5° after the top dead centre (aTDC). The net work done by the simulated engine is -483.81 J and this is derived from a heat energy value of 1564.68 J as released from the combustion of the fuel.

The summary of the deductions made from the simulation of the engine when fitted with inverted truncated cone piston crowns with constant compression ratio is stated in Table 4.3.

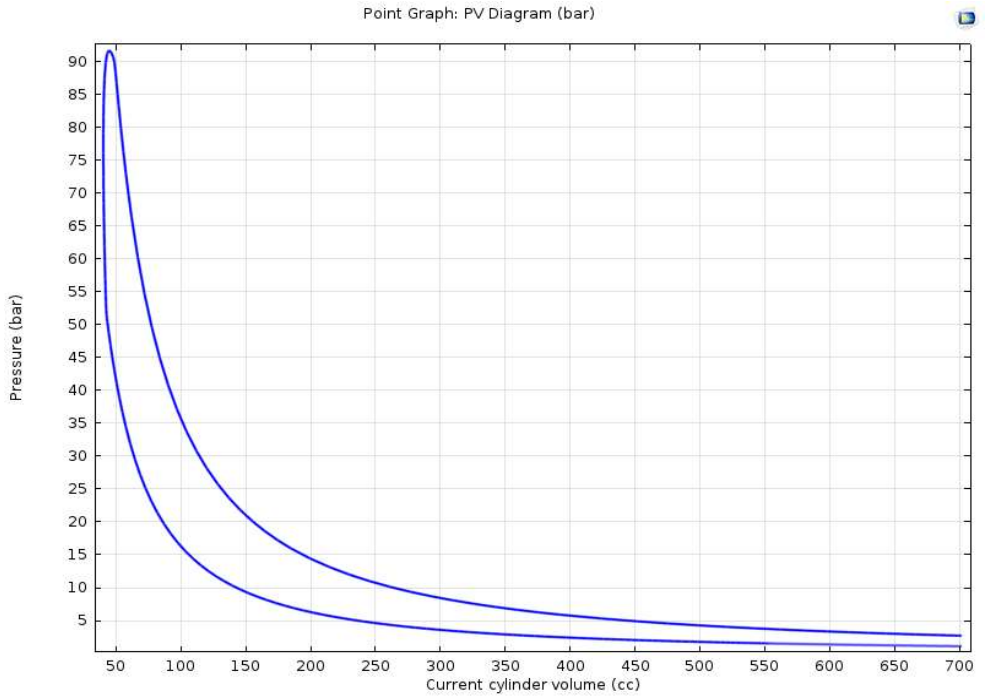

(a)

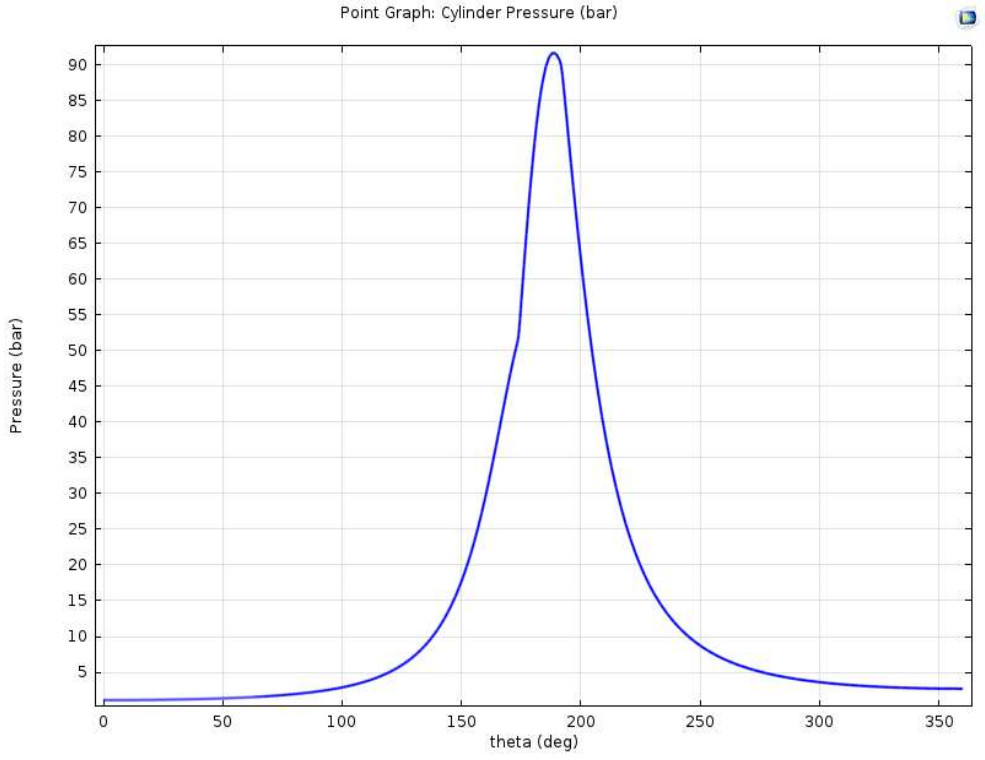

(b)

Crank Angle

Figure 4.26. Pressure curve of the simulated CI Engine fitted with 25^0 inverted truncated cone piston crown with compression ratio of 17.5:1
(a) Pressure-Volume and (b) Pressure-Crank angle

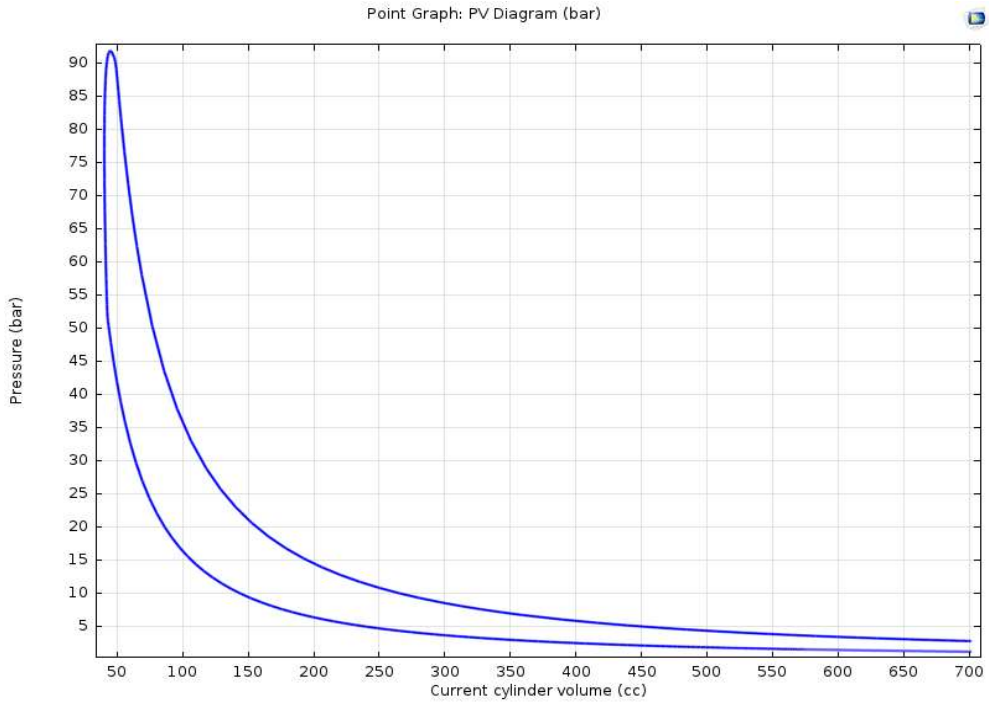

(a)

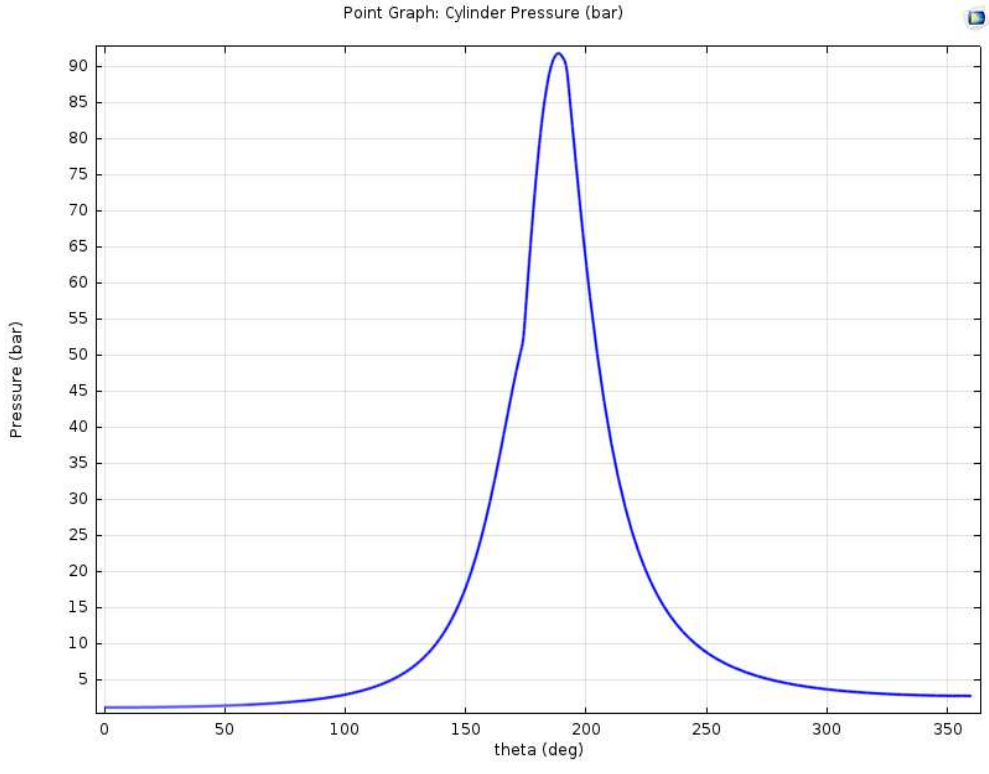

(b)

Crank Angle

Figure 4.27. Pressure curve of the simulated CI Engine fitted with 30^0 inverted truncated cone piston crown with compression ratio of 17.5:1
(a) Pressure-Volume and (b) Pressure-Crank angle

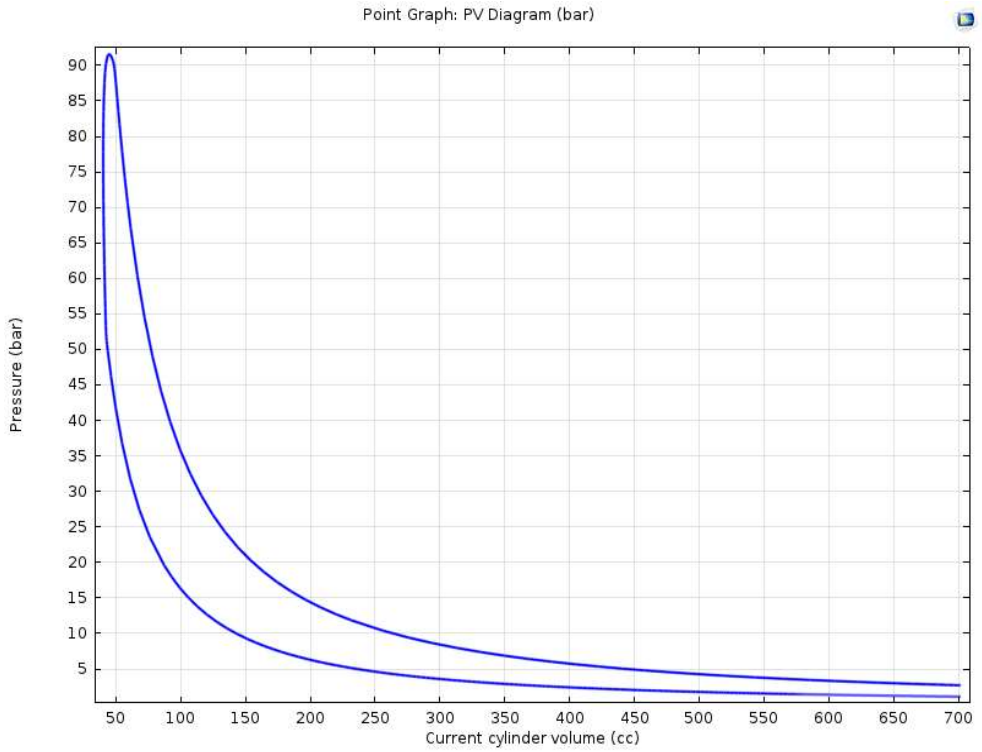

(a)

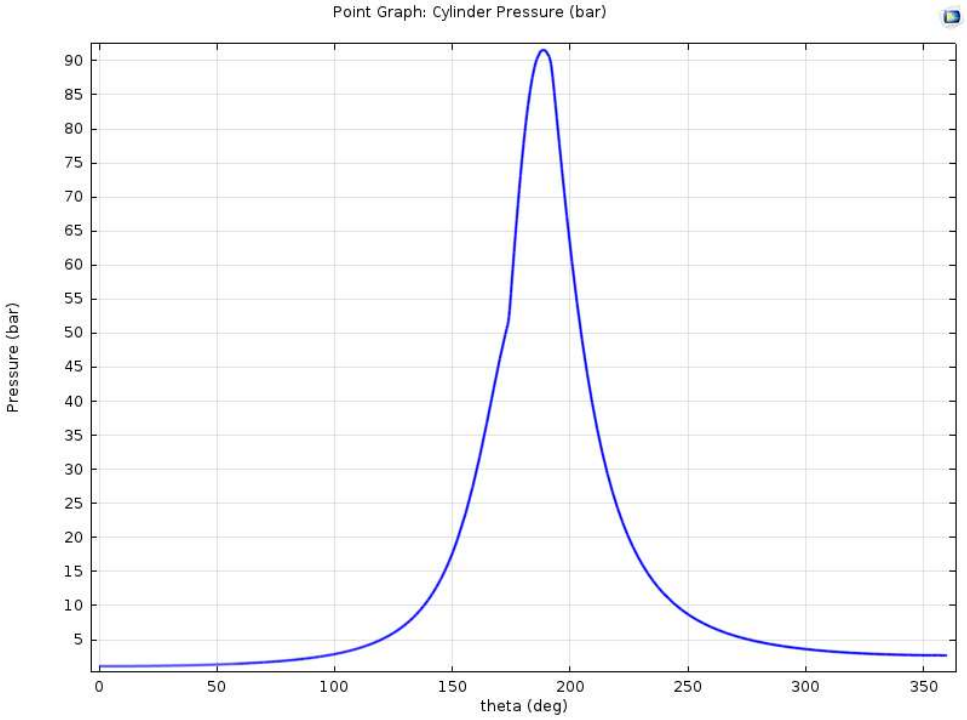

(b)

Crank Angle

Figure 4.28. Pressure curve of the simulated CI Engine fitted with 35^0 inverted truncated cone piston crown with compression ratio of 17.5:1
(a) Pressure-Volume and (b) Pressure-Crank angle

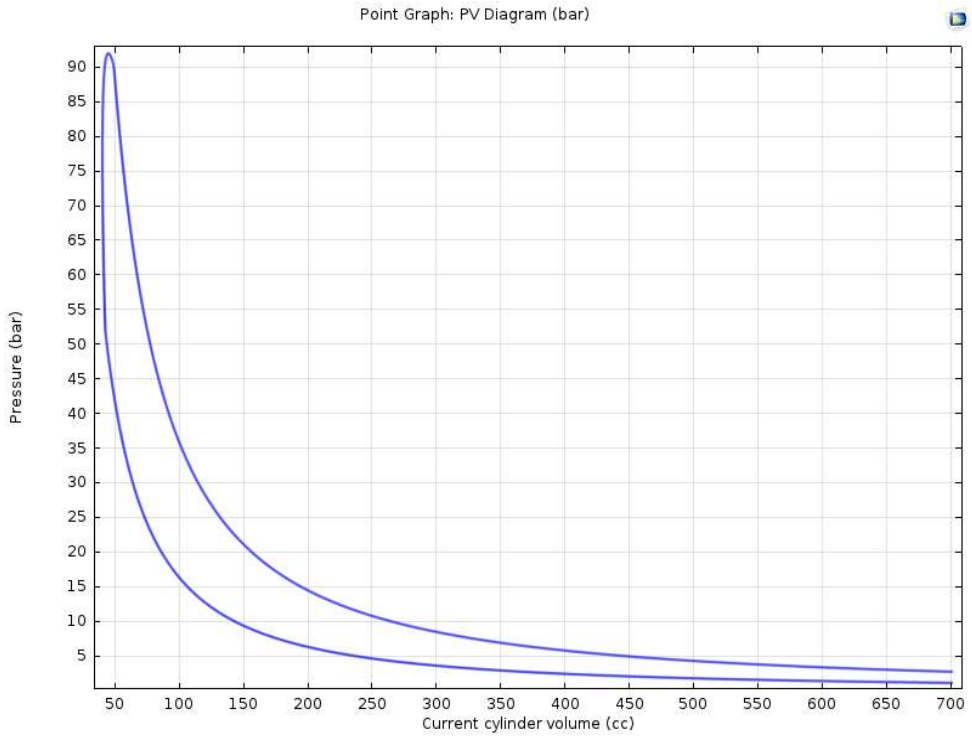

(a)

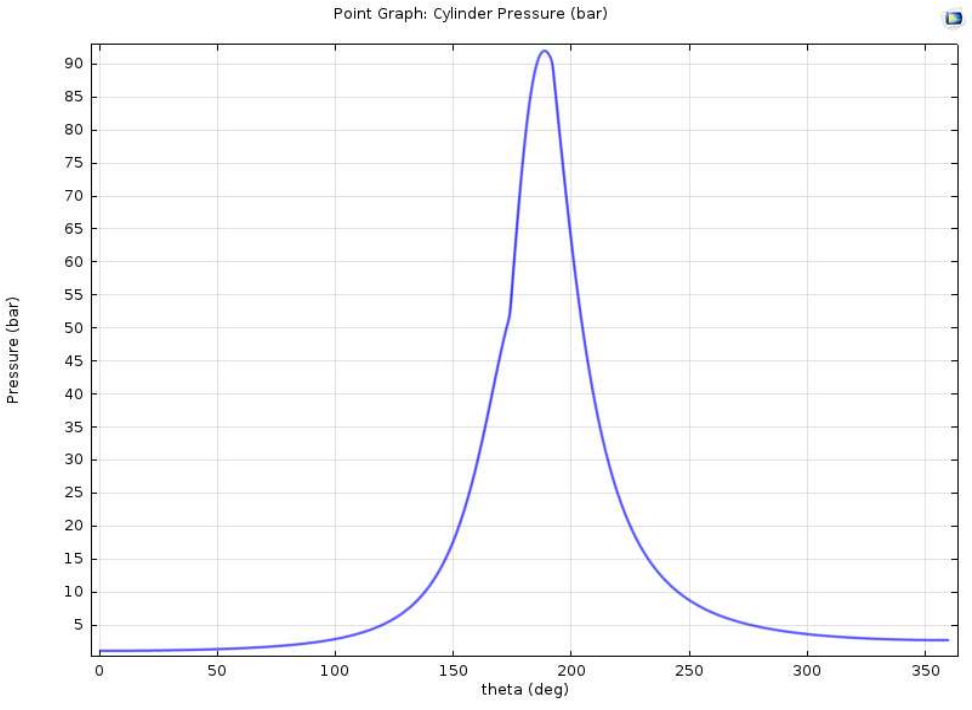

(b)

Crank Angle

Figure 4.29. Pressure curve of the simulated CI Engine fitted with 40^0 inverted truncated cone piston crown with compression ratio of 17.5:1
(a) Pressure-Volume and (b) Pressure-Crank angle

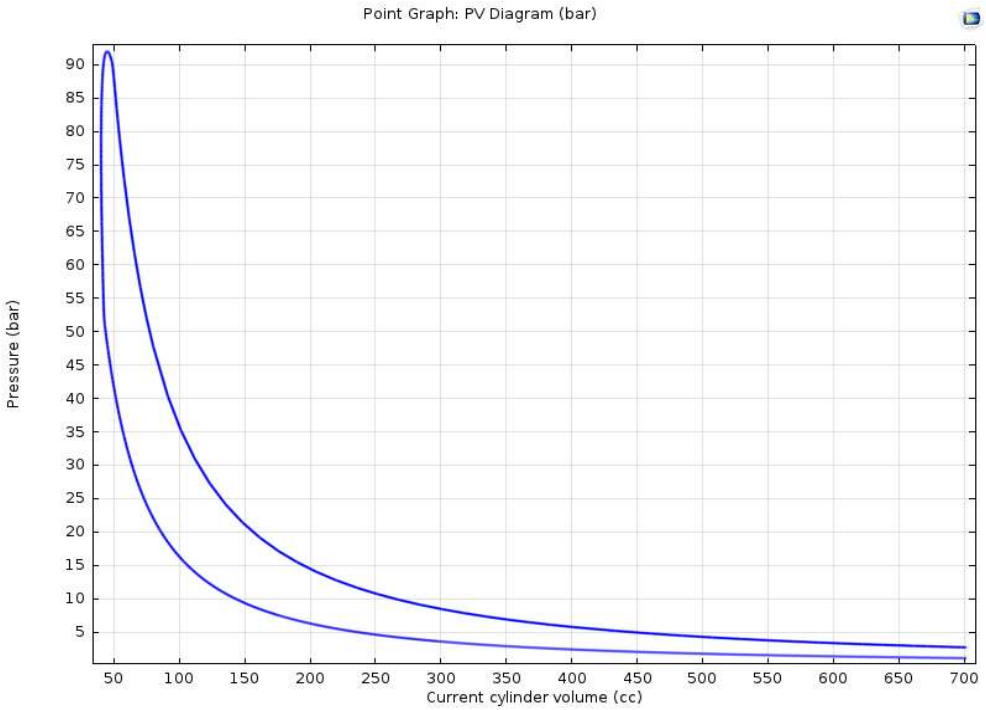

(a)

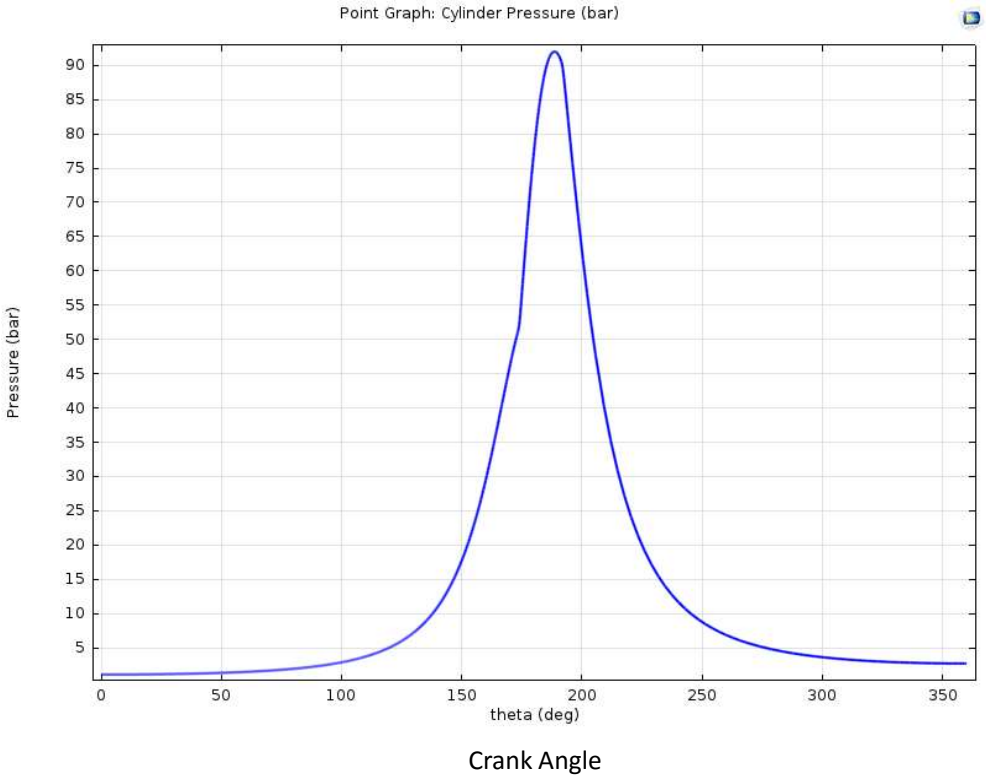

(b)

Crank Angle

Figure 4.30. Pressure curve of the simulated CI Engine fitted with 45^0 inverted truncated cone piston crown with compression ratio of 17.5:1
(a) Pressure-Volume and (b) Pressure-Crank angle

Table 4.3: Performance parameter estimates for the ITCPC with constant CR for category I

Piston Crown Type (ITCPC)	**Net Work (J)**	**Heat Energy (J)**	**Peak Pressure Value (bar)**	**Peak Pressure position (°aTDC)**
Unmodified	481.64	1558.62	92.72	7.0
25°	480.64	1557.74	92.61	8.3
30°	480.86	1558.52	92.70	8.3
35°	480.06	1556.82	92.43	9.4
40°	483.95	1564.74	92.93	8.7
45°	483.81	1564.68	92.91	8.5

The peak pressure values as determined from the plots for the angles of inclination 40° and 45° were higher than for the unmodified piston; the reason for their greater values of net work done in comparison to the unmodified piston, while it was lower for the angles of 25°, 30° and 35° respectively.

As reported by Nataraj *et al.* (2015), the use of the toroidal combustion chamber led to the increase in the engines mean pressure, an indication of an optimized geometry. The use of the inverted truncated cone piston crown with truncated cone base angles of 40° and 45° can be said to have led to an optimized combustion chamber geometry from this studies.

4.5.4 Engine Cylinder Pressure Simulations of Inverted Truncated Cone Piston Crown with Different Compression Ratio for Category I

The pressure versus volume and pressure versus crank angle plots from the simulation results for the various angles of inclination for the inverted truncated cone piston crown with different compression ratio is shown in figure 4.31.

The peak pressure value attained from the engine simulation was highest for the unmodified truncated cone which has the highest compression ratio value of 17.5:1. The same trend was followed for the modified pistons with the peak pressure value decreasing as the compression ratio reduces.

The pressure – volume and corresponding pressure – angle plots of the individual modified pistons of the different inclination angles follows in Figure 4.32 to 4.36.

From Figure 4.32, a peak pressure of 55.95 bar was attained at 11.7° after the top dead centre (aTDC). The net work done from the simulation of the engine of compression ratio 10.645:1 fitted with a modified piston crown of inverted truncated cone geometry with truncated cone base angle of 25° was -433.45 J while generated amount of heat energy from the fuel combustion is 1564.74 J.

The net work done as simulated for the engine when fitted with an inverted truncated cone piston crown with a truncated cone base angle of 30° and a compression ratio of 10.697:1 in Figure 4.33 is -432.41 J, while the heat energy derived from the combustion of the fuel is 1561.84 J. A peak pressure was 56.10 bar was attained at 11.5° after the top dead centre (aTDC).

A peak pressure of 56.55 bar attained at 11.7° after the top dead centre (aTDC) was derived from the simulation of the engine when fitted with a modified inverted truncated cone piston crown with an inclination angle of 35°.

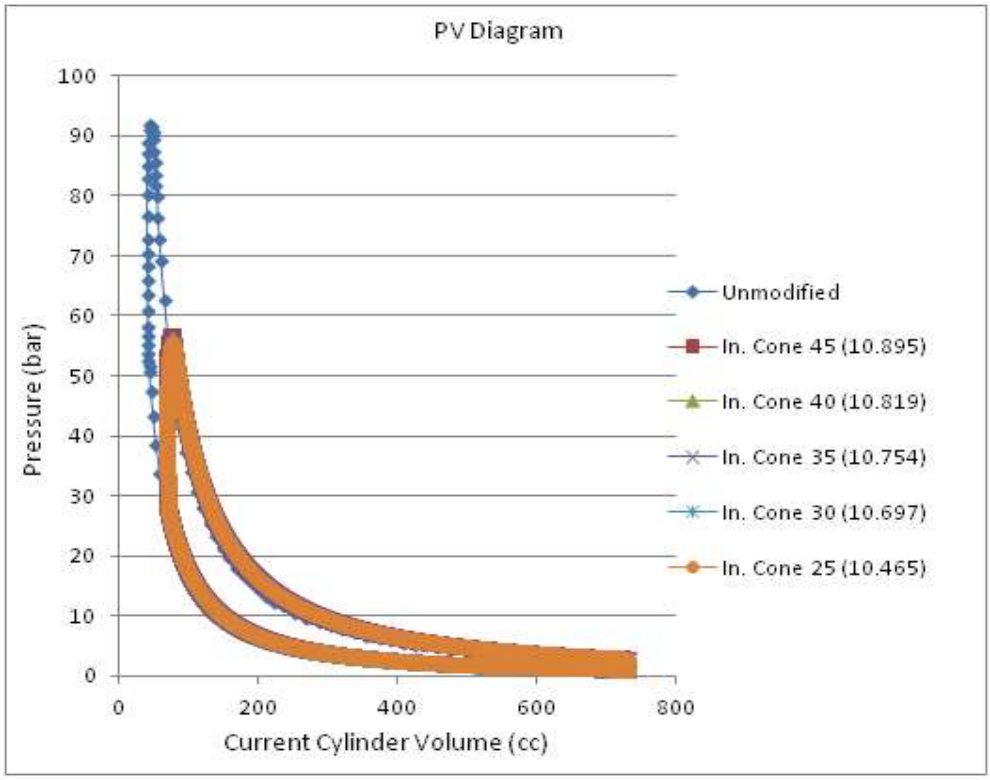

(a)

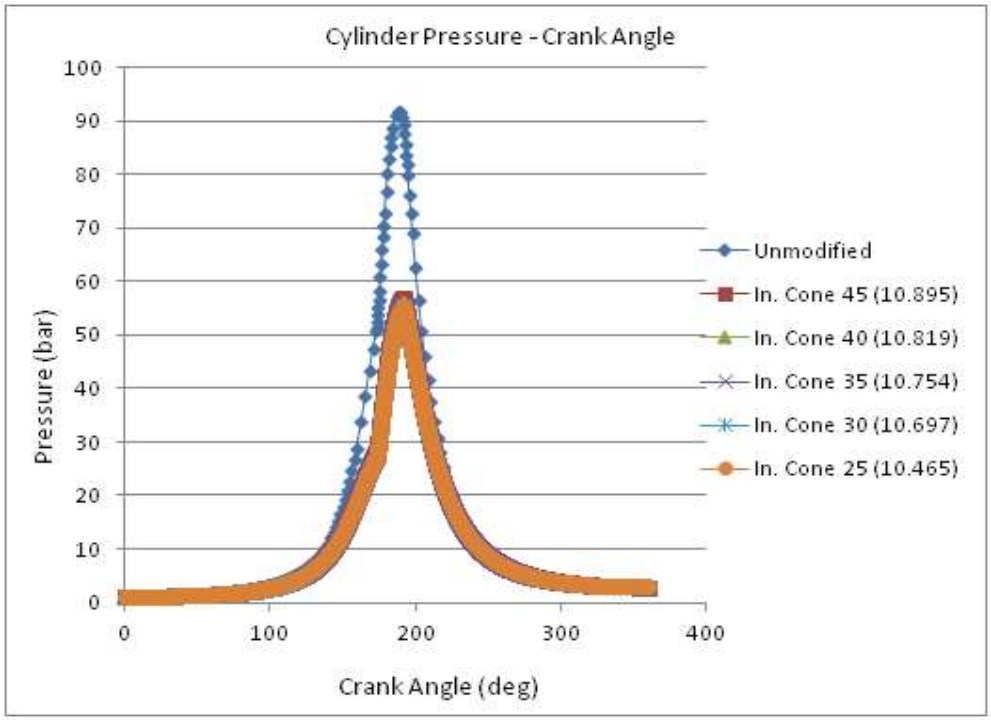

(b)

Figure 4.31. Pressure curve of the simulated CI Engine fitted with inverted truncated cone piston crown at different compression (a) Pressure-Volume and (b) Pressure-Crank angle

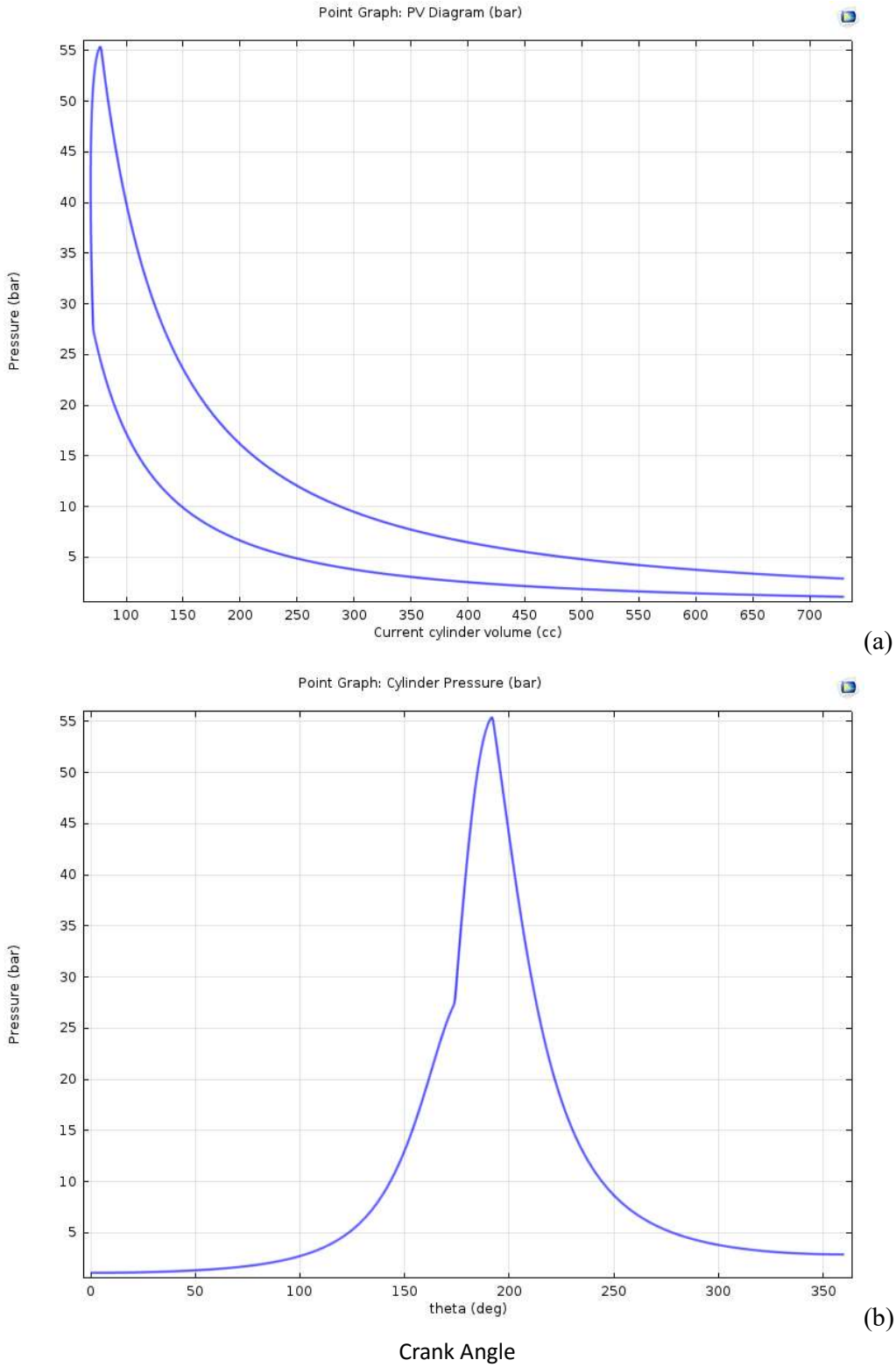

Figure 4.32. Pressure curve of the simulated CI Engine fitted with 25^0 inverted truncated cone piston crown with compression ratio of 10.645:1 (a) Pressure-Volume and (b) Pressure-Crank angle

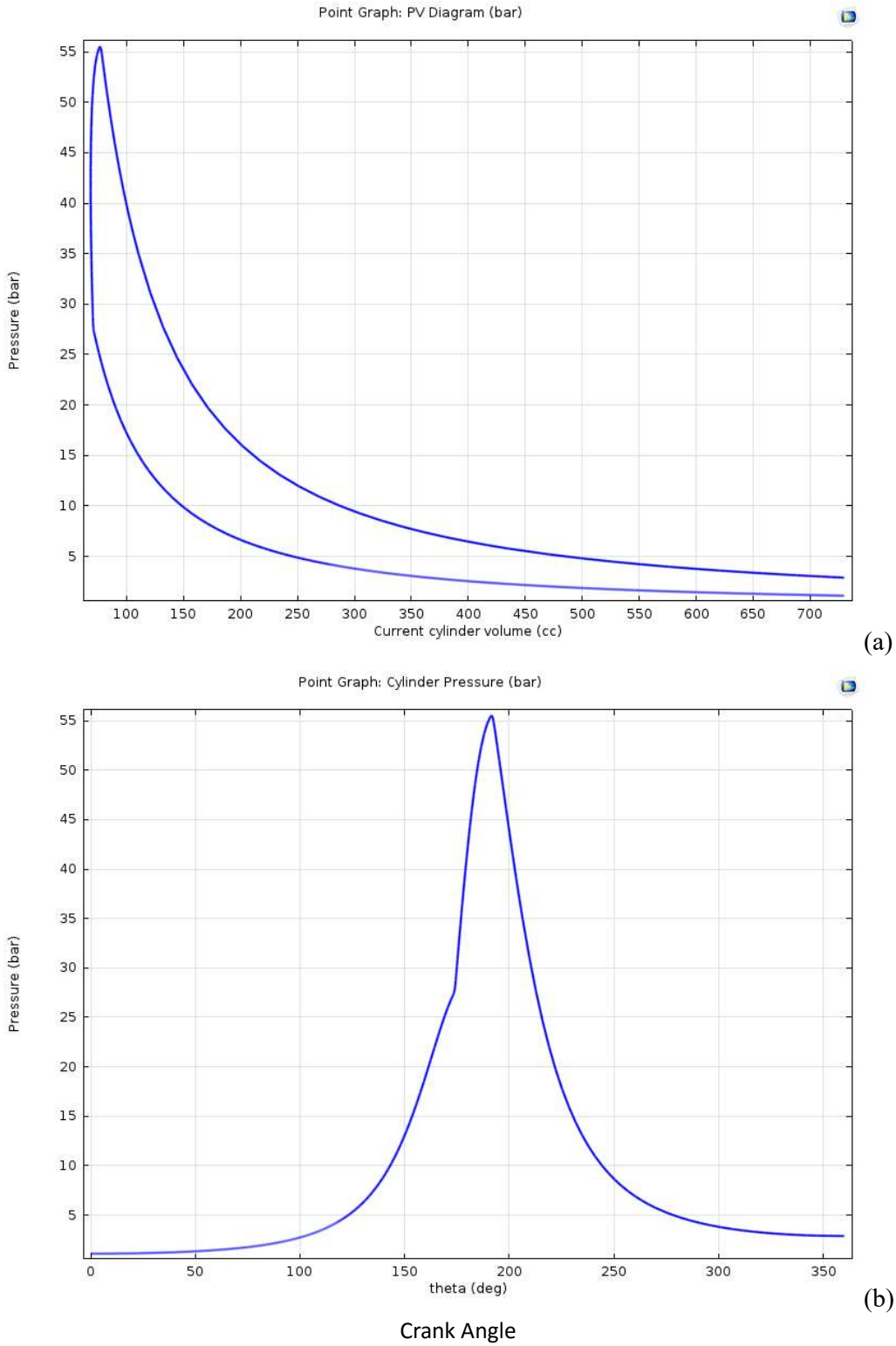

Figure 4.33. Pressure curve of the simulated CI Engine fitted with 30^0 inverted truncated cone piston crown with compression ratio of 10.697:1 (a) Pressure-Volume and (b) Pressure-Crank angle

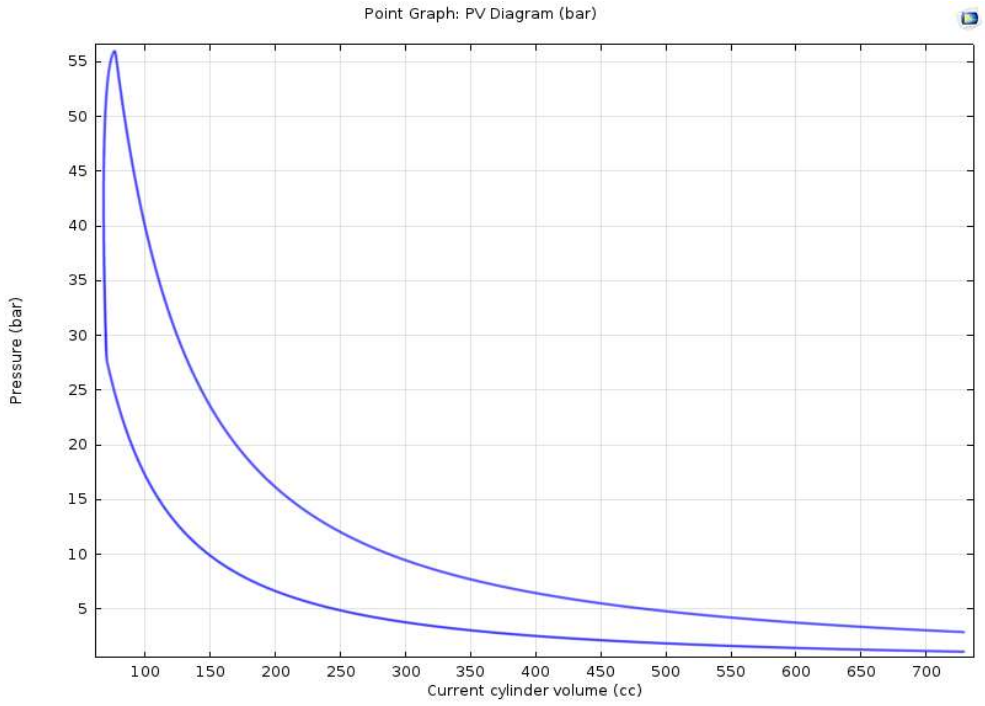

(a)

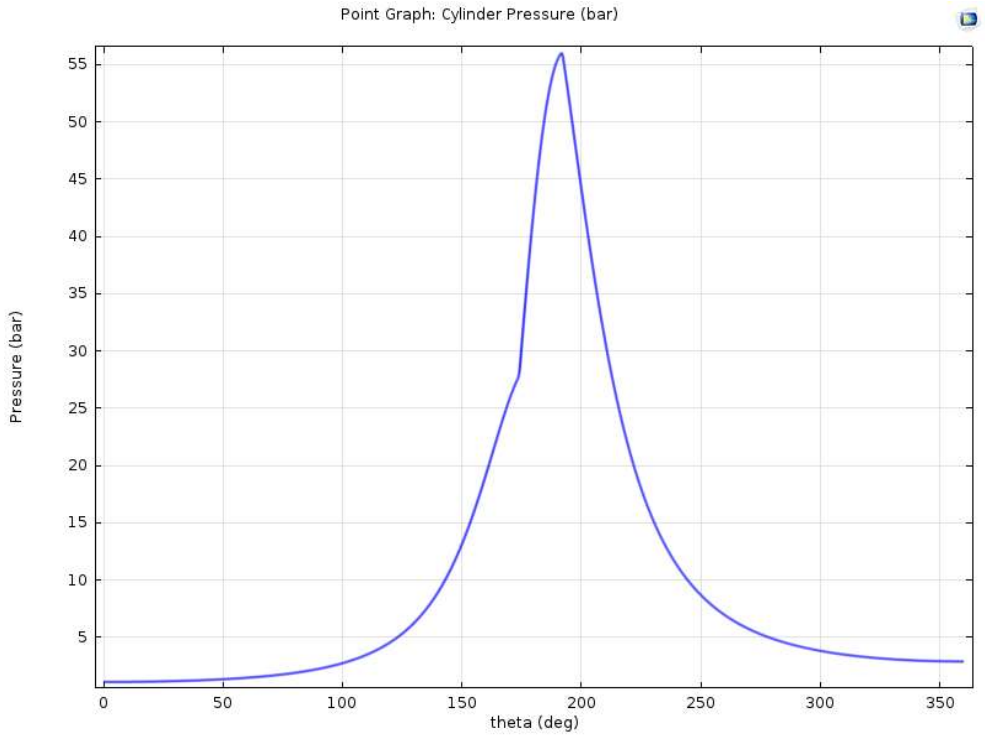

(b)

Crank Angle

Figure 4.34. Pressure curve of the simulated CI Engine fitted with 35^0 inverted truncated cone piston crown with compression ratio of 10.754:1 (a) Pressure-Volume and (b) Pressure-Crank angle

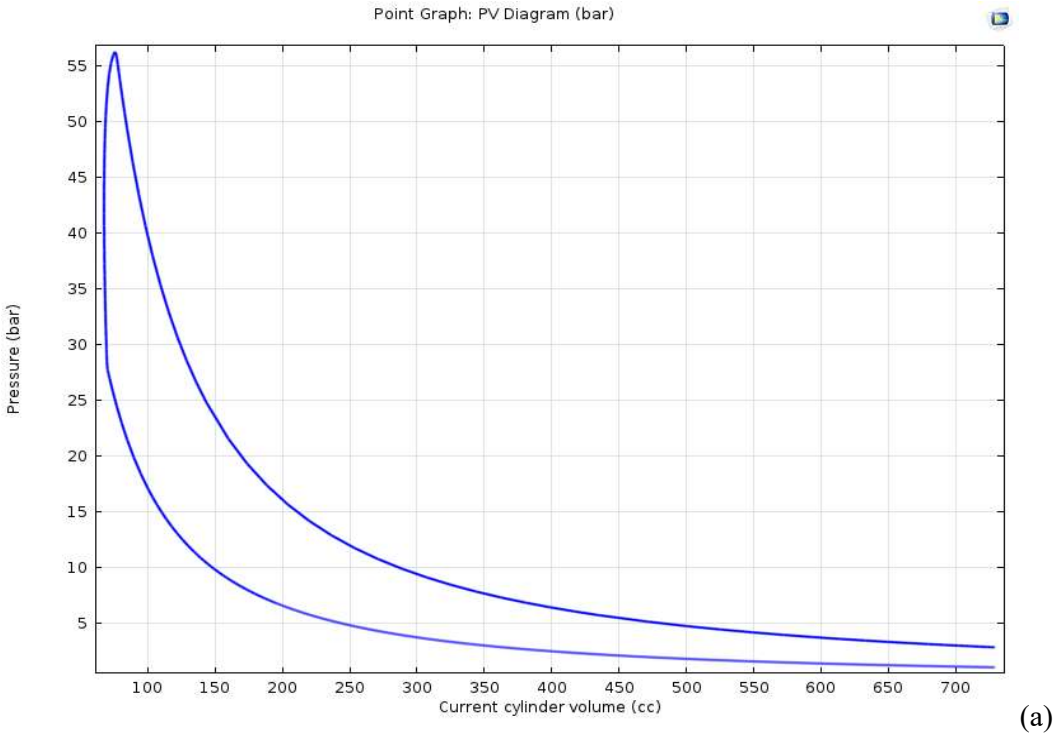

(a)

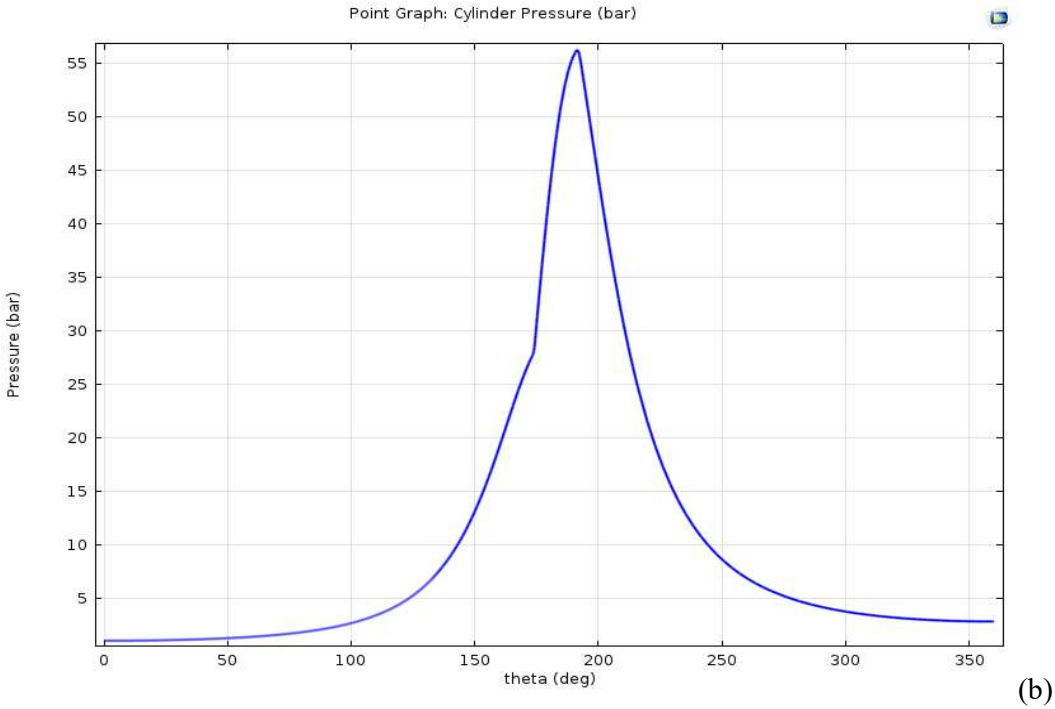

(b)

Crank Angle

Figure 4.35. Pressure curve of the simulated CI Engine fitted with 40^0 inverted truncated cone piston crown with compression ratio of 10.819:1 (a) Pressure-Volume and (b) Pressure-Crank angle

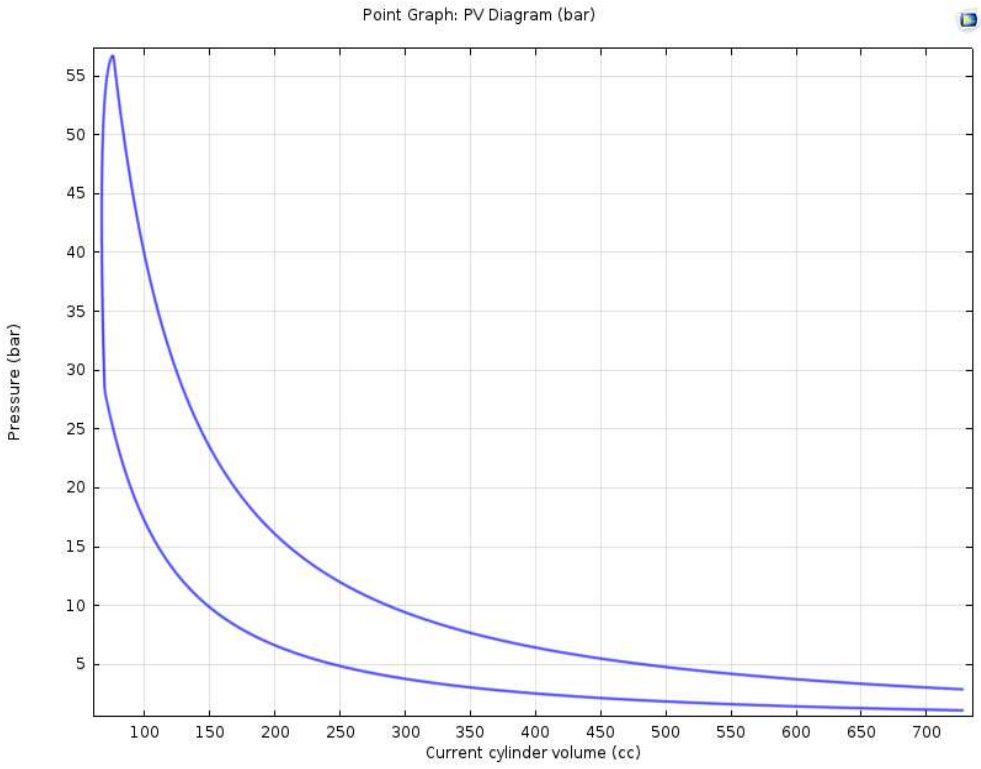

(a)

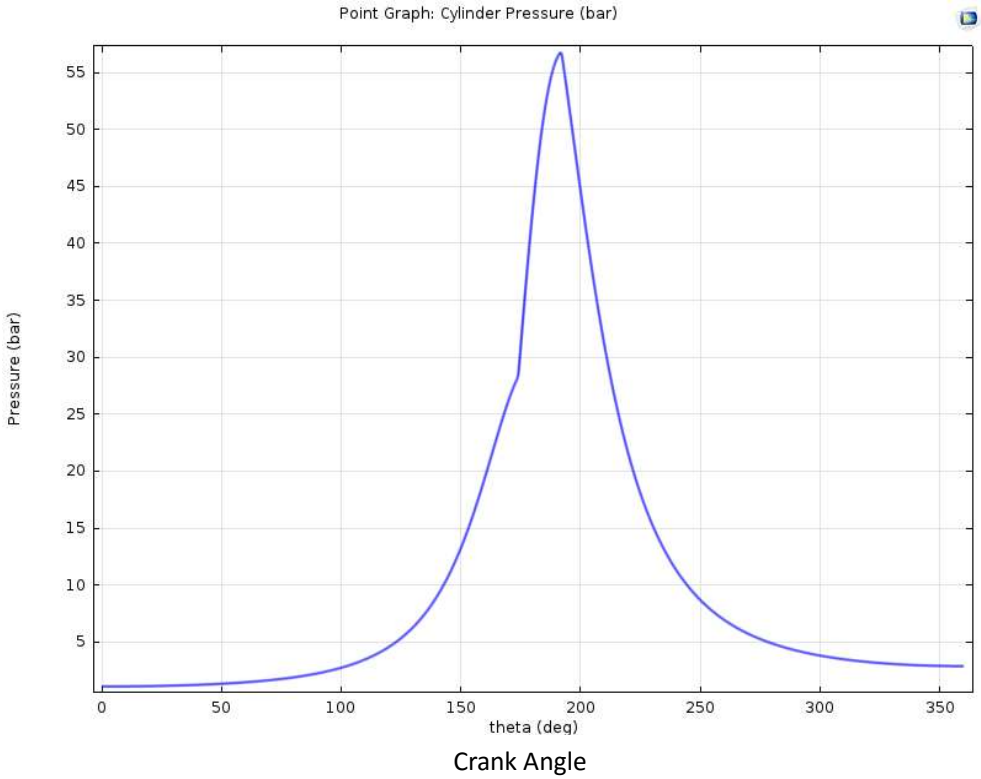

(b)

Crank Angle

Figure 4.36. Pressure curve of the simulated CI Engine fitted with 45^0 inverted truncated cone piston crown with compression ratio of 10.895:1 (a) Pressure-Volume and (b) Pressure-Crank angle

The net work done by the engine with a compression ratio of 10.754:1 is -434.59 J, and the heat energy generated from the fuel combustion is 1564.76 J as derived from Figure 4.34.

From Figure 4.35, at 11.3° after the top dead centre (aTDC), a peak pressure of 56.82 bar was attained by the engine when fitted with an inverted truncated cone piston crown of inclination angle of 40°. Heat energy of 1567.40 J was generated by the combustion of fuel and the net work done is -435.51 J for a compression ratio is 10.819:1.

A peak pressure value of 57.31 bar was obtained at 11.7° after the top dead centre (aTDC) from the simulation of the engine when fitted with a modified inverted truncated cone piston crown with truncated cone base angle of 45°. The net work done as evaluated from the area of the PV diagram as indicated in Figure 4.36 is -436.03 J, and the heat energy derived from the fuel combustion is 1564.74 J.

The summary of the deductions made from the simulation of the engine when fitted with inverted truncated cone piston crowns with constant compression ratio are stated in Table 4.4.

The net work done as derived from the engine simulations using the inverted truncated cone modified pistons are much lower than that evaluated for the unmodified piston. This can be attributed to the reduced values of the compression ratio in each case, as compression ratio is one of the major parameters that determine the performance characteristics of compression ignition engines.

The peak pressure for the engine when fitted with the modified piston crowns are markedly different from that reported by Basha *et al.* (2009), Ghafouri *et al.* (2014) and, Jafarmadar and Khanbabazadeh, (2008) mainly because of the lower values of compression ratios. The percentage difference between the obtained peak pressure was approximately 22% lower compared to the peak pressure reported by Basha *et al.* (2009). Engine compression ratio is a major determinant of its pressure.

4.5.5 Temperature Plots of Simulated Engine fitted with Truncated Cone Piston Crown having Constant Compression Ratio for Category I

The combustion temperature and exhaust gas temperature of an engine also affects its performance, as it determines its thermal efficiency and formation of emission products.
Figure 4.37 presents the temperature versus crank angle plots for the unmodified and truncated cone pistons for the different angles of inclination while maintaining a constant compression ratio.

Table 4.4: Inverted truncated cone piston crown values with different CR for category I

Piston Crown Type (ITCPC)	**CR**	**Net Work (J)**	**Heat Energy (J)**	**Peak Pressure Value (bar)**	**Peak Pressure position (°aTDC)**
Unmodified	17.500	481.64	1558.62	92.72	7.0
25°	10.645	433.45	1564.74	55.95	11.7
30°	10.697	432.41	1561.84	56.10	11.5
35°	10.754	434.59	1564.76	56.55	11.7
40°	10.819	435.51	1567.40	56.82	11.3
45°	10.895	436.03	1564.74	57.31	11.7

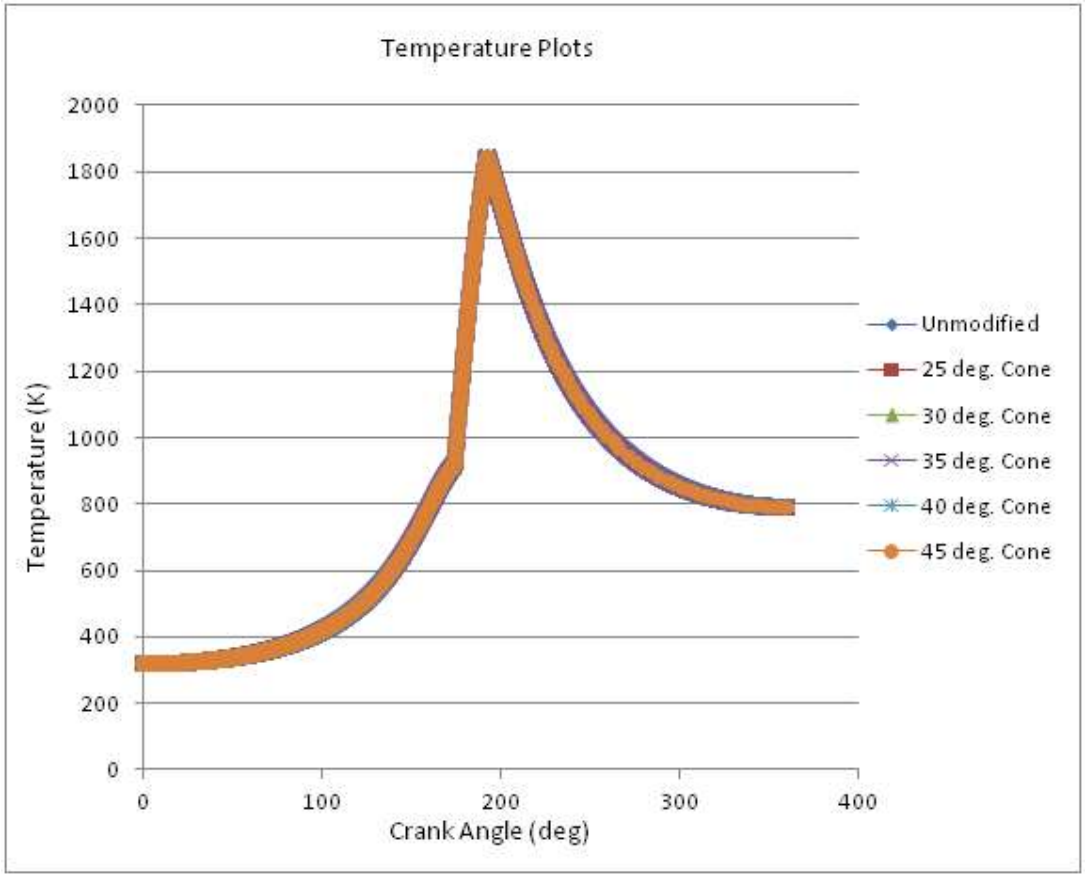

Figure 4.37. Temperature versus crank angle plots for unmodified and truncated cone piston crown (CR 17.5)

The temperature plots as it relates to the crankshaft rotation of the engine when fitted with the unmodified piston and the truncated cone piston crowns of inclination angle 25°, 30°, 35°, 40° and 45° while maintaining a uniform compression ratio is depicted in Figure 4.37.

The temperature plots for the engine when equipped with the truncated cone piston crown with the selected cone base angles are close, and this is the reason why the last plot showed a domineering appearance over the others. However, the temperature plot for the 35° truncated cone piston crown is still conspicuously visible indicating that some differences exists between the plots for the different piston crowns.

The peak temperature values are in good agreement with the findings of Jarfarmada and Khanbabazadeh, (2008), however the exhaust gas temperature obtained from this study are relatively lower. Also, a good correlation exists between the peak and exhaust gas temperatures derived in this studies and the results reported by Basha *et al.* (2009) with percentage difference less than 8%.

4.5.6 Temperature Plots of Simulated Engine fitted with Truncated Cone Piston Crown with Different Compression Ratios for Category I

The temperature plots for the engine when fitted with the unmodified and the truncated cone piston crown with the compression ratio varied from 16.243 to 16.877 as a result of some material from the piston when modified is depicted in Figure 4.38.

The temperature plots of the engine when fitted with the unmodified piston and truncated cone piston crowns of cone base angles 25°, 30°, 35°, 40° and 45° with different compression ratios are depicted in Figure 4.38. The plots are close despite being gotten from different compression ratio values and truncated cone base angles.

The unmodified piston engine plot appears conspicuously underneath the other plots, giving an indication that it has the highest peak temperature and least exhaust temperature values.

The peak temperature and exhaust gas temperature derived from this studies compares favourably with results of literature, as evidenced in the works of Basha *et al.* (2009). The exhaust gas temperatures are however higher than that reported by Reddy *et al,* (2012), although the engines rated power are different; the one used in this studies being higher.

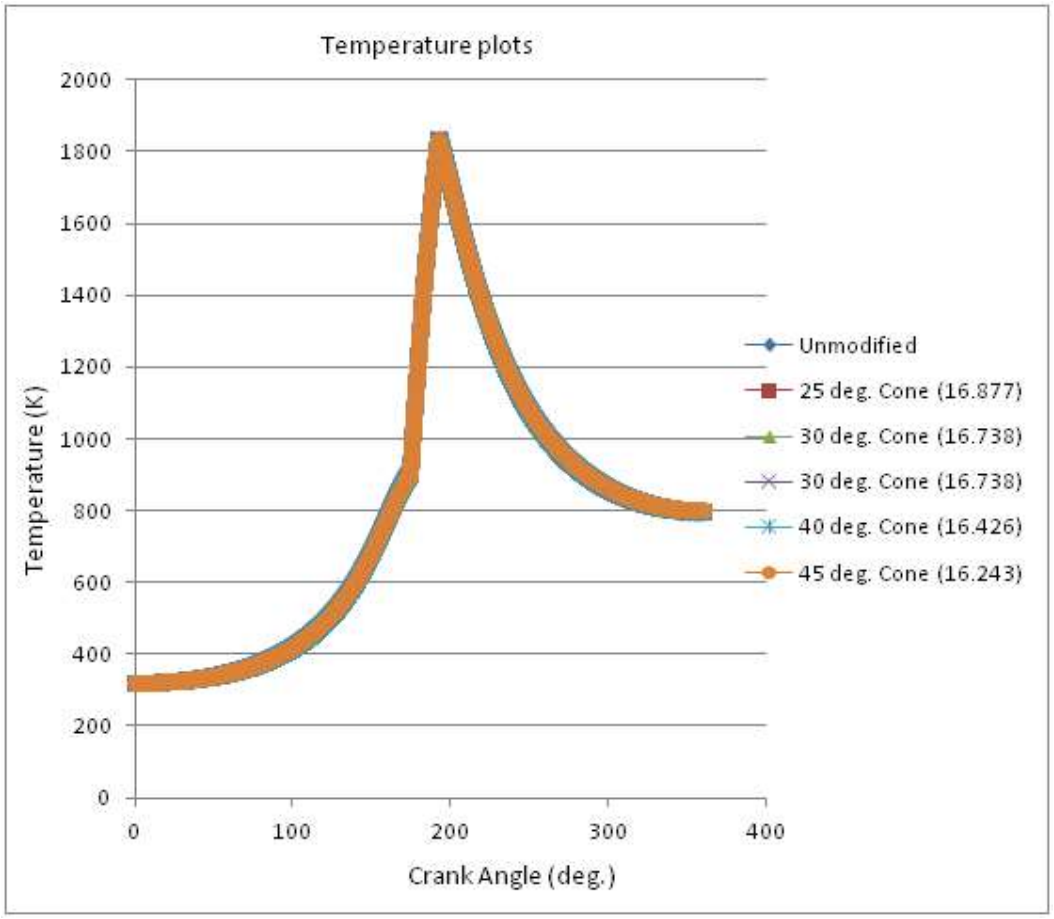

Figure 4.38. Temperature versus crank angle plots for unmodified and truncated cone piston crown with different CR for category I

4.5.7 Temperature Plots of Simulated Engine fitted with Inverted Truncated Cone Piston Crown having Constant Compression Ratio for Category I

The temperature plots for the simulated engine fitted with the unmodified and the inverted truncated cone piston crowns such that the compression ratio of the modified piston crown fitted engine are the same as that of the unmodified piston crown fitted engine is depicted in Figure 4.39.

The plot from the 40° inclination angle is conspicuously visible and has the peak temperature value as depicted in Figure 4.39 giving an indication of an optimized combustion chamber geometry at that cone base angle.

4.5.8 Temperature Plots of Simulated Engine fitted with Inverted Truncated Cone Piston Crown with Different Compression Ratio for Category I

The temperature versus crank angle plots of the engine with different compression ratios when fitted with the unmodified piston and inverted truncated cone piston crowns of inclination angle 25°, 30°, 35°, 40° and 45° is depicted in Figure 4.40.

The unmodified piston engine plot appears glaringly visible underneath the other plots, giving an indication that it has the highest peak temperature and least exhaust temperature values, also clearly visible is the plot of the 45° inclination angle inverted truncated cone piston and thus with higher value of peak temperature than the others.

The compression ratio of the standard piston equipped engine is remarkably higher than that of the inverted truncated cone piston crown equipped engine, and its peak temperature value is higher while its exhaust gas temperature is lower. The dependence of the engine combustion process and performance on compression ratio is clearly visible from the temperature versus crank angle plots; high value of peak temperature and lower value of exhaust gas temperature are required for better performance.

4.5.9 Simulated Engine Peak Temperature Plots for Category I

The peak temperature plots of the engine when fitted with different piston crowns are as depicted in Figure 4.41.

Maximum peak temperature value was obtained in the engine when the compression ratio was as that with the unmodified piston crown when fitted with a truncated cone piston crown having cone base angle of 35°.

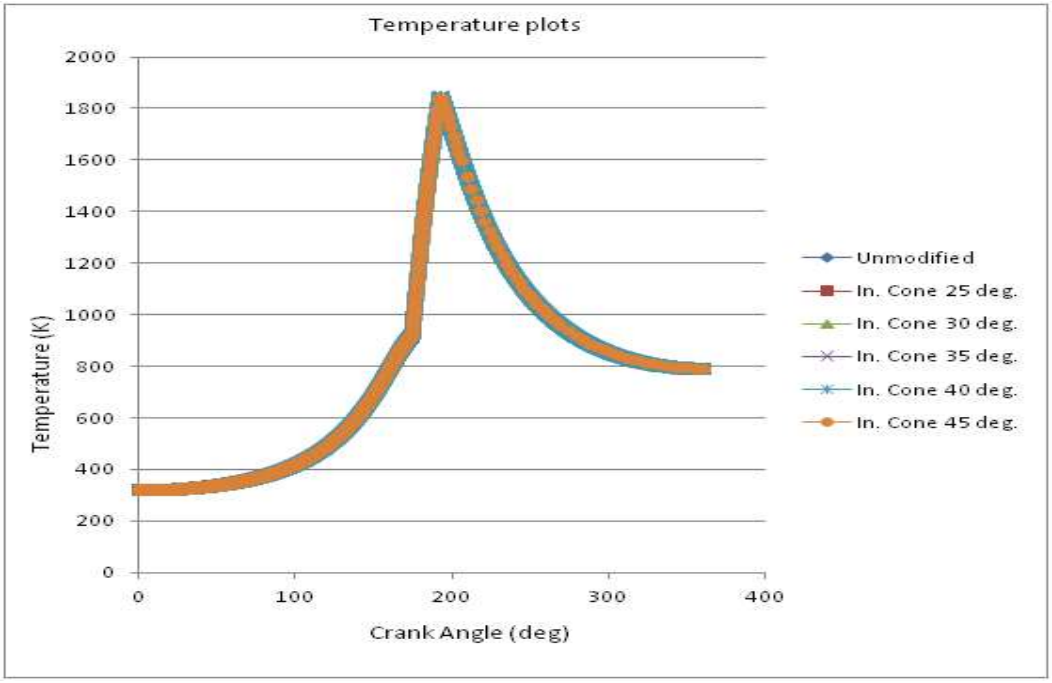

Figure 4.39. Temperature versus crank angle plots for unmodified and inverted truncated cone piston crown (CR 17.5)

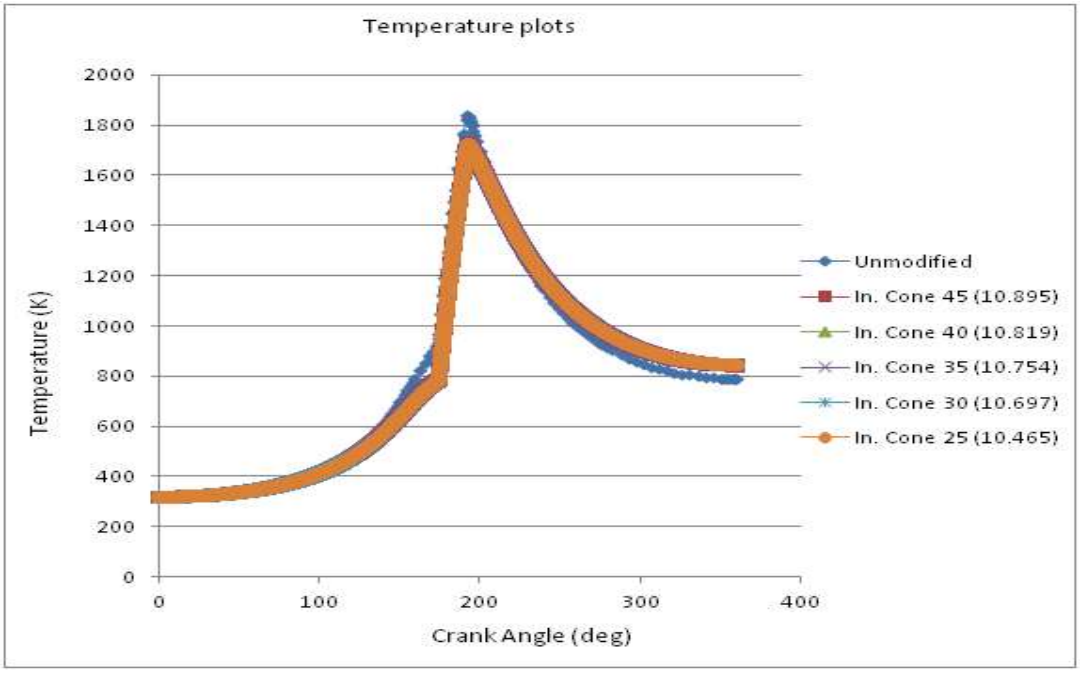

Figure 4.40. Temperature versus crank angle plots for unmodified and inverted truncated cone piston crown with different CR for category I

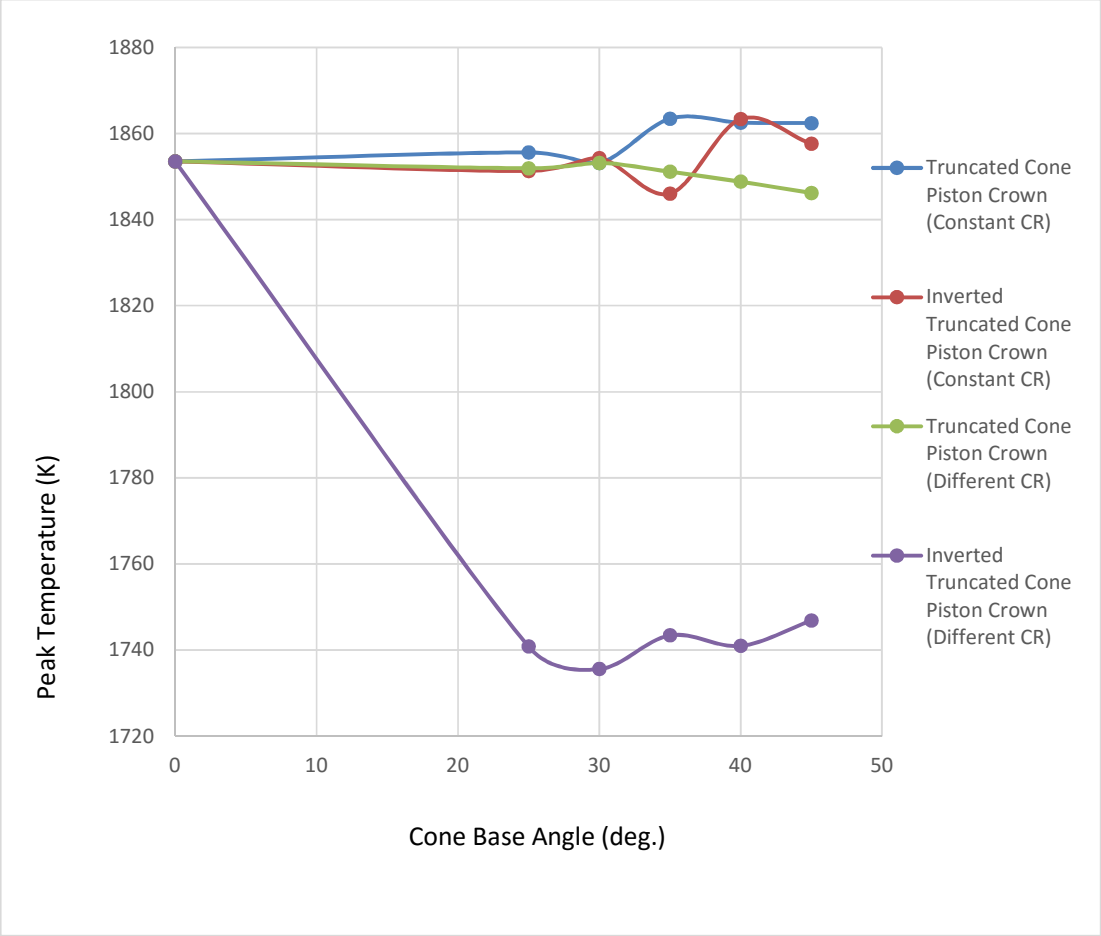

Figure 4.41. Effect of cone base angle on the Engine peak temperature for category I

The peak temperature value obtained for higher degree of inclinations of 40° and 45°, for both the truncated cone piston crown and the inverted truncated cone piston crown whose compression ratios are of the same value as the unmodified piston crown are also relatively higher, giving an indication of the possibility of better engine performance.

With different engine compression ratios, the peak temperature values for the engine with modified piston crowns are relatively lower. However at an inclination angle of 30°, peak temperature was almost the same as that of the unmodified piston crown.

The peak temperature versus crank angle plot for the inverted truncated cone piston crown equipped engine with compression ratio been a function of the truncated cone base angle is distinct from the other plots. This is because of the engine's low compression ratio in comparison with the others giving further credence to the fact that the performance characteristics of an engine is dependent on its compression ratio.

4.5.10 Simulated Engine Exhaust Gas Temperature Plots for Category I

The exhaust gas temperature plots of the engine when fitted with different piston crowns are as shown in Figure 4.42.

Based on the Carnot efficiency, the efficiency of an engine is a function of its peak and least temperature values, as the amount of obtainable work is dependent on the difference between these two temperature values. Asides its requirement for better performance in terms of power, low values of exhaust gas temperature are required for the metallurgical stability of the engine exhaust components.

The engine when fitted with the inverted truncated cone piston with an inclination angle of 35° having a similar compression ratio as that of the unmodified piston recorded the least value of exhaust gas temperature as depicted in Figure 4.42.

The exhaust gas temperature of the engine is affected by the angle of inclination of the modified piston crowns and this is the reason why even at similar compression ratios as that of the unmodified piston crown, the exhaust gas temperature values differs. The plot also gives an indication of the dependency of the exhaust gas temperature with compression ratios, and this is the reason for the marked difference between the plot for the inverted truncated cone piston crown equipped engine whose compression ratio is a function of the truncated cone base angle and the other plots.

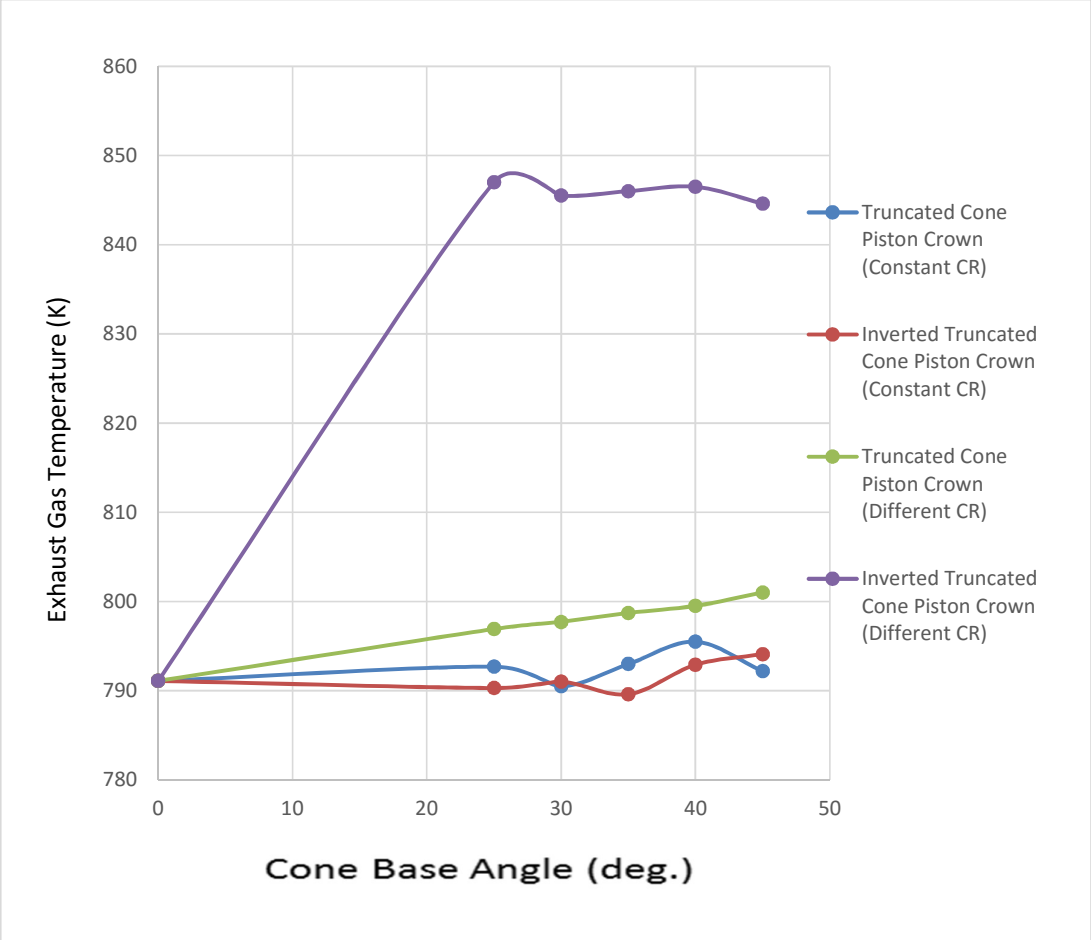

Figure 4.42. Effect of cone base angle on the Engine exhaust gas temperature for category I

4.5.11 Thermal Efficiency of Simulated Engine for Category I

The thermal efficiency of the engine when fitted with the unmodified and modified pistons was calculated using the relation in Equation (3.55);

$$\eta_{Th} = \frac{W_{net}}{Q_{in}}$$

For the engine fitted with the unmodified piston;

$$\eta_{Th} = \frac{481.64}{1558.62} = 30.901\%$$

The thermal efficiencies of the modelled engine when fitted with the truncated cone and the inverted truncated cone piston crowns for the test cone base angles are shown in Figure 4.43;

The engine has its maximum value of thermal efficiency when fitted with a truncated cone piston crown of an inclination angle of 35° having compression ratio of 17.5:1 (see Figure 4.43). When fitted with the inverted truncated cone piston crown of same compression ratio as that of the unmodified piston crown, the thermal efficiency of the engine with cone base angle of 40° and 45° also have thermal efficiency that are almost the same in value as the maximum attained value with the use of the truncated cone piston crown with a cone base angle of 35°.

The thermal efficiencies of the engine when fitted with the truncated cone and inverted truncated cone piston crowns but with the compression ratios lower than that of the standard are lesser implying that compression ratio contributes significantly to engine performance.

The derived thermal efficiencies are in agreement with the findings of Reddy *et al.* (2012) who conducted experiments on a Kirsloskar engine, Sundarraj (2011) with a percentage difference of 1.29%, Sundarraj and Saravannan (2012) with a percentage difference of 0.97%, Banarpumath *et al.* (2014), and Velappan and Sivaprakasam (2014) who separately conducted experiments on Kirsloskar TV1 compression ignition engines.

4.5.12 Mean Effective Pressure of Simulated Engine for Category I

The mean effective pressure in each case was also computed as follows using the relation in Equation (3.34); i.e.

$$P_m = \frac{W_{net}}{V_d}.$$

When the engine was fitted with the unmodified piston;

$$P_m = \frac{481.64}{0.00066145} = 7.282 \text{ x } 10^5 \text{ N/m}^2$$

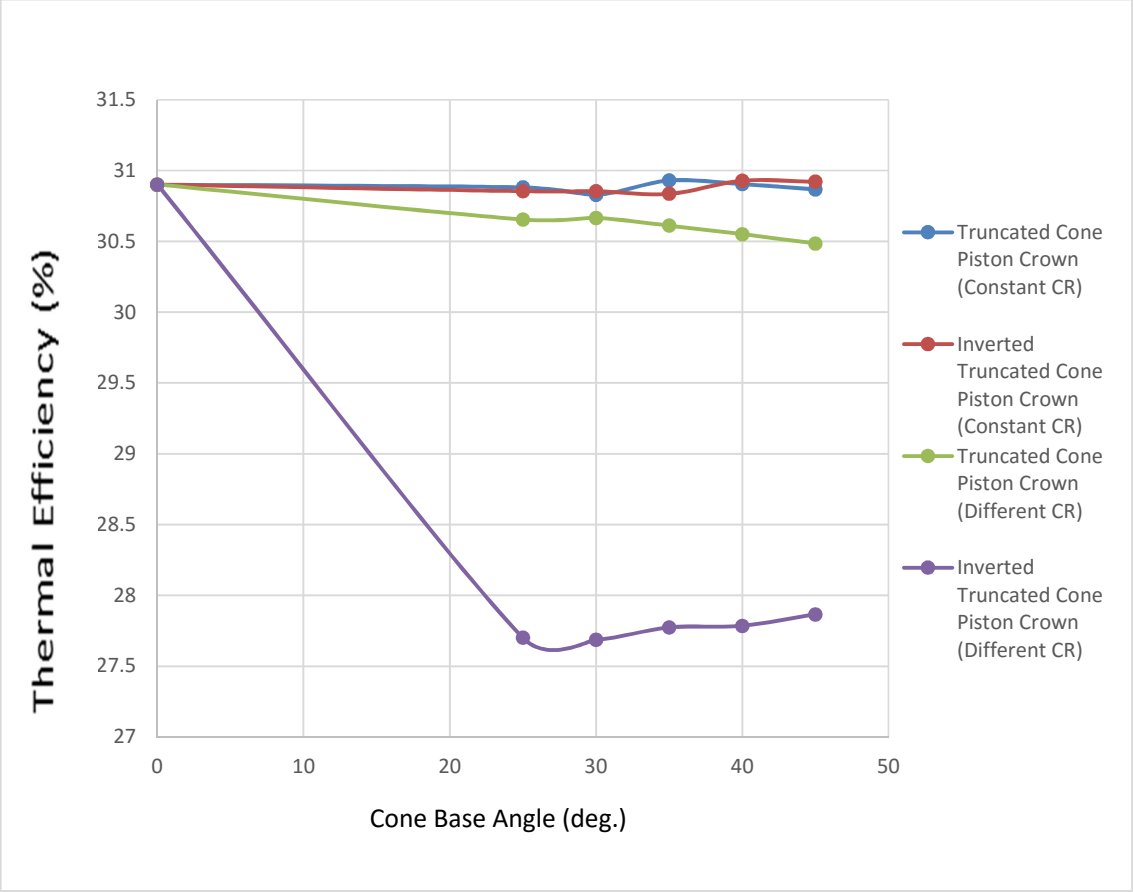

Figure 4.43. Effect of cone base angle on Engine thermal efficiency for category I

The mean effective pressures of the modelled engine when fitted with the truncated cone and the inverted truncated cone piston crowns for the selected truncated cone base angles is depicted Figure 4.44;

For the truncated cone piston crown equipped engine having the same compression ratio as that of the standard engine, the mean effective pressure values were higher for all the selected cone base angles except for 30° than the unmodified piston crown equipped engine. However, the mean effective pressure values are higher only for cone base angle of 40° and 45° with the use of the inverted truncated cone piston crown having the same compression ratio as that of the standard engine.

The values are lower for the engine when fitted with the truncated cone and inverted truncated cone piston crowns at all angle of inclinations as it was expected with lower values of compression ratio and was found to be a function of the compression ratio. The inverted truncated cone piston crown with an inclination angle of 30° however, has a considerable lower value of mean effective pressure in comparison to that at an inclination angle of 25° despite having a higher value of compression ratio. The combustion chamber geometry created at a cone base angle of 30° is thus more suited for a better in-cylinder fluid motion.

4.5.13 Brake Power from Simulations for Category I

The power generated by the engine when fitted with the unmodified piston and the modified piston crown was computed using the relation in Equation (3.35);

$$P = \frac{P_m LAN}{n_c}$$

The area 'A' of the engine cylinder is;

$$\frac{\pi D^2}{4}$$

where D is the cylinder bore

$A = \frac{\pi x 0.0875^2}{4} = 0.006013$ m^2

L = 0.11m, N = 1500 RPM, n_c = 2 (4 – stroke engine)

$\frac{LAN}{n_c} = \frac{0.11x\ 0.006013x1500}{60\ x\ 2} = 0.008268$

When the engine is fitted with the unmodified piston;

$P = 728200x\ 0.008268 = 6.021$ kW

When the engine was fitted with the truncated cone and the inverted truncated cone piston crowns for the selected test inclination angles, the respective generated power is as shown in Figure 4.45.

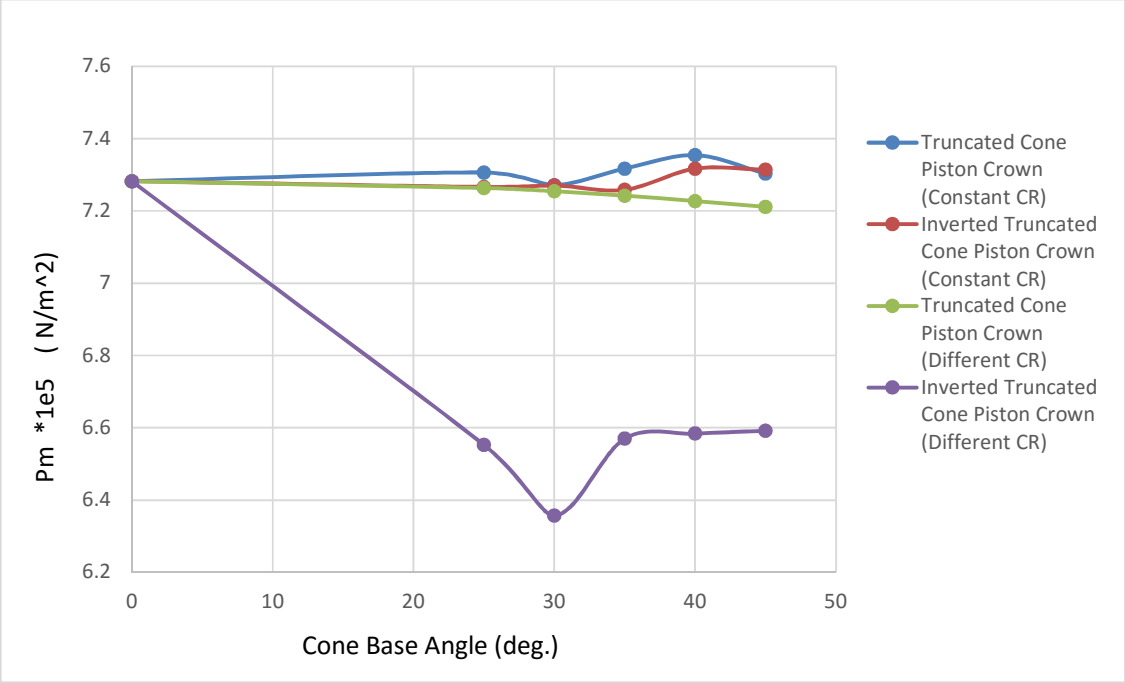

Figure 4.44. Effect of cone base angle on mean effective pressure plots for category I

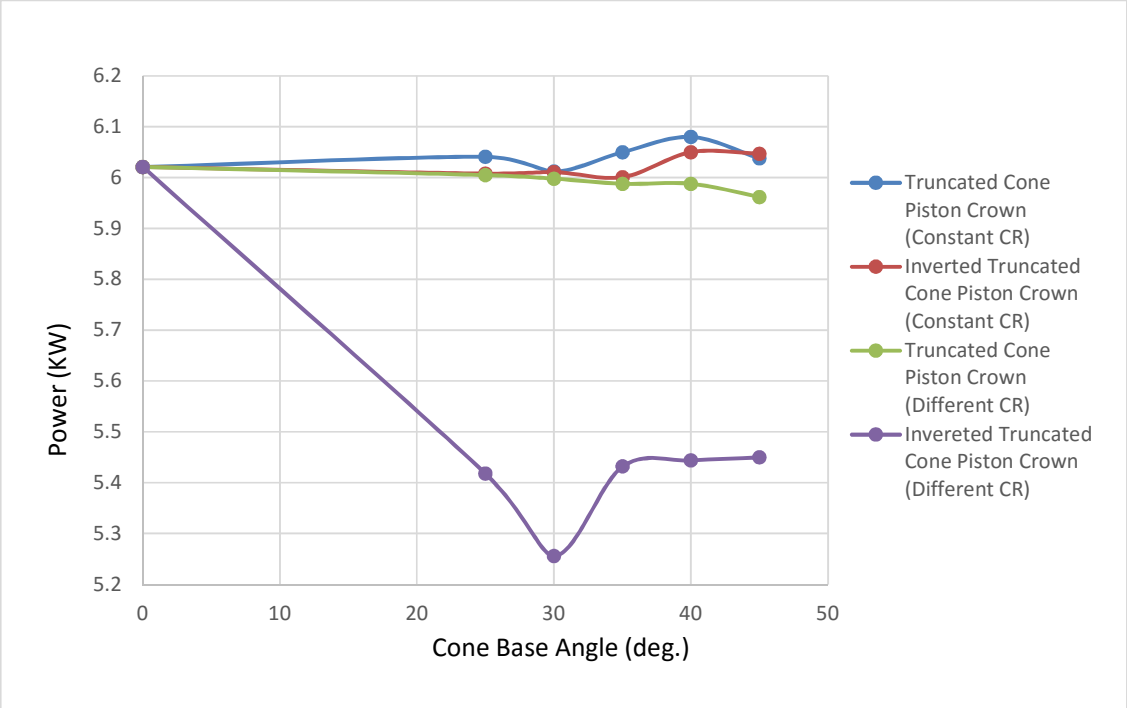

Figure 4.45. Effect of cone base angle on Engine power for category I

The trend observed in the mean effective pressure values of the engine when fitted with the different inclination angle pistons was also observed for the generated power. As shown in Figure 4.45, the power generated by the engine when fitted with the truncated cone piston crown having a compression ratio as that of the unmodified piston crown are higher at all cone base angles except for that of 30°, and this could have resulted from the cone-base angle not creating a combustion chamber geometry that favours improved in-cylinder air motion.

The obtained brake power results are in good agreement with the findings of Sundarraj (2011), Velappan and Sivaprakasam (2014), and Sreedhar and Prassad (2015), all with a percentage difference value lower than 14%. However, for the case of the inverted truncated piston crown equipped engine where the compression ratio is a function of the cone base angle, there exists a marked distinction.

The maximum value of generated power was recorded at a cone-base angle of 40°. However, for the case of the engine when fitted with the inverted truncated cone piston crown, the generated power values are higher only for the inclination angles of 40° and 45°.

The values are lower for the engine when fitted with the truncated cone and inverted truncated cone piston crowns at all angle of inclinations as it was expected with lower values of compression ratio.

The inverted truncated cone piston with an inclination angle of 30° however has a considerable lower value in comparison to that at an inclination angle of 25° just as was the case for the mean pressure value.

4.5.14 Engine Torque from Simulations for Category I

The engine torque for each of the piston crown geometry was calculated using Equation (3.36);

$$T_q = \frac{60}{2\pi N}$$

When the engine is fitted with the unmodified piston;

$$T_q = \frac{60*6021}{2\pi*1500}$$

= 38.33 Nm

When the engine was fitted with the truncated cone and the inverted truncated cone piston crowns for the selected test inclination angles, the respective torques are plotted in Figure 4.46.

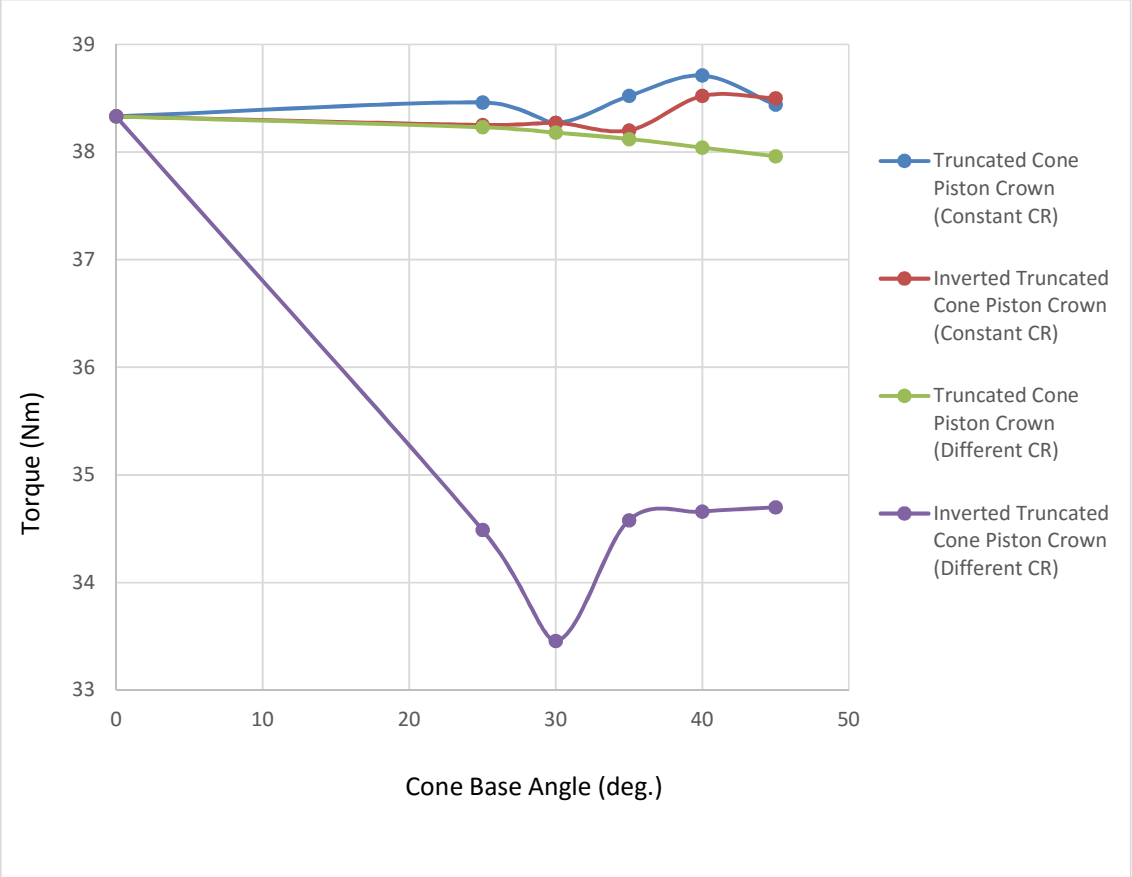

Figure 4.46. Effect of cone base angle on Engine torque for category I

The torque developed by the engine was observed to be least when it was fitted with the inverted truncated cone piston crown of inclination angle of 30° and has its peak value when fitted with a truncated cone piston crown of the same compression ratio as the unmodified piston crown with an inclination angle of 40°.

The same trend as observed in the mean effective pressure and the generated power was also noticed in the generated torque. The use of the modified piston crowns led to the modification of the engines combustion chamber geometry.

4.5.15 Brake Specific Fuel Consumption of Simulated Engine for Category I

The specific fuel consumption was calculated using Equation (3.37);

$$SFC = \frac{\rho_{atm}}{(A/F)P_m} = \frac{\dot{m}_f}{P} = \frac{\rho_f q}{P}$$

Using

$SFC = \frac{\rho_{atm}}{(A/F)P_m}$,

ρ_{atm} = 1.1886 kg/m^3

(A/F); from Equation (3.20);

$((A/F)_{stoc} = \frac{m_{air}}{m_{fuel_{stoc}}} = \frac{4.76*11*m_{air}}{1*m_{fuel}})$

And from Equation (3.21);

$(\psi = \frac{(A/F)_{stoc}}{(A/F)})$

m_{air} = 28.96 kg/Kmol, m_{fuel} = 100 kg/Kmol (C_7H_{16}), ψ = 0.5

$$(A/F) = \frac{(A/F)_{stoc}}{\psi}$$

$$= \frac{4.76*11*m_{air}}{\psi*1*m_{fuel}}$$

$$= \frac{4.76*11*28.96}{0.5*100} = 30.33$$

When the engine is fitted with the unmodified piston;

$$SFC = \frac{\rho_{atm}}{(A/F)P_m}$$

$$= \frac{1.1886}{30.33*728200}$$

$= 5.382 * 10^{-8}$ kg/Ws

= 0.1938 kg/kWh

When the engine was fitted with the truncated cone and the inverted truncated cone piston crowns for the selected test inclination angles, the respective specific fuel consumption is depicted in Figure 4.47.

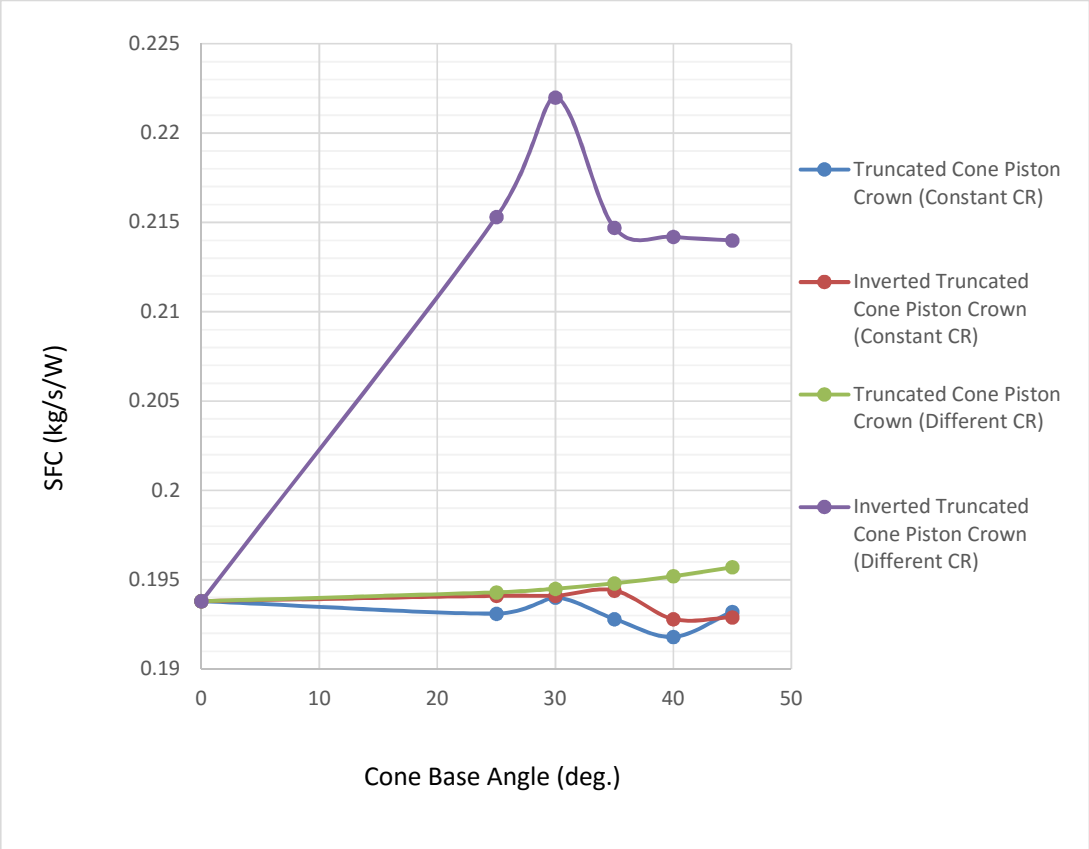

Figure 4.47. Engine specific fuel consumption versus cone base angle for category I

The specific fuel consumption is the amount of fuel consumed for a unit power output. From the plots of generated power in Figure 4.45, the peak amount of power generated for the same amount of fuel was recorded for the engine when fitted with the truncated cone piston crown of inclination angle of 40° and having the same compression ratio as that of the unmodified piston crown. At this same piston crown geometry, the specific fuel consumption has the least value, giving an indication of a better engine performance.

The specific fuel consumption as depicted in Figure 4.47 follows the reverse trend of the generated power; the truncated cone piston crown of inclination angle 40° with compression ratio as that of the unmodified piston has the least value of specific fuel consumption.

It is expected that the specific fuel consumption values will be different, and this is so because the use of the modified piston crown equipped engine changes the combustion chamber geometry, which is a major determinant of the performance characteristics of an engine.

The specific fuel consumption values of the engine when fitted with inverted truncated cone piston crowns having compression ratios equal to that of the unmodified piston are lower only for inclination angles of 40° and 45°. The engine when fitted with an inverted truncated cone piston crown with inclination angle of 30° however has a considerable higher value in comparison to that with inclination angle of 25°.

The derived specific fuel consumption from the studies compares fairly with the findings of Veleppan and Sivaprakasam (2014) who conducted experiments on a Kirloskar TV1 compression ignition engine. A percentage difference of about 19.25% exists between the results of this study and that of the work of Veleppan and Sivaprakasam (2014).

4.5.16 Carbon monoxide (CO) Emissions of Simulated Engine for Category I

The CO emissions as estimated using the developed numerical model for the engine when fitted with the unmodified piston crown and the modified piston crown for all the cases considered were taken, and the resultant plots are depicted in Figure 4.48.

Carbon monoxide (CO) is a poisonous gas and is one of the products formed by the incomplete combustion of fuels.

The CO emissions from the engine when fitted with the inverted truncated cone piston crown having compression ratios lower than standard (due to the modification) are relatively higher than the CO emissions from the engine with unmodified piston. The emission level decreases with increasing piston crown cone base angle.

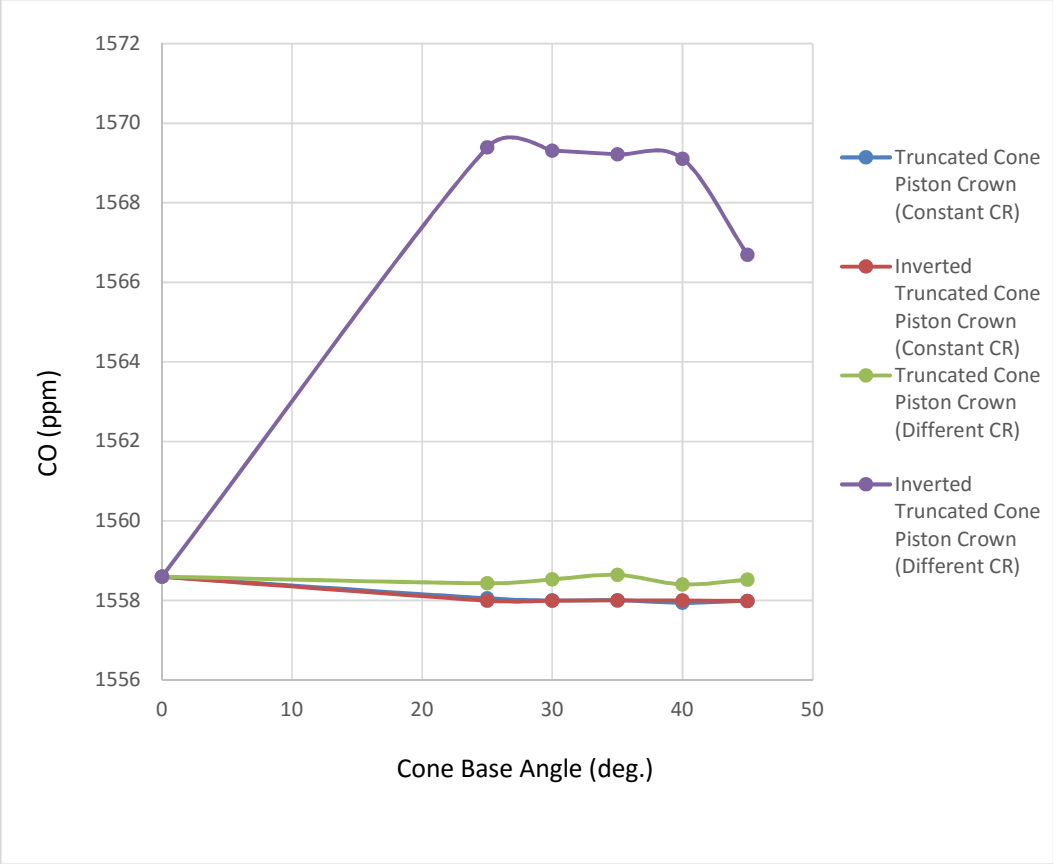

Figure 4.48. Effects of cone base angle on Carbon monoxide (CO) emissions for category I

For the case of the engine with truncated cone piston crown having compression ratios lower than standard due to the modification, the CO emission levels in comparison to that from the unmodified piston crown does not follow a straight forward trend.

It was found to be lower for the cases of 25°, 30° and 40° and higher for the cases of 35° and 45°, giving an indication that the CO emission levels for an engine is not just dependent on the compression ratio, but also on the combustion chamber geometry.

The CO emission level for the engine when fitted with either a truncated cone or the inverted truncated cone piston crown having a compression ratio as that of the unmodified piston crown are lower in comparison to that emitted from the engine when fitted with the unmodified piston crown, corroborating further the idea that the CO emission level is also dependent on the shape of the combustion chamber. The least value of CO emission was from the simulated engine fitted with a truncated cone piston crown at an inclination angle of 35° having a compression ratio of 17.5:1 just as that of the unmodified piston crown.

The CO emission level is in conformity with the findings of Banarpumath *et al.* (2014) and Periyasamy and Vadivel (2015), however, the case of the inverted truncated cone piston crown equipped engine with compression ratios being a function of the truncated cone base angle, there exists a difference. This is as a result of the lower compression ratios.

4.5.17 Carbon dioxide (CO_2) Emissions of Simulated Engine for Category I

The plots of CO_2 emission levels in percentage by volume from the simulation of the engine when fitted with the unmodified piston crown and the modified piston crown for the cases and different angles considered are shown in Figure 4.49.

CO_2 is formed by the complete oxidation (combustion) of the carbon molecules present in fuels.

The CO_2 and CO emissions from the engine when equipped with the inverted truncated cone piston crown having lower compression ratios values due to the modification are higher than the emissions from the unmodified piston crown engine; the emission level decreases for increasing cone base angle.

For the case of the truncated cone piston crown having compression ratio values lower than that for the standard, the CO_2 emission levels were higher, and this is due to the reasons explained earlier that the engine performance is affected by its compression ratio. The emission ratio level witnessed a gradual increase with the increase in inclination angle until at 40° where it showed a decrease, however an increase was observed at an inclination angle of 45°.

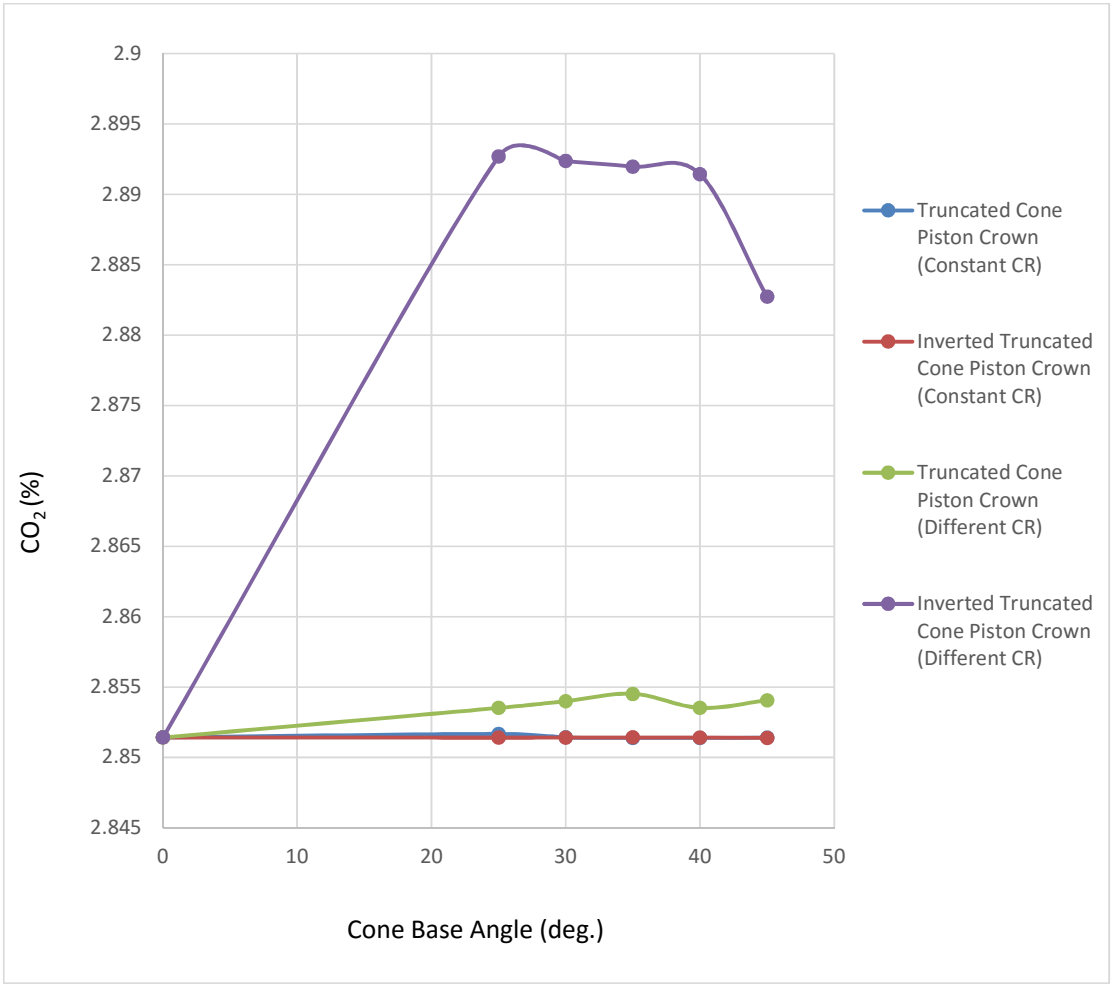

Figure 4.49. Effect of cone base angle on Carbon dioxide (CO_2) emission for category I

The CO_2 emission level for the engine when fitted with either a truncated cone or the inverted truncated cone piston crown having a compression ratio as that of the unmodified piston crown are lower in comparison to that emitted from the engine when fitted with the unmodified piston crown. The CO_2 emission was however, higher for the case of the truncated cone piston crown at inclination angle of 25°. The least value of CO_2 emission was from the simulated engine fitted with a truncated cone piston crown at an inclination angle of 40° having a compression ratio of 17.5:1. The differences in CO_2 emission level is largely due to the differences in combustion type occasioned by the modification of the combustion chamber.

4.6 Category II Simulation Results

The estimated values of the considered performance parameters for the numerical simulation of the category II engine follows in the sub-sections below. Numerical simulations were carried out for the unmodified piston crown, truncated cone piston crowns, and for inverted truncated cone piston crowns with different inclination angles of 25°, 30°, 35°, 40°, and 45° for a constant compression ratio.

4.6.1 Simulated Engine Exhaust Gas Temperature Plots for Category II

The exhaust gas temperature plots of the engine when fitted with the standard piston, truncated cone, and inverted truncated cone piston crowns with inclination angles of 25°, 30°, 35°, 40° and 45° are depicted in Figure 4.50.

The exhaust gas temperature of the engine was affected by the angle of inclination of the modified piston crowns and this explained why even at same compression ratios as that of the unmodified piston crown, the exhaust gas temperature values differs. The unmodified piston crown has the least value of exhaust gas temperature.

The obtained exhaust gas temperature values are similar with the findings of Reddy *et al.* (2012), although an engine of a different power rating was used in his studies.

4.6.2 Thermal Efficiency of Simulated Engine for Category II

The thermal efficiency of the engine when fitted with the unmodified and modified pistons was calculated using the relation in Equation (3.55);

$$\eta_{Th} = \frac{W_{net}}{Q_{in}}$$

For the engine fitted with the unmodified piston;

$$\eta_{Th} = \frac{109.54}{340.22} = 32.200\%$$

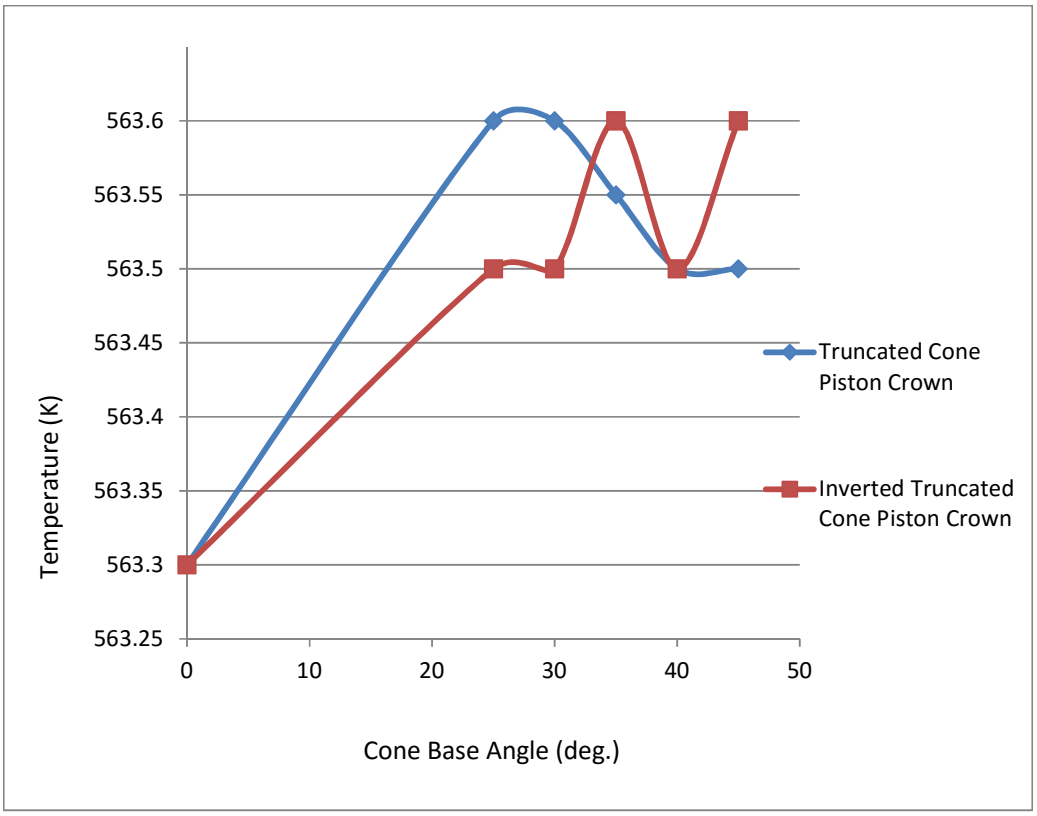

Figure 4.50. Effect of cone base angle on the Engine exhaust gas temperature for category II

The thermal efficiencies of the modelled engine when fitted with the truncated cone and the inverted truncated cone piston crowns for the test inclination angles are as shown in Figure 4.51.

The engine has its maximum value of thermal efficiency when fitted with a truncated cone piston crown with an inclination angle of 40° as depicted in Figure 4.51. The thermal efficiencies of the truncated cone piston crown were in all cases found to be greater than that of the unmodified piston fitted engine, and the same was the results for the thermal efficiency values for the inverted truncated cone piston crowns. This is attributable to the difference in combustion chamber geometry occasioned by the use of truncated cone piston crown with different cone base angles.

The thermal efficiency results compare favourably with the findings of Mamilla *et al.* (2013), Al-Dawody and Bhatti (2014), Periyasamy and Vadivel (2015), and not markedly different from the findings of Laguitton *et al.* (2006).

4.6.3 Mean Effective Pressure of Simulated Engine for Category II

The mean effective pressure in each case was also computed using the relation in Equation (3.56);

$P_m = \frac{W_{net}}{V_d}$.

When the engine was fitted with the unmodified piston;

$P_m = \frac{109.64}{0.00026939}$ = 4.0699 x 10^5 N/m^2

The mean effective pressures of the modelled engine when fitted with the truncated cone and the inverted truncated cone piston crowns for the selected test inclination angles is depicted in Figure 4.52.

The mean effective pressure values for the engine when fitted with the truncated cone piston crowns and the inverted truncated cone piston crowns are higher at all inclination angles than that of the unmodified piston crown with the maximum value recorded at an angle of inclination of 40° for both the truncated and the inverted truncated cone piston crown.

The differences in the mean effective pressure values as obtained was because of the different combustion geometry which is created with the use of the modified piston crown having different truncated cone base angles.

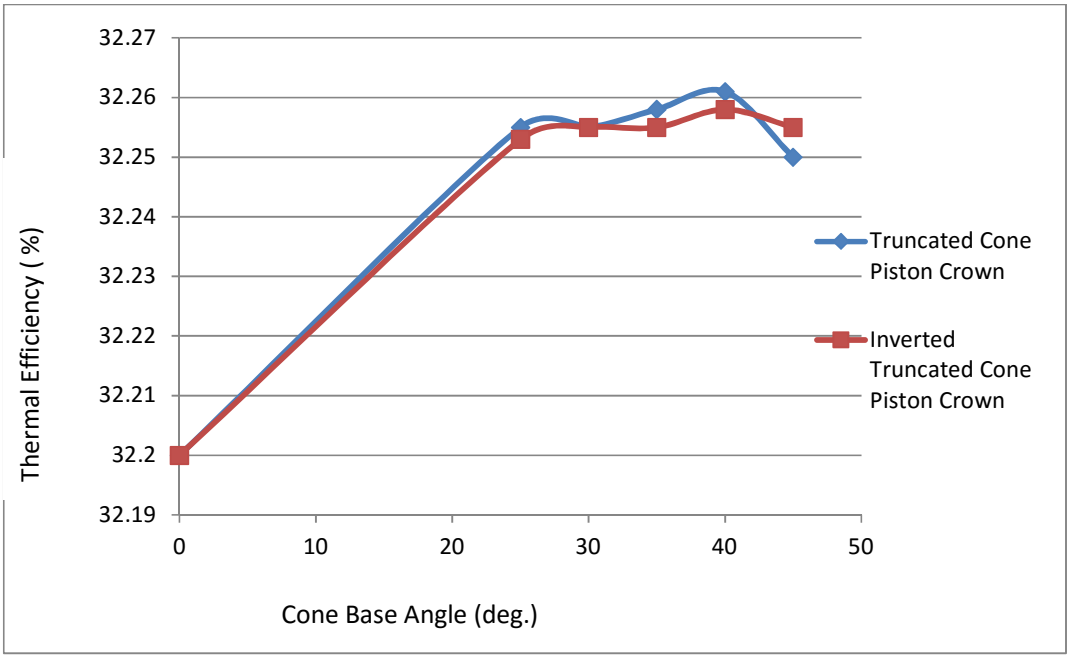

Figure 4.51. Effect of cone base angle on Engine thermal efficiency for category II

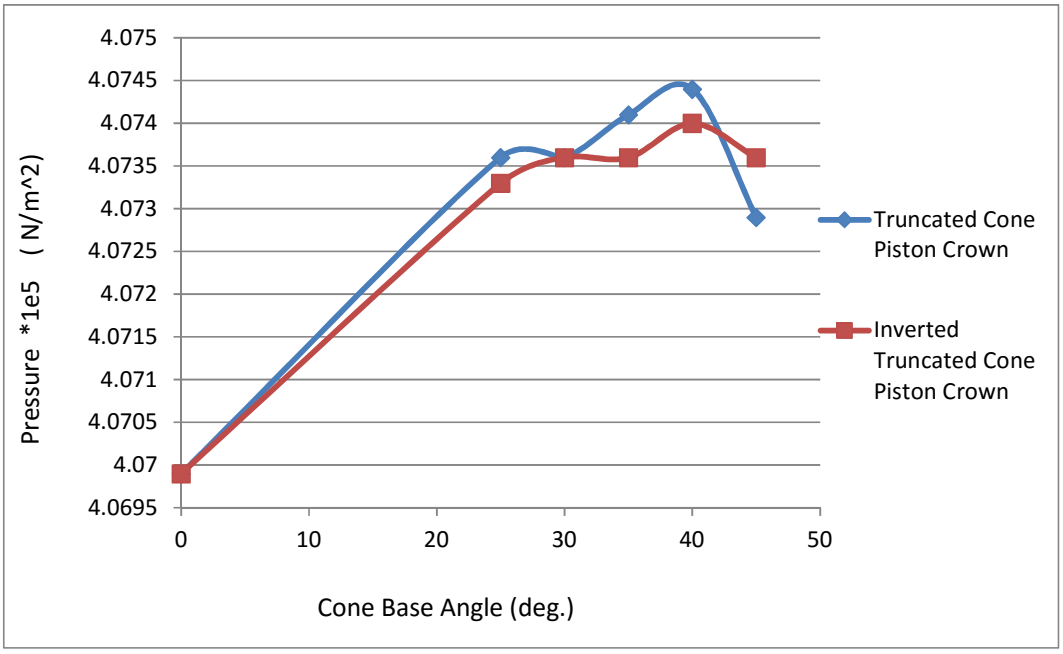

Figure 4.52. Effect of cone base angle on mean effective pressure plots category II

4.6.4 Brake Power from Simulations for Category II

The power generated by the engine when fitted with the unmodified piston and the modified piston crown was computed using the relation in Equation (3.35) i.e.

$P = \frac{P_m LAN}{n_c}$

The area 'A' of the engine cylinder is;

$\frac{\pi D^2}{4}$,

where D is the cylinder bore

A = $\frac{\pi x 0.07^2}{4}$ = 0.003848 m^2

L = 0.07m, N = 2600 RPM, n_c = 2 (4 – stroke engine)

$\frac{LAN}{n_c} = \frac{0.07 * 0.003848 * 2600}{60 * 2}$ = 0.005839

When the engine is fitted with the unmodified piston;

$P = 406990 * 0.005839$ = 2.3764 kW

When the engine was fitted with the truncated cone and the inverted truncated cone piston crowns for the selected test inclination angles, the respective generated power is as shown in Figure 4.53.

The power generated by the engine when fitted with the truncated and the inverted truncated cone piston crowns are higher at all inclination angles than for the unmodified piston crown with the maximum value recorded at an angle of inclination of 40° for the truncated cone piston crown.

The combustion chamber geometry is optimized with the use of the truncated cone piston crown with a cone base angle 40^0 resulting into better combustion process and ultimately better engine performance in comparison to the other piston crowns.

4.6.5 Engine Torque from Simulations for Category II

The engine torque for each of the piston crown geometry was calculated using Equation (3.58), i.e.

$T_q = \frac{60}{2\pi N}$

When the engine is fitted with the unmodified piston;

$T_q = \frac{60 * 2376.4}{2\pi * 2600}$

= 8.728 Nm

Figure 4.53. Effect of cone base angle on Engine power for category II

When the engine was fitted with the truncated cone and the inverted truncated cone piston crowns for the selected test inclination angles, the respective torques are depicted in Figure 4.54.

The torque developed by the engine was observed to be the least when it was fitted with the unmodified piston crown, and has its peak value when fitted with a truncated cone piston crown with an inclination angle of 40°.

The trend observed in the mean effective pressure and the generated power was also noticed in the generated torque. The engine torque was optimized with the use of the 40^0 cone base angle truncated cone piston crown as a result of the combustion chamber modification.

4.6.6 Brake Specific Fuel Consumption of Simulated Engine for Category II

The specific fuel consumption was calculated using Equation (3.37);

$$SFC = \frac{\rho_{atm}}{(A/F)P_m} = \frac{\dot{m}_f}{P} = \frac{\rho_f q}{P}$$

Using

$SFC = \frac{\rho_{atm}}{(A/F)P_m}$,

ρ_{atm} = 1.1886 kg/m^3

(A/F); from Equation (3.20);

$((A/F)_{stoc} = \frac{m_{air}}{m_{fuel_{stoc}}} = \frac{4.76*11*m_{air}}{1*m_{fuel}})$

And from Equation (3.21);

$(\psi = \frac{(A/F)_{stoc}}{(A/F)})$

m_{air} = 28.96 kg/Kmol, m_{fuel} = 100 kg/Kmol (C_7H_{16}), ψ = 0.5

$$(A/F) = \frac{(A/F)_{stoc}}{\psi}$$

$$= \frac{4.76x11x\,m_{air}}{\psi x1x\,m_{fuel}}$$

$$= \frac{4.76x11x28.96}{0.5x100} = 30.33$$

When the engine is fitted with the unmodified piston;

$$SFC = \frac{\rho_{atm}}{(A/F)P_m} = \frac{1.1886}{30.33x406990}$$

= 9.629 x 10^{-8} kg/Ws = 0.3466 kg/kWh

When the engine was fitted with the truncated cone and the inverted truncated cone piston crowns for the selected test inclination angles, the respective brake specific fuel consumption values are depicted in Figure 4.55.

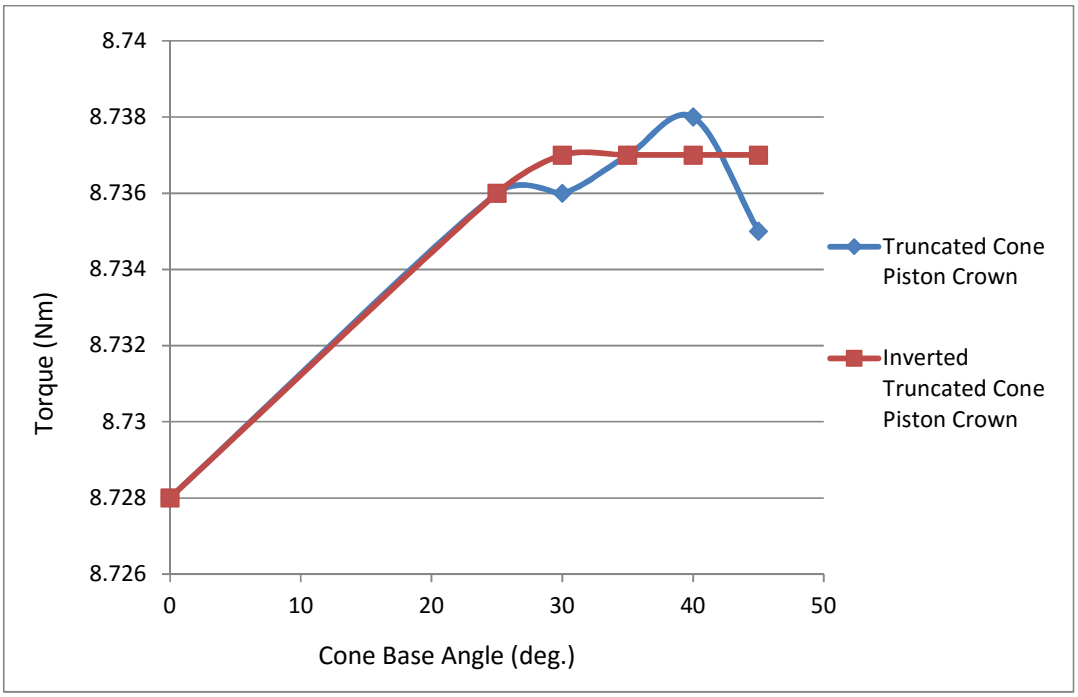

Figure 4.54. Effect of cone base angle on Engine torque for category II

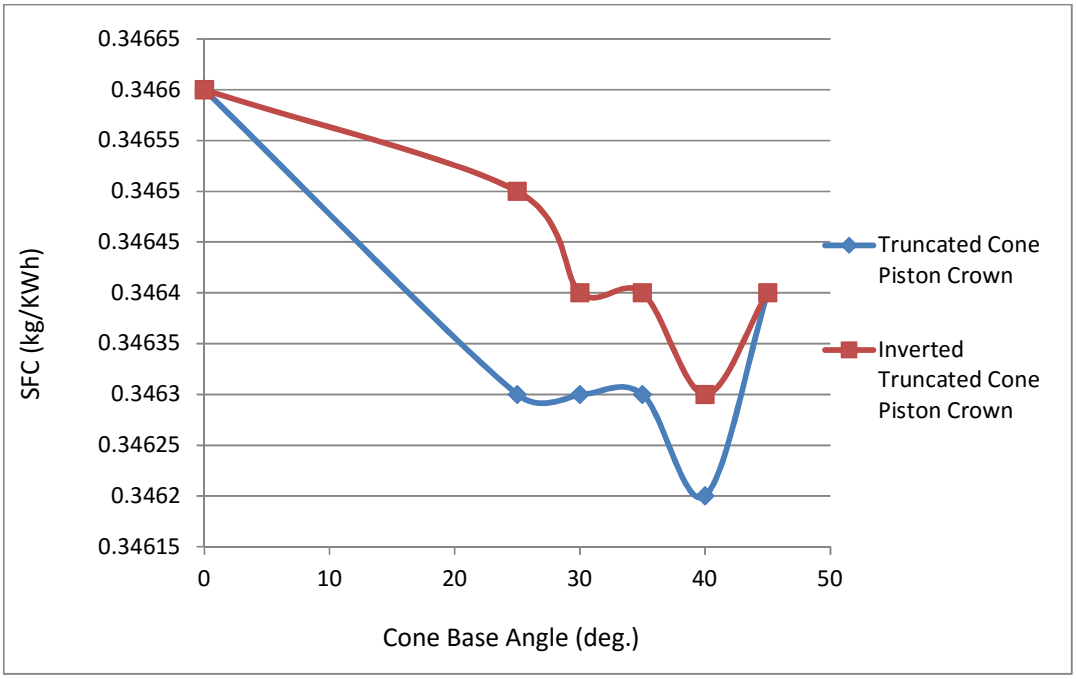

Figure 4.55. Engine specific fuel consumption versus cone base angle for category II

As stated earlier in section 4.5.15, the specific fuel consumption is the amount of fuel consumed for a unit power output. From the plots of generated power in Figure 4.53, the peak amount of power generated for the same amount of fuel was recorded for the engine when fitted with the truncated cone piston crown of inclination angle of 40°. This same piston crown geometry has the least value of specific fuel consumption, giving an indication of its better performance.

The specific fuel consumption results obtained were of different values, and this was because of the differences that occurred in the combustion processes as a result of the combustion chamber modification using the modified piston crown on one hand, and the differences in compression ratio on the other hand.

The results compare favourably with the findings of Periyasamy and Vadivel (2015) for an engine with brake power of 2.3 KW.

The specific fuel consumption curves as depicted in Figure 4.55 follows the reverse trend of the generated power curves; the truncated cone piston crown of inclination angle 40° has the least value of specific fuel consumption.

4.6.7 Carbon monoxide (CO) Emissions of Simulated Engine for category II

The carbon monoxide emissions obtained from the simulation of the engine when fitted with the unmodified piston crown, the truncated cone piston crowns, and the inverted truncated piston crowns for all the values of inclination angles are as shown in Figure 4.56.

The carbon monoxide emission level was observed to be highest for the unmodified piston crown and have the least values for the 25° truncated cone and inverted truncated cone piston crown fitted engine as depicted in Figure 4.56. The modifications of the piston crown thus have an effect on the engine's emission of carbon monoxide.

The modification of the piston crown led to better performance in terms of carbon II oxide emission giving an indication of a better combustion process.

The carbom II oxide emission are in close agreement with the findings of the studies conducted by Periyasamy and Vadivel (2015).

4.6.8 Carbon dioxide (CO_2) Emissions of Simulated Engine for category II

The plots of carbon dioxide emission levels in percentage by volume from the simulation of the engine when fitted with the unmodified piston crown and the modified piston crown for the different angles considered are shown in Figure 4.57.

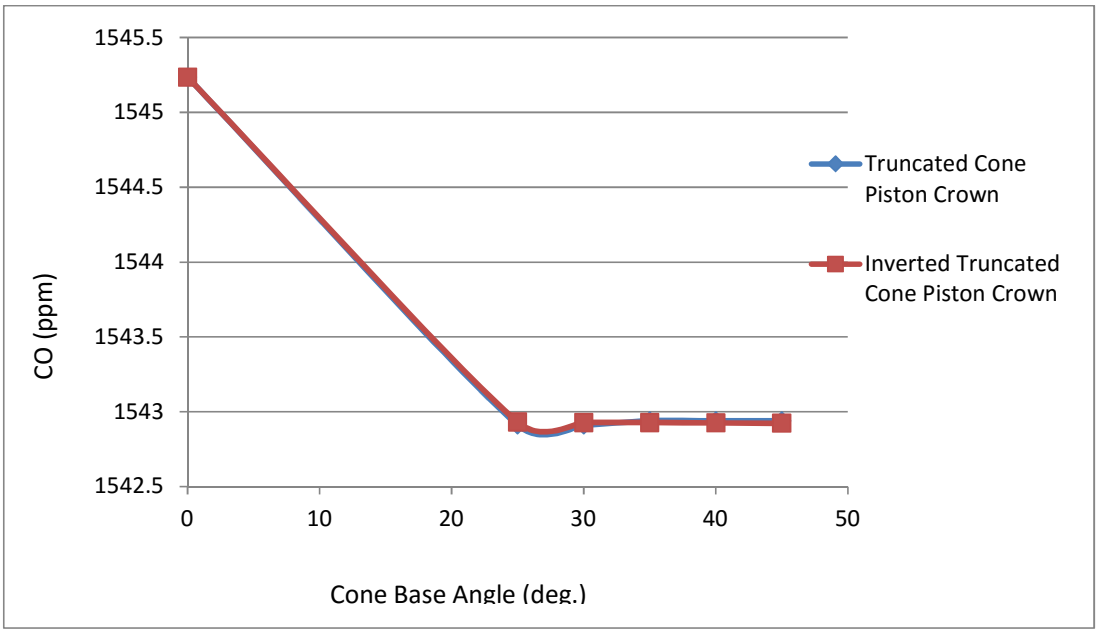

Figure 4.56. Effects of cone base angle on Carbon monoxide (CO) emissions for category II

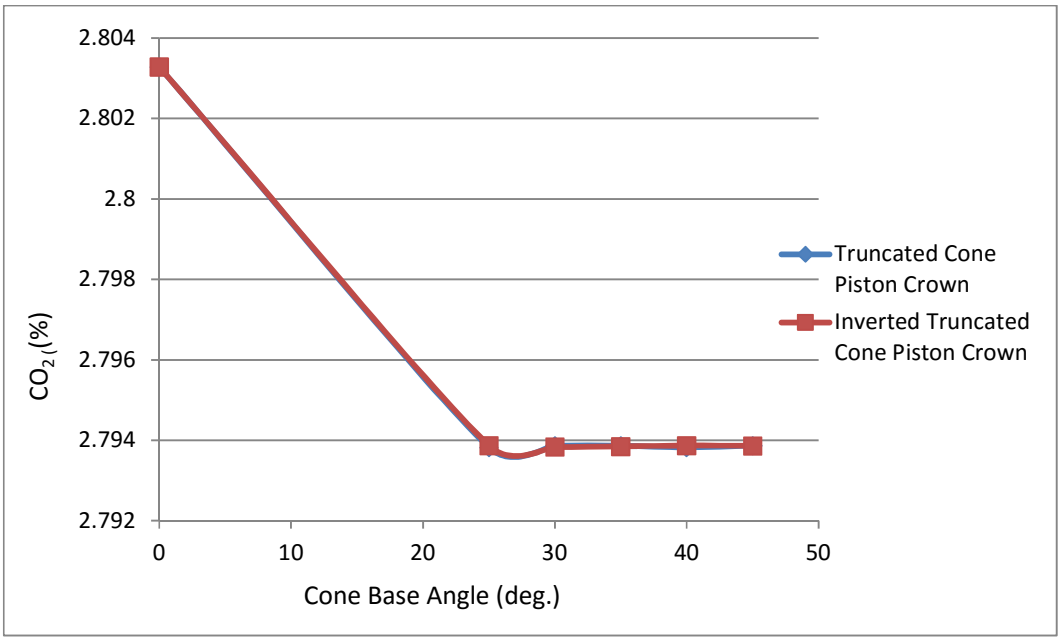

Figure 4.57. Effects of cone base angle on Carbon dioxide (CO_2) emission for category II

The carbon dioxide emission level for category II is similar to that of category I. The emission level was observed to be lower for all considered angles of inclination of the truncated cone and inverted truncated cone piston crowns in comparison to the unmodified piston crown just as it was the case for carbon monoxide emission. The piston crown modification is thus observed to have led to an improvement in the emission level of the engine, by favouring a better combustion process.

4.7 Quantitative Summary of Findings from Numerical Analyses

The mean and standard deviation values of the compression ignition engine termed category I with a compression ratio of 17.5:1 and the weighted performance parameters for all the configurations of the truncated cone piston crown and the inverted truncated cone piston crown with compression ratio of 17.5:1 and of range 10.645 to 16.877 with stepping of V_s/V_{cc} as presented in the previous sections are summarized in Table 4.5. The Category I engine having truncated cone and inverted truncated cone piston crowns with compression ratio of 17.5:1 showed better performance. The compression engine with truncated cone piston crown with compression ratio of 17.5:1 and inclination angle of 40° showed the best performance. The mean and standard deviation values for Category II engine with all the inclination angles of the truncated cone piston crown and the inverted truncated piston crown are summarized in Table 4.6. Just as it was obtained in the modelling results of the Kirloskar TV1 engine, the Yoshita 165F engine equipped with a truncated cone piston crown with a cone base angle of 40° was observed to have the greatest improvement in the performance parameters considered. The numerical modelling predictions of one can thus be used to predict the behaviour of another.

The grand mean values and standard deviations of engine power, thermal efficiency, specific fuel consumption, mean effective pressure, torque, exhaust gas temperature, peak temperature, carbon-monoxide and carbon dioxide for all the variations of the TCPC and ITCPC with compression ratios of 17.5:1 and of range 10.645 to 16.877 are depicted in Table 4.5. As shown in Table 4.7 which shows that the variance ratios (F) were markedly greater than the probability values (F – Critical), the performance of the compression ignition engine was significantly affected by truncated cone and inverted truncated cone piston crown configurations.

Table 4.5: The weighted values of the performance parameters of the TCPC and ITCPC against the standard piston for Category I

Performance Parameters	**TCPC and ITCPC with CR of 17.5:1**	**TCPC and ITCPC with CR of range 10.645 to 16.877**
Power (kW)	6.032±0.023	5.748±0.311
Thermal Efficiency (%)	30.89±0.03	29.47±1.51
Specific Fuel Consumption (kg/kWh)	0.1934±0.0008	0.2035±0.0112
Mean Effective Pressure (10^5 N/m^2)	7.2950±0.0282	6.9514±0.3762
Torque (N/m)	38.40±1.5	36.59±1.98
Exhaust Gas Temperature (K)	792.0±1.7	817.1±25.6
Peak Temperature (K)	1856.2±5.7	1805.5±56.5
Carbon-monoxide emission (ppm)	1558.102±0.233	1562.789±5.304
Carbon-dioxide emission (%)	2.8514±7.77E-5	2.8686±1.92E-2

Table 4.6: The weighted values of the performance parameters of the standard piston, TCPC and ITCPC for Category II

Performance Parameters	**TCPC and ITCPC with CR of 20.5:1**
Power (kW)	2378.28±0.86
Thermal Efficiency (%)	32.25±0.02
Specific Fuel Consumption (kg/kWh)	0.3464±0.0001
Mean Effective Pressure (10^5 N/m^2)	4.0730±0.0015
Torque (Nm)	8.74±0.0034
Exhaust Gas Temperature (K)	563.50±0.11
Carbon-monoxide emission (ppm)	1543.3129±0.8983
Carbon-dioxide emission (%)	2.7954±0.0037

Table 4.7: The ANOVA results for the estimates of numerical model of the performance parameters of the compression ignition engines

	Source of Variation	**Sums of Squares**	**Degrees of Freedom**	**Mean Squares**	**Variance Ratios (F)**	**Probability value (F-Critical)**
Torque (Nm)	Between samples	59.3213	4	14.8303	180.1984	3.01
	Within Samples	1.3710	16	0.0823	-	-
	Total	60.6923	20	-	-	-
Thermal Efficiency (%)	Between samples	37.6785	4	9.4196	2545.8378	3.01
	Within Samples	0.0589	16	0.0037	-	-
	Total	37.7374	20	-	-	-
Specific Fuel Consumption (kg/kWh)	Between samples	0.00180	4	0.000450	144.2308	3.01
	Within Samples	0.00005	16	0.000003	-	-
	Total	0.00185	20	-	-	-

4.8 Results of Experiment

The chemo-physical properties of the fuel; petroleum diesel and Shea-butter biodiesel used to power the engine are tabulated in the Table 4.8.

The biodiesel has the highest values of density, kinematic viscosity, ash content, cloud point, flash point, fire point and pour point, but a lower value of carbon content.

The calorific value and cetane number of the biodiesel were higher than that of petroleum diesel; the calorific value and cetane number of the petroleum diesel sample were relatively lower than that which is available in literature, a possibility of the petroleum diesel being of low quality

The flash point, fire point, pour point and cloud point of the petroleum diesel is also an attestation to the low quality of the diesel fuel.

The results gotten from the test engine; a horizontal single cylinder four-stroke air cooled engine Yoshita 165F model with fuel injection pressure of 140 bar, when fitted with the unmodified piston and the modified truncated cone piston crown with an inclination angle of 40° are stated in Tables 4.9 to 4.10. The engine was operated at no load and full load conditions and the observed output are as tabulated in Tables 4.9 to 4.10.

The obtained values for speed, exhaust gas temperature, torque, average time for 2ml of fuel consumption, vibrations and CO emission are depicted in Tables 4.9 to 4.10.

Using the data depicted in Tables 4.9 to 4.10, the flow rate of the fuel into the engine was computed using Equation (3.45)

$Q = \frac{V_{fuel}}{t}$,

The flow rates values are as computed in Table 4.11. It shows the derived values of the fuel flow rate based on the average time it took for the consumption of 2 ml of the fuel. The computed values were later used for the determination of the respective brake specific fuel consumption of the engine.

4.8.1 Exhaust Gas Temperature of Test Engine at Full Load

The engine's exhaust gas temperature at full load when operated on the test fuels; AGO and Shea-butter biodiesel separately as obtained during the test using the unmodified and the modified piston crown in each case is shown in Table 4.12.

Exhaust gas temperature is an indication of the combustion and emission characteristics of an engine, normally, high temperature exhaust gas tends to have higher amount of NOx emissions.

Table 4.8: Chemo-physical properties of the test fuels

Properties	**AGO**	**Biodiesel**
Density (g/ml)	0.84	0.92
Specific gravity	0.84	0.923
Kinematic viscosity at 30℃ mm^2/s	3.7	5.4
Pour Point ℃	-35	+18
Flash Point ℃	+114	+191
Fire Point ℃	+132	+212
Cloud Point ℃	-28	+32
Carbon Content %	97.20	8.39
PH Value	8.10	4.5
Sulphur content (ppm)	4.28	3.96
Ash content	0.05	0.21
Cetane Number	39.6	44.8
Calorific Value (MJ/kg)	36	40.1

Table 4.9: Unmodified piston crown experimental test output

Parameters	**No Load**		**Full load**	
	AGO	**Biodiesel**	**AGO**	**Biodiesel**
Speed (RPM)	2600	2400	1900	2000
Exhaust Temperature (℃)	150	130	410	370
Torque (Nm)	-	-	9	9
Average Time for 2ml (s)	19.28	18.48	4.64	6.42
Vibration (m/s^2)	16.2	15.2	19.4	12.8
CO emission (ppm)	13	16	1598	1859
O_2 emission (%)	20.9	20.9	19.3	17.2

Table 4.10: Modified truncated cone piston crown experimental test output

Parameters	**No Load**		**Full load**	
	AGO	**Biodiesel**	**AGO**	**Biodiesel**
Speed (RPM)	2600	2400	1950	2300
Exhaust Temperature (℃)	150	150	360	300
Torque (Nm)	-	-	8.8	8
Average Time for 2ml (s)	18.28	18.66	4.24	9.60
Vibration (m/s^2)	34.9	36.2	25.8	39.2
CO emission (ppm)	38	58	1463	780
O_2 emission (%)	19.5	19.2	19.1	18.2

Table 4.11: Flow rate computations

Engine Condition	**Piston Type**	**AGO**	**Biodiesel**
		q ($1*10^{-7}(m^3/s)$)	**q ($1*10^{-7}(m^3/s)$)**
No Load Condition	Unmodified Piston Crown fitted Engine	1.037	1.082
	Modified Piston Crown fitted Engine	1.094	1.072
Full Load Condition	Unmodified Piston Crown fitted Engine	4.310	3.115
	Modified Piston Crown fitted Engine	4.717	2.083

q – Flow Rate

Table 4.12: Exhaust gas temperature of test engine at full load

Piston Crown Type	**AGO (K)**	**Biodiesel (K)**
Unmodified Piston Crown fitted Engine	683	643
Modified Piston Crown fitted Engine	633	573

The unmodified piston crown fitted engine operated on AGO recorded the highest value of exhaust gas temperature, and for all cases of the test fuels, the exhaust gas temperature values of the unmodified piston crown fitted engine are greater than that of the modified piston crown fitted engine.

The least value of exhaust gas temperature value was recorded for the modified piston crown fitted engine operated on Shea-butter biodiesel as fuel. The peak value of the exhaust gas temperature for the modified piston crown fitted engine was found to be lower than the least value for the unmodified piston crown fitted engine for all the two test fuels.

For the modified piston crown fitted engine, the exhaust gas temperature decreased with the use of Shea-butter biodiesel an attestation to its better physicochemical properties.

4.8.2 Speed of Test Engine at Full Load

The designed speed for the test engine was 2600RPM, however when loaded, the engine speed drops. The plots of the engine speed fitted with the unmodified and the modified piston crown and operated on the various test fuels in succession at full load conditions is depicted in Table 4.13.

As stated in Equations (3.35) and (3.36), it can be seen that the brake power is directly proportional to the engine speed and the torque, meaning high values of the two terms gives a high value for power.

The full load speed of the engine when fitted with the modified piston crown was higher than that of the unmodified piston crown fitted engine for all the test fuels, and the reason for their higher values of brake power.

4.8.3 Engine Vibration

Engine body vibration signatures are rich in information regarding its operating parameters and physical conditions as vibration monitoring has the widest applications and benefits in condition monitoring programme (Alhouli *et al*., 2015).

The engines vibration level is expected to always be below a certain designed threshold to ensure its durability. The acceptable vibrations limit for reciprocating engines of this class being 44 m/s^2 for value 1 and 50 m/s^2 for value 2 as stated in IS/ISO 8528-9: (1995) (BIS, 2012)

The engines vibration level when fitted with the unmodified piston crown and the modified piston crown when operated on the two test fuel at full load conditions is as depicted in Table 4.14.

Table 4.13: Engine speed at full load

Piston Crown Type	**AGO (RPM)**	**Biodiesel (RPM)**
Unmodified Piston Crown fitted Engine	1900	2000
Modified Piston Crown fitted Engine	1950	2300

Table 4.14: Vibration of engine at full load

Piston Crown Type	**AGO (m/s^2)**	**Biodiesel (m/s^2)**
Unmodified Piston Crown fitted Engine	19.4	12.8
Modified Piston Crown fitted Engine	25.8	39.2

The engine is better balanced with minimal vibration when fitted with the unmodified piston crown and operated on the Shea-butter biodiesel. Its vibration level at every point at full load when fitted with the unmodified piston and operated on any of the two test fuels is lesser in comparison to that of the modified piston crown fitted engine, and this could have resulted from an imbalance introduced into the system as a result the changes in engine cylinder pressure brought about by the modification.

The peak vibration level was recorded for the modified piston crown fitted engine operated on Shea-butter biodiesel. The engine fitted with the modified piston crown fared better when operated on AGO.

4.8.4 Experimental Test Engine Brake Power

The brake engine power for the cases of the engine when fitted with the unmodified piston crown and with the modified piston crown and operated on the two test fuels; AGO and Shea-butter biodiesel was calculated using Equation (3.36),

$T_q = \frac{60P}{2\pi N}$,

Therefore;

$P = \frac{2\pi N T_q}{60}$,

The brake power generated by the test engine when fitted with the unmodified and the modified piston crown with inclination angle of 40° while being operated on the two test fuels respectively is depicted in Table 4.15. The corresponding values for "T_q" and "N" were taken from the data depicted in tables above for torque and engine speed respectively.

The brake power is a function of the amount of inherent energy "Calorific value" of the fuel and the mass of injected fuel.

The brake power of the engine was found to show an improvement when the engine was fitted with the modified piston crown over that which was fitted with the unmodified piston. A percentage increase of 0.36% and 4.44% respectively was recorded after the modification of the piston crown to truncated cone geometry with inclination angle of 40° over that of the corresponding unmodified piston operated on AGO and Shea-butter biodiesel fuels respectively as depicted in Table 4.15.

The modified piston crown fitted engine operated on Shea-butter biodiesel had the highest value of brake power. The brake power of the modified piston crown fitted engine increased with the use of Shea-butter biodiesel as fuel.

Table 4.15: Brake power of test engine

Piston Crown Type	**AGO**	**Biodiesel**
	Brake Power (W)	**Brake Power (W)**
Unmodified Piston Crown fitted Engine	1790.71	1844.96
Modified Piston Crown fitted Engine	1796.99	1926.84

4.8.5 Experimental Test Engine Brake Specific Fuel Consumption

The brake specific fuel consumption for the cases of the engine when fitted with the unmodified piston crown and with the modified piston crown and operated on the two test fuels; AGO and Shea-butter biodiesel was calculated using Equation (3.37)

BSFC $= \frac{\rho_f q}{P}$.

The brake specific fuel consumption of the test engine when fitted with the unmodified and the modified piston crown with inclination angle of 40° while operated on the two test fuels respectively are depicted in Table 4.16.

The value was relatively high when the engine was operated solely on petroleum diesel 'AGO' than when operated on Shea-butter biodiesel as fuel and this is in agreement with the findings of Carlos *et al.* (2012) who reported that the specific fuel consumption of a compression ignition engine operated on Olive biodiesel as fuel showed an improvement over that when operated on petroleum diesel as fuel.

For the unmodified piston crown and the modified piston crown fitted engine, the brake specific fuel consumption was better when it was operated on Shea-butter biodiesel as fuel. An improvement of 45.02% was recorded by the modified piston crown fitted engine over that of the unmodified piston crown fitted engine when the engines were operated with Shea-butter biodiesel as fuel.

The modified piston crown fitted engine operated on Shea-butter biodiesel fuel thus recorded the best value for the brake specific fuel consumption.

4.8.6 Experimental Engine Mean Effective Pressure

The mean effective pressure for the experimental engine for the two cases considered; unmodified piston and the modified piston crown using the test fuels are derived using Equation (3.35).

$P_m = \frac{Pn_c}{V_d N}$,

where;

$V_d = V_s$, $= V_s = \frac{\pi D^2 S}{4}$, (from Equation (3.15))

$V_d = \frac{\pi * 0.07^2 * 0.07}{4} = 0.0002694$ m^3

The mean effective pressures of the test engine when fitted with the unmodified and the modified piston crown with inclination angle of 40° while operated on the two test fuels respectively are shown in Table 4.17.

Table 4.16: Brake specific fuel consumption of test engine

Piston Crown Type	**AGO**	**Biodiesel**
	BSFC (kg/kWh)	**BSFC (kg/kWh)**
	ρ_f =840 kg/m^3	ρ_f =920 kg/m^3
Unmodified Piston Crown fitted Engine	0.7278	0.5992
Modified Piston Crown fitted Engine	0.7936	0.3294

BSFC – Brake Specific Fuel Consumption

Table 4.17: Mean effective pressure of test engine

Piston Crown Type	**AGO**	**Biodiesel**
	$\boldsymbol{P_m}$ ***(10^5 N/m^2)**	$\boldsymbol{P_m}$ ***(10^5 N/m^2)**
Unmodified Piston Crown fitted Engine	4.198	4.109
Modified Piston Crown fitted Engine	4.105	3.732

P_m – Mean Effective Pressure

The mean effective pressure values of the unmodified piston crown fitted engine are for all cases higher than that of the modified piston crown fitted engine. The trend obtained in the mean effective pressure as shown in Table 4.17 was seen to be the reciprocal of that of the vibration values as shown in Table 4.14. This is in agreement with the findings of Barelli *et al.* (2009) where it was stated that engines vibration have a direct correlation to the mean effective pressure.

4.8.7 Thermal Efficiency of Experimental Test Engine

The thermal efficiency for the cases of the engine when fitted with the unmodified piston crown and with the modified piston crown and operated on the two test fuels; AGO and Shea-butter biodiesel is calculated using Equation (3.33);

$$\eta_{Th} = \frac{P}{FC * CV}$$

$$FC = \rho_f q$$

The thermal efficiencies of the test engine when fitted with the unmodified and the modified piston crown with inclination angle of 40° while operated on the two test fuels respectively are shown in Table 4.18.

The thermal efficiency of shea-butter biodiesel powered engine is higher than that of AGO for both the unmodified and modified piston crown. The thermal efficiency of the biodiesel run engine is higher than that of the petroleum diesel in agreement to the findings of Jehad *et al*. (2009) who conducted experiments on the performance of compression ignition engines using biodiesel made from corn oil as fuel and reported an increase in thermal efficiency of the engine with the use of the biodiesel. It is however in variance with what was reported by Savararaj *et al*. (2011) of a reduced value of thermal efficiency when Mahua biodiesel was used as fuel in a diesel engine and by Anbarasu and Karthikeyan (2014) that used Canola oil biodiesel as fuel.

The thermal efficiency is an indication of the efficacy on how the chemical energy input in the form of fuel is converted into useful work (Jaichandar and Annamalai, 2012b), so the amount of the extractable energy from a fuel sample is a function of its inherent internal energy; its calorific value.

The calorific value of the biodiesel utilized in this studies; shea-butter biodiesel was found to be higher than the value for the petroleum diesel sample. However, the calorific value of the biodiesels used by Savararaj *et al*. (2011) and Anbarasu and Karthikeyan (2014) was remarkably lower than that of their utilized petroleum diesel sample.

Table 4.18: Thermal efficiency of test engine

Piston Crown Type	**AGO**	**Biodiesel**
	η_{Th} **(%)**	η_{Th} **(%)**
Unmodified Piston Crown fitted Engine	13.741	16.059
Modified Piston Crown fitted Engine	12.600	25.079

. η_{Th} – Thermal Efficiency

The thermal efficiency of the engine increased when fitted with the modified piston crown over that of the unmodified piston crown except for the case of AGO as fuel. An improvement of 9.03% was recorded for the engine when fitted with the modified piston crown as against when fitted with the unmodified piston crown using Shea-butter biodiesel as fuel.

4.8.8 Mechanical efficiency of the Experimental Engine

The mechanical efficiency for the engine when fitted with the unmodified piston crown and the modified piston crown and operated on the two test fuels; AGO and Shea-butter biodiesel is calculated using Equation (3.46);

$$\eta_M = \frac{Brake\ power}{Indicated\ power}$$

As depicted in Table 3.3, the indicated power of the test engine is 2.67 kW. The corresponding values for brake power were taken from the computations depicted in Table 4.15.

The mechanical efficiencies of the test engine when fitted with the unmodified and the modified piston crown with inclination angle of 40° while operated on the two test fuels respectively are shown in Table 4.19.

The mechanical efficiency of the modified piston crown fitted engine showed an improvement over that of the unmodified piston crown fitted engine for the used test fuels; AGO and Shea-butter biodiesel. The mechanical efficiency was observed to improve with the use of Shea-butter biodiesel for both the unmodified piston crown and the modified piston crown equipped engine.

The best mechanical efficiency value was recorded for the modified piston crown fitted engine operated on Shea-butter biodiesel, and it recorded an increase of 3.03% over that of the unmodified piston crown fitted engine.

Modification of the combustion chamber brought about with the use of the truncated cone piston crown led to the observed changes in the mechanical efficiency of the test engine.

4.8.9 CO Emission of Experimental Engine at Full Load

The carbon monoxide emission from the engine when equipped with the unmodified piston crown and the modified piston crown and operated on the two test fuel at full load conditions is as shown in Table 4.20.

With AGO as fuel, the CO emission level decreased for the modified piston crown fitted engine as compared to that of the unmodified crown fitted engine.

Table 4.19: Mechanical efficiency

Piston Crown Type	**AGO**	**Biodiesel**
	η_M **(%)**	η_M **(%)**
Unmodified Piston Crown fitted Engine	67.07	69.10
Modified Piston Crown fitted Engine	67.30	72.13

. η_M – Mechanical Efficiency

Table 4.20: CO Emissions of experimental engine at full load

Piston Crown Type	**AGO (ppm)**	**Biodiesel (ppm)**
Unmodified Piston Crown fitted Engine	1598	1859
Modified Piston Crown fitted Engine	1463	780

An improvement was recorded for the modified piston crown fitted engine when ran on AGO and Shea-butter biodiesel fuels over that of the unmodified piston crown fitted engine.

The CO emission values for the modified piston crown fitted engine improve for Shea-butter biodiesel as fuel over that of AGO and this is in conformity with literature as reported by Al-Dawody and Bhatti (2014) that operated a diesel engine on Soybean biodiesel.

For the unmodified piston crown fitted engine, the CO emission value recorded was higher when Shea-butter biodiesel was used as fuel.

The reason for the observed differences is not far-fetched, the in-cylinder process in an engine cylinder is dictated by its combustion chamber geometry, this in turn determines the engines emission products (Dec., 2009). The use of the truncated cone piston crown changes the engine's combustion chamber, and thus, a change in the emission characteristics of the engine is expected.

4.9 Comparison of the Numerical Results with Literature and Experimental Data

The numerical estimates obtained for the compression ignition engine with piston length of 106 mm, cylinder bore of 87.5 mm and compression ratio of 17.5:1 (Kirloskar TV-1) compared favourably to a great extent with experimental results gotten from literature. The estimated and literature values for the engine power as given in the works of Sundarraj (2011), Sreedhar and Prassad (2015), Sundarraj and Saravannan (2012), Velappan and Sivaprakasam (2014) have a correlation of 5.61±0.58, and a percentage difference of 13.64%. The estimated thermal efficiency and values for literature at a brake power of 5.2 kW have values of 30.75±0.21 and a percentage difference of 0.97% (Sundarraj and Saravannan, 2012) a percentage difference of 1.29%, and 31.35±0.64 (Sundarraj, 2011) and a percentage difference of 2.83% (Velappan and Sivaprakasam, 2014). The estimated specific fuel consumption and the values from literature at a brake power of 5.2 kW are 0.22±0.03 with a percentage difference of 19.25% (Velappan and Sivaprakasam, 2014). This is depicted in Table 4.21.

The numerical estimates gotten for the compression ignition engine with piston length of 75 mm, cylinder bore of 70 mm and compression ratio of 20.5:1 and the truncated cone piston crown with an inclination angle of 40° with the experimental results for the same engine when operated on AGO as fuel are now compared below.

Table 4.22 depicts the correlation between the estimates of the numerical model and experimental results for the engine.

The engine torque, mean effective pressure, brake specific fuel consumption, power, exhaust gas temperature and thermal efficiency derived from the numerical model and

experimental results have a grand mean and standard deviation of 8.81±0.13, 4.1117±0.0596, 0.5536±0.2407, 2085.78±337.10, 610.70±58.31, and 22.70±11.01 respectively.

The numerical and experimental derived values for the engine torque, mean effective pressure, brake specific fuel consumption, exhaust gas temperature, power and thermal efficiency have an average difference of 1.91 %, 1.90 % 54.18%, 14.24%, 24.5% and 59.14% respectively giving an indication that the numerical modelling and experimental results are similar.

The average percentage difference for the thermal efficiency was however observed to be high, and this could be attributed to the fact that the engine cylinder wall was assumed to be thermally insulated in the numerical model, whereas the heat loss by the cooling of the cylinder to ensure smooth piston operation by an actual engine utilized in the experiment has effects on the engine's thermal efficiency. Also asides the non-instantaneous combustion nature that takes place in an actual engine, the calorific value of the utilized AGO was relatively low; 36 MJ as against a normal average value of 45.5 MJ been quoted in literature and 48 MJ for n-heptane which was used as the diesel representative in the numerical model. This also had its toll on the generated power from the experimental test.

4.10 Analysis of Variance (ANOVA) of the Numerical and Experimental Data

The grand mean values and standard deviations of the weighted engine torque, mean effective pressure, exhaust gas temperature, and CO emission from numerical and experimental results for Category II engine and with TCPC of inclination angle of 40° are presented in Table 4.23. Also, the tables of ANOVA at $\alpha_{0.05}$ of the engine torque, mean effective pressure, exhaust gas temperature, and the CO emission from the numerical and experimental analyses are as shown in Table 4.24. The numerical and experimental results of the engine torque, mean effective pressure, and exhaust gas temperature were not significantly different at $\alpha_{0.05}$ as it can be seen that their respective variance values (F) and well below the probability values (F – Critical).

Table 4.21: Correlation between numerical model estimates and literature

Performance Parameter	**Sundarraj (2011)**	**Sreedhar and Prassad (2015)**	**Sundarraj and Saravannan (2012)**	**Velappan and Sivaprakasam (2104)**
Power (kW)	Average: 5.61±0.58	Average: 5.61±0.58	Average: 5.61±0.58	Average: 5.61±0.58
	% Difference: 13.64	% Difference: 13.64	% Difference: 13.64	% Difference: 13.64
Thermal Efficiency (%)	Average: 31.35±0.64	-	Average: 30.75±0.21	-
	% Difference: 1.29	-	% Difference: 0.97	% Difference: 2.83
Brake Specific Fuel	-	-	-	Average: 0.22±0.03
Consumption (kg/kWh)	-	-	-	% Difference: 19.25

Table 4.22: Correlation between numerical model estimates and experimental results

Performance Parameter	**Average**	**% Difference**
Torque (Nm)	8.81±0.13	1.91
Mean Effective Pressure (100 kN/m^2)	4.1117±0.0596	1.90
Brake Specific Fuel Consumption (kg/kWh)	0.5536±0.2407	54.18
Exhaust Gas Temperature (℃)	610.70±58.31	14.24
Power (W)	2085.78±337.10	24.5
Thermal Efficiency (%)	22.70±11.01	59.14

Table 4.23: The grand mean values of the performance parameters from the numerical and experimental analyses

	CI2 and TCPC
Experimental and Numerical Torque (N/m)	8.81±0.13
Experimental and Numerical Mean Effective Pressure (KN/m^2)	411.17±5.96
Experimental and Numerical Exhaust Gas Temperature (K)	610.70±58.30
CO (ppm)	1537.29±55.68

Table 4.24: The ANOVA results for the performance parameters of the estimates of numerical model and experimental results

Performance Parameter	**Source of Variation**	**Sums of Squares**	**Degrees of Freedom**	**Mean Squares**	**Variance Ratios (F)**	**Probability value (F Critical)**
Torque (N/m)	Between samples	0.0306	1	0.0306	3.0524	18.51
	Within Samples	0.0200	2	0.0100	-	-
	Total	0.0506	3	-	-	-
Mean Effective Pressure (N/m^2)	Between samples	0.0063	1	0.0063	2.9302	18.51
	Within Samples	0.0043	2	0.0021	-	-
	Total	0.0106	3	-	-	-
Exhaust Gas Temperature (K)	Between samples	8817.70	1	8817.70	14.1081	18.51
	Within Samples	1250.02	2	625.01	-	-
	Total	10067.72	3	-	-	-
CO (ppm)	Between samples	184.60	1	184.60	0.0405	18.51
	Within Samples	9115.14	2	4557.57	-	-
	Total	9299.74	3	-	-	-

CHAPTER FIVE
CONCLUSIONS AND RECOMMENDATIONS

5.1 Conclusions

The following conclusions could be drawn from this study;

i. The use of the truncated cone piston crowns and inverted truncated cone piston crowns equipped Kirloskar TV1 compression ignition engine led to a change in the engines' performance characteristics as observed during the numerical analysis.

ii. The truncated cone piston crown fitted Kirloskar TV1 engine with equal compression ratio as that of the unmodified, performed better in terms of thermal efficiency, brake power, specific fuel consumption, CO emission, and CO_2 emission levels for truncated cone base angles of 35°, 40° and 45° as observed during the numerical analysis.

iii. Improved performance in terms of thermal efficiency, brake power, specific fuel consumption, CO emission, and CO_2 emission levels were observed for the inverted truncated cone piston crown fitted Kirloskar TV1 engine with equal compression ratio to that of the unmodified, at truncated cone base angles of 40° and 45° during the numerical analysis.

iv. Lower CO emissions level were obtained for the truncated cone piston crown equipped Kirloskar TV1 engine with varying chamber volume at truncated cone base angles of 25°, 30° and 45° respectively in comparison to the unmodified piston as observed during the numerical analysis.

v. The truncated cone piston crown equipped Kirloskar TV1 engine with a cone base angle of 40° showed the overall best improvement in performance against the unmodified piston with equal compression ratio, and is therefore the most suitable among all the modified piston crown configurations investigated as observed during the numerical analysis.

vi. The numerical analysis results compared favourably with experimental results from literature for the Kirloskar TV1 engine.

vii. The use of the truncated cone piston crowns and inverted truncated cone piston crowns equipped Yoshita 165F compression ignition engine led to a change in the engines' performance characteristics.

viii. The thermal efficiency, brake power, specific fuel consumption, CO emission and CO_2 emission were observed to improve with the use of the truncated cone piston crowns

and the inverted truncated cone piston crowns equipped Yoshita 165F compression ignition engine as against the unmodified piston as observed during the numerical analysis.

ix. The modified truncated cone piston crown equipped Yoshita 165F compression ignition engine with a truncated cone base angle of 40° showed the best overall improvement in performance characteristics as obtained from the numerical analysis.

x. The experimental studies results showed an improvement in brake power, mechanical efficiency, CO emission, and exhaust gas temperature using AGO as fuel, when the test engine (Yoshita 165F) was fitted with truncated cone piston crown having a cone base angle of 40° in comparison with the unmodified piston.

xi. The thermal efficiency, brake specific fuel consumption, brake power, mechanical efficiency, CO emission, and exhaust gas temperature using Shea-butter as fuel improved, when the test engine was fitted with truncated cone piston crown having a cone base angle of 40° in comparison with the unmodified piston during experimental studies.

xii. The vibration level of the unmodified piston crown fitted test engine was lower than that of the truncated cone piston crown having a cone base angle of 40° for the two used fuels as obtained from the experimental results.

xiii. The performance characteristics of the test engine fitted with the truncated cone piston crown with a cone base angle of 40° was optimized with the use of Shea-butter biodiesel, hence the truncated cone piston crown fitted engine with a cone base angle of 40° will be preferred when operated on Shea-butter biodiesel as against with AGO.

xiv. The numerical and experimental results for the Yoshita 165F engine are comparatively in good agreement, however, there were some disparity in the thermal efficiencies and specific fuel consumption. This may be due to the simplifications introduced in the numerical method of taking the cylinder walls to be thermally insulated, whereas experimentally, heat loss from the cylinder walls cannot be ruled out completely.

xv. The comparative agreement and the consistencies of performance of the standard engines and modified piston crown engines from both the numerical and experimental methods showed that any of the two methods can be used to independently investigate the performance of a compression ignition engine.

The stated objectives of this research were fully realized; the performance characterization of a compression ignition engine equipped with truncated cone piston crown was carried out using the numerical and experimental approach, while the performance characterization of a

compression ignition engine equipped with an inverted truncated cone piston crown was carried out numerically.

5.2 Recommendations

For further research, the following are recommended;

i. Better quality AGO can still be sourced for, and use to carry out the test.
ii. More and different values of piston crown inclination angles both for the truncated cone and inverted truncated cone can still be investigated both numerically and experimentally.
iii. Other piston crown shapes besides conical could also be explored to investigate their effects on an engine performance.
iv. The performance parameters at different engine loads could be investigated.
v. A three-dimensional analyses model could be used in the numerical analysis.

REFERENCES

Abagnale, C., Cameretti, M. C., Luigi, D. S., Gambino, M., Iannaccone, S., and Tuccillo, R. (2014). Combined numerical-experimental study of dual fuel diesel engine. *68th Conference of the Italian Thermal Machines Engineering Association, ATI2013, 45,* (721-730). Napoli: Energy Procedia.

Agarwal, A., Soni, S. L., Sharma, D. K., and Bhaskar, S. K. (2015). Effect of Variation of Compression Ratio and Injection Pressure on the Performance and Emission Characteristics of CI Engine using various Alternative Fuels: A Review. *IJRET: International Journal of Research in Engineering and Technology*, *4(1),* 40-45.

Agrawal, A. K., Singh, S. K., Sinha, S., and Shukla, M. K. (2004). Effect of EGR on the exhaust gas temperature and exhaust opacity in compression ignition engines. *Sadhana*, *29(3)* 275-284.

Al-Dawody, M. F., and Bhatti, S. (2014). Effect of Variable Compression Ratio on the Combustion, Performance and Emission Parameters of a Diesel Engine Fuelled with Diesel and Soybean Biodiesel Blending. *World Applied Sciences Journal*, *30(12),* 1852-1858.

Alessio, F., Gianluca, D., Tommaso, L., Alessandro, S., Alberto, C., Tiziano, et al. (2015). Reduced kinetic mechanisms of diesel fuel surrogate for engine CFD simulations. *Combustion and Flame*, *162(10),* 3991-4007.

Alhouli, Y., Alkhaledi, A., Alzayedi, A., Alardhi, M., and Abed, A. I. (2015). Study of Diesel Engine Vibration Monitoring. *Global Journal of Researches in Engineering; J General Engineering*, *15(6),* 36-44.

Anandan, M., Sampath, S., and Sudharsan, N. M. (2014a). Effect of Compression Ratio and Exhaust Gas Recirculation (EGR) on Combustion, Emission and Performance of DI Diesel Engine with Biodiesel Blends. *Global Journal of Researches in Engineering: A Mechanical and Mechanics Engineering, 14(7)*, 1-16.

Anandan, M., Sampath, S., and Sudharsan, N. M. (2014b). Study of Combustion and Performance Characteristics on a Single Cylinder DI Diesel Engine with Jatropha and Pongamia Methyl Ester Blends. *Global Journal of Researches in Engineering: A Mechanical and Mechanics Engineering, 14(7)*, 26-40.

Anbarasu, A., and Karthikeyan, A. (2014). Performance and Emission Characteristics of Direct Injection Diesel Engine Running On Canola Oil / Diesel Fuel Blend. *American Journal of Engineering Research (AJER), 3(8)*, 202-207.

Arcoumanis, D. (2011). *Internal combustion engines.* Retrieved December 20, 2017, from Thermopedia: http://www.thermopedia.com/content/880/

Argakiotis, C., Mishra, R., Stubbs, C., and Weston, W. (2014). The Effect of using an Ethanol blended fuel on Emissions in an SI Engine. *Renewable Energy and Power Quality Journal (RE&PQJ), 12,* 1-6.

Balki, M. K., Sayin, C., and Canakci, M. (2014). The effect of different alcohol fuels on the performance, emission and combustion characteristics of a gasoline engine. *Fuel, 115*, 901-906.

Banapurmath, R., Dodamani, B., Khanda, S., Hiremath, S., and Math, V. (2014). Performance, Emission Characteristics of Dual Fuel (DF) & Homogeneous Charge Compression Ignition (HCCI) Engines Operated on Compressed Natural Gas (CNG) – Uppage Oil Methylester (UOME). *Universal Journal of Renewable Energy, 2*, 32-44.

Barelli, L., Bidini, G., Buratti, C., and Mariani, R. (2009). Diagnosis of internal combustion engine through vibration and acoustic pressure non - intrusive measurements. *Applied Thermal Engineering, 29(8-9)*, 1707-1713.

Basavarajappa, Y., Banapurmath, N., and Sangameshwar, A. (2014). Performance, Combustion & Emission Characteristics of a Dual Fuel Engine Operated with Compressed Natural Gas (CNG) & Honge & Jatropha Biodiesels. *Universal Journal of Petroleum Sciences, 2*, 46-73.

Basha, J. S., Prasad, P. I., and Rajagopal, K. (2009). Simulation of In-Cylinder Processes in a DI Diesel Engine with Various Injection Timings . *ARPN Journal of Engineering and Applied Sciences, 4(1)*, 1-7.

Bell, A. (2014). *Transcript of Combustion Engine Impacts.* Retrieved March 3, 2018, from https://prezi.com/29x_9mn5loaz/combustion-engine-impacts/

Bhabani, P. P., Chandrakanta, N., and Basanta, K. N. (2013). Investigation on utilization of Biogas & Karanja Oil biodiesel in dual fuel mode in a Single Cylinder DI Diesel engine. *International Journal of Energy and Environment, 4(2)*, 279-290.

Bharathi, V. V., and Prasanthi, G. (2013). The Influence of Air Swirl on Combustion and Emissions in a Diesel Engine. *International Journal of Researh in Mechanical Engineering and Technology, 3(2)*, 14-16.

BIS. (2012). Indian Standard Reciprocating Internal Combustion Engine Driven Alternating Current Generating Sets, Part 9:Measurement and Evaluation of Mechanical Vibrations. New Delhi, India.

Carlos, E. S., Alexon, d. P., Jackson, A. B.,and Nilson, S. (2012). Performance of cycle diesel engine using Biodiesel of olive oil (B100). *Ciência e Agrotecnologia, 36(3)*, 348-353.

Charalambides, A. G. (2013). Homogenous Charge Compression Ignition (HCCI) Engines. In *Advances in Internal Combustion Engines and Fuel Technologies* (pp. 119-148). Cyprus: Intech.

COMSOL (2012), "Homogenous Charge Compression Ignition of Methane" COMSOL 4.3.

COMSOL (2014), "Three-Cylinder Reciprocating Engine" COMSOL 5.0 (Build: 202).

Curran, H., Gaffuri, P., Pitz, W. J., and Westbrook, C. (1998). A Comprehensive Modeling Study of n-Heptane Oxidation. *Combustion And Flame, 114(1-2)*, 149-177.

De Risi, A., and Manieri, D. F. (1999). A Theoretical Investigation on the Effects of Combustion Chamber Geometry and Engine Speed on Soot and NOx Emissions. *Proceedings of ASME 1999 fall technical conference, ICE-vol. 33/1; 1999* (1-10). ASME.

Dec, J. E. (2009). Advanced Compression- Engines - understanding the incylinder processs. *The Combustion Institute, 32*, 2727-2742.

Diesel cycle vs Otto cycle. (2016). Retrieved may 3, 2017, from mech4study.com: http://mech4study.com/2016/08/diesel-cycle-vs-otto-cycle.html

Electric car use by country. (2018). Retrieved April 2, 2018, from Wikipedia: https://en.wikipedia.org/wiki/Electric_car_use_by_country

Etheridge, J., Mosbach, S., Kraft, M., and Wu, H. (2008). Investigating Cycle to Cycle Variations in an SI Engine Through Experiments and a New Computational Model. *Cambridge Centre for Computational Chemical Engineering, 62*, 1-34.

Fischer, H. and Keating, D. (2017). *How eco-friendly are electric cars?* Retrieved March 2, 2018, from Green Transport: http://www.dw.com/en/how-eco-friendly-are-electric-cars/a-19441437

Franco, M. (2017). *OBQ: Do electric cars really harm the environment less than gasoline-powered cars?* Retrieved January 2, 2018, from Environment: https://newatlas.com/obi-electric-cars/47489/

Ghafouri, J., Shafee, S., and Maghbouli, A. (2014). Investigation on Effect of Equivalence Ratio and Engine Speed on Homogeneous Charge Compression Ignition Combustion Using Chemistry Based CFD Code . *Thermal Science, 18(1)*, 89-96.

Goldwine, G. (2008). *The Effect of Fuel Injection Profile on Diesel Engine Performance.* Beer-Sheva: PhD Thesis, Ben-Gurion University.

Gowthaman, S., and Sathiyagnanam, A. (2015). A review of Homogeneous charge compression ignition (HCCI) engine. *International Journal of Scientific & Engineering Research, , 6 (1),* 779-798.

Gustavo, F., and Enzo, G. (2006). Knock Resistance in a Small Turbocharged Spark-Ignition Engine. *SAE International*, 2006-01-2995, 1-8.

Hanania, J., Jenden, J., Stenhouse, K., & Donev, J. (n.d.). *Internal combustion engine.* Retrieved March 1, 2018, from Energyeducation.ca: https://energyeducation.ca/encyclopediay/internal_combustion_engine

Hanlon, M. (2004). *Most powerful diesel engine inthe world.* Retrieved March 30, 2018, from https://newatlas.com/go/3263/

Havens, J. (2015). *A brief history of internal combustion engine.* Retrieved October 14, 2017, from Vintage machinery org: http//wiki.vintagemachinery.org/A-Brief-History-of-the-Internal-Combustion-Engine.ashx.

Hebbar, G. S., and Bhat, A. K. (2012). Control of NOx from A DI Diesel Engine With Hot EGR And Ethanol Fumigation: An Experimental Investigation. *IOSR Journal of Engineering (IOSRJEN), 2(7)*, 45-53.

Himmatsinh, R. C., Syham, K. D., Preksha, K., and Vivek, G. T. (2015). A Technical Review of HCCI Combustion in Diesel engine. *IJIRST-International Journal for Innovative Research in Science & Technology, 1(10)*, 28-31.

History of internal combustion engine. (2018). Retrieved January 15, 2018, from wikipedia: http//en.wikipedia.org/wiki/Internal-combustion-engine#History

Indrodia, A., Chotai, N., and Ramani, B. (2014). Investigation of Different Combustion Chamber Geometry on Diesel Engine using CFD Modelling of In-cylinder Flow for Improving the Performance of Engine. *5th International & 26th All India Manufacturing Technology, Design and Research Conference (AIMTDR 2014)*, (489-1 - 489-6). Assam.

Ingram, A. (2014). *Toyota Gasoline Engine Achieves Thermal Efficiency Of 38 Percent.* Retrieved November 22, 2017, from Green car report: https://www.greencarreports.com/news/1091436_toyota-gasoline-engine-achieves-thermal-efficiency-of-38-percent

Internal combustion engine. (2014). Retrieved November 11, 2017, from New world encyclopedia: http://www.newworldencyclopedia.org/p/index.php?title=Internal_combustion_engine&oldid=980420

Internal combustion engine. (2018). Retrieved March 30, 2018, from en.m.wikipedia.org: https://en.wikipedia.org/wiki/Internal_combustion_engine

Internal Combustion Engines. (2015). Retrieved March 11, 2018, from Quadrennial Technology Review 2015, U.S. department of energy: https://www.energy.gov/sites/prod/files/2015/11/f27/QTR2015-8C-Internal-Combustion-Engines.pdf

Jääskeläinen, H. (2013). *Early history of the Diesel engine.* Retrieved january 15, 2018, from DieselNet.com: https://www.dieselnet.com/tech/diesel_history.php

Jafarmadar, S., and Khanbabazadeh, M. (2008). A Computational Study of the Effects of Combustion Chamber Geometries on Combustion Process and Emission in a DI Diesel Engine. *Journal of Fuel and Combustion, 1(1)*, 1-16.

Jaichandar, S., and Annamalai, K. (2012a). Effects of open combustion chamber geometries on the performance of pongamia biodiesel in a DI diesel engin. *Fuel, 98*, 272-279.

Jaichander, S., and Annamalai, K. (2012b). Performance and Exhaust Emission Analysis on Pongamia Biodiesel with Different Open Combustion Chambers in a DI Diesel Engine. *Journal of Scientific and Industrial Research, 71*, 487-491.

Jehad, Y., Nina, S., and Hamdan, M. (2009). Performance of CI engines using Biodiesel as fuel. *GCREEDER international conference* (1-13). Amman: GCREEDER.

Joshi, A., Poonia, M., and Jethoo, A. (2012). Mathematical Modeling of the Dual Fuel Engine Cycle. *International Journal of Engineering and Innovative Technology (IJEIT), 2(1)*, 19-25.

Kerdsuwan, S., Lekpradit, T., Tongorn, S., and Nipattummakul, N. (2008). Effect of Advanced Injection Timing on the Performance Improvement of a Dual-Fuel Diesel Engine with Producer Gas from a Down-Draft Gasifier for Power Generation. *The Second International Energy 2030 Conference* (313-318). Abu-Dhabi: Energy 2030.

Khemani, H. (2008a). *Types of Internal Combustion (IC) Engines.* Retrieved December 22, 2017, from bright hub engineering: https://www.brighthubengineering.com/machine-design/1401-types-of-internal-combustion-ic-engines/

Khemani, H. (2008b). *Comparison of Spark Ignition (SI) and Compression Ignition (CI) Engines.* Retrieved March 1, 2018, from Bright hub engineering: https://www.brighthubengineering.com/machine-design/1537-comparison-of-spark-ignition-si-and-compression-ignition-ci-engines/

Krishnan, A., Sekar, V. C., Balaji, J., and Boopathi, S. (2006). Prediction of NOx reduction with Exhaust Gas Recirculation using the Flame Temperature Correlation Technique. *Proceedings of the National Conference on Advances in Mechanical Engineering* (378-385). Kota: Engineering College Kota, Kota (Rajasthan) India.

Kumar, R. N., Sekhar, Y., and Adinarayana, S. (2013). Effects of Compression Ratio and EGR on Performance, Combustion and Emissions of Di Injection Diesel Engine. *International Journal of Applied Science and Engineering, 11(1)*, 41-49.

Laguitton, O., Crua, C., Cowell, T., Heikal, M., and Gold, M. (2006). Effect of Compression ratio on Exhaust Emissions from a PCCI Diesel engine. *Proceedings of the 19th International Conference on Efficiency, Cost, Optimization, Simulation and Environmental Impact of Energy Systems* (2918-2924). Crete: Energy conversion and management.

Larson, A. (2015). *World's Largest Internal Combustion Engine Power Plant Inagurated.* Retrieved January 25, 2018, from www.powermag.com/worlds-largest-internal-combustion-engine-power-plant-inaugurated/

Laukkonei, J. D. (2013). *History of internal combustion engine.* Retrieved November 11, 2017, from http://www.crankshift.com/history-internal-combustion-engine/

Lehtiniemi, H., Zhang, Y., Rawat, R., and Mauss, F. (2014). *Advanced Combustion Modeling withSTAR-CD using Transient Flamelet Models:TIF and TFPV*. Retrieved July 31, 2015, from www.cd-adapco.com

Li, D.-g., Zhen, H., Xingcai, L., Zhang, W., and Yang, J. (2005). Physico-chemical properties of ethanol-diesel blend fuel and its effect on performance and emissions of diesel engines. *Renewable Energy, 30*, 967-976.

Ma, B. (2014). *How has the internal combustion engine changed our perspective on time and space.* Retrieved January 25, 2018, from Time, Space and More: http://blackgold36.weebly.com/time-space-and-more/how-has-the-internal-combustion-engine-changed-our-perspectives-on-time-and-space-by-brian-ma

Mamilla, V. R., Mallikarjun, M., and Rao, G. N. (2013). Effect of Combustion Chamber Design on a DI Diesel Engine Fuelled with Jatropha Methyl Esters Blends with Diesel. *International Conference On DESIGN AND MANUFACTURING, IConDM 2013* (479-490). India: Elsevier Ltd.

Mikalsen, R., and Roskilly, A. (2009). Coupled dynamic–multidimensional modelling of free-piston engine combustion. *Applied Energy, 86(1)*, 89-95.

Mozaffari, B. (2010). Performance of Homogeneous Charge _ Dual Engine. *New Aspects of Fluid Mechanics, Heat Transfer and Environment*, 79-83.

Mueller, C. J., Cannella, W. J., Bays, J. Timothy, Bruno, Thomas J., DeFabio, Kathy, Dettman, Heather D., Gieleciak, Rafal M., Huber, Marcia L., Kweon, Chol-Bum, MCConnell, Steven S., Pitz, William J., and Ratcliff, Matthew A. (2016). Diesel Surrogate Fuels for Engine Testing and Chemical-Kinetic Modelling: Compositions and Properties. *Energy Fuels, 30*, 1445-1461.

Mueller, C., WJ, B. T., Bunting, B., Dettman, H., Franz, J., Huber, M.L., Natarajan, M., Pitz, W.J., Ratcliff, M.A., and Wright, K. (2012). Methodology for formulating diesel surrogate fuels with accurate compositional, ignition-quality, and volatility characteristics. *Energy Fuels, 26*, 3284-3303.

Najafabadi, M. I., and Aziz, N. A. (2013). Homogeneous Charge Compression Ignition Combustion: Challenges and Proposed Solutions. *Journal of Combustion,* 2013, 1-14.

Nataraj, K., Banapurmath, N., Manavendra, G. Y., Vaibhav, K., and Satish, G. (2015). Effect of Combustion Chamber Shapes on the Performance of Mahua and Neem Biodiesel Operated Diesel Engines. *Petroleum & Environmental Biotechnology, 6(4)*, 1-7.

Naveen, K., Parameshwaran, T. P., and Azhagiri, P. (2014). Experimental Investigation of Variable Compression Ratio Diesel Engine using Ziziphus Jujuba oil. *2014 International Conference on Innovations in Engineering and Technology (ICIET'14)* (1134-1139). Madurai, Tamil Nadu: International Journal of Innovative Research in Science, Engineering and Technology.

Nureddin, D., and Nuri, Y. (2008). Numerical Simulation of Flow and Combustion in an Axisymmetric Internal Combustion Engine. *International Journal of Engineering and Applied Sciences, 4(3)*, 179-184.

Nwafor, O. (2000). Effect of advanced injection timing on the performance of natural gas in diesel engines. *Sadhana, 25(1)*, 11-20.

Parvaneh, Z., Ali, A. Z., and Barat, G. (2017). Comparative Assessment of Performance and Emission Characteristics of Castor, Coconut and Waste Cooking based Biodiesel as fuel in a Diesel Engine. *Energy, 139*, 883-894.

Pei, Y., Mehi, M., Liu, W., Lu, T., Pitz, W. J., and Som, S. (2015). A Multicomponent Blend as a Diesel Fuel Surrogate for Compression Ignition Engine Applications. *Journal of Engineering Gas Turbine and Power, 137(11)*, 1-9.

Periyasamy, M., and Vadivel, N. (2015). Experimental Investigation On LPG-Biodiesel (Pongamia) Dual Fuelled Engine. *International Journal on Applications in Mechanical and Production Engineering, 1(3)*, 3-7.

Periyasamy, S., Alwarsamy, T., and Rajasekar, V. (2012). Analysis on Combustion of a Primary Reference Fuel. *International Journal of Engineering Science and Technology (IJEST), 4(5)*, 2244-2250.

Pirouzpanah, V., and Khoshbakhti, S. R. (2006). A Predictive Model for the Combustion Process in Dual Fuel Engines at Part Loads using a Quasi Dimensional Multi Zone Model and Detailed Chemical Kinetics Mechanism. *IJE Transactions B: Applications, 19(1)*, 83-98.

Pitz, W. J., and Mueller, C. J. (2011). Recent progress in the development of diesel surrogate fuels. *Progress in Energy and Combustion Science, 37(3)*, 330-350.

Pokharkar, S., Pansare, S., Khandve, T., and Pagare, M. (2016). REVIEW ON HCCI ENGINE. *International Conference on Emerging Trends in Engineering and Management Research* (113-122). Anjaneri, Nashik: ICETEMR.

Poonia, M., and Mathur, Y. (2012). Effect of Exhaust Gas Recirculation on the Combustion of an LPG Diesel Dual Fuel Engine. *IRACST – Engineering Science and Technology: An International Journal (ESTIJ), 2(4),* 616-626.

Prasad, G. R., Goud, S. C., and Meheswar, D. (2012). Alternative Fuels for HCCI engine technology and recent developments. *International Journal of Advanced Research in Engineering and Applied Science, 1(2)*, 1-19.

Puiu, T. (2017). *This is what 109,000 horsepower looks like - meet the biggest engine in the world.* Retrieved February 11, 2018, from ZME Science: https://www.zmescience.com/science/biggest-most-poweful-engine-world

Rajashekhar, C. R., Chandrashekar, T. K., Umashankar, C., and Kumar, R. H. (2012). Studies on Effects of Combustion Chamber Geometry and Injection Pressure on Biodiesel Combustion. *Transactions of the Canadian Society for Mechanical Engineers, 36(4)*, 429-438.

Ranganatha, S. L., Chandrashekar, T., Banapurmath, N., and Nashipudi, P. (2014). Effect of Injection Timing, Combustion Chamber Shapes and Nozzle Geometry on the Diesel Engine Performance. *Universal Journal of Petroleum Sciences, 2*, 74-95.

Ravi, M., Vijayakumar, K., Ashok, K. M., and Gunaseelan, T. (2015). Experimental Investigation on Emission and Performance Charecteristics of Single Cylinder Diesel Engine using Lime Treated Biogas. *International Journal of ChemTech Research, 7(4)*, 1720-1728.

Reddy, C. S., Reddy, C. E., and Reddy, K. H. (2012). Effect of Tangential Grooves on Piston Crown of D.I. Diesel Engine with Blends of Cotton Seed Oil Methyl Easter. *IJRRAS, 13(1)*, 150-159.

Reifarth, S. (2010). *EGR-Systems for Diesel Engines.* Stockholm: Department of Machine Design Royal Institute of Technology.

Sankararaj, S. (2013). *Internal Combustion Engine- Introduction and Types.* Retrieved March 3, 2018, from MechTeacher.com: http://mechteacher.com/internal-combustion-engine/

Savariraj, S., Ganapathy, T., and Saravanan, C. (2011). Experimental Investigation of Performance and Emission Characteristics of Mahua Biodiesel in Diesel Engine. *Renewable Energy, 2011*, 1-6.

Scott, W., (2018). *Slider Crank Method*. Retrieved June 4, 2016, from http://www.engr.colostate.edu/~allan/thermo/page2/page2.html

Serrano, J. R. (2017). Imagining the Future of the Internal Combustion Engine for Ground Transport in the Current Context. *Applied Sciences, 7(10)*, 1-5.

Seyedmohsen, H., Rushed, A., and Amir, K. (2008). A Developed Quasi-Dimensional Combustion Model in Spark-Ignition Engines. *Proceedings of the World Congress on Engineering 2008 Vol II* (3-7). London: World Congress on Engineering.

Shehata, M., and Razek, A. S. (2008). Engine Performance Parameters. *Engineering Research Journal, 120,* M32-M57.

Sorathia, H. S., Rahhod, P. P., and Sorathiya, A. S. (2012). "Effects of Exhaust Gas Recirculation (EGR) on NOx Emission on C.I. Engine" - A Review Study. *International Journal of Advanced Engineering Research and Studies, 1(3)*, 223-227.

Sreedhar, C., and Prassad, B. D. (2015). Performance evaluation of four-stroke single cylinder DI diesel engine using different blends of diesel and grape seed biodiesel. *International Journal of Engineering and Innovative Technology (IJEIT), 4(11)*, 255-261.

Sundarraj, C. S. (2011). Influence of hexanol-diesel blends on constant speed diesel engine. *Thermal Science, 15(4)*, 1215-1222.

Sundarraj, C. S., and Saravannan, G. (2012). Performance and emission analyses of a single cylinder constant speed diesel engine fuelled with Diesel-Methanol- Isopropyl alcohol blends. *SAE Technical Paper 2012-01-1683*, 1-7.

Tao, F., Reitz, R. D., and Foster, D. E. (2007). Revisit of Diesel Reference Fuel (n-Heptane) Mechanism Applied to Multidimensional Diesel Ignition and Combustion Simulations. *Seventeenth International Multidimensional Engine Modelling User's Group Meeting at the SAE Congress* (1-8). Detroit, Michigan: SAE.

Tatschl, R., Bogensperger, M., Kotnik, G., Priesching, P., and Gouda, M. (2005). Flame Propagation and Knock Onset Analysis For Full Load SI Engine Combustion Optimisation Using AVL FIRE. *Proceedings of International Multidimensional Engine Modelling Users Group Meeting at the SAE Congress* (1-8). Detroit: SAE.

Valipour, A. (2014). Effect of Injection Pressure on Ignition Delay and Combustion Duration of Diesel Engine with Biodiesel (Jatropha Oil) and Its Blends. *International Journal of Modern Engineering Research (IJMER), 4(1)*, 9-14.

Vancoillie, J., and Verhelst, S. (2010). Modelling the Combustion of Light Alcohols in SI Engines: A Preliminary Study. *F2010-SC-O-04*, 1-12.

Velappan, R., and Sivaprakasam, S. (2014). Invesstigation of single cylinder diesel engine using bio diesel from marine algae . *International Journal of Innovative Science, Engineering and Technology (IJISET), 1(4)*, 399-403.

Venkatesan, M., Moorthi, N. S., Franco, P. A., Manivannan, A., and Karthikeyan, R. (2015). Hydrous Methanol Fuelled HCCI Engine. *Mechanics and Mechanical Engineering, 19(1)*, 31-49.

Wade, L. (2016). *Tesla's Electric cars aren't as green as you might think.* Retrieved March 2, 2018, from https://www.wired.com/2016/03/teslas-electric-cars-might-not-green-think/

Wartsilä-Sulzer RTA96-C. (2018). Retrieved March 31, 2018, from Wikipedia.org: https://en.wikipedia.org/wiki/W%C3%A4rtsil%C3%A4-Sulzer_RTA96-C

Yang, S., Reitz, R. D., Iyer, C. O., and Yi, J. (2008). A Transport Equation Residual Model Incorporating a Damkohler Criterion for Predicting the Flame Propagation in Gasoline Direct Injection Engines. *Eighteenth International Multidimensional Engine Modeling User's Group Meeting at the SAE Congress* (1-10). Detroit, Michigan: SAE.

Yuhua, (. Z., Nameer, S., Kevin, F., Ronald, R. I., Zihan, W., Riccardo, S., et al. (2013). Numerical Studies of the Combustion Characterisstics of a Diesel Micro Pilot Ignited DI Gasoline Engine with Turbocharging and EGR. *Proceedings of the ASME 2013 Internal Combustion Engine Division Fall Technical Conference ICEF2013* (1-13). Michigan: ASME.

Zelimir, D., Blaz, V., Stanislaw, P., and Breda, K. (2009). Influence of Fuel Properties on Engine Characteristics and Tribology Parameters. *Goriva I Maziva, 48(2)*, 131-158.

Zhang, M., Wang, J., Huang, Z., and Iida, N. (2014). Numerical Study of Effects of the Intermediates and Initial Conditions on Flame Propagation in a Real Homogeneous Charge Compression Ignition Engine. *Thermal science, 18(1)*, 79-87.

APPENDIX

TABLES OF THE ENGINE PERFORMANCE PARAMETERS

Thermal efficiency of modelled engine for category I

Cone Base Angle (°)	**Truncated Cone Piston Crown**				**Inverted Truncated Cone Piston Crown**			
	CR	η_{Th} (%)	CR	η_{Th} (%)	CR	η_{Th} (%)	CR	η_{Th} (%)
25	17.5:1	30.881	16.877:1	30.654	17.5:1	30.855	10.645:1	27.701
30	17.5:1	30.829	16.738:1	30.665	17.5:1	30.854	10.697:1	27.686
35	17.5:1	30.930	16.589:1	30.611	17.5:1	30.836	10.754:1	27.773
40	17.5:1	30.905	16.426:1	30.551	17.5:1	30.928	10.819:1	27.785
45	17.5:1	30.867	16.243:1	30.485	17.5:1	30.921	10.895:1	27.866

CR – Compression Ratio

η_{Th} - Thermal Efficiency

Mean effective pressure of modelled engine for category I

Cone Base Angle (°)	**Truncated Cone Piston Crown**				**Inverted Truncated Cone Piston Crown**			
	CR	P_m (10^5 N/m^2)	CR	P_m (10^5 N/m^2)	CR	P_m (10^5 N/m^2)	CR	P_m (10^5 N/m^2)
25	17.5:1	7.306	16.877:1	7.263	17.5:1	7.266	10.645:1	6.553
30	17.5:1	7.271	16.738:1	7.254	17.5:1	7.270	10.697:1	6.357
35	17.5:1	7.317	16.589:1	7.242	17.5:1	7.258	10.754:1	6.570
40	17.5:1	7.354	16.426:1	7.227	17.5:1	7.317	10.819:1	6.584
45	17.5:1	7.303	16.243:1	7.211	17.5:1	7.314	10.895:1	6.592

CR – Compression Ratio

P_m – Mean Effective Pressure

Generated power of modelled engine for category I

Cone Base Angle (°)	**Truncated Cone Piston Crown**				**Inverted Truncated Cone Piston Crown**			
	CR	Power (kW)	CR	Power (kW)	CR	Power (kW)	CR	Power (kW)
25	17.5:1	6.041	16.877:1	6.005	17.5:1	6.008	10.645:1	5.418
30	17.5:1	6.012	16.738:1	5.998	17.5:1	6.011	10.697:1	5.256
35	17.5:1	6.050	16.589:1	5.988	17.5:1	6.001	10.754:1	5.432
40	17.5:1	6.080	16.426:1	5.988	17.5:1	6.050	10.819:1	5.444
45	17.5:1	6.038	16.243:1	5.962	17.5:1	6.047	10.895:1	5.450

CR – Compression Ratio

Engine Torque of the modelled engine for category I

Cone Base Angle (°)	**Truncated Cone Piston Crown**				**Inverted Truncated Cone Piston Crown**			
	CR	Torque (N/m)	CR	Torque (N/m)	CR	Torque (N/m)	CR	Torque (N/m)
25	17.5:1	38.46	16.877:1	38.23	17.5:1	38.25	10.645:1	34.49
30	17.5:1	38.27	16.738:1	38.18	17.5:1	38.27	10.697:1	33.46
35	17.5:1	38.52	16.589:1	38.12	17.5:1	38.20	10.754:1	34.58
40	17.5:1	38.71	16.426:1	38.04	17.5:1	38.52	10.819:1	34.66
45	17.5:1	38.44	16.243:1	37.96	17.5:1	38.50	10.895:1	34.70

CR – Compression Ratio

Specific fuel consumption of modelled engine for category I

Cone Base Angle (°)	Truncated Cone Piston Crown				Inverted Truncated Cone Piston Crown			
	CR	SFC (kg/kWh)	CR	SFC (kg/kWh)	CR	SFC (kg/kWh)	CR	SFC (kg/kWh)
25	17.5:1	0.1931	16.877:1	0.1943	17.5:1	0.1941	10.645:1	0.2153
30	17.5:1	0.1940	16.738:1	0.1945	17.5:1	0.1941	10.697:1	0.2220
35	17.5:1	0.1928	16.589:1	0.1948	17.5:1	0.1944	10.754:1	0.2147
40	17.5:1	0.1918	16.426:1	0.1952	17.5:1	0.1928	10.819:1	0.2142
45	17.5:1	0.1932	16.243:1	0.1957	17.5:1	0.1929	10.895:1	0.2140

CR – Compression Ratio

SFC – Specific Fuel Consumption

Thermal efficiency of modelled engine for category II

Cone Base Angle (°)	CR	Truncated Cone Piston Crown	Inverted Truncated Cone Piston Crown
		η_{Th} (%)	η_{Th} (%)
25	20.5:1	32.255	32.253
30	20.5:1	32.255	32.255
35	20.5:1	32.258	32.255
40	20.5:1	32.261	32.258
45	20.5:1	32.250	32.255

CR – Compression Ratio

η_{Th} - Thermal Efficiency

Mean effective pressure of modelled engine for category II

Cone Base Angle (°)	CR	Truncated Cone Piston Crown	Inverted Truncated Cone Piston Crown
		P_m (10^5 N/m^2)	P_m (10^5 N/m^2)
25	20.5:1	4.0736	4.0733
30	20.5:1	4.0736	4.0736
35	20.5:1	4.0741	4.0736
40	20.5:1	4.0744	4.0740
45	20.5:1	4.0729	4.0736

CR – Compression Ratio

P_m – Mean Effective Pressure

Generated power of modelled engine for category II

Cone Base Angle (°)	CR	Truncated Cone Piston Crown	Inverted Truncated Cone Piston Crown
		Power (kW)	Power (kW)
25	20.5:1	2.3786	2.3784
30	20.5:1	2.3786	2.3786
35	20.5:1	2.3789	2.3786
40	20.5:1	2.3790	2.3788
45	20.5:1	2.3782	2.3786

CR – Compression Ratio

Engine Torque of the modelled engine for category II

Cone Base Angle (°)	CR	Truncated Cone Piston Crown	Inverted Truncated Cone Piston Crown
		Torque (N/m)	Torque (N/m)
25	20.5:1	8.736	8.736
30	20.5:1	8.736	8.737
35	20.5:1	8.737	8.737
40	20.5:1	8.738	8.737
45	20.5:1	8.735	8.737

CR – Compression Ratio

Specific fuel consumption of modelled engine for category II

Cone Base Angle (°)	CR	Truncated Cone Piston Crown	Inverted Truncated Cone Piston Crown
		SFC (kg/kWh)	SFC (kg/kWh)
25	20.5:1	0.3463	0.3465
30	20.5:1	0.3463	0.3464
35	20.5:1	0.3463	0.3464
40	20.5:1	0.3462	0.3463
45	20.5:1	0.3464	0.3464

CR – Compression Ratio

SFC – Specific Fuel Consumption